

TABLE OF CONTENTS

| | Page |
|--|------|
| INTRODUCTION | 1 |
| CHAPTER 1 STATE OF THE ART AND LITTERATURE REVIEW OF MICROGRID | 1 |
| 1.1 Introduction..... | 1 |
| 1.2 Concept of Microgrid..... | 2 |
| 1.2.1 Microgrid advantages and disadvantages | 3 |
| 1.2.2 Microgrid classifications..... | 4 |
| 1.3 Distributed energy resource technologies for MG..... | 5 |
| 1.4 Wind Energy Conversion System..... | 6 |
| 1.5 Solar Photovoltaic System | 7 |
| 1.6 Small-Scale Hydroelectric Generation..... | 8 |
| 1.7 Biomass..... | 9 |
| 1.8 Geothermal Energy | 10 |
| 1.9 Stirling Engine | 11 |
| 1.10 Fuel Cells | 11 |
| 1.11 Microturbine | 12 |
| 1.12 Energy Storage System Technology..... | 13 |
| 1.12.1 Battery Energy Storage Technology..... | 14 |
| 1.12.2 Flywheel Energy Storage Technology..... | 16 |
| 1.12.3 Ultra-capacitor Energy Storage Technology..... | 17 |
| 1.13 Vehicle to microgrid (V2G) and microgrid to vehicle (G2V) interaction | 18 |
| 1.13.1 Introduction..... | 18 |
| 1.13.2 Plug-in Hybrid Electric Vehicle (PHEV)..... | 18 |
| 1.13.3 Electric Vehicles | 20 |
| 1.13.4 Battery pack and ultra-capacitor used in PHEV and EV | 21 |
| 1.14 Interface between V2G and G2V..... | 21 |
| 1.15 Mode of charging and discharging of V2G and G2V..... | 22 |
| 1.16 Charging time for PHEV and EV | 23 |
| 1.17 Microgrid operation and islanding..... | 23 |
| 1.17.1 Microgrid Protection..... | 25 |
| 1.17.2 Net Zero Energy House based on Microgrid concept..... | 25 |
| 1.18 Review of the main power electronics converters used in MG | 26 |
| 1.18.1 Factors and Symbols used in AC Power System | 27 |
| 1.18.1.1 Power factor for linear load | 27 |
| 1.18.1.2 Power factor for nonlinear load | 29 |
| 1.18.2 Factor and symbols used in DC power system | 31 |
| 1.18.3 DC-AC Inverter with two level topologies..... | 32 |
| 1.18.4 Single-phase half-bridge voltage source inverter..... | 33 |
| 1.18.5 Single-Phase Full-Bridge VSC | 33 |
| 1.18.6 Three-Phase Full Bridge VSC | 34 |

| | | |
|--|---|----|
| 1.18.7 | Three-Phase Full-bridge current source inverter | 35 |
| 1.18.8 | Impedance source inverter | 35 |
| 1.19 | Multilevel power converter structures | 37 |
| 1.19.1 | Diode-Clamped and Capacitor-Clamped Multilevel Inverters | 38 |
| 1.19.2 | Multilevel Inverters using H-Bridges topologies..... | 40 |
| 1.20 | Power quality problems in Microgrids | 41 |
| 1.21 | Power quality solution for microgrids | 43 |
| 1.21.1 | Dynamic Voltage Restorer..... | 44 |
| 1.21.2 | Transient Voltage Surge Suppressors | 45 |
| 1.21.3 | Static VAR compensators | 45 |
| 1.21.4 | Passive harmonic filter..... | 46 |
| 1.21.5 | Power quality with active filtering devices..... | 47 |
| 1.21.6 | Active filter type of VSC configuration with three phase | 47 |
| 1.21.7 | Three-Phase four wire active filter VSC with midpoint capacitor | 48 |
| 1.21.8 | Three phase four leg of the active filter VSC | 48 |
| 1.21.9 | Hybrid Shunt filter without transformer | 49 |
| 1.21.10 | Hybrid active filter with two legs without transformer | 50 |
| 1.21.11 | Series Active Filter | 51 |
| 1.21.12 | Hybrid filter series | 52 |
| 1.21.13 | Unified power quality conditioner (UPQC)..... | 53 |
| 1.22 | State of the art of the technique modulation control..... | 54 |
| 1.22.1 | Hysterisis control | 54 |
| 1.22.2 | Modulated hysteresis control | 56 |
| 1.22.3 | Pulse-Width Modulation Control..... | 56 |
| 1.22.4 | PWM Space vector modulation (PWM-SVM) | 57 |
| 1.23 | Main controls algorithms used in power quality..... | 58 |
| 1.23.1 | PQ direct instantaneous power control method | 59 |
| 1.23.2 | PQ indirect instantaneous power control method | 60 |
| 1.23.3 | Synchronous Reference Frame (SRF) | 61 |
| 1.23.4 | Nonlinear control | 61 |
| 1.23.5 | Sliding mode control..... | 62 |
| 1.23.6 | Direct adaptive control with reference model..... | 63 |
| 1.23.7 | Indirect adaptive control | 63 |
| 1.23.8 | Control method based on Lyapunov stability | 64 |
| 1.24 | Conclusion | 64 |
| CHAPTER 2 CONCEPT AND DESIGN OF NET ZERO ENERGY HOUSE USING MICROGRID APPROCHES..... | | 65 |
| 2.1 | Introduction..... | 65 |
| 2.2 | Description of under study system..... | 65 |
| 2.3 | Design of photovoltaic system for NZEH | 66 |
| 2.3.1 | Load characteristics and daily energy consumption | 67 |
| 2.3.2 | Power generated from photovoltaic system..... | 68 |
| 2.3.3 | DC bus voltage of VSC-AHF | 70 |
| 2.4 | DC bus capacitor calculation | 70 |

| | | |
|-----------|--|-----|
| 2.4.1 | Design of output VSC-AHF inductor | 71 |
| 2.4.2 | Validation of the VSC-AHF design using Semisel software | 71 |
| 2.4.3 | Proposed Control Algorithm for the NZEH..... | 72 |
| 2.4.3.1 | Synchronous reference frame and direct voltage control | 73 |
| 2.4.3.2 | Nonlinear direct control for current and direct control for voltage | 75 |
| 2.4.3.3 | Nonlinear direct control for current and nonlinear direct control for voltage..... | 76 |
| 2.5 | Modeling of bidirectional battery charger for PHEV | 77 |
| 2.5.1 | Modeling of buck-boost converter and controlling with sliding mode.... | 78 |
| 2.5.1.1 | Modeling of boost converter | 80 |
| 2.5.1.2 | Modeling of buck converter | 81 |
| 2.5.1.3 | Sliding mode control of the buck-boost converter..... | 82 |
| 2.5.2 | Modeling of the five level DC-AC bidirectional battery charger | 84 |
| 2.6 | Simulation results of the Net Zero Energy House | 87 |
| 2.6.1 | Simulation result of bidirectional battery charger for PHEV | 88 |
| 2.6.2 | Simulation result of the house connected to the grid..... | 89 |
| 2.6.3 | Simulation of Net Zero Energy House for ON/OFF grid operation | 91 |
| 2.7 | Economic analysis using PV*Sol software..... | 95 |
| 2.7.1 | System Check and optimisation..... | 96 |
| 2.7.2 | Economic Efficiency Calculation and report..... | 98 |
| 2.8 | Conclusion | 99 |
| | | |
| CHAPTER 3 | SMART HYBRID ENERGY MANAGEMENT OF STANDALONE SYSTEM BASED ON MICROGRID CONCEPT..... | 101 |
| 3.1 | Introduction..... | 101 |
| 3.2 | System description | 101 |
| 3.3 | Step for calculation of total energy demand and power supply | 102 |
| 3.3.1 | Estimated daily energy consumption and specification of the load..... | 102 |
| 3.3.2 | Size evaluation of photovoltaic array | 103 |
| 3.3.3 | Battery energy storage system | 105 |
| 3.4 | Modeling and control strategy of the under study system | 105 |
| 3.4.1 | Modeling and control of photovoltaic system | 105 |
| 3.4.1.1 | Mathematic model of solar cell..... | 106 |
| 3.4.1.2 | Modeling of photovoltaic module..... | 107 |
| 3.4.2 | Gas generator set and its advantages..... | 109 |
| 3.4.2.1 | Control strategy of GGS | 109 |
| 3.5 | Developing of active damping approach for VSC | 110 |
| 3.5.1 | Passive damping approaches and their disadvantages | 111 |
| 3.5.2 | Power losses calculation in the damping resistor R_c | 112 |
| 3.5.3 | Development of active damping approach | 113 |
| 3.5.4 | Approach for reducing the value of output filter $L_f C_f$ using active damping technique | 118 |
| 3.6 | Fuzzy logic supervisor and its application domain..... | 122 |
| 3.6.1 | Fuzzy logic energy management used for the proposed system..... | 123 |

| | | |
|--------------------------------------|---|-----|
| 3.6.2 | Battery overcharging and system protection using water pump | 126 |
| 3.7 | Simulation results of standalone complete system based on MG concept | 127 |
| 3.8 | Conclusion | 128 |
| CHAPTER 4 | EXPERIMENTAL REALIZATION OF NZEH AND STANDALONE SYSTEM BASED ON MICROGRID CONCEPT | 131 |
| 4.1 | Introduction | 131 |
| 4.2 | Net Zero Energy House hardware implementation | 131 |
| 4.2.1 | Step1: Test of dc-dc boost converter with small photovoltaic module... .. | 131 |
| 4.2.2 | Step2: Test of NZEH with the single phase VSC-AHF | 133 |
| 4.2.3 | Step3: Improvement and performance of NZEH with industrial point of view | 135 |
| 4.2.3.1 | Design of printed circuit board for sensing and regulating the signal of V_s , V_{dc} , i_s , i_F and i_L | 136 |
| 4.2.3.2 | Offset of the input ADC signal and protection technique of the DSP | 139 |
| 4.2.3.3 | PCB interface card for the microcontroller eZdsp F28335 | 141 |
| 4.2.3.4 | Implementation of the control algorithm of NZEH | 142 |
| 4.2.3.5 | Experimental result of NZEH | 145 |
| 4.3 | Experimental results for Chapter 3 (standalone system for remote area) | 150 |
| 4.4 | Conclusion | 156 |
| CONCLUSION AND RECOMMENDATIONS | | 157 |
| ANNEX I | OPTIMISATION OF THE INVERTER USING SEMISEL SOFTWARE | 161 |
| ANNEX II | SYSTEM PARAMETERS | 163 |
| ANNEX III | HARDWARE SETUP DETAILS | 165 |
| LIST OF | BIBLIOGRAPHICAL REFERENCES | 174 |

LIST OF TABLES

| | | Page |
|-----------|---|------|
| Table 1.1 | Characteristics of different type of batteries | 15 |
| Table 1.2 | Conductive charging system for electric vehicles..... | 23 |
| Table 1.3 | Different type of Power Quality disturbances..... | 42 |
| Table 2.1 | Load load characteristics and daily energy consumption | 67 |
| Table 2.2 | Switching table of the inverter | 87 |
| Table 2.3 | Report for economic efficiency calculation | 98 |
| Table 3.1 | Daily energy required for the load | 103 |
| Table 3.2 | Characteristics of choosing PV module X21-345..... | 104 |
| Table 3.3 | Power calculation..... | 104 |
| Table 3.4 | Fuzzy logic rules for the power management of the system..... | 124 |
| Table 3.5 | System parameters used in simulation | 163 |

LIST OF FIGURES

| | | Page |
|-------------|---|------|
| Figure 1.1 | Africa's Energy Landscape..... | 2 |
| Figure 1.2 | Distributed energy resources employed in MG | 5 |
| Figure 1.3 | Wind energy conversion systems (WECS)..... | 7 |
| Figure 1.4 | Photovoltaic system | 8 |
| Figure 1.5 | Micro-Hydro Power | 9 |
| Figure 1.6 | Diagram of the biomass gasified system..... | 10 |
| Figure 1.7 | Geothermal energy system..... | 10 |
| Figure 1.8 | Stirling engine..... | 11 |
| Figure 1.9 | Genetic Hydrogen Fuel Cell Operation | 12 |
| Figure 1.10 | Block diagram of a micro-turbine..... | 13 |
| Figure 1.11 | Different energy storage technology..... | 14 |
| Figure 1.12 | Battery energy storage system and primary power component | 14 |
| Figure 1.13 | Flywheel energy storage technology | 16 |
| Figure 1.14 | Family tree of super capacitors | 17 |
| Figure 1.15 | PHEV with a series hybrid power train | 19 |
| Figure 1.16 | PHEV with a parallel hybrid power train | 19 |
| Figure 1.17 | PHEV with a series-parallel hybrid power train..... | 20 |
| Figure 1.18 | 100% Electric Vehicle | 20 |
| Figure 1.19 | Comparison between different batteries technology and super capacitor. 21 | |
| Figure 1.20 | General bi-directional charger for single and three phase systems..... | 22 |
| Figure 1.21 | Net Zero Energy House..... | 26 |

| | | |
|-------------|---|----|
| Figure 1.22 | Power vector diagram for the linear load..... | 28 |
| Figure 1.23 | Fresnel diagram for Power..... | 30 |
| Figure 1.24 | Single-phase half-bridge voltage source inverter | 33 |
| Figure 1.25 | Single-phase full-bridge VSC..... | 34 |
| Figure 1.26 | Three-phase full-bridge VSC..... | 34 |
| Figure 1.27 | Three phase CSI..... | 35 |
| Figure 1.28 | Impedance Source Inverter | 36 |
| Figure 1.29 | Family tree of multilevel level inverters..... | 38 |
| Figure 1.30 | Three-level diode-clamped multilevel inverter..... | 39 |
| Figure 1.31 | Five level diode-clamped multilevel inverter | 40 |
| Figure 1.32 | Multilevel inverter based on the connection of HBs. | 41 |
| Figure 1.33 | ITIC and CBEMA power quality standard curve | 44 |
| Figure 1.34 | Dynamic Voltage restorer operation..... | 45 |
| Figure 1.35 | Passive harmonic filter..... | 46 |
| Figure 1.36 | Three-phase system with active shunt filter..... | 47 |
| Figure 1.37 | Three Phase Four Wire Active VSC with midpoint capacitor..... | 48 |
| Figure 1.38 | Three phase four leg active filter VSC | 49 |
| Figure 1.39 | Hybrid Shunt filter without transformer | 50 |
| Figure 1.40 | Hybrid active filter with two legs and without transformer..... | 51 |
| Figure 1.41 | Three phase system with series active filter | 52 |
| Figure 1.42 | Association d'un filtre actif série et d'un filtre passif..... | 53 |
| Figure 1.43 | Three phase system using Unified Power Quality Conditioner..... | 54 |
| Figure 1.44 | Hysterisis control | 55 |
| Figure 1.45 | Hysteresis control band..... | 55 |

Figure 1.46 Modulation Hysteresis Control 56

Figure 1.47 Output voltage vector in the a, b plane. 58

Figure 1.48 Output line voltages in time domain 58

Figure 1.49 PQ direct instantaneous power method for harmonic currents and reactive power compensation..... 60

Figure 1.50 Algorithm of ‘PQ’ indirect instantaneous power control method..... 60

Figure 1.51 SRF control for the hybrid shunt filter..... 61

Figure 1.52 Nonlinear control by exact linearization..... 62

Figure 1.53 Sliding mode control..... 62

Figure 1.54 Direct adaptive control with reference model..... 63

Figure 1.55 Indirect non linear adaptative control. 63

Figure 2.1a Model of Net Zero Energy House based on MG concept..... 66

Figure 2.1b Daily load profile of the NZEH 70

Figure 2.2 Average daily sunlight hour 69

Figure 2.3 Circuit for secure Start-Stop of the VSC-AHF 72

Figure 2.4 Block diagram of the control scheme for VSC 74

Figure 2.5 Second control 76

Figure 2.6 Third control 77

Figure 2.7 Bidirectional onboard PHEV battery charger 78

Figure 2.8 DC-DC buck boost converter..... 78

Figure 2.9 ON sequence of the boost converter 79

Figure 2.10 OFF sequence of the boost converter..... 80

Figure 2.11 Bloc diagram of sliding mode control for battery charger..... 84

Figure 2.12 Five level dc-ac converter 85

Figure 2.13 Five level battery charger for PHEV..... 88

| | | |
|---------------|--|-----|
| Figure 2.14 | Battery characteristics | 89 |
| Figure 2.15 | Testing the performance of VSC-AHF | 90 |
| Figure 2.16 | Power flow and reactive power control | 91 |
| Figure 2.17 | Net Zero Energy House operating in ON/OFF Grid..... | 92 |
| Figure 2.18 | Zoom of figure 2.25 | 93 |
| Figure 2.19 | Zoom of Figure 2.17 | 94 |
| Figure 2.20 | Unbalance compensation when single phase battery charger connected to the three phase | 94 |
| Figure 2.21 | Climate Data for Oum-Hadjer City..... | 95 |
| Figure 2.22 | Model of the PVS connected to the grid in 2D..... | 96 |
| Figure 2.23 | Check for the compatibility of the system | 97 |
| Figure 2.24 | Check for compatibility of the system and optimization..... | 97 |
| Figure 2.25 | Project profitability after 9 years | 99 |
| Figure 3.1 | Smart MG system designed for remote area..... | 102 |
| Figure 3.2 | From a solar cell to the PVS | 106 |
| Figure 3.3 | Equivalent circuit for solar cell..... | 106 |
| Figure 3.4 | Implementation of photovoltaic module in Matlab | 108 |
| Figure 3.5 | Result of PV module implementation..... | 108 |
| Figure 3.6 | Control diagram of GGS..... | 110 |
| Figure 3.7. | Output filter with damping resistor R_c | 111 |
| Figure 3.8. | Bode diagram of output filter with damping resistor R_c | 113 |
| Figure 3.9 | Output filter with Active Damping technique | 113 |
| Figure 3.10 . | Output filter with active damping coefficient..... | 117 |
| Figure 3.11 | Bode Diagram of R_c and k_c | 117 |
| Figure 3.12 | Harmonic spectrum of load current | 119 |

| | | |
|--------------|--|-----|
| Figure 3.13 | Harmonic spectrum of inverter voltage | 119 |
| Figure 3.14 | New value of output filter $L_{f1}C_{f1}$ with new damping factor | 120 |
| Figure 3.15 | Zero and pole maps for transfer functions of the $L_f C_f$ before and after value reduction..... | 121 |
| Figure 3.16 | Control of VSC inverter with active damping coefficient..... | 121 |
| Figure 3.17 | FLS and typical variable speed of GGS [32]..... | 125 |
| Figure 18a | Operation of a fuzzy controller | 23 |
| Figure 3.18b | Membership function of input variable P_{reg} | 125 |
| Figure 3.19 | Membership function of input variable SOC(%)..... | 126 |
| Figure 3.20 | Membership function of input variable P_{GGS} | 126 |
| Figure 3.21 | Power flow and speed of the GGS..... | 127 |
| Figure 3.22 | Power management and power quality | 128 |
| Figure 4.1 | Mini Setup of NZEH (First step) | 132 |
| Figure 4.2 | eZdsp F28335 description..... | 132 |
| Fig. 4.3. | DC-DC boost converter | 132 |
| Figure 4.4 | Laboratory setup for experimental validation (Second step)..... | 133 |
| Figure 4.5 | Result of single phase VSC-AHF connected to the grid..... | 134 |
| Figure 4.6 | Result of single phase VSC-AHF connected to the grid..... | 134 |
| Figure 4.7 | Experimental setup of NZEH..... | 135 |
| Figure 4.8 | Control Box of the NZEH..... | 136 |
| Figure 4.9 | Schematic for V_{dc} and V_s | 137 |
| Figure 4.10 | PCB for sensing and regulating V_s and V_{dc} output signal | 137 |
| Figure 4.11 | Schematic for signal i_L and i_F | 138 |
| Figure 4.12 | PCB for regulating the output signal of i_L and i_F | 138 |
| Figure 4.13 | Schematic circuit for offset signal from ± 1.5 to 3V | 139 |

| | | |
|----------------|--|-----|
| Figure 4.14 | Simulation of the DSP protection | 140 |
| Figure 4.15 | Experimental result of the DSP protection | 140 |
| Figure 4.16 a) | PCB interface card (version2) of eZdsp F28335 | 141 |
| Figure 4.17 | Code composer studio V.3 with its main icons on the right | 143 |
| Figure 4.18 | Graphical display with CCS..... | 143 |
| Figure 4.19 | Input and output of signal from ADC to PWM | 144 |
| Figure 4.20 | Control algorithm Diagram..... | 144 |
| Figure 4.21 | Result of VSC-AHF connected to the grid and load (V_{dc} , V_s , i_L , i_{sa})... | 145 |
| Figure 4.22 | Result of VSC-AHF connected to the grid and load (V_{dc} , V_s , i_f , i_{sa}) ... | 146 |
| Figure 4.23 | Steady state response of VSC-AHF | 146 |
| Figure 4.24 | Experimental result for start from transient to steady state | 147 |
| Figure 4.25 | Experimental result for transient and steady state of the startup | 147 |
| Figure 4.26 | Experimental validation of the VSC-AHF during a shutdown..... | 148 |
| Figure 4.27 | Experimental validation of the VSC-AHF during stop and start..... | 149 |
| Figure 4.28 | Experimental validation of the NZEH with PVS and grid | 150 |
| Figure 4.29 | Experimental setup for standalone PVS, PHEV and GGS system | 151 |
| Figure 4.30 | Steady state response of the system..... | 152 |
| Figure 4.31 | Reference load voltage variation from 30 to 45 V..... | 152 |
| Figure 4.32 | Feeding of load from PVS and batteries of PHEV | 153 |
| Figure 4.33 | Load voltage with GGS and batteries without PVS..... | 154 |
| Figure 4.34 | Experimental results with disconnection of one phase of the load..... | 154 |
| Figure 4.35 | Voltage Quality of system without active damping..... | 155 |
| Figure 4.36 | Voltage Quality of system with active damping..... | 156 |

LIST OF ABBREVIATIONS

| | |
|------|------------------------------------|
| AC | Alternative Current |
| AF | Active Filter |
| AVR | Automatic Voltage Regulation |
| BESS | Battery Energy Storage System |
| BHMI | Binary Hybrid Multilevel Inverters |
| CSI | Current Source Inverter |
| CHP | Combined Heat and Power |
| DC | Direct Current |
| DER | Distributor Energy Ressources |
| DF | Distortion Factor |
| DG | Diesel Generator |
| DSM | Demand Side Management |
| DPF | Displacement Power Factor |
| DSP | Digital Signal Procesing |
| DVR | Dynamic Voltage Restorer |
| ES | Energy Source |
| EV | Electric Vehicles |
| FF | Form Factor |
| GGs | Gas Generator Set |
| G2V | Grid to vehicle |
| HEVs | Hybrid Electric Vehicles |
| HBs | H-bridges |

XXIV

| | |
|------|-------------------------------------|
| ICE | Internal Combustion Engine |
| ZSI | Impedance Source Inverter |
| MW | Megawatts |
| MEVs | More-Electric Vehicles |
| MG | Migrogrid |
| MPPT | Maximum Power Point Tracking |
| NZEH | Net Zero Energy House |
| VSC | Voltage Source Converter |
| PCC | Point Common Coupling |
| PVS | Photovoltaic System |
| PWM | Pulse Width Modulation |
| FLS | Fuzzy Logic Supervisor |
| PHEV | Plug-in Hybrid Electric Vehicle |
| RES | Renewable Energy Source |
| RF | Ripple Factor |
| SRF | Synchronous Reference Frame |
| SOC | State of Charge |
| THD | Total Harmonic Distorsion |
| THMI | Trinary Hybrid Multilevel Inverters |
| TVSS | Transient Voltage Surge Suppressors |
| UPS | Uninterruptible Power Supply |
| UPQC | Unified Power Quality Conditioner |
| WECS | Wind Energy Conversion Systems |

LIST OF SYMBOLS AND UNIT OF MEASUREMENTS

| | |
|----------|---|
| ω | Angular frequency |
| Φ | Phase angle between source current w.r.t. to source voltage |
| C_{dc} | DC link capacitor |
| C_f | Ripple filter capacitor |
| D | Distorted power eff Effective value |
| f | network frequency |
| f_s | Switching frequency |
| G | Gain proportional to current harmonics |
| h | Harmonic order |
| Hz | Hertz |
| i_s | Source current |
| i_L | Load current |
| i_h | Source harmonic current |
| i_b | Battery Current |
| V_s | Voltage source |
| V_{dc} | DC bus voltage |
| L | Inductance |
| P | Active power |
| Q | Reactive power |
| R or r | Resistance |
| s | Second |
| S | Apparent power |
| W | Watt |
| Z | Impedance |

INTRODUCTION

In recent years, the term "*Microgrid*" has gained significant importance, especially in renewable energy related fields as a solution to energy deficiency. The term microgrid (MG) is defined as a group of interconnected loads and multiple distributed generators (renewable energy, electric vehicles and others sources) that are usually integrated via voltage source converters and is able to operate in grid-connected or island-mode. The MG is a new formula developed to face the problem of public network during disturbances and also helps to reach remote areas. MG represents one of the three legs of the smart grid stool, together with enhanced megagrid operations and grid-customer interaction. Recent reports claim dramatic growth in projects planned to around 116 GW total worldwide (Navigant Research, 2016). Notably, following many natural disasters in some countries, the concept of MG and its perceived benefits shifted beyond economic and environmental goals towards resilience. In addition, the MG could help reduce the pollution caused by fossil fuels and conventional transportation. However, power quality is a big concern of MG to guarantee reliable and clean energy for the customers.

The ever-increasing interest in the subject of MG can be explained in the context of its major advantages:

- During network (grid) disturbances, the MG has the ability to isolate itself from grid and continue to supply loads safely;
- During peak load demand, the MG assists the network by injecting more power to the grid to compensate the deficit;
- With renewable energies integration, MG help maintaining very low or zero emission generators;
- Improvement in power quality and reliability are achieved due to the decentralization of power supply sources, better power management, and reduction in the impact of large-scale transmission.

Research Objectives

This work was conducted at GREPCI (Groupe de Recherche en Électronique de Puissance et Commande Industrielle) with support from Concordia Institute for Water, Energy and Sustainable Systems (CIWESS). The research objectives are summarized below:

- To carry out an in-depth analytical study on how the different energy resources of MGs are integrated and managed and also to understand how the MG may behave under different operating conditions;
- To perform feasibility analyze of MGs under a realistic network environment;
- To reduce the number of electronic component and optimize the size of the output filter $L_f C_f$ of VSC while keeping high performance of operation;
- To develop a new control approaches for battery charger for vehicle to grid (V2G) and grid to vehicle (G2V) application;
- To simulate a model of the MG for the Central African State regions.

Methodology

To accomplish the objectives highlighted above, three important steps are followed which are outlined below:

- This thesis contains basic laws of mathematics, circuit theory, and electrical engineering. The proposed control approaches are first put forward through adequate mathematical formulation supported with detailed control schemes and diagram representations. MATLAB/ Simulink is used for simulation and validation of the MG under different operating conditions;
- Implementation of the hardware setup by following predefined plan and steps;
- Developing an interface card based on microcontroller eZdspF28335 to control the hardware setup of MG. Finally, different tests and adjustments are done to validate the functionality and performance of the system.

Thesis Contributions

The contribution of the thesis is to deal with three significant problems: 1) Smart energy management for Grid Connect and Standalone Systems, 2) Control strategies approaches to reduce the number of sensors in Net Zero Energy House, 3) Reduction of the number of components of the voltage source converter the size. The remarkable accomplishments of this work are as follows:

- The developed control approach ensures a high operating performance of MG in ON and OFF mode in order to reach the Net Zero Energy House concept which is serving as benchmark for the future work;
- The reduction of sensors' number helps reducing the cost and degree of control complexity;
- The smart energy management is achieved through fuzzy logic supervisor built on 25 rules. The mixed operation of photovoltaic system and gas generator set has contributed in the battery size reduction while ensuring an uninterruptible power supply.
- The development of a new approach of active damping control technique without using any additional sensor has allowed reducing the losses of the output filter, reducing the component of the system by eliminating the passive damping resistor and finally contributing in the voltage quality improvement;
- The proposed technique of resonant frequency shifting had allowed reducing five times the size of $L_f C_f$ output filter of the voltage source converter while keeping high performance of operation. This is providing an additional option for the hardware MG optimization.

Finally, the experimental prototype of MG is consisted of three-phase VSC, gas generator set, photovoltaic system, batteries, PHEV, Network and water pump (using as a damp load). A control box based on the microcontroller eZdsp F28335 is developed to control the system.

Thesis Outline

This thesis is organized as follows:

CHAPTER 1 presents a literature review of the most research work being done in the area of MG and power quality using different approaches. The MG basics, including key concepts and operating principles, are explained which serve as a foundation for this thesis work. Different control algorithm for power quality and power management are also developed and supported with a diagram and schema.

CHAPTER 2 is fully dedicated to the Net Zero Energy House design and control based on MG concept. The power quality issue, the stability and reliability of the system to work in ON/OFF grid mode of operation is largely studied. The charging and discharging of electric vehicle have been carefully investigated. Many control approaches have been analyzed in order to find an optimal way to reduce the sensors' number, degree of control complexity and relatively cost of the system. Many simulations, experimental and economic results have been analyzed.

CHAPTER 3, special attention is given to the design of MG for remote area in order to enhance power balance and uninterruptible power supply. A new simplified approach for controlling the MG is concentrated on smart energy management using fuzzy logic supervisor and power quality using active harmonic filter. A new technique of active damping approach and reduction of the output $L_f C_f$ filter size of VSC is largely discussed. Interesting experimental results are discussed for the MG system.

CHAPTER 4 discusses the hardware implementation and experimental result of the previous chapters 2 and 3. The experimental results of NZEH for chapter 2 are done in three steps. The control approach allows compensating the harmonic current, unbalanced load, improving power factor and managing the power flow. Many promised results are obtained for the microgrid of standalone and grid connected system. Finally, a general conclusion and recommendation for the future work have been highlighted.

CHAPTER 1

STATE OF THE ART AND LITERATURE REVIEW OF MICROGRID

1.1 Introduction

Microgrid (MG) is attracting considerable attention as a solution to energy deficiency. The MG, as defined by the U.S. Department of Energy, is “a group of interconnected loads and distributed energy resources (DERs) with clearly defined electrical boundaries that acts as a single controllable entity with respect to the grid and can connect and disconnect from the grid to enable it to operate in both grid-connected or island modes" (Banerji, Biswas, & Singh, 2016a). There is a new wave of interest in recent years to deploy MG which is driven in part by the need for higher energy management reliability and power quality, advancements in power electronics and DER technologies.

This chapter presents a general review of all issues concerning:

- Summarizes the research areas related to MG, including a variety of issues associated to distributed energy resources (DER) as well as energy storage system (ESS) deployment;
- Applications to support grid performance, with a focus on improving grid reliability, resiliency, and power quality;
- Application of power electronics in MG as the integration of DERs necessitates a broader application of power electronics;
- MG scheduling, demand side management (DSM), market pricing, and optimal planning;
- MG operation, control, and islanding, covering the existing literature on MG control methodologies and architectures as well as the control of tie-line power, power electronic converters, uninterruptible power supply (UPS) systems and resynchronization of MG;
- MG clusters in which two or more electrically coupled MG are controlled and operated in a coordinated fashion;

- MG protection, which includes the modeling of faults in MG, protection of power-electronically coupled MG, and protection schemes based on microprocessors and communications, protection of DC MG, and fault current limiters;
- Discusses the issues related to MG communications necessary to achieve MG efficient protection and control;
- Conclusion.

In addition, a part of chapter will focus on the perspective of MG integration in the Central African Countries (CAC). Figure.1.1 shows the Africa's energy landscape (Agency, 2015a).

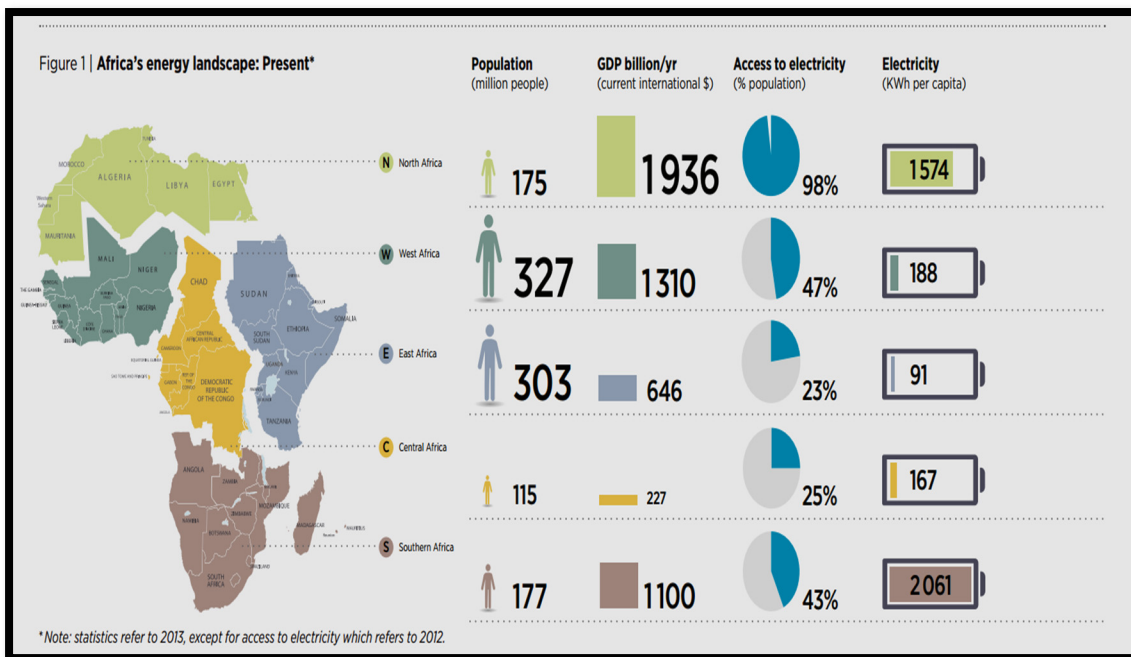


Figure 1.1 Africa's Energy Landscape

1.2 Concept of Microgrid

Microgrid (MG) consists of low voltage, combined heat and electrical power designed to supply loads for a small community, such as a suburban locality, villages, education areas

(university, school, etc....), a commercial and industrial site, a trading estate, or a municipal region. MG is the conglomerate of DG systems and different loads at distribution voltage level. These DG employed in a MG are usually hybrid system which consists of renewable/non-conventional energy sources integrated together to generate power at distribution voltage. MG must be equipped with power electronic interfaces controls to ensure reliability, security, flexibility for specified power quality and smart energy management in order to meet local energy needs. The MG is an ideal solution for supplying power to remote areas of a country where supply from the public grid system is either difficult to prevent due to the topology or frequently disrupted due to severe climatic conditions, or man-made disturbances (Akagi, Srianthumrong, & Tamai, 2003; S. Chowdhury, 2009).

1.2.1 Microgrid advantages and disadvantages

The development of MG is very promising because of the following advantages (Khan, 2009; Talei et al., 2015):

- MG has the ability during public grid disturbance, to isolate itself from the grid and to continue to supply other loads safely;
- During peak load demand periods, MG assists utility public grid from overcharging by injecting more power to the public grid;
- MG participates by integration of the renewable energies to extract the environmental benefits to maintain very low or zero emission generators;
- The combination of using both electricity and heat allow increasing the overall energy efficiency;
- Improvement in power quality and reliability is achieved due to:
 - Decentralization of power supply sources;
 - Better power management;
 - Reduction of the impact of large-scale transmission and generation outages;

- Minimization of downtimes and enhancement of the restoration process through black start operations of micro-sources. A black start is the process of restoring an electric power station or a part of an electric grid to operation without relying on the external transmission network.

The disadvantages of the MG are given by:

- Complexity of control to keep voltage, frequency and power quality to an acceptable standards;
- Energy Storage System requires more space and maintenance;
- Resynchronisation with the utility grid is difficult;
- MG protection is one of the important challenges facing the implementation of MG.

Interconnection standards need to be developed to ensure consistency.

1.2.2 Microgrid classifications

There are different classifications of MG that are summarized in four main categories (Lilienthal, 2013; Puthenpurakel & Subadhra, 2016):

- **Large grid-connected MGs:** it concerns large campus applications and military bases connected to a main public grid or operate in island mode;
- **Small grid-connected MGs:** with a single generator supported by energy storage system and renewable energy;
- **Large remote micro-grids:** such as island utilities with multiple generators and sub-station distribution;
- **Small remote MGs:** it will not usually have more than one generator and the smallest may have none. Some of the very small ones may have DC distribution. Innovations in billing and payment methods could greatly enhance the potential for these types of MG.

1.3 Distributed energy resource technologies for MG

The distributed energy resources (DERs) employed in MG is known as a combination of Renewable Energy Sources (RES) or non-conventional electricity generators. The MG has flexibility to integrate non-conventional/ RES included combined heat and power (CHP) to form a high-efficiency system as shown in Figure 1.2 (Lab; Zubieta, 2016).

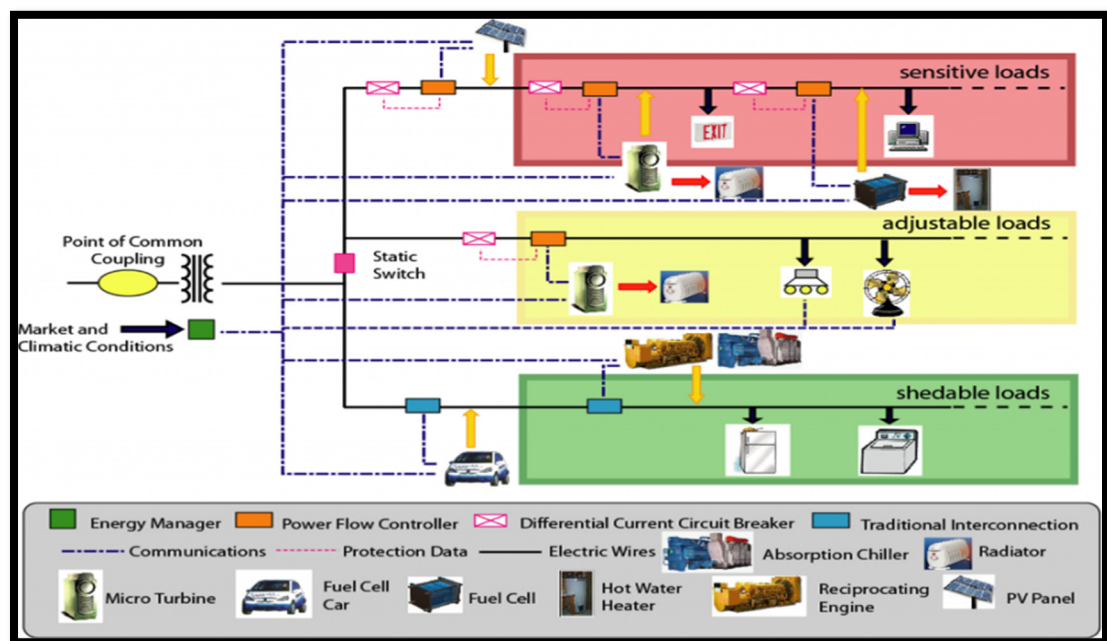


Figure 1.2 Distributed energy resources employed in MG

Many researchers are investigating the possibilities of using hybrid system with various energy storage system (ESS) technologies like flywheel, batteries and ultra- capacitors, etc.... The optimal choice of a DER depends mostly on the climate, the topology of the region and the fuel availability. Prospective DERs for MG are mostly based on:

- Wind energy conversion systems (WECS);
- Solar photovoltaic (PV) systems;
- Small-scale hydroelectric generation;
- Biomass;
- Geothermal energy;

- Stirling engines;
- Fuel cells;
- Energy storage system (battery, flywheel, ultracapacitor).

1.4 Wind Energy Conversion System

The wind energy conversion system (WECS) based wind turbines that convert wind energy into mechanical energy through a multiple-ratio gearbox and then to electrical energy via the generator. The main parts of a wind turbine shown in Figure 1.3 consist of:

- The tower;
- The rotor;
- The nacelle.

The wind turbine captures the kinetic energy of wind that flows through rotor blades and transfers the energy to the induction generator side through the gearbox (Edremitlioglu, 2010). The generator shaft is driven by the wind turbine to generate electric power. Wind turbines may have horizontal or vertical axis configuration. The average commercial turbine size of WECS was 300 kW until the mid-1990s, but recently machines of larger capacity, up to 5 MW, have been developed and installed.

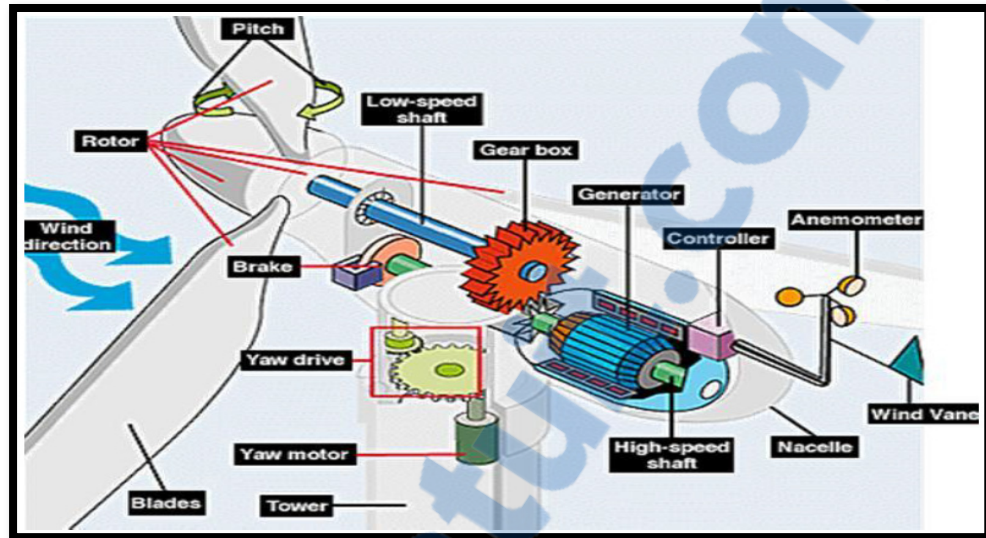


Figure 1.3 Wind energy conversion systems (WECS) (Edremitlioglu, 2010)

1.5 Solar Photovoltaic System

The solar photovoltaic system (PVS) (see Figure 1.4) generates electricity from solar energy irradiation and their major advantages are:

- Sustainable nature of solar energy;
- Minimum environmental impact;
- Reduction in customers' electricity bills;
- Long lifetime over 30 years with minimum maintenance;
- Silent operation.

Today PVS technology is encouraged by governments, environmental and commercial organizations to supply a significant part of the world's energy needs. It has been studied that small PVS installations are more cost-effective than larger ones, which indicates the effectiveness of feeding PVS generation directly into customer circuits at low voltage distribution networks (MG). However, the nature of PVS generation being DC, suitable power converter circuits are to be employed to convert DC power into AC at the specified frequency level (S. Chowdhury, 2009).

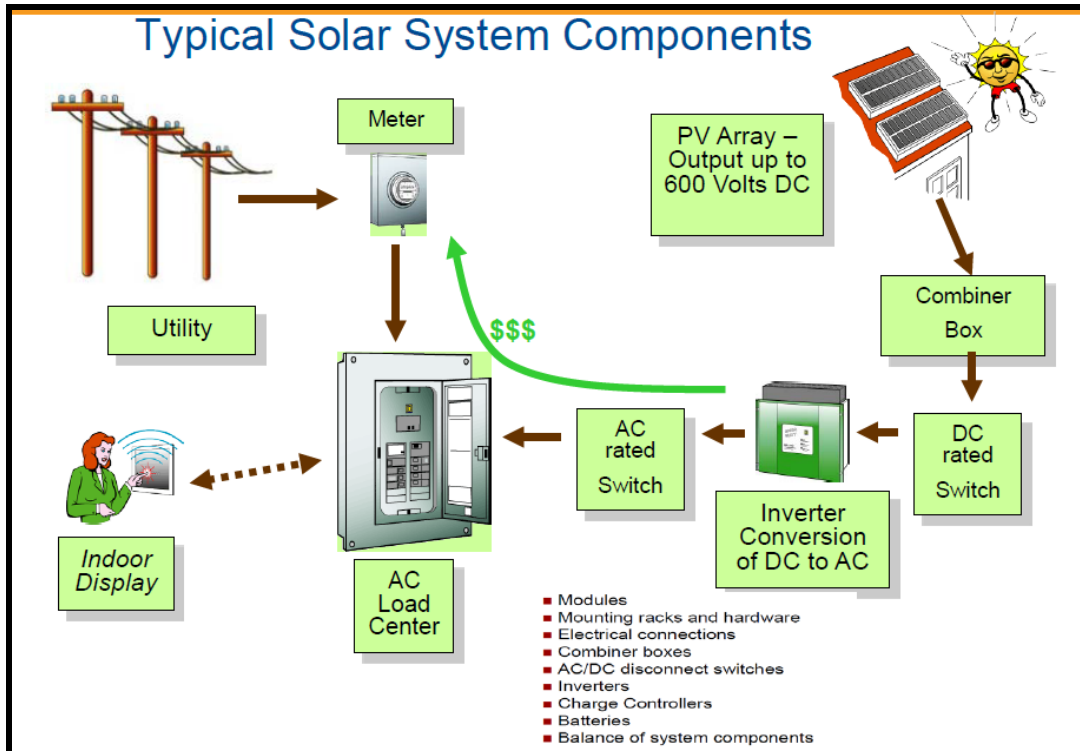


Figure 1.4 Photovoltaic system (S. Chowdhury, 2009)

1.6 Small-Scale Hydroelectric Generation

Small-scale hydroelectric generation as shown in Figure 1.5, serves a small community or a limited industrial plant that corresponds to the concept of distributed generation.

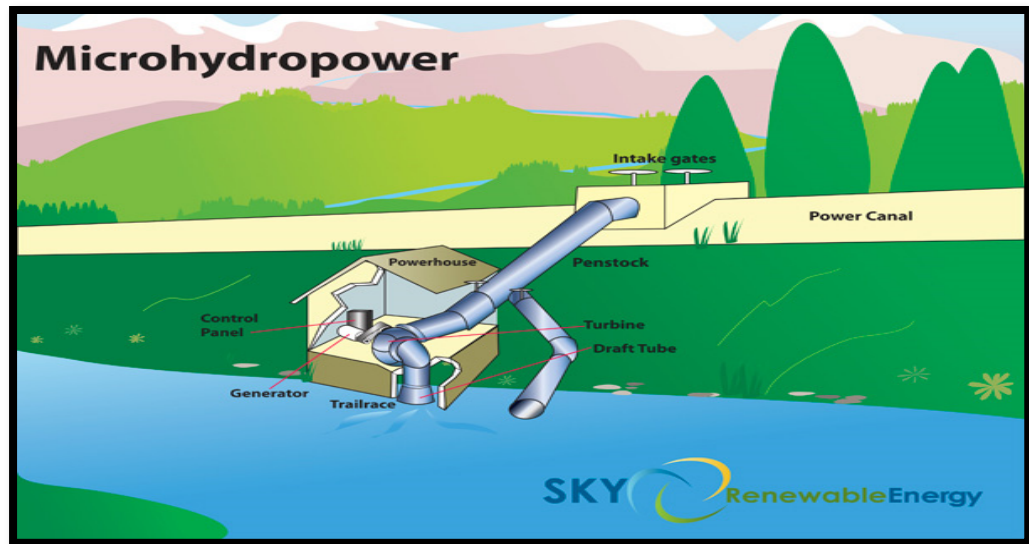


Figure 1.5 Micro-Hydro Power (Energy, 2012).

1.7 Biomass

The term biomass refers to land and water-based vegetation, organic wastes and photosynthetic organisms like wood, grasses, crops, agricultural and municipal wastes. Biomass can be burned to produce heat that is used to create steam to turn turbines to produce electricity. Liquid biofuels can also be derived from biomass crops. Energy from biomass and waste is often referred to as bioenergy. The Figure 1.6 shows the gasification process (IRENA, 2012).

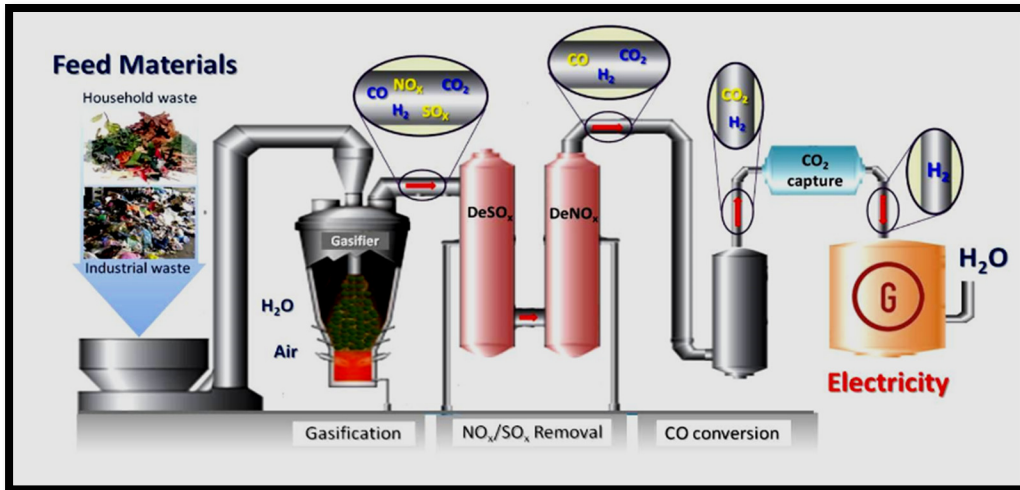


Figure 1.6 Diagram of the biomass gasified system (IRENA, 2012)

1.8 Geothermal Energy

Geothermal energy is the heat produced from the earth's core and then distributed amongst the earth's layers through thermal induction where it is exploited. Thermal energy (see Figure 1.7) produces steam for a turbine that converts it into electricity through a generator ((A.P.E.S), 2012; Setel, Gordan, & Gordan, 2016).

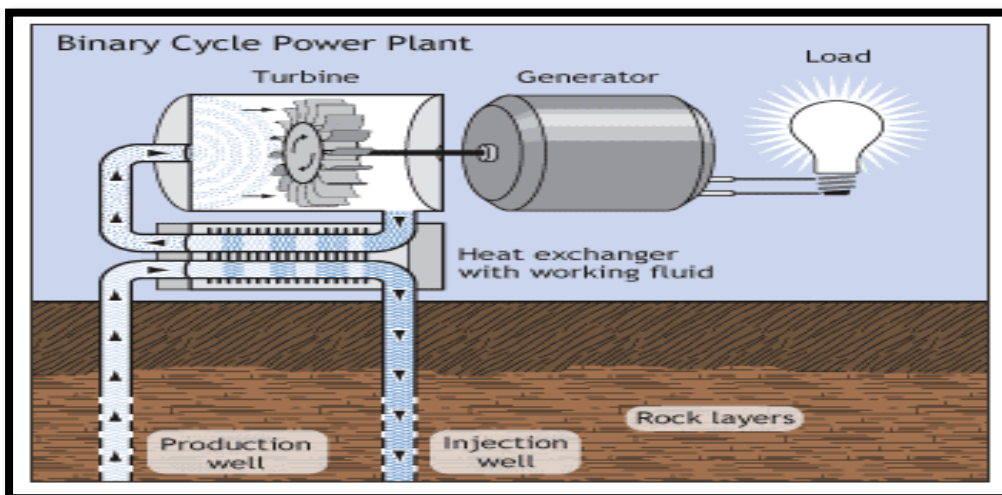


Figure 1.7 Geothermal energy system

1.9 Stirling Engine

Stirling engine (Figure 1.8) is a closed-cycle piston heat engine where the working gas is permanently contained within the cylinder (Hauser & Bamieh, 2015).

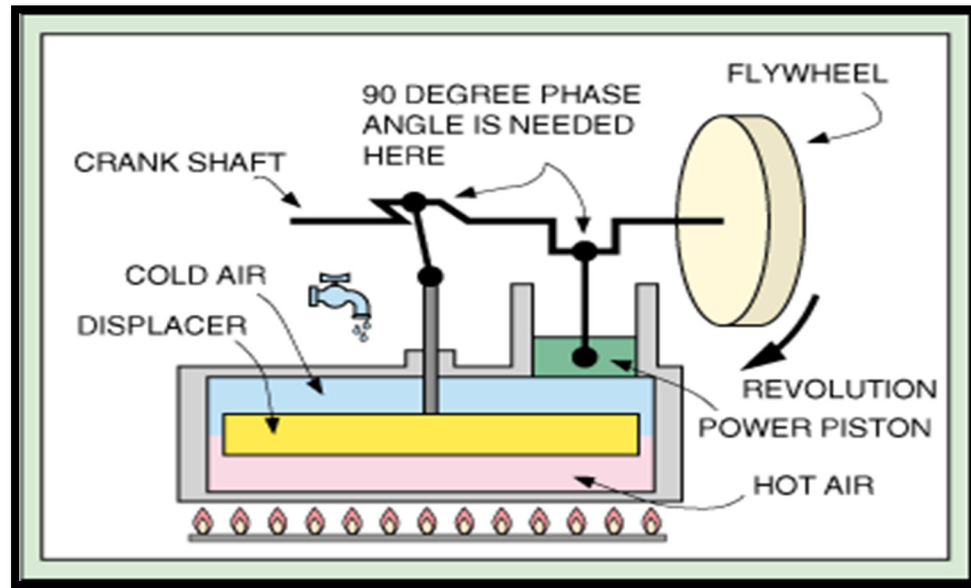


Figure 1.8 Stirling engine (Hauser & Bamieh, 2015)

1.10 Fuel Cells

A fuel cell converts chemical energy of a fuel directly into electrical energy (see Figure 1.9). It consists of two electrodes (an anode and a cathode) and an electrolyte, retained in a matrix (Szasz, 2008). The types of fuel cells under active development are summarized in Figure 1.9.

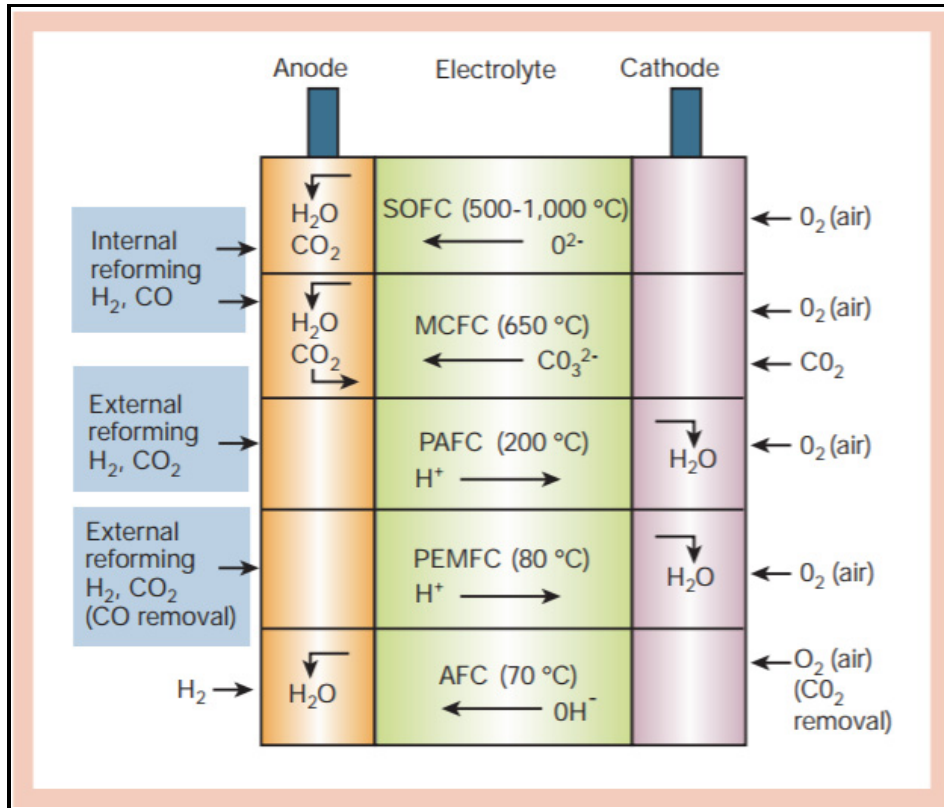


Figure 1.9 Hydrogen Fuel Cell Operation (B. C. Steele & A. Heinzel, 2001)

1.11 Microturbine

Micro-turbines are widely popular as generating units in the distributed generator (DG) systems and as energy producers in CHP systems. At present they hold maximum prospect to be used as micro-sources for Micro-grids (Pavinatto, Peres, Reis, Pereira, & Salles, 2008). Micro-turbines are small and simple-cycle gas turbines. Figure 1.10 shows the diagram of micro turbine and hybrid microturbine.

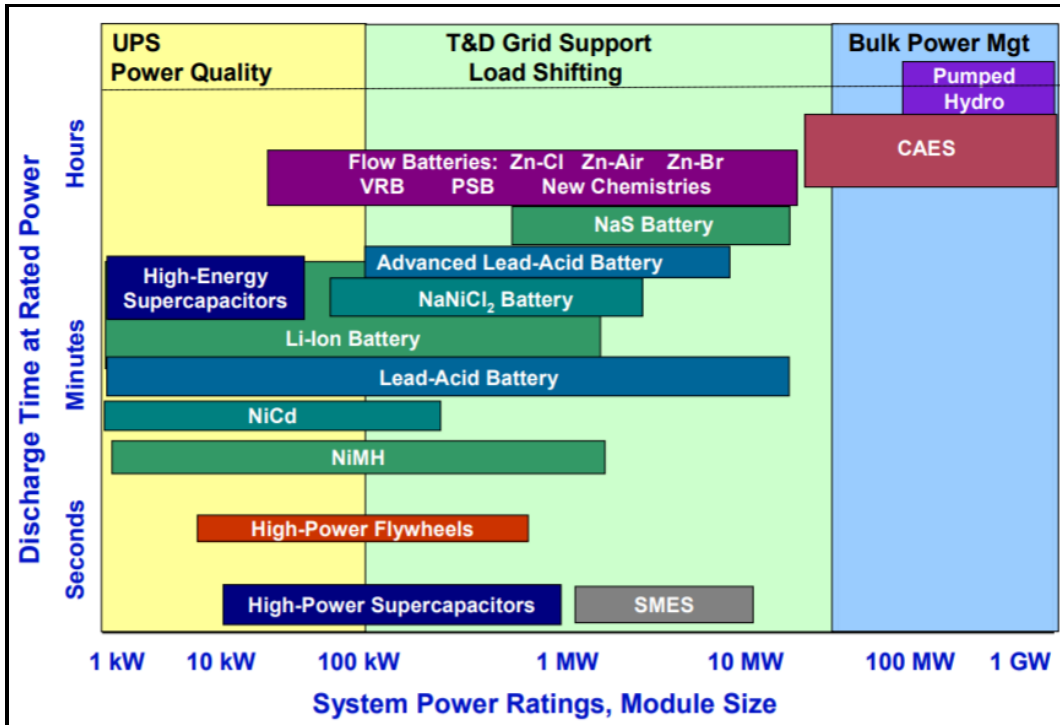


Figure 1.11 Positioning energy storage technology (A. A. Akhil & G. Huff, 2013)

1.12.1 Battery Energy Storage Technology

Battery energy storage system (BESS) contains several primary components, including battery monitoring, control, and power conversion as shown in Figure 1.12 (Agency, 2015b).

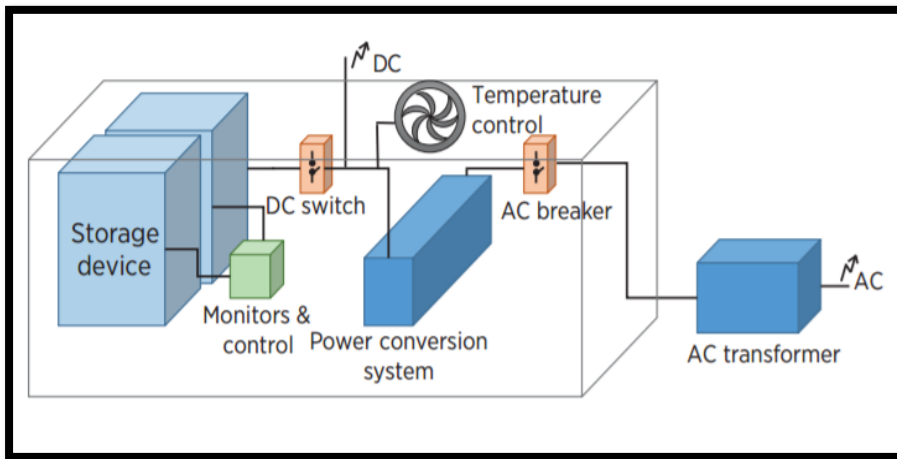


Figure 1.12 Battery energy storage system and primary power component

The different type of BESS technology is summarized in Table 1.1 (K.C. Divya, 2009).

Table 1.1 Characteristics of different type of batteries

| Battery type | Largest capacity (commercial unit) | Location & application | Characteristics |
|-----------------------------|--|--|--|
| Lead acid (flooded type) | 10 MW/40 MWh California-Chino Load Leveling | 10 MW/40 MWh California-Chino Load Leveling | $\eta = 72\text{--}78\%$, life span 1000–2000 cycles at 70% depth of discharge, operating temperature -5 to 40°C , 25 Wh/kg, self-discharge 2–5%/month, frequent maintenance to replace water lost in operation, heavy |
| Lead acid (valve regulated) | 300 kW/580 KWh Turn key system Load Leveling | 300 kW/580 KWh Turn key system Load Leveling | $\eta = 72\text{--}78\%$, life span 200–300 cycles at 80% depth of discharge, operating temperature -5 to 40°C , 30–50 Wh/kg, self-discharge 2–5%/month, less robust, negligible maintenance, more mobile, safe (compared to flooded type) |
| Nickel Cadmium (NiCd) | 27 MW/6.75 MWh ^c GVEA Alaska Control power supply Var compensation | 27 MW/6.75 MWh ^c GVEA Alaska Control power supply Var compensation | $\eta = 72\text{--}78\%$, life span 3000 cycles at 100% depth of discharge, operating temperature -40 to 50°C , 45–80 Wh/kg, self-discharge 5–20%/month, high discharge rate, negligible maintenance, NiCd cells are poisonous and heavy |
| Sodium Sulphur (NaS) | 9.6 MW/64 MWh Tokyo Japan Load Leveling | 9.6 MW/64 MWh Tokyo Japan Load Leveling | $\eta = 89\%$ (at 325°C), life span 2500 cycles at 100% depth of discharge, operating temperature 325°C , 100Wh/kg, no self-discharge, due to high operating temperature it has to be heated in stand-by mode and this reduces its overall η , have pulse power capability of over 6 times their rating for 30 s |
| Lithium ion | 1.5 MW/1.5 MWh Japan Voltage sag Peak load shaving | 1.5 MW/1.5 MWh Japan Voltage sag Peak load shaving | $\eta \approx 100\%$, life span 3000 cycle at 80% depth of discharge, operating temperature -30 to 60°C , 90–190 Wh/kg, self-discharge 1%/month, high cost due to special packaging and internal over charge protection |
| Vanadium redox (VRB) | 1 MW/4 MWh Kyushu EPC | 1 MW/4 MWh Kyushu EPC | $\eta = 85\%$, Life span 10,000 cycles at 75% depth of discharge, operating temperature $0\text{--}40^\circ\text{C}$, 30–50 Wh/kg, negligible self-discharge |
| Zinc Bromine | 15 MW/120 MWh (under development) Innogy's Little Barford station UK | 15 MW/120 MWh (under development) Innogy's Little Barford station UK | $\eta = 75\%$, operating temperature $0\text{--}40^\circ\text{C}$, 70 Wh/kg, negligible self-discharge, low power, bulky, hazardous components |
| Metal air | | | $\eta = 50\%$, Life span few 100 cycles, operating temperature -20 to 50°C , 450–650 Wh/kg, negligible self-discharge, recharging is very difficult and inefficient, compact |
| Regenerative fuel cell | | | $\eta = 75\%$, operating temperature $0\text{--}40^\circ\text{C}$, negligible self-discharge |

1.12.2 Flywheel Energy Storage Technology

A flywheel is a simple form of mechanical (kinetic) energy storage. The Energy is stored by causing a disk or rotor to spin on its axis as shown in Figure 1.13.

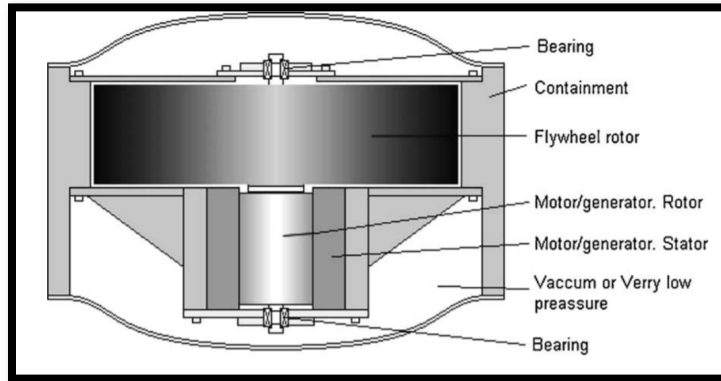


Figure 1.13 Flywheel energy storage technology (B. Bolund & H. Bernhoff, 2007)

The kinetic energy stored in a flywheel is proportional to the mass and to the square of its rotational speed according to Equation (1.1).

$$E_k = \frac{1}{2} I \omega^2 \quad (1.1)$$

where E_k is the kinetic energy stored in the flywheel, I is the moment of inertia and ω is the angular velocity of a rotating disc.

Advances in power electronics, magnetic bearings, and flywheel materials coupled with innovative integration of components have resulted in direct current (DC) flywheel energy storage systems that can be used as a substitute or supplement to batteries in uninterruptible power supply (UPS) systems. Although generally more expensive than batteries in terms of first cost, the longer life, simpler maintenance, and smaller footprint of the flywheel systems makes them attractive (Leijon, 2014).

1.12.3 Ultra-capacitor Energy Storage Technology

An ultra-capacitor or super-capacitor is a high-capacity electrochemical capacitor with capacitance values much higher but with lower voltage limits that bridge the gap between electrolytic capacitors and rechargeable batteries. They typically store 10 to 100 times more energy per unit volume or mass than electrolytic capacitors. They can accept and deliver charge much faster than batteries, and tolerate many more charge and discharge cycles. Super capacitors are being developed as an alternative to pulse batteries. Contrary to the battery, the super-capacitor has much cycle life, high power but low density. The Figure 1.14 shows the family tree of super-capacitors types (Marin S. H, 2006).

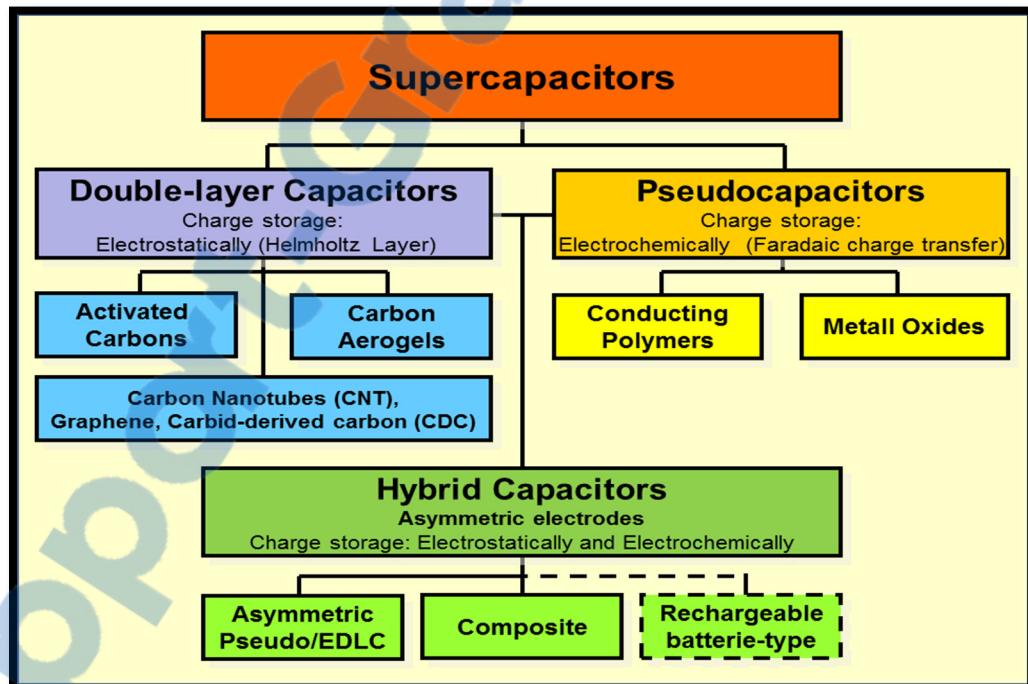


Figure 1.14 the family tree of super capacitors (Marin S.H, 2006)

1.13 Vehicle to microgrid (V2G) and microgrid to vehicle (G2V) interaction

1.13.1 Introduction

Most of current road vehicles have an internal combustion engines (ICE) technology that depends on fossil fuels which are one of the main sources of pollution. There is, in fact, a new vision in the transportation industry toward more efficient and environmentally friendly vehicles. The new transportation electrification vision is more and more designed on the generating of electricity from carbon-free and renewable energy sources. Power electronics and advanced electromechanical energy conversion systems provide the enabling technology (Bedir, Ozpineci, & Christian, 2010a; Freire, Delgado, Santos, & de Almeida, 2010). The different types of electrified vehicles existing in the market are: “more-electric vehicles” (MEVs), hybrid electric vehicles (HEVs), plug-in hybrid electric vehicles (PHEVs), and electric vehicles (EVs)(Kramer, Chakraborty, & Kroposki, 2008; Ota et al., 2012; Yonghua, Xia, & Zongxiang, 2010). Based on researchers’ estimations, advanced electric-drive vehicles will reach an important part of the global new vehicle market. The new generations of electrified vehicles PHEVs and EVs (called also Vehicle to grid (V2G) or grid to vehicle (G2V)) can be integrated with MG systems for charging and discharging.

As part of a connection to a household outlet distribution system of a building standard, the charge is limited to 10 A, which results in a longer charging time, on the order of 10-12 hours. When the connection is made via a dedicated circuit, the charging time will be greatly reduced.

1.13.2 Plug-in Hybrid Electric Vehicle (PHEV)

PHEVs are, in fact, dual-fuel vehicles that consume electricity and another source of energy as gasoline. The energy storage system of PHEVs can be charged onboard or externally from the utility grid through a bidirectional battery charger. In addition, the bidirectional charger allows for V2G, G2V, vehicle-to-building (V2B), and vehicle-to-home (V2H) operating modes with high quality power and can, thus, address the problem of energy storage in a

smart grid. A PHEV can have a series, parallel or series-parallel hybrid power train as shown in Figure 1.15; 1.16 and 1.17 (Emadi, 2011).

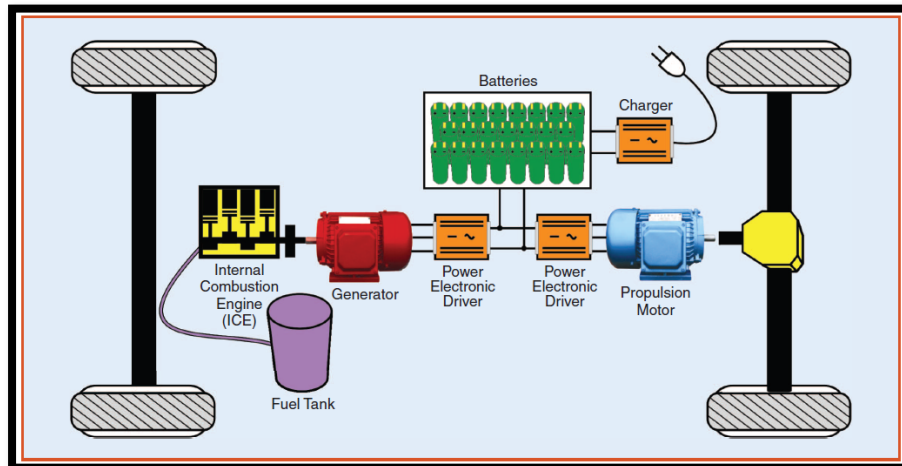


Figure 1.15 PHEV with a series hybrid power train

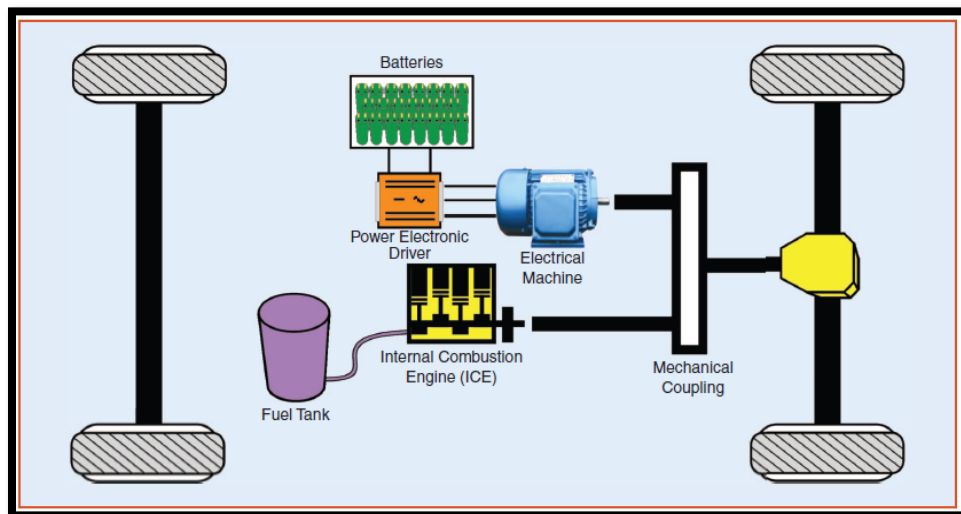


Figure 1.16 PHEV with a parallel hybrid power train



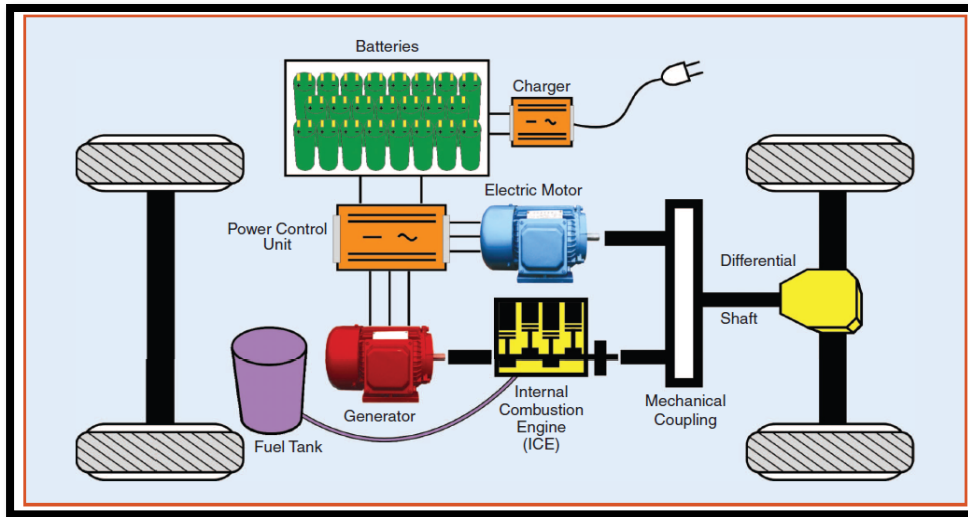


Figure 1.17 PHEV with a series-parallel hybrid power train

1.13.3 Electric Vehicles

Contrary to PHEVs, EVs have 100% electric propulsion systems without any integrated onboard internal combustion engine (ICE) or engine-generator as shown in Figure 1.18. The energy storage system used for EVs could be battery pack or a hybrid system as the combination of battery and ultra-capacitor(Emadi, 2011).

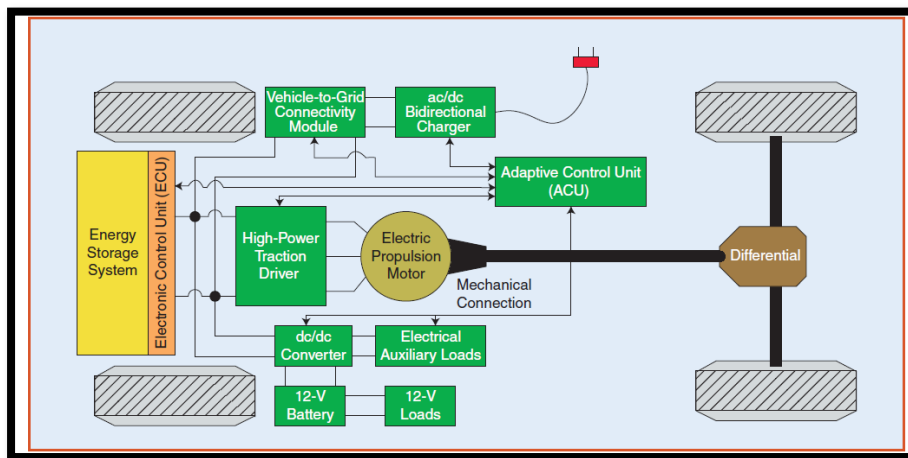


Figure 1.18 100% Electric Vehicle

1.13.4 Battery pack and ultra-capacitor used in PHEV and EV

The lithium-Ion batteries are the most used in electric transportation because of their very high energy and mass power as shown in Figure 1.19 (Thounthong, Chunkag, Sethakul, Davat, & Hinaje, 2009). The batteries are used for energy and long term voltage stability. However, the super capacitor is used for short term and high instantaneous power. It is, therefore, an ideal solution to combine the technology of battery and super capacitor to form a robust EES and to increase their performance as well as their life cycle. In this way, the battery will not suffer significant transient current and its life span will increase.

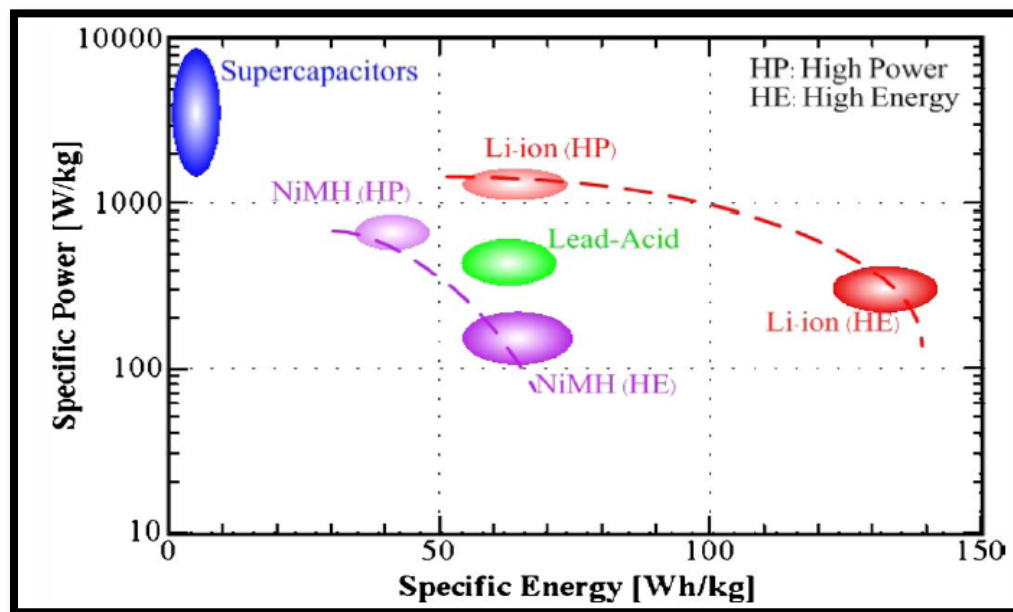


Figure 1.19 Comparison between different batteries technology and super capacitor

1.14 Interface between V2G and G2V

Among the most important points in the subject of the V2G and G2V is the battery charger converter that plays the role of interface between the grid and the electric vehicle in order to ensure the control of power flow, power management and protection. A bad design of battery charger can cause problems of resonance and distortion of the power quality. A dynamic control strategy to prevent overcharging or deep discharge of the battery as well as network

overload during peak hours is a requirement. The manner and time of charging and discharging plays an important role in the PHEV technologies. The Figure 1.20 shows the General bi-directional charger for single and three phase systems (Erb, Onar, & Khaligh, 2010).

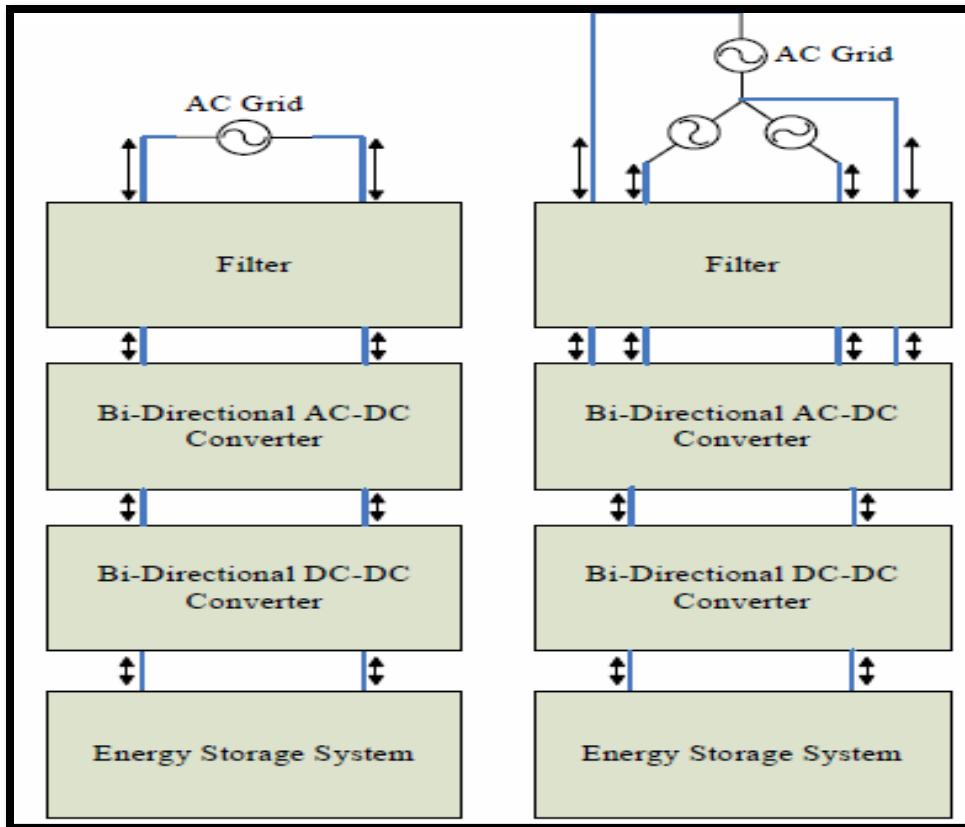


Figure 1.20 General bi-directional charger for single and three phase systems

1.15 Mode of charging and discharging of V2G and G2V

The batteries pack of EV is charged by a continuous power which is often converted from an AC power. The capacity of the batteries pack and the corresponding autonomy vary from one company to another, it is usually in the range of 6 kWh to 35 kWh, assuring with about 150 kilometers of autonomy (Rutherford & Yousefzadeh, 2011). The mode of recharging depends on the daily or weekly habit of the driver.

1.16 Charging time for PHEV and EV

The time required for optimum recharging of the EV (or PHEV) battery is directly related to the amount of injected electrical power (Table 1.2). For the domestic standard outlet, the load will be limited to 10 A, which results in a longer recharge time in the range of 10 to 12 hours. When the connection is made via a dedicated circuit, the charging time is between one hour for three phase, 63 A system and 8 hours for single phase, 16 A systems. In fast DC charging stations, with 500V/125 A dc, the battery pack will be recharged until 80% in just 15 minutes (Yilmaz, 2013).

Table 1.2 Conductive charging system for electric vehicles

| Charging time | Power Supply | Voltage | Current Max |
|---------------|------------------------|---------------|-------------|
| 6-8 hours | Single phase - 3,7 kVA | 230 VAC | 16 A |
| 2-3 hours | Three phase - 11 kVA | 400 VAC | 16 A |
| 3-4 hours | Single phase - 7 kVA | 230 VAC | 32 A |
| 1-2 hours | Three phase - 22 kVA | 400 VAC | 32 A |
| 20–30 minutes | Three phase - 43 kVA | 400 VAC | 63 A |
| 20–30 minutes | DC- 50 kVA | 400 - 500 VDC | 100 - 125 A |

1.17 Microgrid operation and islanding

MG operates in grid-connected and islanded mode. In the grid connected mode, MGs has an active interaction with the utility grid in order to send or receive the power. In the islanded mode, when the MGs is not connected to the utility grid, a special design of ESS is a requirement to ensure an autonomous operation. One of the important features of a MG is the ability to be islanded from the utility grid at the PCC. During utility grid disturbances, MG is disconnected from the grid to operate in autonomous mode and uninterrupted supply of consumer loads. The MG master controller would offer the optimal operation by maintaining the frequency and voltages within permissible ranges. The islanded MG would be

resynchronized with the utility grid once the disturbance problem is resolved (Chaoyong, Xuehao, & Dong, 2010).

Because of the complex characteristics of the MGs such as the bidirectional power flow, presence of different energy sources, power management, power quality problem and considerable presence of power electronics, the control of the MG in each operation mode or the switching between one mode to another are problematic and need an optimal solution in order to increase the efficiency and reliability (Dörfler, Simpson-Porco, & Bullo, 2016), (Bidram & Davoudi, 2012).

There are two common control architectures included in centralized and decentralized approaches:

- Centralized control approach has advantages in standardization procedures and easy implementations and the central controller makes decisions about the dispatch of all DGs and ESSs according to the objective function and constraints (Olivares, Cañizares, & Kazerani, 2011);
- In decentralized control approach, each controller makes decisions locally. This has an advantage to reduce the number of messages and solving the problems locally.

Multi-agent and cooperative approaches are one of the controls used in decentralized MG (Cai, Xu, & Mitra, 2011).

We can also find in literature other kinds of control strategies used in MG as:

- Voltage and frequency control (Reigosa et al., 2009);
- Adaptive control: It is used to control the systems with varying or uncertain parameters because the MG operating modes can unexpectedly change as a result of the disturbances in the utility grid (Mehrizi-Sani & Iravani, 2012); (Bevrani, Habibi, Babahajyani, Watanabe, & Mitani, 2012).

1.17.1 Microgrid Protection

MG necessitates high protection to be able to adapt itself to any undesired conditions as the fault current, reduction in fault current capacity, disruption in fault detection, and protection sensitivity. Considering these problematic issues, many studies have investigated the topic of dc and ac MGs protection. The study in (Nikkhajoei & Lasseter, 2007) explains the integration of protection in the generation in order to detect the over current via the detection of the current magnitude as a fault. In (Ustun, Ozansoy, & Ustun, 2013) an arc model is presented to study series faults in low-voltage DC MGs. In (Jayawarna et al., 2005), the fault current distribution is studied and a grounding electrode system is developed to ensure the MGs safety. In (Ustun, Ozansoy, & Zayegh, 2011), (Etemadi & Iravani, 2013), the relay hierarchy, the overload technique and anti-false-alarm method are presented. Many other protections in dc and ac MGs are largely discussed in (Prasai et al., 2010), (Park & Candelaria, 2013).

1.17.2 Net Zero Energy House based on Microgrid concept

Net Zero Energy House (NZEH) is still a relatively new movement; however efforts are increasing. NZEH is defined as a residential house can generate as much energy on site as they consume. The NZEH (Figure 1.21) goal is being pursued by combining energy efficient technologies and methods, on-site photovoltaic system power generation, and smart energy-management appliances (Bedir, Ozpineci, & Christian, 2010b; Etz, Patarau, Daraban, & Petreus, 2012; Ferraro et al., 2016; Harkouss, Fardoun, & Biwole, 2016; Longo, Roscia, & Zaninelli, 2015; Tidjani & Chandra, 2012).

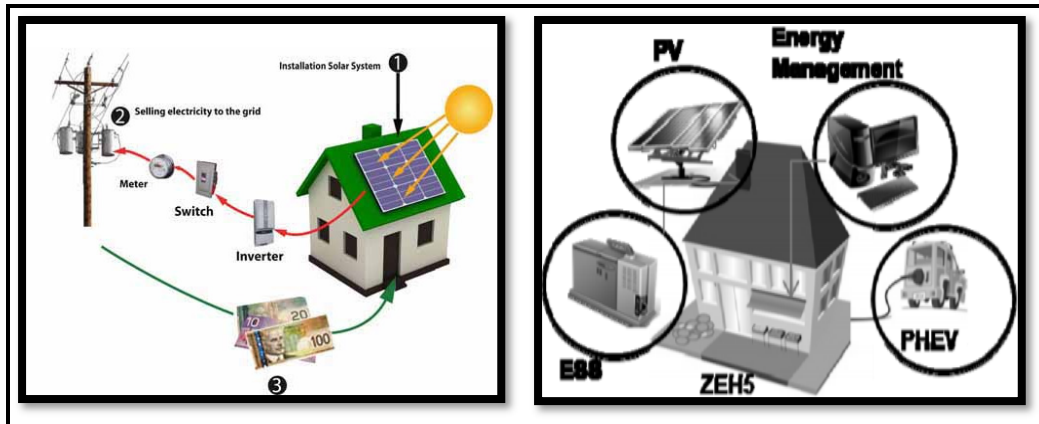


Figure 1.21 Net Zero Energy House

1.18 Review of the main power electronics converters used in MG

Many of DERs are not suitable to be directly connected to the MG network. Hence, power electronic converters are required to interface their integration in order to improve the power quality, frequency and power management.

There are four categories of converters:

- DC/AC: Inverter refers to the converter when the power flows from the DC to the AC side;
- AC/DC: Rectifier refers to a converter when the power flows AC to the DC side converters;
- AC/AC refers to converter that changes an AC wave form to another AC with a different voltage, frequency, phase or shape;
- DC/DC: It is a converter that converts a source of direct current (DC) from one voltage level to another (up or down level).

Before exploring the different type of converters, some basics factors and symbols are very necessary to understand the role and functionalities of converters.

1.18.1 Factors and Symbols used in AC Power System

The input AC voltage can be single-phase or three-phase voltages. They are usually a pure sinusoidal wave function. For a single-phase input voltage $v(t)$, the function can be expressed as (Eddin, 2002).

$$v(t) = \sqrt{2}V\sin\omega t = V_m \sin\omega t \quad (1.2)$$

$$i(t) = \sqrt{2}I\sin(\omega t - \varphi) = I_m \sin(\omega t - \varphi) \quad (1.3)$$

where v is the instantaneous input voltage, V and I are the rms value, V_m and I_m are the maximum values, $\omega = 2\pi f$ is the angular frequency and f is the supply frequency and φ is the phase-delay angle.

1.18.1.1 Power factor for linear load

For a sinusoidal signal, the power factor is given by the ratio of the active power P and the apparent power S . The generators, transformers, transmission lines and measuring devices are sized for the nominal values of voltage and current.

The power factor for this case is:

$$PF = \frac{P}{S} \quad (1.4)$$

Where the S is the apparent power and its power diagram is shown in Figure. 1.22.

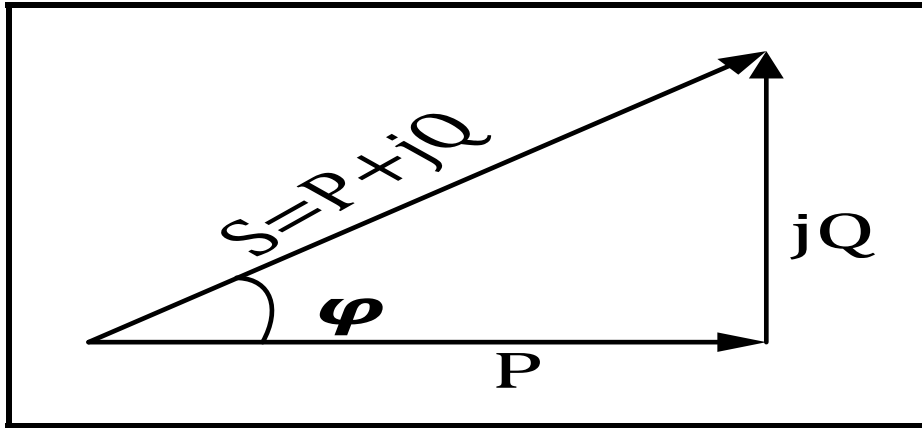


Figure 1.22 Power vector diagram for the linear load

The basic formulas derived from the power vector diagram are:

$$S = VI^* = \frac{V^2}{Z^*} = P + jQ = S \angle \varphi \quad (1.5)$$

The module of S is defined as:

$$S = \sqrt{P^2 + Q^2} \quad (1.6)$$

$$\varphi = \tan^{-1} \frac{Q}{P} \quad (1.7)$$

$$P = S \cos \varphi \quad (1.8)$$

$$Q = S \sin \varphi \quad (1.9)$$

Where P and Q are the active and reactive power, respectively. Z is the impedance (Ω).

1.18.1.2 Power factor for nonlinear load

In case of nonlinear load, the input current is distorted by harmonic contents where its fundamental harmonic can be expressed as:

$$i_1 = \sqrt{2}I_1 \sin(\omega t - \varphi_1) = I_{m1} \sin(\omega t - \varphi_1) \quad (1.10)$$

where i_1 is the fundamental harmonic instantaneous value, I_1 is the rms value, I_{m1} is the amplitude, and φ_1 its phase angle.

The apparent power of the Fresnel diagram of Figure 1.23 for a balanced network is defined as:

$$i_1 = \sqrt{2}I_1 \sin(\omega t - \varphi_1) = I_{m1} \sin(\omega t - \varphi_1) \quad (1.11)$$

$$S = 3V_{rms} * I_{rms} = 3V_{rms} \sqrt{\sum_{h=1}^{\infty} I_{Lh}^2} = \sqrt{P^2 + Q^2 + D^2} \quad (1.12)$$

With h - Rank of the harmonic; I_{Lh} - Value of the harmonic order h

D: Power distortion, V_{rms} , I_{rms} are the rms of the voltage and current respectively.

The active power P resulting from a phase shift between the fundamentals of the current and the voltage, is then:

$$P = 3V_{rms1} * I_{rms1} \cos \varphi_1 \quad (1.13)$$

$$D = 3V_{rms} \sqrt{\sum_{h=2}^{\infty} I_{Lh}^2} \quad (1.14)$$

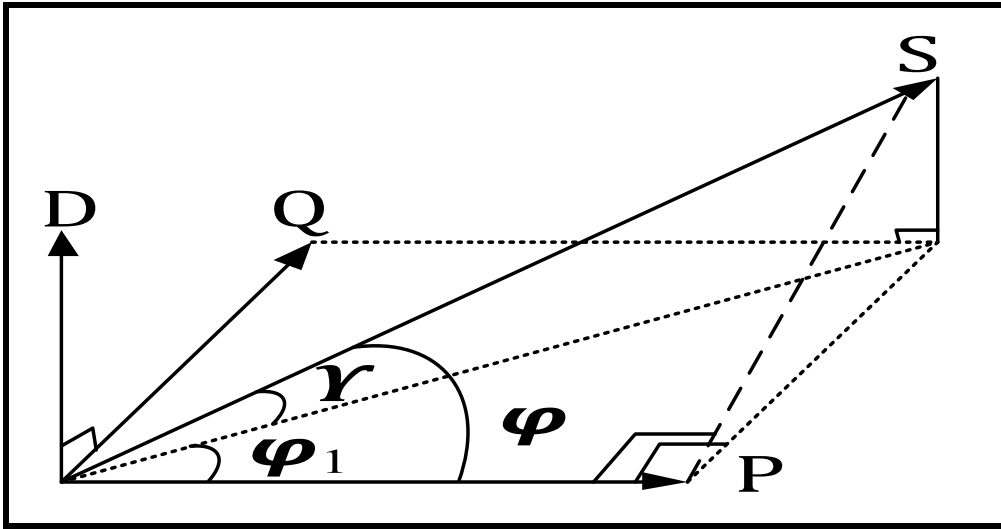


Figure 1.23 Fresnel diagram for Power

The power factor is then:

$$PF = \frac{P}{\sqrt{P^2 + Q^2 + D^2}} = \cos\phi_1 * \cos\gamma \quad (1.15)$$

Hence, it can be seen that the power factor is degraded by the presence of harmonics and the reactive power. The displacement power factor in this case, (DPF) is defined as:

$$DPF = \cos\phi_1 \quad (1.16)$$

The distortion factor is given by:

$$DF = \cos\gamma = \frac{1}{\sqrt{1 + THD^2}} \quad (1.17)$$

where THD is defined as the total harmonic distortion and can be used to measure both voltage and current waveforms. The THD gives an immediate measure of the inverter output voltage waveform distortion. The current THD is defined as:

$$THD_I = \frac{\sqrt{\sum_{h=2}^{\infty} I_h^2}}{I_{rms1}} \quad (1.18)$$

The voltage THD is defined as:

$$THD_V = \frac{\sqrt{\sum_{h=2}^{\infty} V_h^2}}{V_{rms1}} \quad (1.19)$$

where V_h is the amplitude of the n th harmonic order. The power factor could be written also as:

$$PF = DPF * DF \quad (1.20)$$

1.18.2 Factor and symbols used in DC power system

We define the output DC voltage instantaneous value to be v_d and the average value V_d [5]. A pure DC voltage has no ripple; it is then called ripple-free DC voltage. Otherwise, a DC voltage is distorted and consists of a DC component and AC harmonics. Its rms value is V_{drms} . For a distorted DC voltage, V_{drms} is constantly higher than V_d . The ripple factor (RF) is defined as:

$$RF = \frac{\sqrt{\sum_{h=1}^{\infty} V_h^2}}{V_d} \quad (1.21)$$

where V_h is the n th order harmonic.

The form factor (FF) is defined as:

$$FF = \frac{V_{d-rms}}{V_d} = \frac{\sqrt{\sum_{h=0}^{\infty} V_h^2}}{V_d} \quad (1.22)$$

Therefore, we obtain $FF > 1$, and the relation will be

$$RF = \sqrt{FF^2 - 1} \quad (1.23)$$

The form factor FF and ripple factor RF are used to describe the quality of the voltage and current DC waveform parameters. For a pure DC voltage, $FF = 1$ and $RF = 0$.

1.18.3 DC-AC Inverter with two level topologies

DC-AC inverters are generally used in the following applications:

- Variable voltage/variable frequency AC supplies in adjustable speed drive (ASD); devices such as induction motor drives, synchronous machine drives, and so on;
- Constant regulated voltage AC power supplies, such as uninterruptible power supplies (UPSs);
- Static variability (reactive power) compensations;
- Passive/active series and parallel filters;
- Flexible AC transmission systems (FACTSs);
- Voltage compensations.

The generally used DC/AC inverters topologies are:

1. Single-phase half-bridge voltage source inverter (VSC);
2. Single-phase full-bridge VSC;
3. Three-phase full-bridge VSC;
4. Three-phase full-bridge current source inverter (CSI),
5. Impedance source inverter (ZSI).

1.18.4 Single-phase half-bridge voltage source inverter

A single-phase half-bridge voltage source converter (VSC) is shown in Figure 1.24. In order to provide a neutral point N , two capacitors are required where each of capacitors keeps half of the input DC voltage. Since the output voltage is referring to the neutral point N , the maximum output voltage is smaller than half of the DC-link voltage if it is operating in linear modulation. Two switches are used to operate in an exclusive state with small dead time to avoid a short-circuit (Abouelmahjoub et al., 2014).

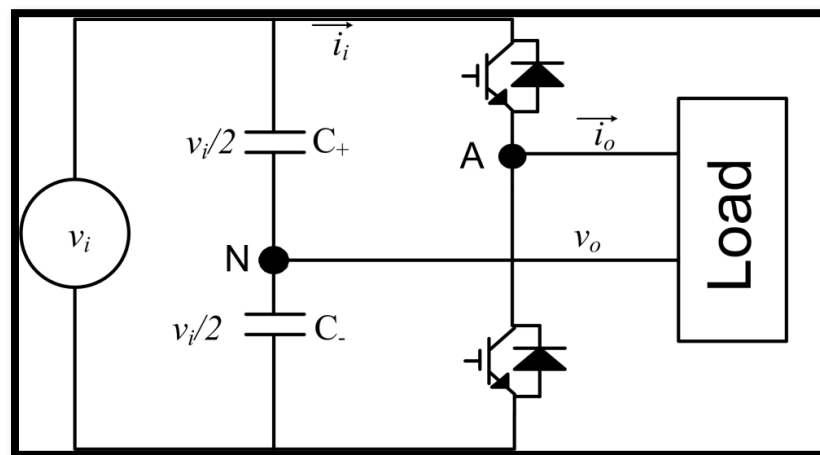


Figure 1.24 Single-phase half-bridge voltage source inverter

1.18.5 Single-Phase Full-Bridge VSC

A single-phase full-bridge voltage source inverter (VSC) is shown in Figure 1.25. Two large capacitors may be used to provide a neutral point N , but are not a requirement. Since the output voltage is not referring to the neutral point N , the maximum output voltage is possibly greater than the half of the DC-link voltage. If it is operating in linear modulation the output voltage is smaller than the DC-link voltage. The modulation operation of multi-leg VSI is different from that of single-leg (single-phase half-bridge). Four switches, S_{1+}/S_{1-} and S_{2+}/S_{2-} , in two legs are applied and switched by the PWM signal or other control (Roy, Xia, & Ayyanar, 2016).

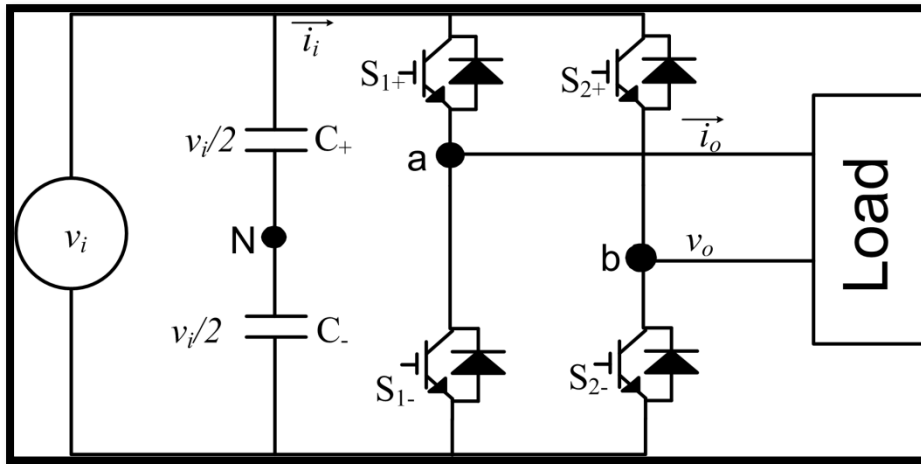


Figure 1.25 Single-phase full-bridge VSC

1.18.6 Three-Phase Full Bridge VSC

A three-phase full-bridge VSC is shown in Figure 1.26. The carrier-based pulse width modulation (PWM) technique is applied in this single-phase full-bridge VSC. Two large capacitors may be used to provide a neutral point N , but are not necessary. Six switches S_1 – S_6 in three legs are applied and switched by the PWM signal (Sunan, Kucuk, Goto, Guo, & Ichinokura, 2014).

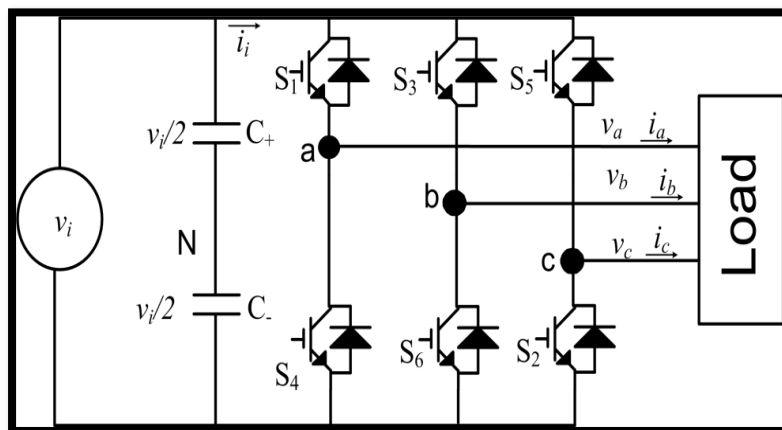


Figure 1.26 Three-phase full-bridge VSC

1.18.7 Three-Phase Full-bridge current source inverter

The current source inverter (CSI) consists of a current switch with a DC side inductor and a capacitive grid-side filter (Sharma, Saini, Garg, & Negi, 2016). The CSI (Figure 1.27) is not widely applied in industrial applications; because it has many disadvantages among them:

- Less efficiency compared to voltage source inverter;
- For its protection, the main switches of the I-source converter have to block reverse voltage that requires a series diode to be used in combination with high-speed and high-performance transistors such as IGBTs. This addition of extra component increases the cost;
- The CSI cannot be used with conventional multi-level topologies.

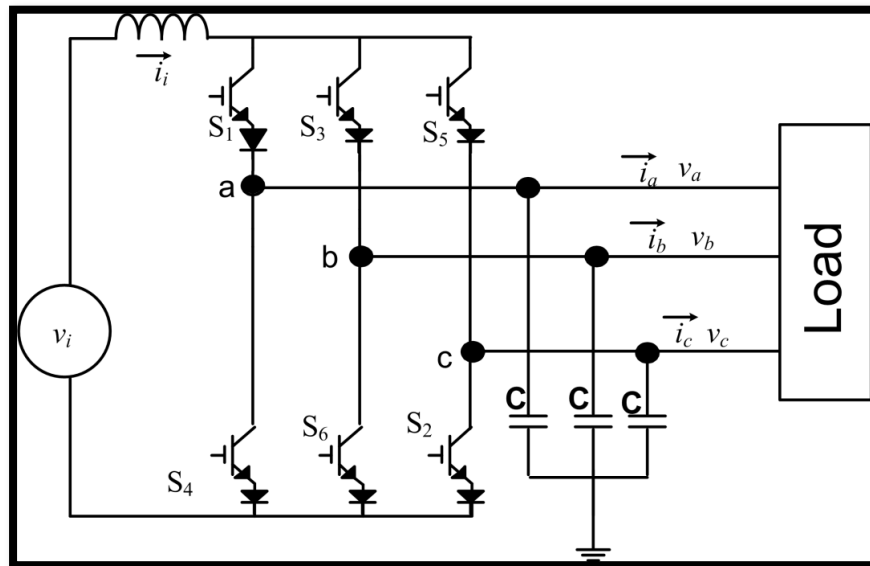


Figure 1.27 Three phase CSI

1.18.8 Impedance source inverter

The ZSI consists of an x-shaped impedance network formed by two capacitors and two inductors, and it provides unique buck–boost characteristics (Figure 1.28). The ZSI is considered as a new inverter different from traditional VSC and CSI. Due to these attractive

features, it has found numerous industrial applications. On the other hand, the presence of the x-shaped impedance network and the need for short-circuiting the inverter arm to boost the voltage would complicate the controlling of ZSI (Mahale & Patil, 2016). The ZSI presents many advantages as:

- The need for dead time would not arise with this topology;
- The source can be either a voltage source or a current source. The DC source of a ZSI can either be a battery, a diode rectifier or a thyristor converter, a fuel cell stack or a combination of these;
- The main circuit of a ZSI can either be the traditional VSC or the traditional CSI;
- Works as a buck-boost inverter.

The load of a ZSI can either be inductive or capacitive or another Z-Source network (Mahale & Patil, 2016).

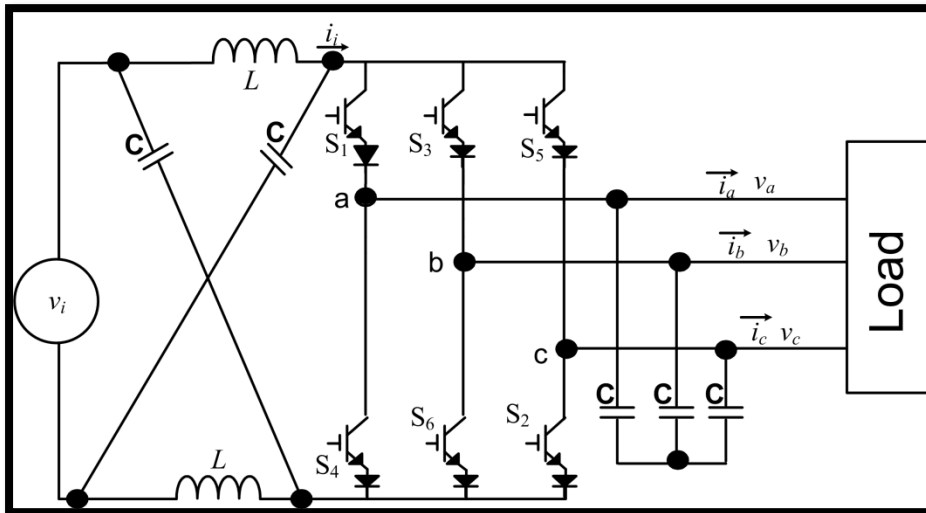


Figure 1.28 Impedance Source Inverter

1.19 Multilevel power converter structures

Nowadays, more industrial applications have begun to require higher power apparatus in recent years. Some medium voltage motor drives and utility applications require medium voltage and megawatt power level. As a result, a multilevel power converter structure has been introduced as an alternative in high power and medium voltage situations (Gupta & Jain, 2014; Gupta, Ranjan, Bhatnagar, Sahu, & Jain, 2016). A multilevel converter has several advantages over a conventional two-level converter that uses high switching frequency pulse width modulation (PWM). Various kinds of multilevel inverters have been proposed, tested, and installed like:

- Multilevel inverters using diode/capacitor clamped topologies;
- Multilevel inverters using H-bridges topologies;
- Capacitor-clamped (flying capacitors) multilevel inverters;
- Multilevel inverters using ladder;
- Other kinds of multilevel inverters.

The family tree of multilevel level inverters is shown in Figure 1.29.

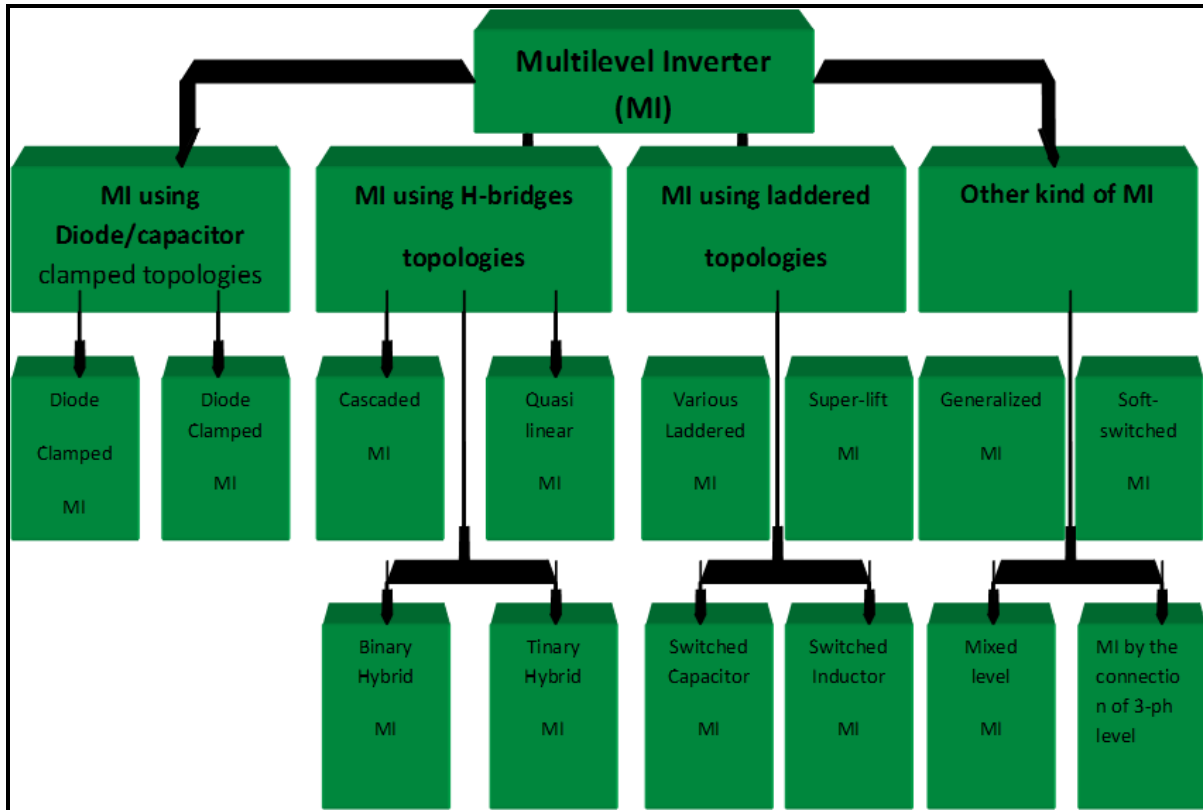


Figure 1.29 Family tree of multilevel level inverters

1.19.1 Diode-Clamped and Capacitor-Clamped Multilevel Inverters

The Figures 1.30 and 1.31 show the configuration of three and five level of Diode-Clamped multilevel inverter respectively. In this category, the switching devices are connected in series to make up the desired voltage rating and output levels. The inner voltage points are clamped by either two extra diodes or one high-frequency capacitor. The switching devices of an m -level inverter are required to block a voltage level of $V_{dc}/(m-1)$. The clamping diode needs different voltage ratings for different inner voltage levels. In summary, an m -level diode clamped inverter has:

- Number of power electronic switches = $2(m - 1)$;
- Number of DC-link capacitors = $(m - 1)$;
- Number of clamped diodes = $2(m - 2)$;
- Voltage across each DC-link capacitor = $\frac{V_{dc}}{m-1}$.

where V_{dc} is the DC-link voltage. A three-level diode-clamped inverter (Figure 1.30) with $V_{dc} = 2E$. In this circuit, the DC-bus voltage is split into three levels by two series-connected bulk capacitors, C_1 and C_2 . The middle point of the two capacitors, n , can be defined as the neutral point. The output voltage v_{an} has three states: E , 0 , and $-E$. For voltage level E , switches S_1 and S_2 need to be turned on; for $-E$, switches S_1' and S_2' need to be turned on; and for the 0 level, S_2 and S_2' need to be turned on. The key components that distinguish this circuit from a conventional two level inverter are D_1 and D_1' . These two diodes clamp the switch voltage to half the level of the DC-bus voltage. When both S_1 and S_2 turn on, the voltage across a and 0 is $2E$, that is, $v_{a0} = 2E$. In this case, D_1' balances out the voltage sharing between S_1' and S_2' with S_1' blocking the voltage across C_1 and S_2' blocking the voltage across C_2 . Notice that output voltage v_{an} is AC, and v_{a0} is DC. The difference between v_{an} and v_{a0} is the voltage across C_2 , which is E . If the output is removed between a and 0 , then the circuit becomes a DC/DC converter that has three output voltage levels: E , 0 , and $-E$.

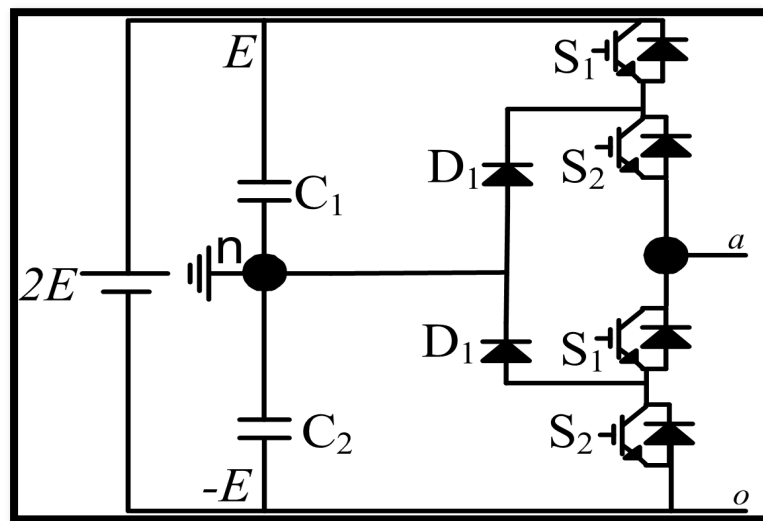


Figure 1.30 Three-level diode-clamped multilevel inverter

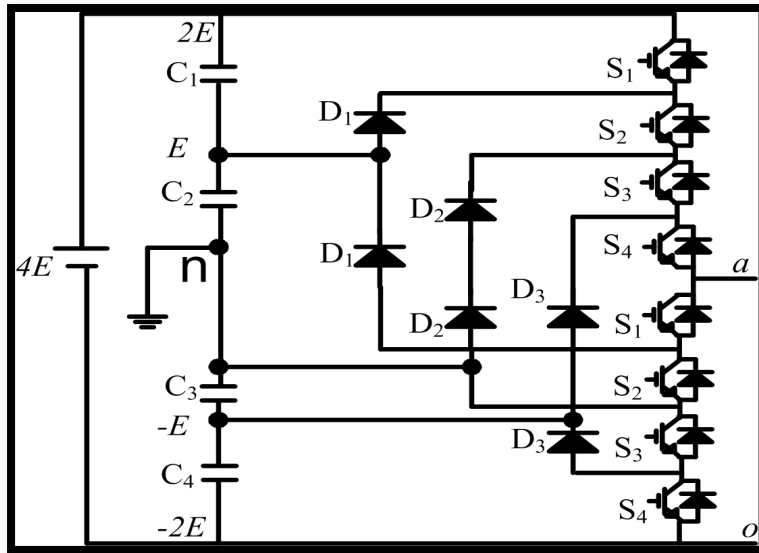


Figure 1.31 Five level diode-clamped multilevel inverter

The structure of flying capacitors inverter is similar to the diode-clamped inverter topology but instead of using clamping diodes, it uses capacitors (Gawande et al., 2016; Karugaba, Muetze, & Ojo, 2012).

1.19.2 Multilevel Inverters using H-Bridges topologies

The different multilevel topologies using HBs are 1) Cascaded Multilevel inverters; 2) Quasilinear multilevel inverters; 3) Binary hybrid multilevel inverters (BHMI); 4) Trinary hybrid multilevel inverters (THMI). The basic structure is based on the connection of H-bridges (HBs). Figure 1.32 shows the power circuit for one phase leg of a multilevel inverter with three HBs (HB1, HB2, and HB3) in each phase. Each HB is supplied by a separate DC source. The resulting phase voltage is synthesized by the addition of the voltages generated by the different HBs. If the DC link voltages of HBs are identical, the multilevel inverter is called the cascaded multilevel inverter (Vigneshkumar & Prabakaran, 2016).

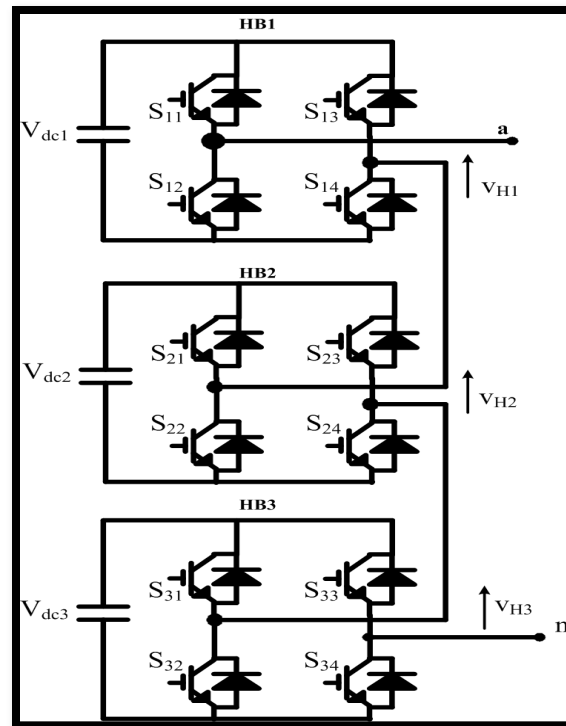
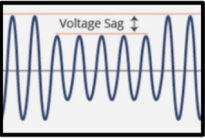


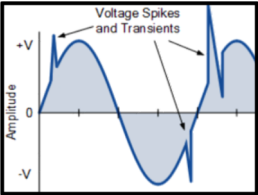
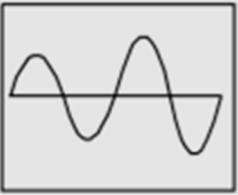


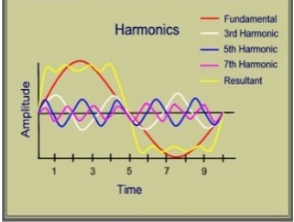
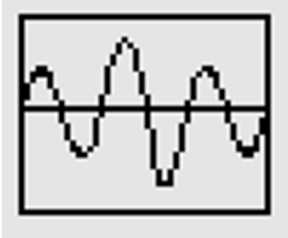
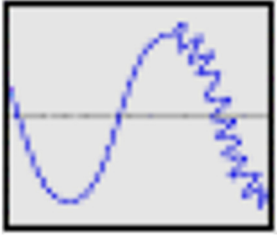
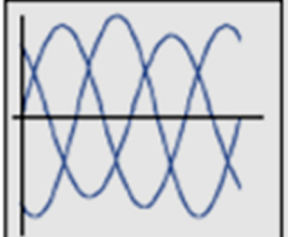
Figure 1.32 Multilevel inverter based on the connection of HBs.

1.20 Power quality problems in Microgrids

Many electrical types of equipment are designed to operate within a predefined range of voltage and frequency and any deviation from that band may lead to deterioration in the performance of this equipment. Power quality disturbances arise when certain deviations in magnitude and frequency beyond the specified range take place, creating problems to customer equipment (Parhizi, Lotfi, Khodaei, & Bahramirad, 2015). The most common types of Power Quality disturbances are presented in Table 1.3 (A. de Almeida, 2003).

Table 1.3 Different type of Power Quality disturbances

| | |
|---|---|
| <p>1. Voltage sag (or dip)</p>  | <p>Description: A decrease of the normal voltage level between 10 and 90% of the nominal rms voltage at the power frequency, for durations of 0,5 cycle to minute.</p> <p>Causes: Faults on the transmission or distribution network (most of the times on parallel feeders). Faults in consumer's installation. Connection of heavy loads and start-up of large motors. Consequences: Malfunction of information technology equipment, namely microprocessor-based control systems (PCs, PLCs, ASDs) that may lead to a process stoppage. Tripping of contactors and electromechanical relays. Disconnection and loss of efficiency in electric machines.</p> |
| <p>2. Very short Interruptions</p>  | <p>Description: Total interruption of electrical supply for duration from few milliseconds to one or two seconds. Causes: Mainly due to the opening and automatic reclosure of protection devices to decommission a faulty section of the network. The main fault causes are insulation failure, lightning and insulator flashover. Consequences: Tripping of protection devices, loss of information and malfunction of data processing equipment. Stoppage of sensitive equipment, such as ASDs, PCs, PLCs, if they're not prepared to deal with this situation.</p> |
| <p>3. Long interruptions</p>  | <p>Description: Total interruption of electrical supply for duration greater than 1 to 2 seconds. Causes: Equipment failure in the power system network, storms and objects (trees, cars, etc) striking lines or poles, fire, human error, bad coordination or failure of protection devices. Consequences: Stoppage of all equipment.</p> |
| <p>4. Voltage spike</p>  | <p>Causes: Lightning, switching of lines or power factor correction capacitors, disconnection of heavy loads.</p> <p>Consequences: Destruction of components (particularly electronic components) and of insulation materials, data processing errors or data loss, electromagnetic interference.</p> |
| <p>5. Voltage swell</p>  | <p>Description: Momentary increase of the voltage, at the power frequency, outside the normal tolerances, with duration of more than one cycle and typically less than a few seconds.</p> <p>Causes: Start/stop of heavy loads, badly dimensioned power sources, badly regulated transformers (mainly during off-peak hours).</p> <p>Consequences: Data loss, flickering of lighting and screens, stoppage or damage of sensitive equipment, if the voltage values are too high.</p> |
| <p>6. Harmonic distortion</p> | <p>Description: Voltage or current waveforms assume non-sinusoidal shape. The waveform corresponds to the sum of different sine-waves with different magnitude and phase, having frequencies that are multiples of power-system frequency. Causes:</p> |

| | |
|--|--|
|  | <p>Classic sources: electric machines working above the knee of the magnetization curve (magnetic saturation), arc furnaces, welding machines, rectifiers, and DC brush motors. Modern sources: all non-linear loads, such as power electronics equipment including ASDs, switched mode power supplies, data processing equipment, high efficiency lighting.</p> <p>Consequences: Increased probability in occurrence of resonance, neutral overload in 3-phase systems, overheating of all cables and equipment, loss of efficiency in electric machines, electromagnetic interference with communication systems, errors in measures when using average reading meters, nuisance tripping of thermal protections.</p> |
| <p>7. Voltage fluctuation</p>  | <p>Description: Oscillation of voltage value, amplitude modulated by a signal with frequency of 0 to 30 Hz. Causes: Arc furnaces, frequent start/stop of electric motors (for instance elevators), oscillating loads.</p> <p>Consequences: Most consequences are common to under voltages. The most perceptible consequence is the flickering of lighting and screens, giving the impression of unsteadiness of visual perception.</p> |
| <p>8. Noise</p>  | <p>Description: Superimposing of high frequency signals on the waveform of the power-system frequency.</p> <p>Causes: Electromagnetic interferences provoked by Hertzian waves such as microwaves, television diffusion, and radiation due to welding machines, arc furnaces, and electronic equipment. Improper grounding may also be a cause.</p> <p>Consequences: Disturbances on sensitive electronic equipment, usually not destructive. May cause data loss and data processing errors</p> |
| <p>9. Voltage Unbalance</p>  | <p>Description: A voltage variation in a three-phase system in which the three voltage magnitudes or the phase angle differences between them are not equal. Causes: Large single-phase loads (induction furnaces, traction loads), incorrect distribution of all single-phase loads by the three phases of the system (this may be also due to a fault).</p> <p>Consequences: Unbalanced systems imply the existence of a negative sequence that is harmful to all three phase loads. The most affected loads are three-phase induction machines.</p> |

1.21 Power quality solution for micro-grids

The most common interface devices used to solve PQ problems are: 1) Dynamic Voltage Restorer (DVR), 2) Transient Voltage Surge suppressors (TVSS), 3) Constant Voltage Transformers, 4) Noise Filters, 5) Static VAR Compensators, 7) Harmonic Filters, 8) Energy

storage system. In addition, some measures have been taken to regulate the minimum PQ level that utilities have to provide to consumers and the immunity level that equipment should have to operate properly when the power supplied is within the standards. One major step in this direction was taken with the ITIC-CBEMA curve (Horak, 2006) (Figure 1.33).

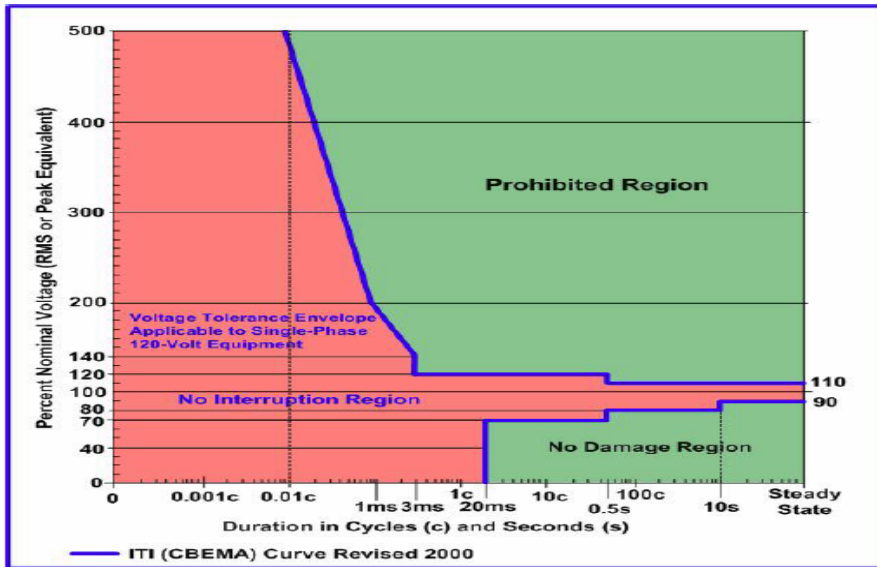


Figure 1.33 ITIC and CBEMA power quality standard curve

1.21.1 Dynamic Voltage Restorer

A dynamic voltage restorer (DVR) acts like a voltage source connected in series with the load where the output voltage is kept approximately constant at the load terminals by injecting active and reactive power in the output supply using transformer and/or ESS via voltage source converter (Awaar, Jugge, & Tara Kalyani, 2016) (see Figure 1.34).

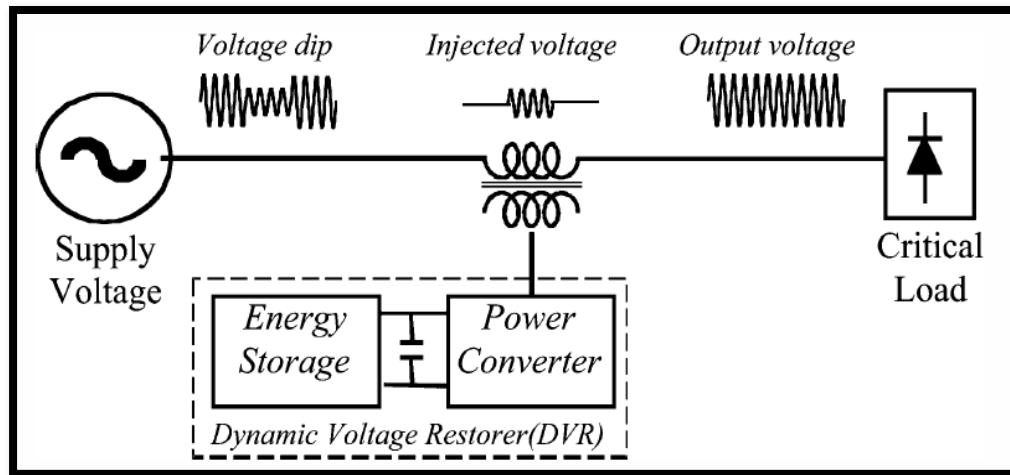


Figure 1.34 Dynamic Voltage restorer operation

1.21.2 Transient Voltage Surge Suppressors

Transient voltage surge suppressors (TVSS) are used as interface between the power source and sensitive loads, so that the transient voltage is clamped by the TVSS before it reaches the load. TVSSs usually contain a component with a nonlinear resistance (a metal oxide varistor or a zener diode) that limits excessive line voltage and conduct any excess impulse energy to ground (Bustamante et al., 2006).

1.21.3 Static VAR compensators

Static VAR compensators (SVR) use a combination of capacitors and reactors to regulate the voltage quickly. The switches control the insertion of the capacitors and reactors at the right magnitude to prevent the voltage from fluctuating. The main application of SVR is the voltage regulation in high voltage and the elimination of flicker caused by large loads (such as induction furnaces) (Mukhopadhyay, Maiti, Banerji, S. K., & Deb, 2017).

1.21.4 Passive harmonic filter

The passive filter (PF) is the first device used for harmonic compensation. It consists of only passive component (inductor, capacitor, resistor) and do not provide amplification. There are four kind of PF:

- Band reject filter that rejects or stop frequencies in a narrow range but passes others;
- Low-pass filter that passes frequencies below a critical frequency, and attenuates those above;
- High-pass filter that passes frequencies above the critical frequency but reject those below;
- Band pass filter that passes only frequencies in a narrow range between upper and lower cutoff frequencies.

The most common choice for the high power thyristor rectifier is to use a combination of several filters tuned to the 5th and 7th harmonics as shown in Figure 1.35 (Akagi, 2005; Fujita, Yamasaki, & Akagi, 2000; Rivas, Moran, Dixon, & Espinoza, 2003).

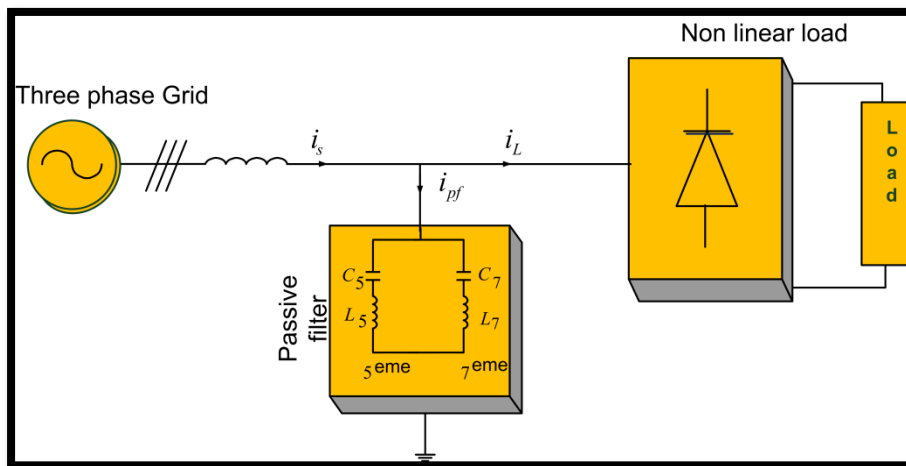


Figure 1.35 Passive harmonic filter

1.21.5 Power quality with active filtering devices

Unlike traditional passive filters, active filters devices have multiple functions as harmonic filtering, damping, reactive-power compensation for power factor improvement and voltage regulation, load balancing and voltage-flicker reduction etc.... The different family of active filtering devices as Active filter (AF), Hybrid Active Filter, Unified power quality conditioner (UPQC) and Series Active Filter have lots of advantages to solve the power quality problems in medium voltage (Akagi, 2005). Generally the VSC is most preferred than CSI, because of its better efficiency, lower cost and lower volume. In addition, the IGBT modules currently available on the market are well adapted to VSC. There are different types of active filtering configurations.

1.21.6 Active filter type of VSC configuration with three phase

The Figure 1.36 shows the diagram of the active filter (AF) type of VSC that is also able to improve the compensation performance with low switching (Akagi et al., 2003).

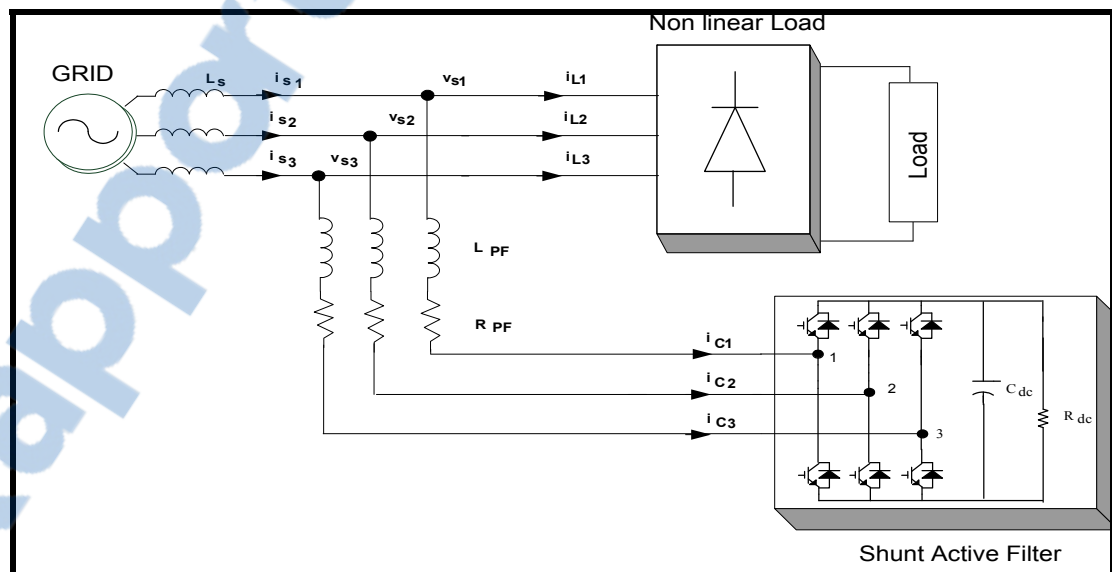


Figure 1.36 Three-phase system with active shunt filter

1.21.7 Three-Phase four wire active filter VSC with midpoint capacitor

A numerous of single-phase loads can be supplied from a three-phase system with the neutral. They can cause excessive harmonic current in the neutral, an overload of reactive power and an imbalance. To reduce these problems, some solutions have been proposed in the literature (Ferreira, Monteiro, Afonso, & Couto, 2008; Kedjar & Al-Haddad, 2008; Missanda, Al-Haddad, & Mendalek, 2016). Figure 1.37 illustrates the diagram of a three phase four wire active filter VSC with a midpoint capacitor. This topology is used for limited powers because the neutral current flows through the capacitors (Aredes, Hafner, & Heumann, 1997; Escobar, Valdez, Torres-Olguin, & Martinez-Montejano, 2007; Grino, Cardoner, Costa-Castello, & Fossas, 2007; Pal, Swarup, & Singh, 2008; R. Zhang, Prasad, Boroyevich, & Lee, 2002).

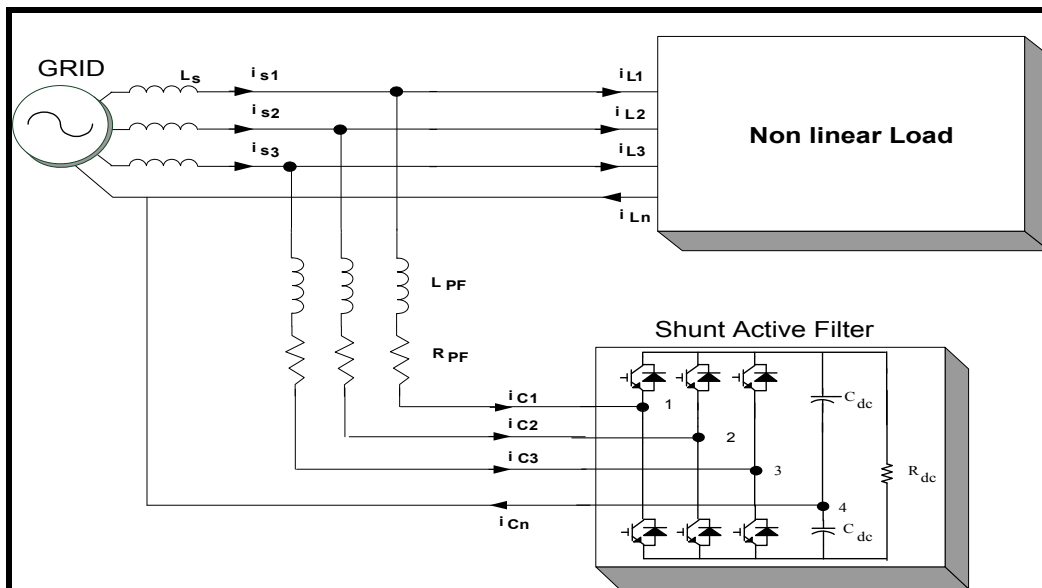


Figure 1.37 Three Phase Four Wire Active VSC with midpoint capacitor

1.21.8 Three phase four leg of the active filter VSC

The Figure 1.38 shows the configuration of three phase four leg active filter VSC where the four leg (used instead of midpoint capacitor of preview Figure 1.38) is controllable and could

help stabilizing more the neutral current (Hirve, Chatterjee, Fernandes, Imayavaramban, & Dwari, 2007).

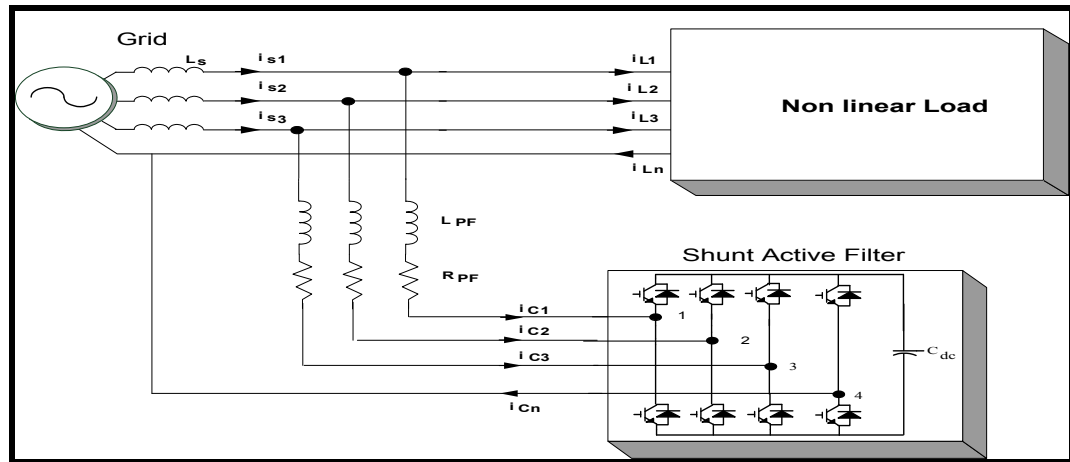


Figure 1.38 Three phase four leg active filter VSC

1.21.9 Hybrid Shunt filter without transformer

The topology of the hybrid shunt filter without integrated transformer (Figure 1.39) is composed of a passive filter tuned to the 7th harmonic, and an active filter with reduced size type of VSC. The active filter compensates the current harmonics and the passive filter acts as low impedance at the tuning frequency and as high impedance at the fundamental frequency. This system has two advantages: 1) the power sizing of the active filter is even more reduced because the current flowing through it is lower and 2) the active filter is protected from a possible short circuit of the load (Tangtheerajaronwong, Hatada, Wada, & Akagi, 2007).



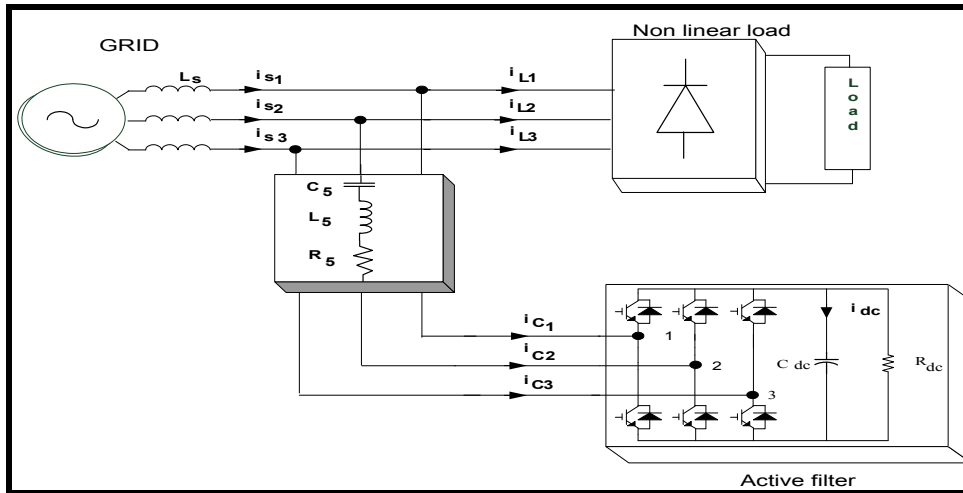


Figure 1.39 Hybrid Shunt filter without transformer

1.21.10 Hybrid active filter with two legs without transformer

This topology (Figure 1.40) composed of a single-phase inverter and a three-phase passive filter, tuned to the fifth harmonic. These both filters are directly connected in series each other without any intermediary transformer and then connected in parallel at the PCC. The passive filter acts as low impedance at the tuning frequency and as high impedance at the fundamental frequency. This passive filter absorbs the 5th harmonic currents generated by the load and the active filter improves the efficiency of the passive filter (Bor-Ren, Yuan-An, & Tsung-Yu, 2004).

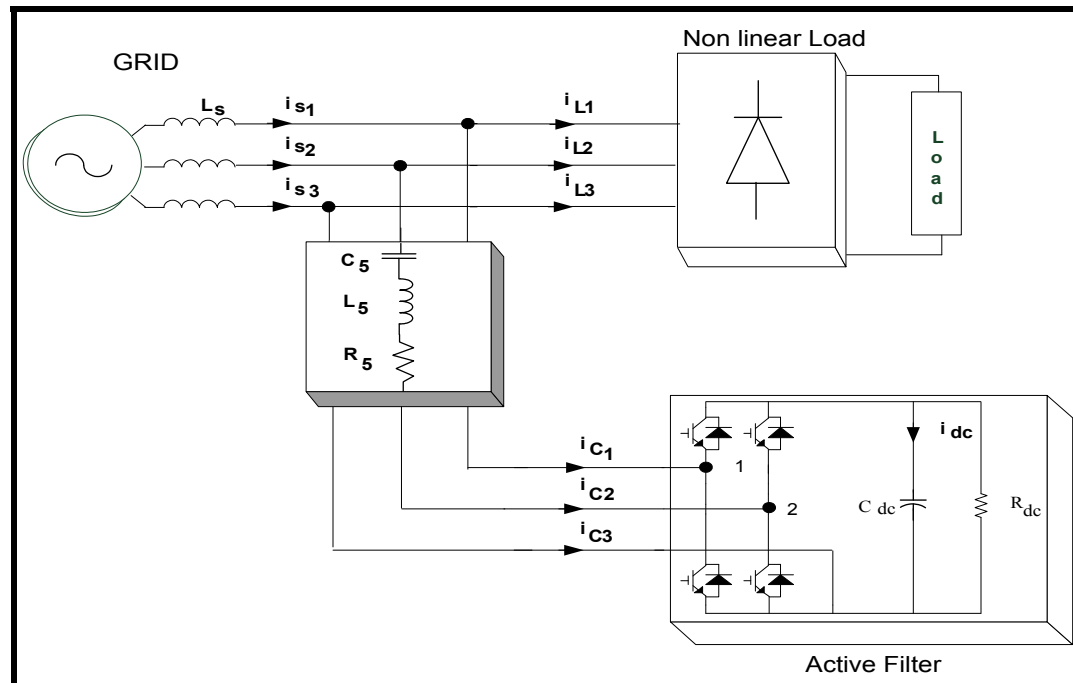


Figure 1.40 Hybrid active filter with two legs and without transformer

1.21.11 Series Active Filter

The series active filter (SAF) allows cancelling voltage harmonics, unbalancing and regulating the voltage at the PCC. This configuration allows also avoiding any risk of resonance between the elements of the passive filter and the impedance of the grid (Figure 1.41), (Benchaita, Saadate, & Salem nia, 1999; Pal et al., 2008; Sawant & Chandorkar, 2009; Srianthumrong, Fujita, & Akagi, 2002; Zhaoan, Qun, Weizheng, & Jinjun, 2001).

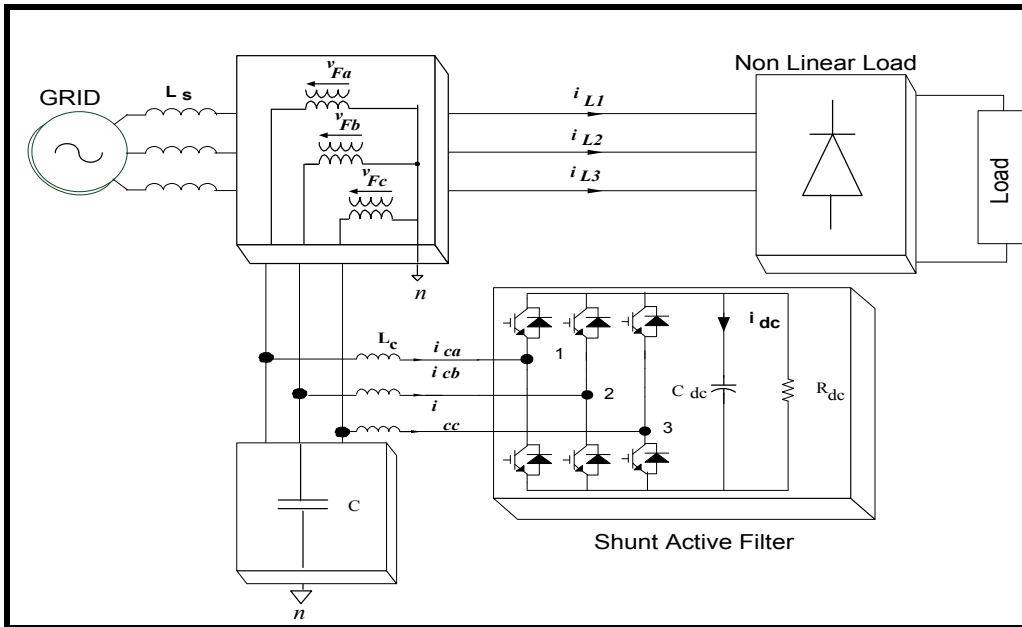


Figure 1.41 Three phase system with series active filter

1.21.12 Hybrid filter series

This configuration (Figure 1.42) reduces the risk of resonances between the elements of the passive filters and the impedance of the grid. In this case, the serial active filter acts as a resistance to the frequency of the harmonics with respect to the harmonic currents and forces them to circulate in the passive filter without cutting the fundamental frequency. This configuration is a very popular because the used semiconductors in the active filter design can be reduced in volume and in price (5% of the load). The passive filter is used to eliminate current harmonics of order 5, 7 and greater than 11 (Hamadi, Al-Haddad, & Rahmani, 2006).

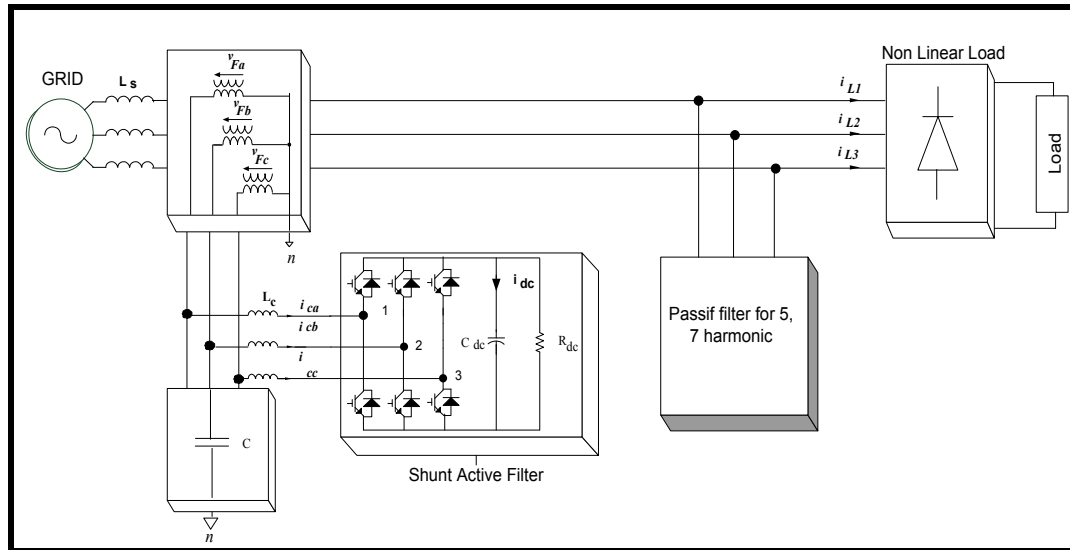


Figure 1.42 Association d'un filtre actif série et d'un filtre passif

1.21.13 Unified power quality conditioner (UPQC)

Figure 1.43 shows the schematic of the universal active filter known under the name of Unified Power Quality Conditioner (UPQC). A UPQC consists of combination of series and shunt converters for simultaneous compensation of voltage and current imperfections at the PCC. It is also able to compensate the voltage and current unbalance. However, the UPQC cost is high and its control is complex because of using many semiconductors (Khadkikar & Chandra, 2008).

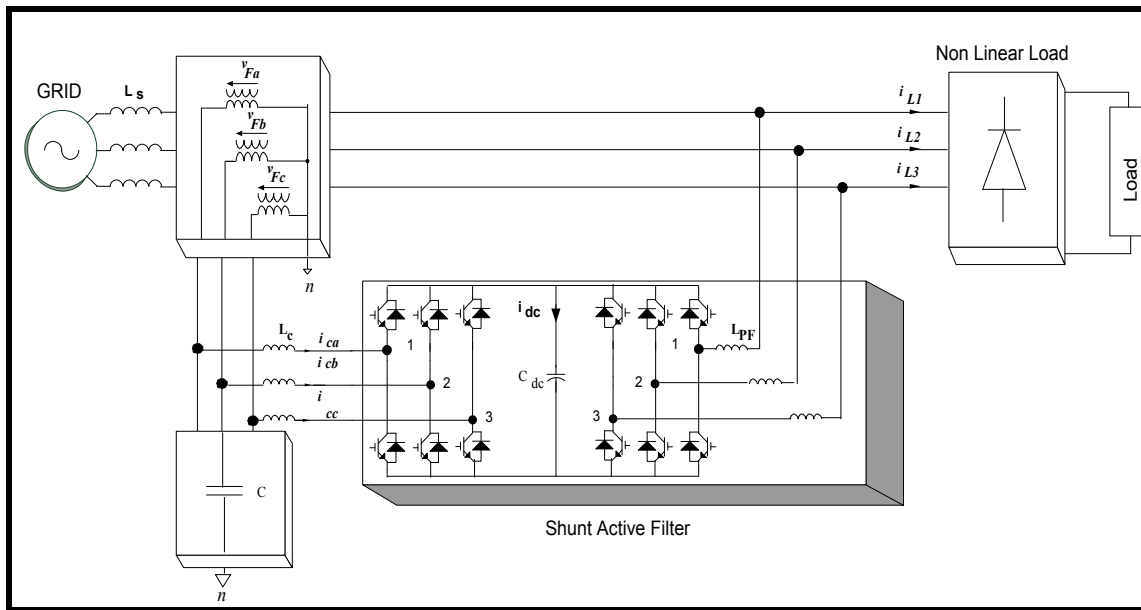


Figure 1.43 Three phase system using Unified Power Quality Conditioner

1.22 State of the art of the technique modulation control

The current current control methods play an important role in power electronic circuits, particularly in current regulated PWM inverters which are widely applied in ac motor drives and continuous ac power supplies where the objective is to produce a sinusoidal ac output. The main task of the control systems in current regulated inverters is to force the current vector in the three phase load according to a reference trajectory. The main different control techniques of inverter are:

- Hysteresis Control;
- Modulated Hysteresis Control;
- Pulse-Width Modulation Control;
- Space vector Modulation Control.

1.22.1 Hysterisis control

Among the various PWM techniques, the hysteresis band current control is used very often because of its simplicity of implementation. Also, besides fast response current loop, the

method does not need any knowledge of load parameters. Hysteresis control (Figure 1.44 and Figure 1.45) is a non-linear control with variable switching frequency to fix the ripple current. The principle consists in establishing, in a first time, the error signal which is the difference between the reference current i_{ref} and the current of the active compensator i_c and then this error is compared with an interval called the hysteresis band which generates the control of the switches (Zabihi & Zare, 2006).

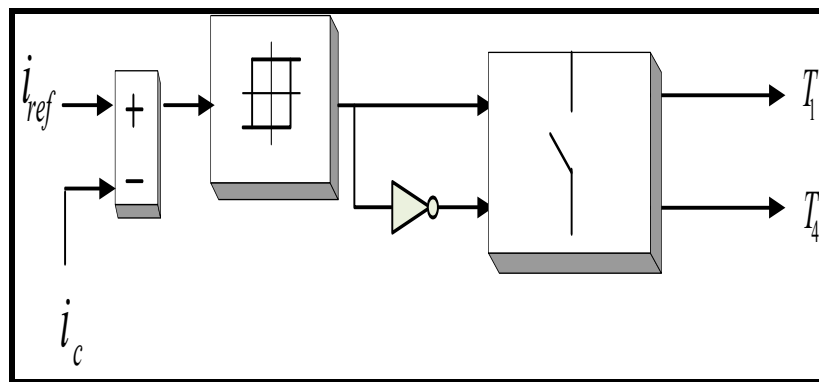


Figure 1.44 Hysterisis control

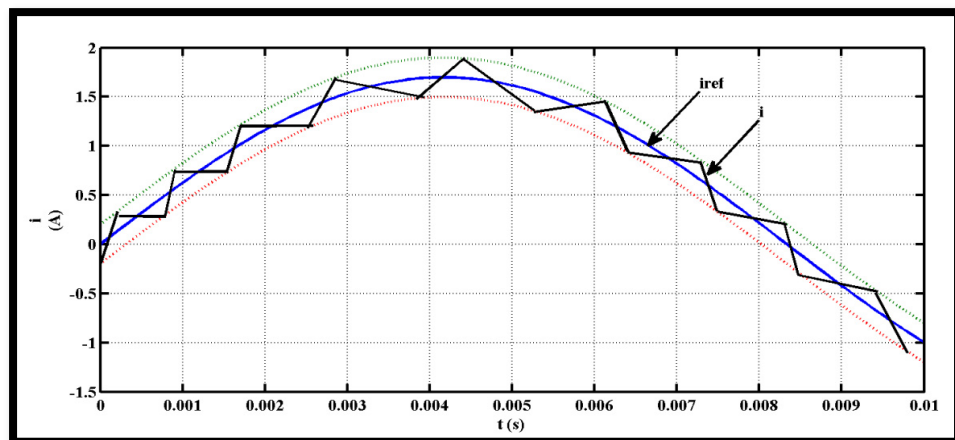


Figure 1.45 Hysterisis control band

1.22.2 Modulated hysteresis control

The disadvantage of the hysteresis control that the PWM frequency varies within a band because peak-to-peak current ripple is required to be controlled at all points of the fundamental frequency wave. Therefore, the purpose of the modulated hysteresis control is to provide an improvement in solving the major disadvantage of conventional hysteresis control by fixing the semiconductor switching frequency. This improvement consists in adding to the error signal ($\mathcal{E} = i_{ref} - i_c$), a triangular signal at the switching frequency. The frequency must be chosen to be equal to the switching frequency that it is desired to impose on the power components (IGBT, MOSFET, etc...). Thus, the obtained signal will be the input of a bandwidth hysteresis regulator 2BH (Band Hysteresis) where the output allows controlling the power switches (Figure 1.46). In the case of modulated hysteresis control, it is important to determine correctly the values of the two main parameters: 1) the amplitude of the triangular signal and 2) the hysteresis regulator bandwidth. If these two parameters are not correctly determined, the switching frequency of semiconductors will be either higher or lower than the desired frequency; therefore the switching losses will increase.

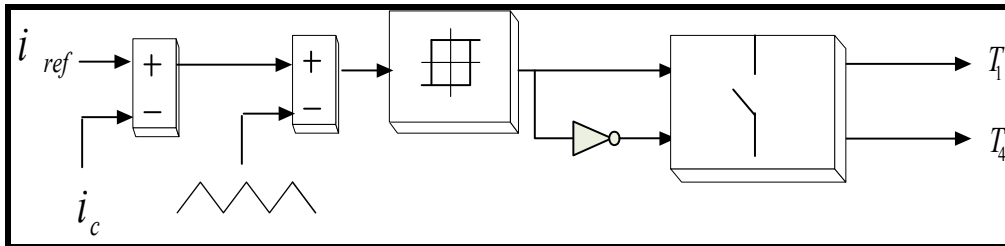


Figure 1.46 Modulation Hysteresis Control

1.22.3 Pulse-Width Modulation Control

The function of the pulse-width modulation (PWM) is to determine the switching times of the semiconductors in order to obtain a switching sequence with the same low frequency spectrum as the original signal. PWM adopts sufficiently high switching frequency with respecting the maximum frequency of the desired output signal and reproducing the mean

value of this signal at each switching period. This is can be done by playing over the duration of application of the positive and negative voltages with respect to the midpoint of the DC bus. The purpose of this command is to decrease the additional and undesired harmonics present in the currents generated by the inverter. The PWM control is applicable to linear systems, with constant switching frequency. The advantages and disadvantages of this control are:

a) Advantages

- Robustness;
- Low control effort;
- High reliability;
- Power losses are very minimal.

b) Disadvantages

- Switching losses due to high switching frequency;
- Weakness control in high noise environment and variable system parameters;
- Mathematical model required;
- No control of current ripples.

1.22.4 PWM Space vector modulation (PWM-SVM)

PWM-SVM is an algorithm for the control of pulse width modulation (PWM) and is conceptually quite a bit different from the standard PWM methods. The SVM method treats the inverter as one unit. That is, the inverter can be driven to eight unique states as shown in Figure 1.47 and Figure 1.48. Unlike PWM techniques which control the phase voltages, SVM controls the voltage vector $[\]$.

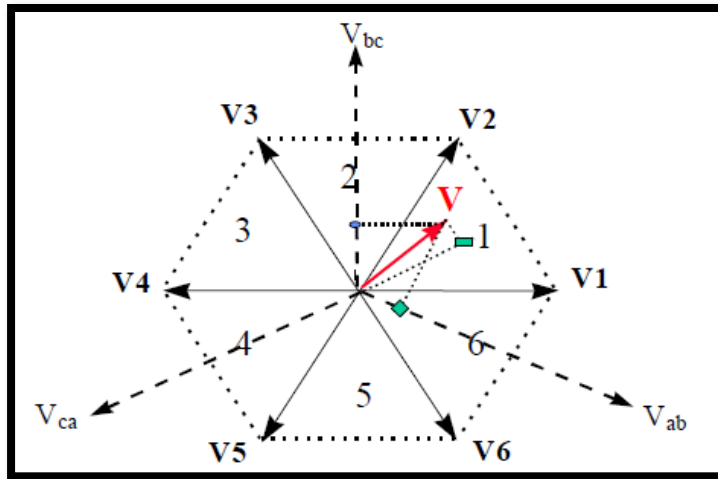


Figure 1.47 Output voltage vector in the a, b plane.

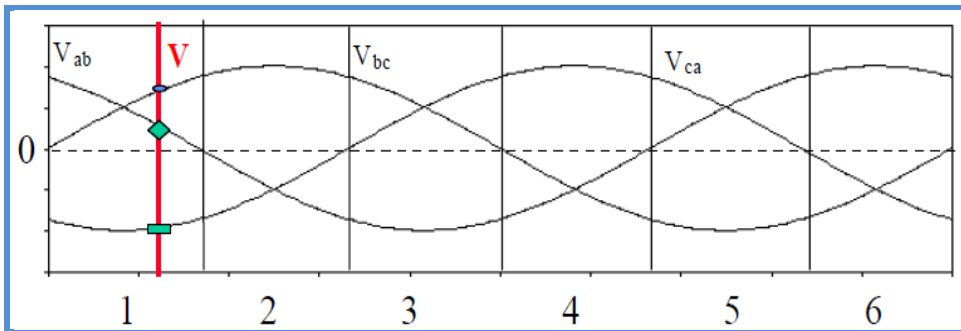


Figure 1.48 Output line voltages in time domain

1.23 Main controls algorithms used in power quality

The most frequent disturbances affecting the power quality in a three-phase system are the imbalance and the distortion of the waveform. In the literature, there are several methods that describe different type of algorithms. These methods are classified into two groups according to the temporal or frequency domain of the developed mathematical concept:

- **Frequency Methods:** Frequency domain methods use Fourier analysis (discrete transform, fast transform, recursive discrete transform, etc.) to identify the current harmonics. These methods are well adapted to loads where the harmonic content varies slowly. Moreover, they have the advantage of identifying the harmonics individually and

then allow a selective compensation. However, the most disadvantages of these methods are the average transient results and the very large computation volume that needs more space in memory (Asiminoaei, Blaabjerg, & Hansen, 2005);

- **Time domain:** Time domain methods allow for faster response and require fewer operations than previous methods. The principle of this method is the separation of the fundamental or certain harmonics by the numerical filtering method (Nava-Segura & Carmona-Hernandez, 1999).

The performance of powers electronic convertors used in MG control depends on many factors:

- The control algorithm used to identify the references of currents or voltages;
- The control mode used (PWM, hysteresis, modulated hysteresis...) for generating control signal for semiconductors;
- Performance of the voltage loop regulation of the capacitive tank.

The main different control techniques in power quality of MG are summarized below.

1.23.1 PQ direct instantaneous power control method

The PQ direct instantaneous power method is a temporal method and uses the load current i_L as a reference in order to compensate at the PCC the harmonic generated by the nonlinear load (Figure 1.49). It was used to avoid the problem due to the high number of computations when implementing frequency methods such as the Fourier method. Its principle is based on the transition from three-phase systems consisting of simple voltages and line currents to a two-phase system (α - β reference) using the Concordia transformation, in order to calculate the instantaneous real and imaginary powers. Then, for the currents harmonic determination generated by the load, the fundamental component is transformed into a continuous component and the harmonic components into alternating components. In this method, one generally uses either a high-pass filter or a low-pass filter in order to keep only the harmonic component of the signal (Y. Zhang & Qu, 2015).

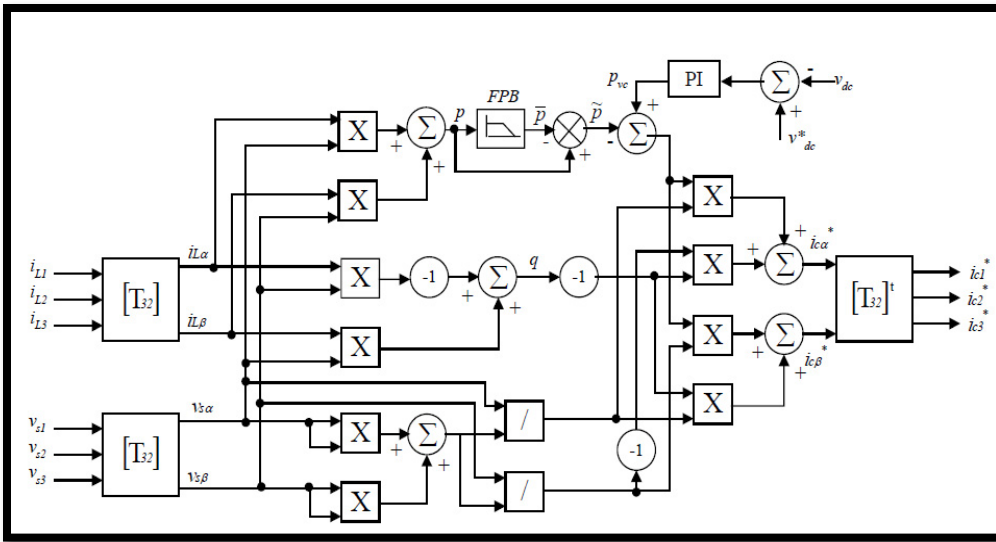


Figure 1.49 PQ direct instantaneous power method for harmonic currents and reactive power compensation

1.23.2 PQ indirect instantaneous power control method

PQ indirect method (Figure 1.50).uses the grid current i_s as a reference in order to compensate at the PCC the harmonic generated by the nonlinear load (HAMADI, 2010).

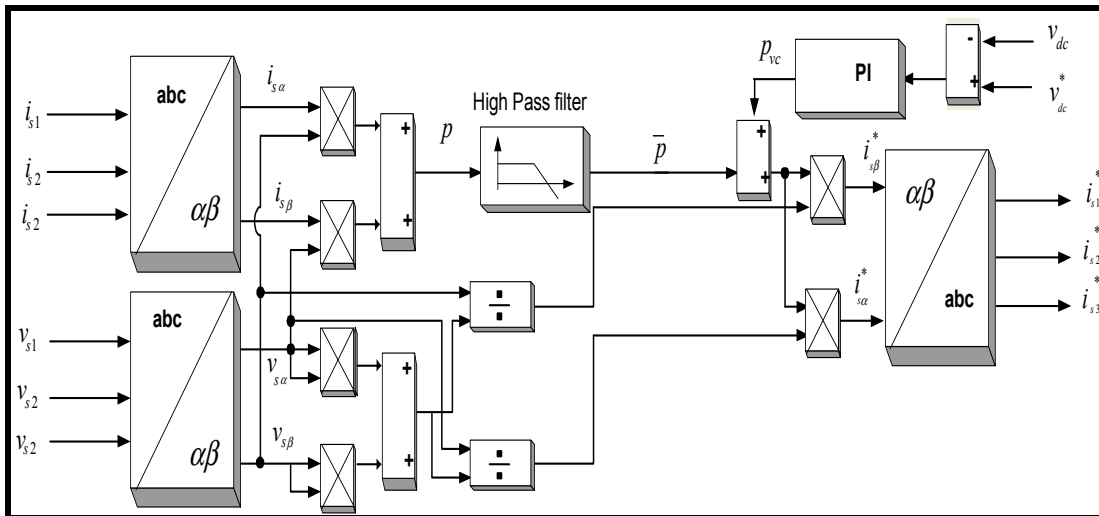


Figure 1.50 Algorithm of ‘PQ’ indirect instantaneous power control method

1.23.3 Synchronous Reference Frame (SRF)

Figure 1.51 shows the classical control scheme for the hybrid shunt filter. For both control loops, the SRF control is used to identify the voltage references of the inverter. The principle of this method is based on the use of a PLL and Concordia transformation to determine the d-q axis components of currents and voltages in the Park reference. Then the alternate components were extracted using two first-order high-pass filters for the feedback loop, and a band pass filter for extracting the fifth harmonic component for the feed forward loop (Wiroj, Hatada, Keiji, & Akagi, 2007).

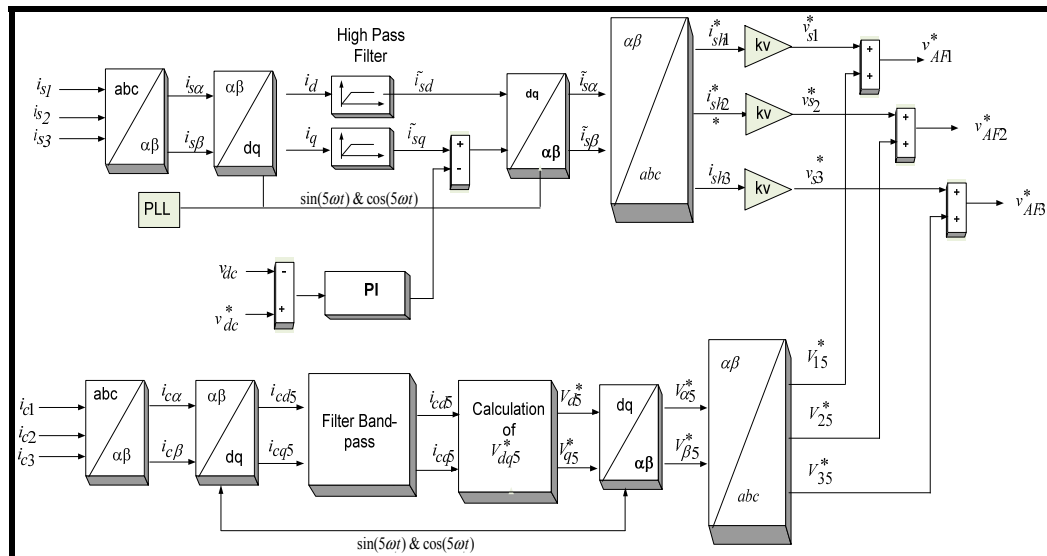


Figure 1.51 SRF control for the hybrid shunt filter

1.23.4 Nonlinear control

The non-linear control is based on two main steps. 1) The first step is the determination of the control law by deriving so many times the output system until the input u of the system appears; 2) The second step is to apply linear controllers to the previously linearized system in order to impose specific dynamics on the closed-loop system. The general principle of this technique is described in Figure 1.52 (Mendalek, Al-Haddad, Fnaiech, & Dessaint, 2003; Yacoubi, Al-Haddad, Dessaint, & Fnaiech, 2006a).

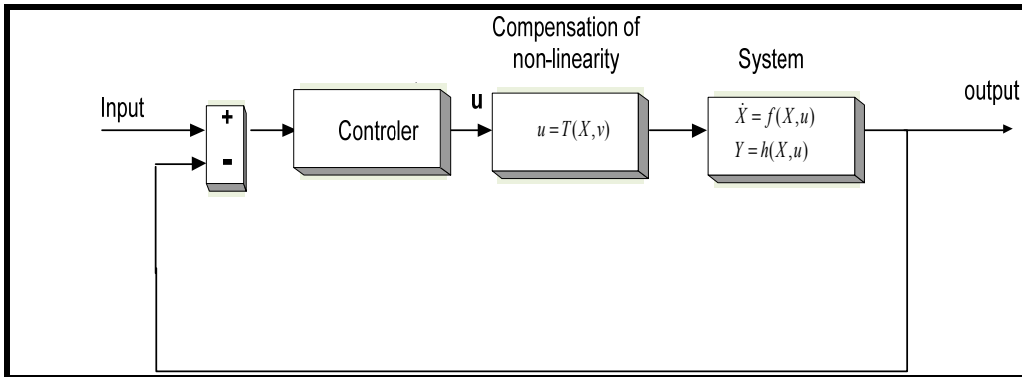


Figure 1.52 Nonlinear control by exact linearization

1.23.5 Sliding mode control

The sliding mode control is a nonlinear control technique with variable structure, where the dynamics of the system are transformed by applying a basic high-frequency switching control law. This control is ideal for active filters where the configuration varies with the sequences of operation (Figure 1.53). The fact that the dynamic model of an active filter varies over time makes the application of this control very appropriate (Gous & Beukes, 2004; Komurcugil, 2009; Matas, de Vicuna, Miret, Guerrero, & Castilla, 2008; Mendalek, 2009; Mendalek, Al-Haddad, Kanaan, & Hassoun, 2008).

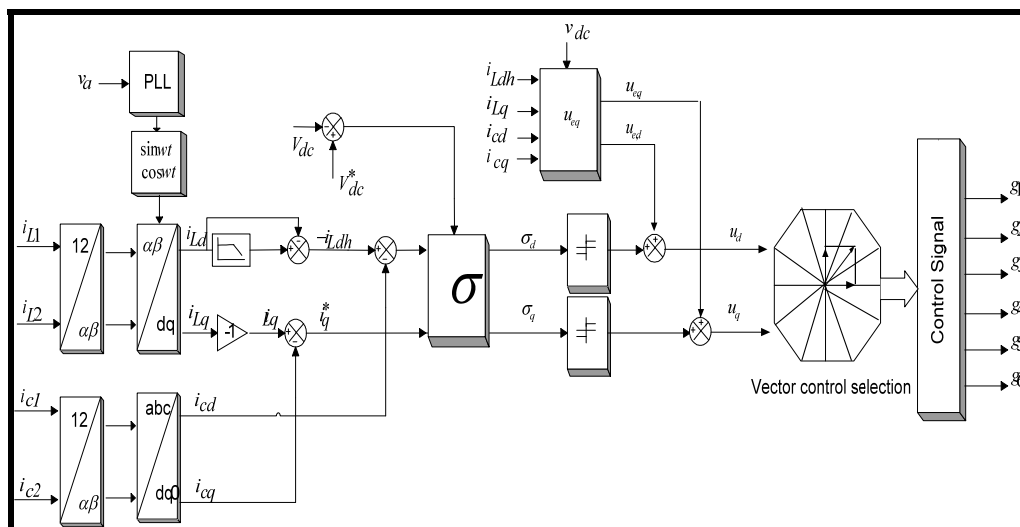


Figure 1.53 Sliding mode control

1.23.6 Direct adaptive control with reference model

The principle of direct adaptive control with reference model (Figure 1.54), the parameters of the controllers are directly updated by an adaptation law in order to have the derivative energy asymptotically stable. The dynamics of the controlled system must follow a reference model, which is called "adaptive control with reference model".

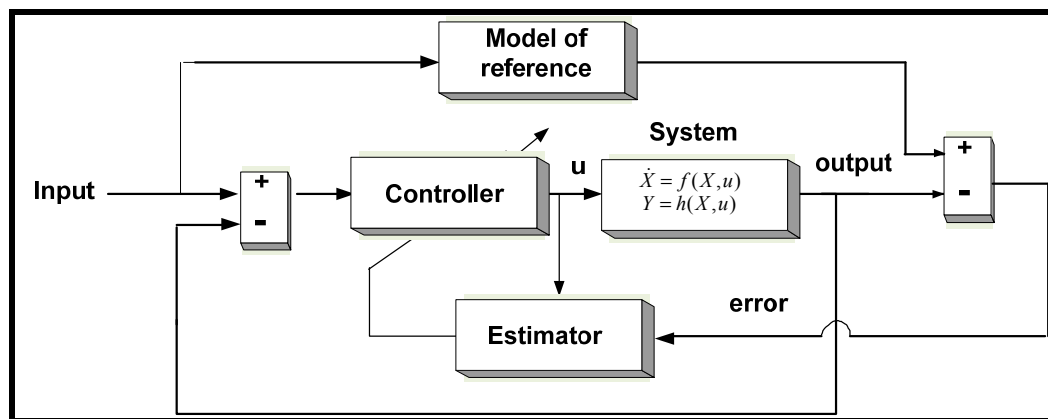


Figure 1.54 Direct adaptive control with reference model

1.23.7 Indirect adaptive control

In the indirect adaptive control, the parameters of controller are estimated from the system parameters (Figure 1.55). This estimate uses a least squares algorithm or other variants (Yacoubi, Al-Haddad, Dessaint, & Fnaiech, 2006b).

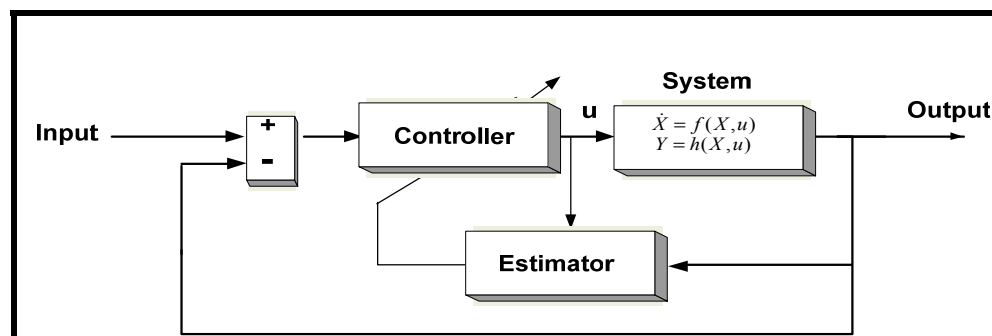


Figure 1.55 Indirect non linear adaptive control.

1.23.8 Control method based on Lyapunov stability

The principle of the Lyapunov method is based on the mathematical extension of a fundamental observation of physics. If the total energy of a system is dissipated continuously, then the system (linear or non-linear) will ultimately have to reach a point of equilibrium. We can therefore conclude that a system is stable by analyzing its total energy.

The basic procedure is to generate an energy function for the dynamic system and to examine its derivative. One can thus define the stability of the system without analyzing the explicit solution of the nonlinear differential equations (Komurcugil, 2007; Komurcugil & Kukrer, 2005).

1.24 Conclusion

In this chapter, different problematics related to MGs issues have been highlighted in order to understand the essential basics of the concept. A state of the art on development of Microgrids and their potential applications for remote areas as well as for grid connected type was discussed. Moreover, it has been pointed out that the most important task of MGs is the power quality and energy management to maintain a reliable uninterruptible power supply to customer's level without which the desired performance cannot be achieved. To reach the desired performance, the relatively new concept of Net Zero Energy House (NZEH) and Net Zero Energy Building is introduced.

However, in spite of the multitude works that already done on the MGs areas, the power quality and optimization issues need effective and efficient control algorithm to improve the performance and well understanding the behavior of different sources of energy connected together. Many controls algorithms will be investigated in this work in order to find the best way to reduce the sensors' number, the installation size and the degree of control complexity, while keeping a better power quality, as well as the system reliability. These problematic will allow situating the original contributions proposed in this thesis and which will be presented in the next chapters.

CHAPTER 2

CONCEPT AND DESIGN OF NET ZERO ENERGY HOUSE USING MICROGRID CONCEPT

2.1 Introduction

This chapter deals on concept and design of Net Zero Energy House (NZEH) based on MGs concept. The idea of the NZEH implies that the integrated energy systems designed for a specific house can generate at least as much energy as the house uses over the year. Photovoltaic system (PVS) and electrical grid are the two main energy sources used for NZEH. Backup energy storage (battery and electric vehicle) is used to ensure an uninterruptible power supply and used only for emergency when the grid is disconnected or over loaded. When the PVS do not generate a sufficient amount of power, the electricity is purchased from the grid and when the PVS produces excess electricity, the difference is sold back to the grid. In addition, a bidirectional battery charger is designed to facilitate the charging of plug-in hybrid electric vehicle (PHEV) from dc or ac source. A three phase system is used in the proposed system in order to have an option for distributing the extra power to the neighborhood.

To achieve these goals, new control approaches based on synchronous reference frames (SRF), indirect and sliding mode control are developed, tested experimentally validated for ON and OFF-grid mode operation of NZEH.

2.2 Description of under study system

Figure 2.1 shows the NZEH, consisting of integrated Photovoltaic System, PHEV and battery energy storage system. A voltage source converter active harmonic filter (VSC-AHF) is used as an interface between energy sources and NZEH to manage the power flow, to cancel the harmonic current, and to keep the power factor at unity. A bidirectional battery charger for PHEV is carefully studied and designed to ensure safe charge and discharge of batteries (Tidjani & Chandra, 2012; Tidjani, Hamadi, Chandra, & Pillay, 2014).

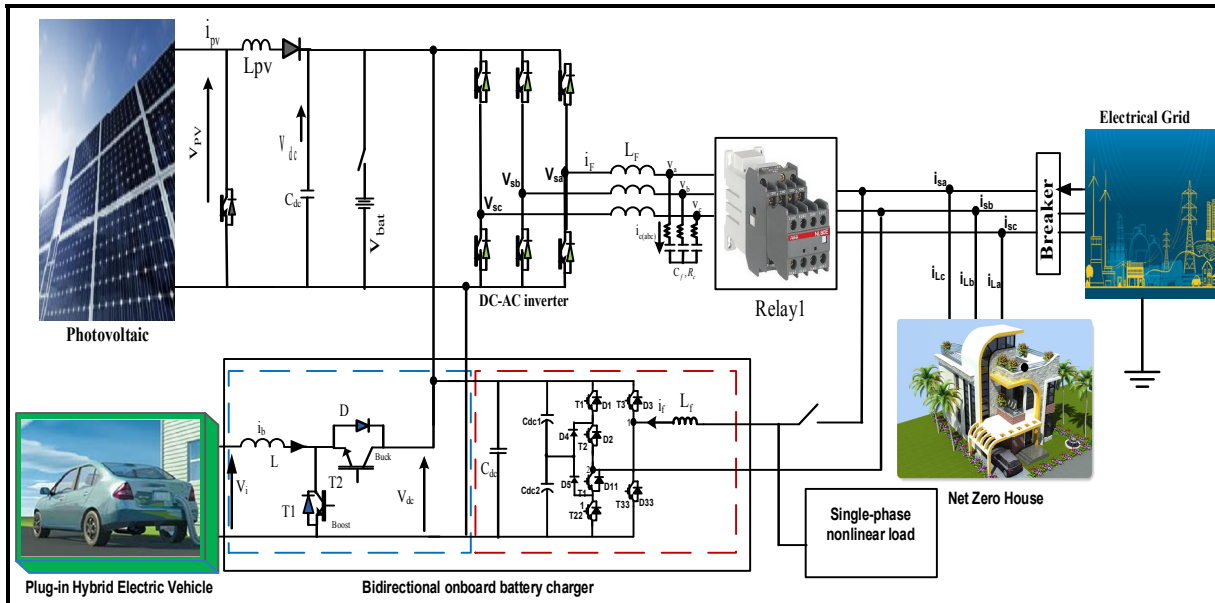


Figure 2.1a Model of Net Zero Energy House based on MG concept

2.3 Design of photovoltaic system for NZEH

Design of photovoltaic system (PVS) requires the collection of detail information about electricity consuming loads and their operation from the customer. The first step is to define the load profile and then the solar potential in the region.

2.3.1 Load characteristics and daily energy consumption

The load characteristics and daily energy consumption are shown in Table 2.1.

Table 2.1 Load characteristics and daily energy consumption

| Bridge diode (in NZEH) | |
|---|---|
| Apparent power (S_L) | $S_L = 5.5 \text{ kVA}$ |
| RMS Line voltage (V_{SL}) | 208 V |
| Source voltage V_s | 120 V |
| RMS load current (I_{La}) | $I_{La} = \frac{S_L}{3 * V_s} = 15.27 \text{ A}$ |
| Frequency source (f_s) | 60 Hz |
| DC load current (I_{dc}) | $I_{dc} = \frac{I_{La}}{\sqrt{\left(\frac{2}{3}\right)}} = \frac{15.27}{\sqrt{\left(\frac{2}{3}\right)}} = 18.70 \text{ A}$ |
| Fundamental load current (I_{La1}) | $I_{La1} = I_{dc} \frac{\sqrt{6}}{\pi} = 14.58 \text{ A}$ |
| Load active power (P_L); $\varphi_1 = 0$ | $P_L = 3 * V_s * I_{La1} * \cos(\varphi_1) = 5.24 \text{ kW}$ |
| Load reactive power (Q_L); $\varphi_1 = 0$ | $Q_L = 3 * V_s * I_{La1} * \sin(\varphi_1) = 0 \text{ kVAR}$ |
| RMS fundamental active load current : I_{La1_active} | $I_{La1_active} = \frac{P_L}{3 * V_s * I_{La1}} = 14.55 \text{ A}$ |
| Load distortion power (D_L) | $D_L = 3 * V_s * \sqrt{I_L^2 - I_{L_active}^2} = \sqrt{15.27^2 - 14.55^2} = 1.62 \text{ kVA}$ |
| Linear load | |
| Power factor, $R = 12 \Omega$, $L = 0.02 \text{ H}$ | $\cos(\varphi_1) = \frac{R}{\sqrt{R^2 + (L\omega)^2}} = \frac{12}{\sqrt{12^2 + (0.02 * 377)^2}} = 0.85$ |
| Current rms | $I_{L1} = \frac{V_s}{Z} = \frac{120}{\sqrt{12^2 + (0.02 * 377)^2}} = 8.47 \text{ A}$ |
| Load active power (P_L); | $P_L = 3 * V_s * I_{L1} * \cos(\varphi_1) = 2.58 \text{ kW}$ with |
| | $\cos(\varphi_1) = \frac{R}{\sqrt{R^2 + (L\omega)^2}} = \frac{12}{\sqrt{12^2 + (0.02 * 377)^2}} = 0.85$ |
| Load active power (Q_L) | $Q_L = 3 * V_s * I_{L1} * \sin(\varphi_1) = 1.62 \text{ kVAR}$ |
| PHEV | |
| Load active power (P_{LV}) | 3 kW |
| active current ($I_{L_PHEV_active}$) | $I_{L_PHEV_active} = \frac{3 \text{ kW}}{3 * 120} = 9.33 \text{ A}$ |
| Fixed daily energy consumption | |
| The total fixed daily energy E_T | $E_T = 50 \text{ kWh}$ |

The Figure 2.1b shows the daily load profile of the NZEH

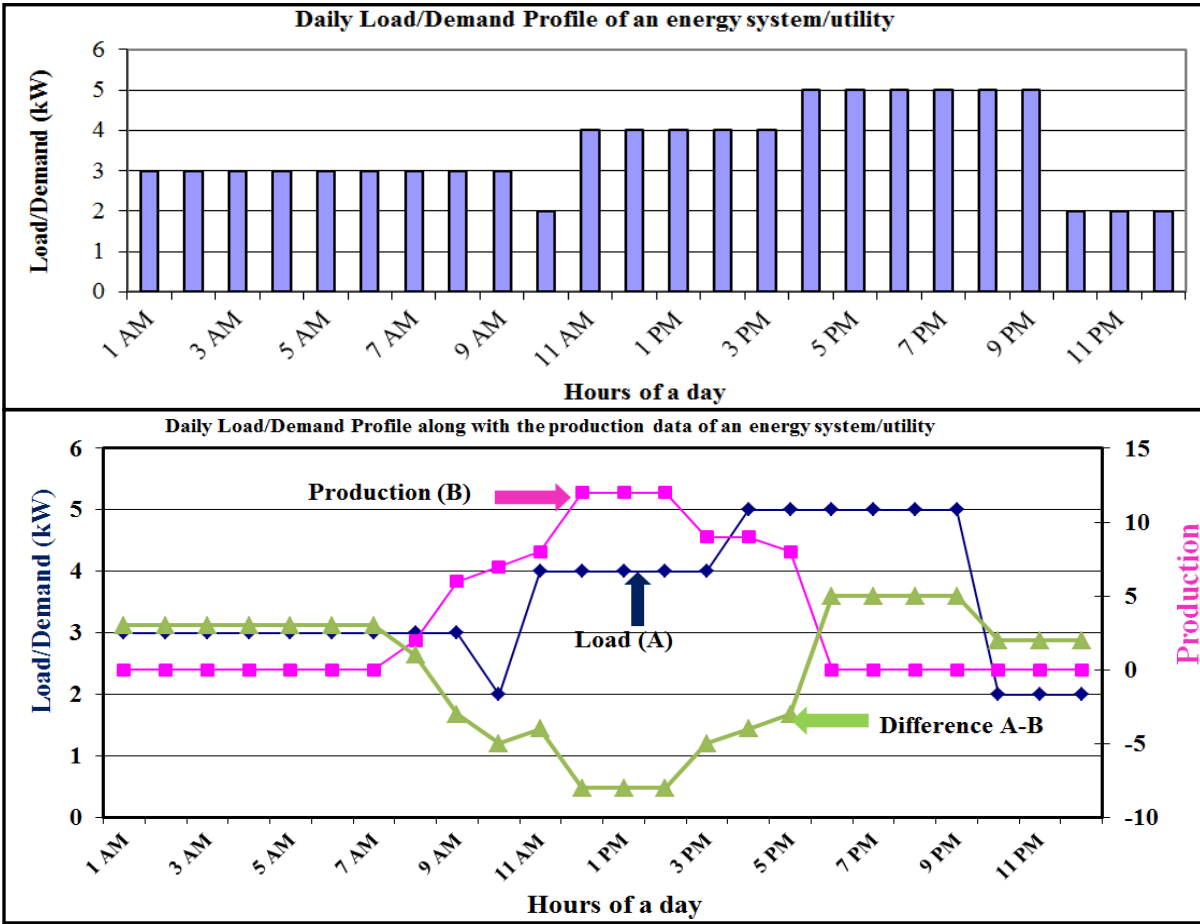


Figure 2.1b Daily load profile of the NZEH

The inverter selection is calculated is the Table 2.2.

2.3.2 Power generated from photovoltaic system

It is very important to know the information regarding the geographical place of the installation before determining the size of the PVS. Information such as how many days in the year does sunshine occur in a year and which month has the maximum average sunshine hour and which month has the minimum. The geographical place chosen for the installation is Republic of Chad and the corresponding average sunshine hour is given in Figure 2.2. The

minimum solar insolation is 4.9 kWh/m²/day (or Peak Sun of 1 kW for 4.9 hour) (Diabate, Blanc, & Wald, 2004).

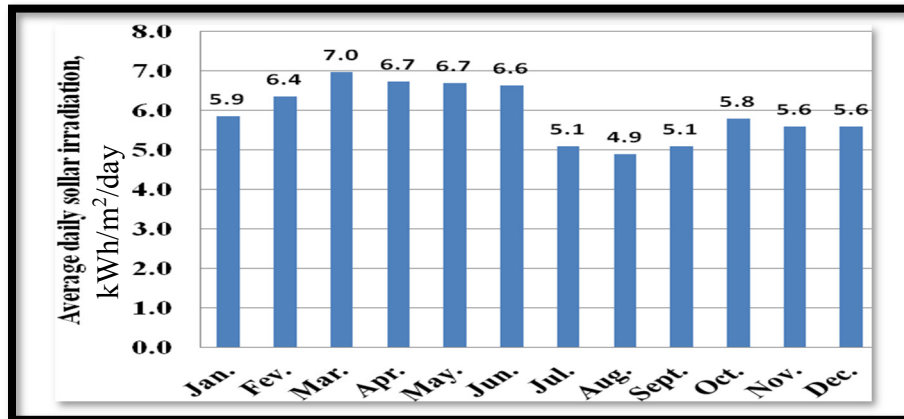


Figure 2.2 Average daily sunlight hour

After determining the Peak Sun, the current to be generated by the PVS is given by using the following Equation.

$$I_{PVS} = \frac{E_T}{T \cdot V_{dc}} = \frac{50000}{4.9 \text{ hr} \cdot 500} = 20.5 \text{ A} \quad (2.1)$$

Where, I_{PVS} = current generated by PVS (Ampere); E_T = required total daily energy (Watt Hour); T = peak sun (hours); V_{dc} = dc bus voltage (Volt).

The out power of photovoltaic is calculated by:

$$P_{PVS} = \frac{E_T}{T \cdot C_p} = \frac{50000}{4.9 \text{ hr} \cdot 0.85} = 12 \text{ kW} \quad (2.2)$$

Where C_p is the power electronic efficiency. Locally, the PVS generates 12kW*4.9hr = 59 kW.hr of energy, but at the charge level, the energy is 50 kWhr, the losses represents 9 kWhr

2.3.3 DC bus voltage of VSC-AHF

There are many approaches to calculate the dc bus voltage (V_{dc}) and the common condition is that V_{dc} must be greater than the maximum peak value of the AC side of VSC. In this approach, the calculation of the V_{dc} is based on the hypothesis that the maximum modulation ($m_a = 1$), the expression of V_{dc} is shown in the following equation (Rastogi, Naik, & Mohan, 1994).

$$V_{dc} = 2\sqrt{2} V_s \quad (2.3)$$

With V_{dc} 20% higher than the maximum input voltage of the inverter, then one takes the security coefficient:

$$V_{dc} = 1.2 \cdot 2\sqrt{2} V_s = 408 V \quad (2.4)$$

Taken into account that the inverter current can reach high value, for the adequate operation, one chooses the dc bus voltage reference $V_{dc} = 500 V$.

2.4 DC bus capacitor calculation

The value of the dc bus capacitor of VSC depends on the ripple voltage and the instantaneous energy needed for normal operation of the inverter (Singh, Jayaprakash, & Kothari, 2008b). The principle of energy conservation is applied to calculate the capacitor.

$$\begin{aligned} \Delta E &= 3 \cdot V_s \cdot I_F \cdot \Delta t = \frac{1}{2} C_{dc} (V_{dc_max})^2 - (V_{dc_min})^2 \\ \Rightarrow C_{dc} &= \frac{6 \cdot V_s \cdot I_F \cdot \Delta t}{(V_{dc})^2 - (V_{dc_min})^2} = \frac{6 \cdot 120 \cdot 7.95 \cdot 0.0083}{(500)^2 - (450)^2} = 1000 \mu F \end{aligned} \quad (2.5)$$

Where $\Delta t = T/2$ corresponding to the maximum time of charge/discharge of the reactive components and current harmonic.

2.4.1 Design of output VSC-AHF inductor

The peak ripple current is chosen as sizing criteria of the inductance design. The equation of inductor filter is then written as (Banerji, Biswas, & Singh, 2016b; Singh, Jayaprakash, & Kothari, 2008a):

$$L_F = \frac{\sqrt{3}}{2 \cdot 6 \cdot a \cdot f_s \cdot \Delta I_F} m_a \cdot V_{dc} = \frac{\sqrt{3}}{2 \cdot 6 \cdot 1.5 \cdot 15000 \cdot 0.795} \cdot 1 \cdot 500 = 4 \text{ mH} \quad (2.6)$$

With ripple $\Delta I_F = 10\% I_F$ $a = 1.5$ $m_a = 1$; $f_s = 15$ Khz.

2.4.2 Validation of the VSC-AHF design using Semisel software

The design calculation of the VSC-AHF is validated by using the SemiSel software. SemiSel is the SEMIKRON online calculation and simulation tool for losses, temperatures and optimal choice of power electronic components. The difference in calculation between the two methods is only 0.5 kW. In addition, the losses are also taken into account with the software. The design and simulation results of VSC-AHF using SemiSel is shown in ANNEX I.

In addition, the test of the VSC-AHF without PVS is tested for start and stop using the preload circuit of Figure 2.3. During start and stop of the VSC-AHF, three relays are used for preload, start-stop and discharging for capacitor of bus dc. The Relay 2 is used to charge the capacitor C_{dc} at a certain voltage level before starting the VSC-AHF; this is to avoid a high inrush current that could damage the power electronics or create transient in network. When the dc capacitor C_{dc} is charged, the relay 1 will be activated to start the operation of AHF. The relay 3 is used to discharge the dc capacitor C_{dc} via the resistor R when the VSC-AHF is stopped.

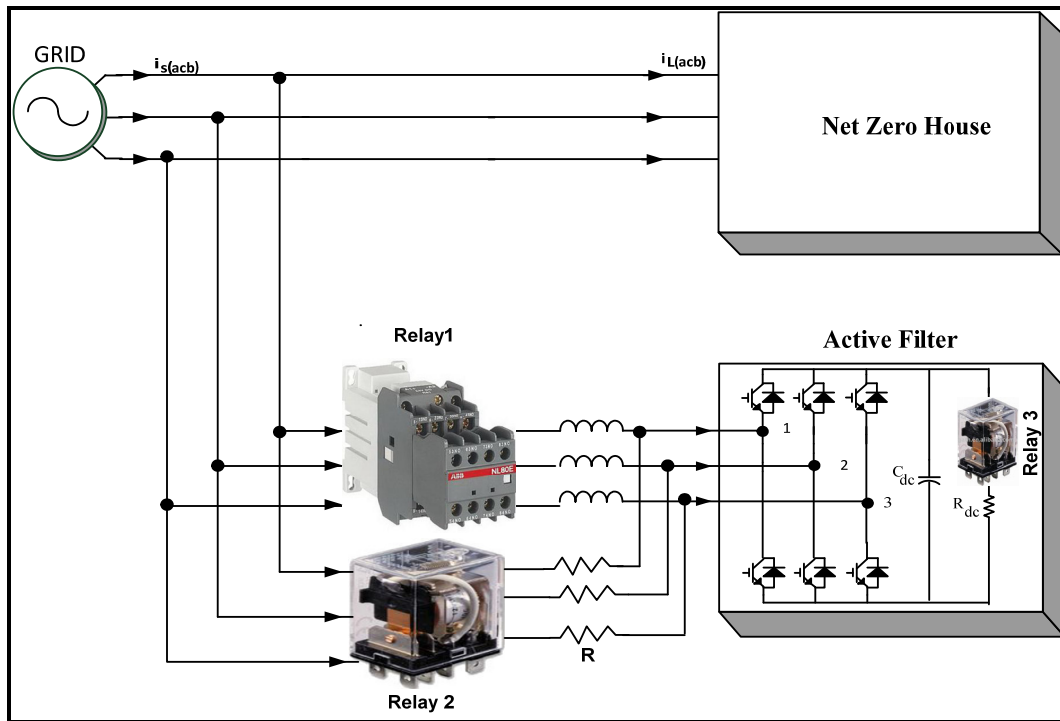


Figure 2.3 Circuit for secure Start-Stop of the VSC-AHF

2.4.3 Proposed Control Algorithm for the NZEH

To ensure the uninterruptible power supply for the Net Zero Energy House, a VSC-AHF is used as interface between different energy sources and load. The VSC-AHF is able to control the system during ON and OFF grid mode of operation. The ON mode is when the NZEH is connected to the grid and the OFF one is when the grid is disconnected and the NZEH is working as a standalone system. When the grid is disconnected, the centralized system of control receives signal from the signal detector indicating the voltage disappearance, the second control is then automatically activate to allow the NZEH operating on standalone mode.

Three control approaches have been analyzed in order to optimize the control of the system:

- Synchronous reference frame (SRF) and direct control;
- Nonlinear direct control for current and direct control for voltage;
- Direct nonlinear approaches for current and direct nonlinear control for voltage.

2.4.3.1 Synchronous reference frame and direct voltage control

The Synchronous reference frame (SRF) control is used to control the system for ON grid mode of operation. The Equations (2.7) to (2.9) of park transformation are used in the mathematical control approaches (Tidjani et al., 2014).

$$\begin{bmatrix} i_{Lq} \\ i_{Ld} \\ i_{L0} \end{bmatrix} = \frac{2}{3} \begin{bmatrix} \cos \theta & \cos(\theta - \frac{2\pi}{3}) & \cos(\theta + \frac{2\pi}{3}) \\ \sin \theta & \sin(\theta - \frac{2\pi}{3}) & \sin(\theta + \frac{2\pi}{3}) \\ \frac{1}{2} & \frac{1}{2} & \frac{1}{2} \end{bmatrix} \begin{bmatrix} i_{La} \\ i_{Lb} \\ i_{Lc} \end{bmatrix} \quad (2.7)$$

The load currents i_{La} , i_{Lb} , i_{Lc} are transformed to stationary coordinate system “dqo” The angle θ is obtained using phase locked loop (PLL).

The SRF control extracts dc quantities of a load current i_{Ld} using low-pass filter. To obtain the reference grid current i_{sd}^* , an active current at the fundamental frequency i_{d0} is added to the I_{Ld_dc} in order to maintain dc bus constant.

$$\begin{cases} i_{sd}^* = I_{Ld_dc} + i_{d0} \\ i_{sq}^* = -I_{Lq_dc} \end{cases} \quad (2.8)$$

The reference source current obtained by the following reverse Park's transformation:

$$\begin{bmatrix} i_{sa}^* \\ i_{sb}^* \\ i_{sc}^* \end{bmatrix} = \begin{bmatrix} \cos \theta & -\sin \theta \\ \cos(\theta - \frac{2\pi}{3}) & -\sin(\theta - \frac{2\pi}{3}) \\ \cos(\theta + \frac{2\pi}{3}) & -\sin(\theta + \frac{2\pi}{3}) \end{bmatrix} \begin{bmatrix} i_{sd}^* \\ i_{sq}^* \\ i_{s0} \end{bmatrix} \quad (2.9)$$

The reference current $i_{s(abc)}^*$ is compared to the sensed source current $i_{s(abc)}$, a PI controller is used to force the measured current to follow the desired reference current. The output signal is forward to digital signal processor in order to generate gate pulses to control the VSC-AHF.

For the OFF mode, when the system is disconnected from the grid, the signal detector (voltage detector) indicating the voltage disappearance and the direct control of voltage is automatically activated to maintain the voltage at the PCC constant and allows system working in standalone mode of operation.

This first control approaches (Figure 2.4) that combined SRF (control for ON grid) and direct control (control for OFF grid) is working very well but the inconvenient is the high number of sensors (13 sensors) that have direct impact on the cost and complexity of power management.

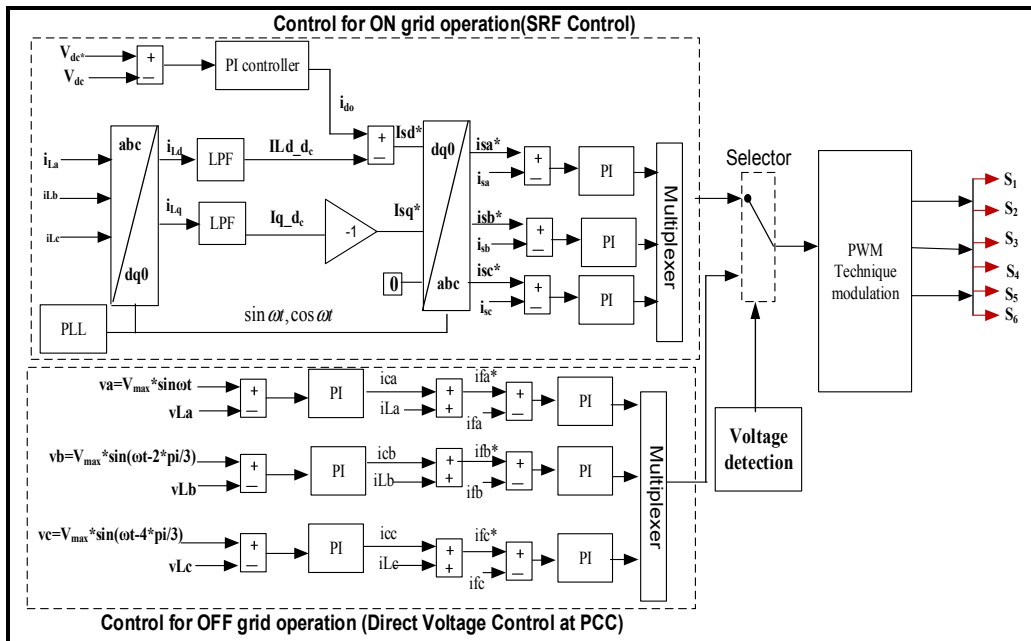


Figure 2.4 SRF control for ON grid and Direct voltage control for OFF grid

To solve the problem of the high number of sensors, another control approaches is developed and compared in the following section 2.4.3.2.

2.4.3.2 Nonlinear direct control for current and direct control for voltage

For the second control approaches, a nonlinear direct control for current is developed to control the NZEH for grid mode of operation. The nonlinear control extracts harmonics quantities of the load current i_{Ld_h} using high-pass filter. To obtain the reference inverter current i_{fd}^* , an active current at the fundamental frequency i_{fd0} is added to the I_{Ld_h} (Equation 2.10) in order to maintain the DC bus constant.

$$\begin{cases} i_{fd}^* = I_{Ld_h} + i_{fd0} \\ i_{fq}^* = -I_{Lq} \end{cases} \quad (2.10)$$

The control laws adopting PI controller are given by (Hamadi, Javadi, Ndtoungou, Rahmani, & Al-Haddad, 2017):

$$d_{nd} = \frac{L\omega i_q - u_d + v_{sd}}{v_{dc}} \quad (2.11)$$

$$d_{nq} = \frac{-L\omega i_d - u_q + v_{sq}}{v_{dc}} \quad (2.12)$$

For the OFF grid mode, the direct control of the voltage is used to maintain the voltage at the PCC constant (Figure 2.5).

Compared to the first control approaches, in this second control, the number of sensors is reduced from 13 to 10 as shown in Figure 2.5.

However, the high accuracy in the power quality compensation depends in part on the sampling time during the analysis of the control signal. The performance is increasing when the sampling time is reducing. In the following section 2.4.3.3, a novel control approaches is

developed to reduce the number of digital block used to calculate and analyze the control signal in order to reduce the sampling time.

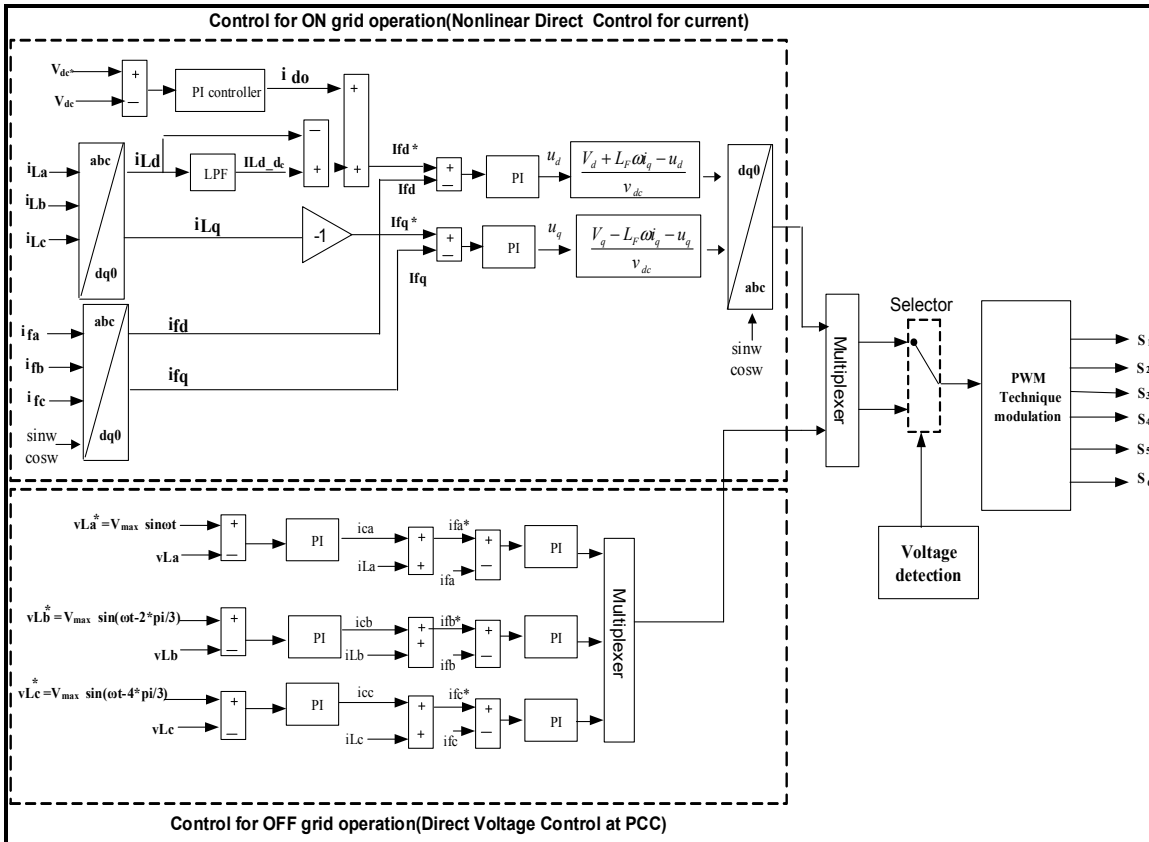


Figure 2.5 Nonlinear direct control for current and direct control for voltage

2.4.3.3 Nonlinear direct control for current and nonlinear direct control for voltage

This third control approaches (Figure 2.6) is developed to reduce the sampling time by reducing the number of digital block using for the calculation and signal analyzing. Two nonlinear direct controls are used to control the VSC-AHF for the current and voltage in the dq frame (Tidjani, Hamadi, Chandra, Pillay, & Ndtoungou, 2017).

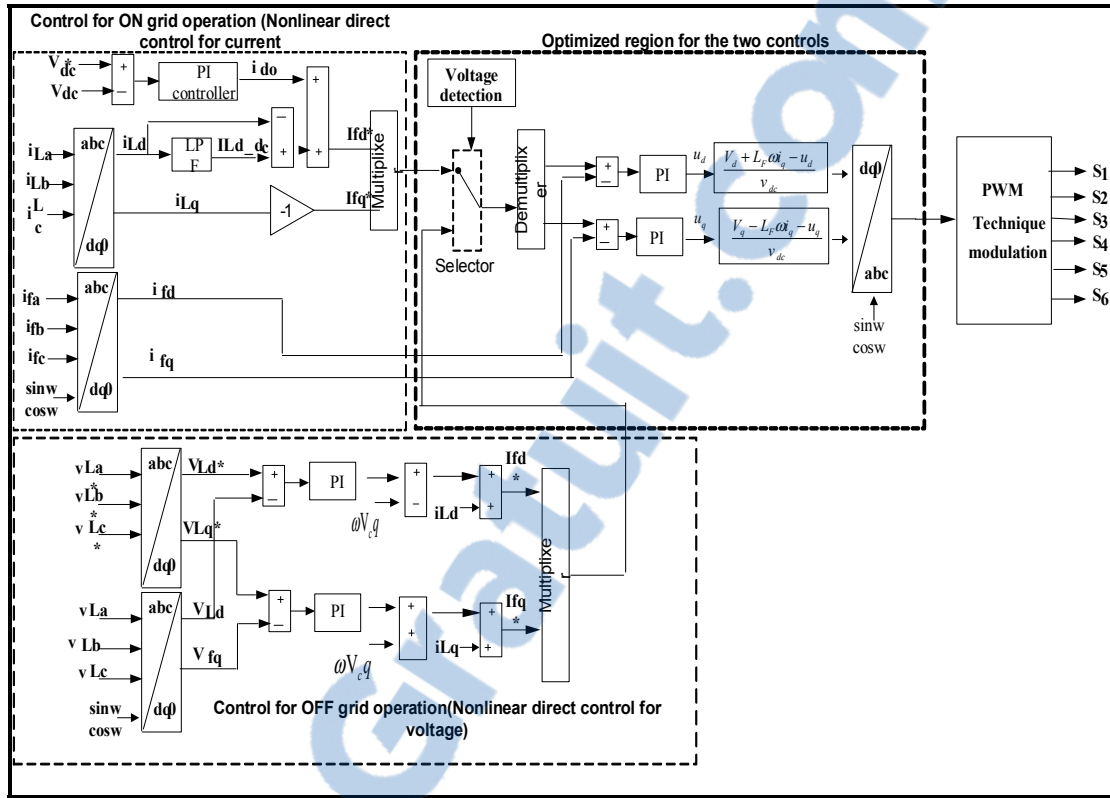


Figure 2.6 Nonlinear direct control for current and nonlinear direct control for voltage

2.5 Modeling of bidirectional battery charger for PHEV

This section is dedicated for designing a bidirectional PHEV charger that is able to be connected directly to DC or AC bus depending on customer using (Figure 2.7). This charger consists of two modules: 1) a DC-DC buck - boost converter, 2). a DC-AC single phase five level inverter.

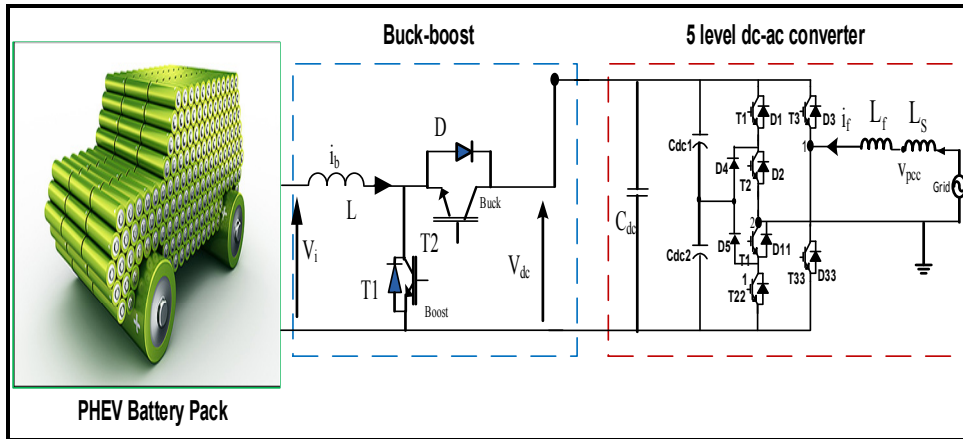


Figure 2.7 Bidirectional onboard PHEV battery charger

2.5.1 Modeling of buck-boost converter and controlling with sliding mode

The buck boost battery charger (Figure 2.8) is modeled using average model theory and is then controlled by sliding mode technique.

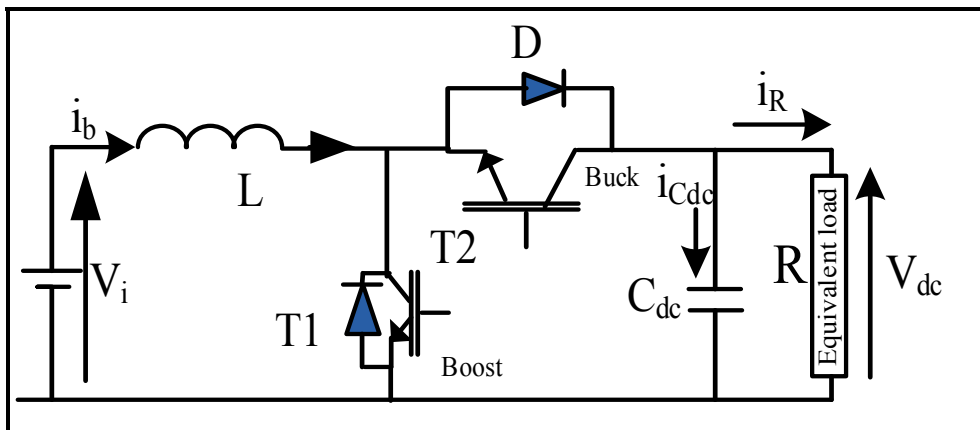


Figure 2.8 DC-DC buck boost converter

2.5.1.1 Modeling of boost converter

The boost converter is modeled following two steps:

1. Switch $T1_{on}$ and the diode D_{off} (See Figure 2.9);

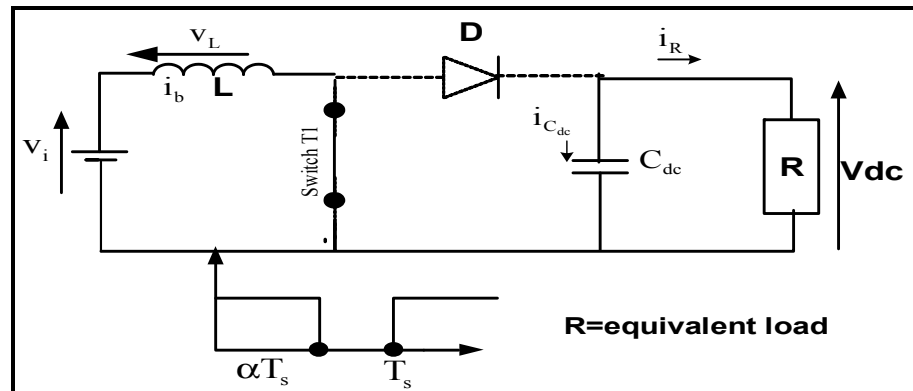


Figure 2.9 ON sequence of the boost converter

α – is the duty cycle, T_s is the conduction time.

When $0 < t < \alpha T_s$ one can write the following equation:

$$\begin{cases} v_L = v_i = L \frac{di_b}{dt} \\ i_{C_{dc}} = -i_R = \frac{-v_{dc}}{R} = C_{dc} \frac{dv_{C_{dc}}}{dt} \end{cases} \Rightarrow \begin{cases} \frac{di_b}{dt} = \frac{v_i}{L} \\ \frac{dv_{C_{dc}}}{dt} = \frac{-v_{dc}}{RC_{dc}} \end{cases} \quad (2.13)$$

The equation (2.13) can be written in matrix form as:

$$\begin{bmatrix} \frac{di_b}{dt} \\ \frac{dv_{C_{dc}}}{dt} \end{bmatrix} = \underbrace{\begin{bmatrix} 0 & 0 \\ 0 & -\frac{1}{RC_{dc}} \end{bmatrix}}_{A_1} \begin{bmatrix} i_b \\ 0 \end{bmatrix} + \underbrace{\begin{bmatrix} \frac{1}{L} \\ 0 \end{bmatrix}}_{B_1} v_i \quad (2.14)$$

The equation (2.14) is the form of:

$$\frac{dx}{dt} = A_1 x + B_1 v_i \quad (2.15)$$

2. Switch T1_{off} and the diode D_{on} (Figure 2.10)

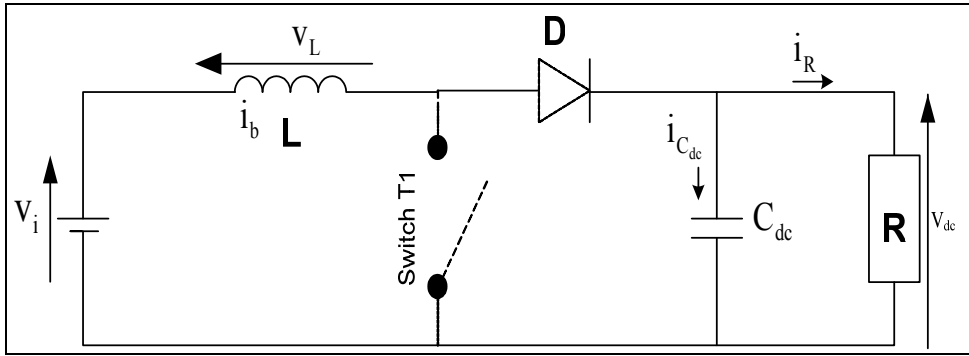


Figure 2.10 OFF sequence of the boost converter

When $\alpha T_s \ll t \ll T_s$ one can write the following equation:

$$\begin{cases} L \frac{di_b}{dt} = v_i - v_{dc} \\ C_{dc} \frac{dv_{C_{dc}}}{dt} = i_b - \frac{v_{dc}}{R} \end{cases} \Rightarrow \begin{cases} \frac{di_b}{dt} = \frac{v_i}{L} - \frac{v_{dc}}{L} \\ \frac{dv_{C_{dc}}}{dt} = \frac{i_b}{C_{dc}} - \frac{v_{dc}}{RC_{dc}} \end{cases} \quad (2.16)$$

The matrix form of equation (2.16) is:

$$\begin{bmatrix} \frac{di_b}{dt} \\ \frac{dv_{C_{dc}}}{dt} \end{bmatrix} = \underbrace{\begin{bmatrix} 0 & -1 \\ 1 & -1 \end{bmatrix}}_{A_2} \begin{bmatrix} i_b \\ v_{C_{dc}} \end{bmatrix} + \underbrace{\begin{bmatrix} 1 \\ 0 \end{bmatrix}}_{B_2} v_i \quad (2.17)$$

The form of equation (2.17) is:

$$\frac{dx}{dt} = A_2x + B_2v_i \quad (2.18)$$

The average model of the boost can be written as:

$$\left\{ \begin{array}{l} A = A_1d + A_2(1-d) \Rightarrow A = \begin{bmatrix} 0 & \frac{d-1}{L} \\ 1-d & -1 \\ C_{dc} & RC_{dc} \end{bmatrix} \\ B = B_1d + B_2(1-d) \Rightarrow B = \begin{bmatrix} 1 \\ L \\ 0 \end{bmatrix} \end{array} \right. \quad (2.19)$$

So the control law of boost with current or voltage parameters is given by:

$$\left\{ \begin{array}{l} L \frac{di_b}{dt} = v_i - (1-d)v_{dc} \\ C_{dc} \frac{dv_{dc}}{dt} + \frac{v_{dc}}{R} = (1-d)i_b \end{array} \right. \quad (2.20)$$

$$\frac{di_b}{dt} = \frac{v_i}{L} - \frac{(1-d)v_{dc}}{L} \quad (2.21)$$

2.5.1.2 Modeling of buck converter

The mathematic model of the buck converter is the inverse of the boost converter and the control law is given by:

$$\text{So, } \left\{ \begin{array}{l} L \frac{di_b}{dt} = v_i d - v_{dc} \\ C_{dc} \frac{dv_{dc}}{dt} = i_L - \frac{v_{dc}}{R} \end{array} \right. \quad (2.22)$$

2.5.1.3 Sliding mode control of the buck-boost converter

Knowing the buck-boost mathematic model, one uses sliding mode to control the charging and discharging of PHEV battery pack and also study its stability. For this purpose, let's choose the sliding surface S:

$$\text{So, } S = k_1 (x_1 - x_1^*) = 0 \quad (2.23)$$

Where $x_1 = i_b$ and $x_1^* = i_b^*$ are respectively the measured and the reference current of PHEV battery pack.

The equivalent control d_{eq} is extracted from the derivate of sliding surface Sd.

$$\text{So, } \frac{dS}{dt} = k_1 (\dot{x}_1 - \dot{x}_1^*) = k_1 \left(\frac{V_i}{L} - \frac{(1-d_{eq})v_{dc}}{L} - \dot{x}_1^* \right) = 0 \quad (2.24)$$

$$\text{So, } d_{eq} = 1 - \frac{V_i}{v_{dc}} + \frac{\dot{x}_1^* \cdot L}{v_{dc}} \quad (2.25)$$

An optimal control has an infinite number of switches on a finite-time interval and this phenomena is called chattering. The control law of the global system is given by:

$$\text{So, } d = d_{eq} + d_s = d_{eq} - k \text{sign}(S) \quad (2.26)$$

Where d_s is the switching control and k is the coefficient of stability convergence.

To ensure stability of the sliding mode and its convergence to the surface, one chooses a Lyapunov function candidate V and its derivate $\frac{dV}{dt}$ as shown in Equations (2.27) and (2.28).

The derivate should be negative definite. The global control law d is introduced to verify the asymptotic stability of the derivative function $\frac{dV}{dt}$.

$$V = \frac{1}{2} S S^T \quad (2.27)$$

$$\text{So, } \frac{dV}{dt} = S \frac{dS}{dt} = S \cdot \dot{S} < 0 \quad (2.28)$$

$$\text{So, } \frac{dS}{dt} = k_1 \left(\frac{V_i}{L} - \frac{(1-d)v_{dc}}{L} - \dot{x}_1 \right) = k_1 \left(\frac{V_i}{L} - \frac{(1-(d_{eq} - k \cdot \text{sign}(S)))v_{dc}}{L} - \dot{x}_1 \right) \quad (2.29)$$

Knowing that the expression $k_1 \left(\frac{V_i}{L} - \frac{(1-d_{eq})v_{dc}}{L} - \dot{x}_1 \right) = 0$, the equation (2.31) became:

$$\text{So, } \frac{dS}{dt} = -k_1 k \cdot \text{sign}(S) \frac{v_{dc}}{L} \quad (2.30)$$

The expression of Equation (2.28) can be written as:

$$\frac{dV}{dt} = S \dot{S} = -k_1 k S \text{sign}(S) \frac{v_{dc}}{L} \quad (2.31)$$

Using the following inequality one gets (Tidjani et al., 2014):

$$\text{So, } \text{sign}(S) \leq S \quad (2.32)$$

$$\text{So, } \frac{v_{dc}}{L} S \text{sign}(S) \leq |S| \left| \frac{v_{dc}}{L} \right| \quad (2.33)$$

$$\text{One gets for } \frac{dV}{dt} = -k_1 k \left| \frac{v_{dc}}{L} \right| < 0 \quad (2.34)$$

The Lyapunov function is negative definite if $k > 0$ and $k_1 > 0$.

The implementation of sliding mode control is shown in Figure 2.11.

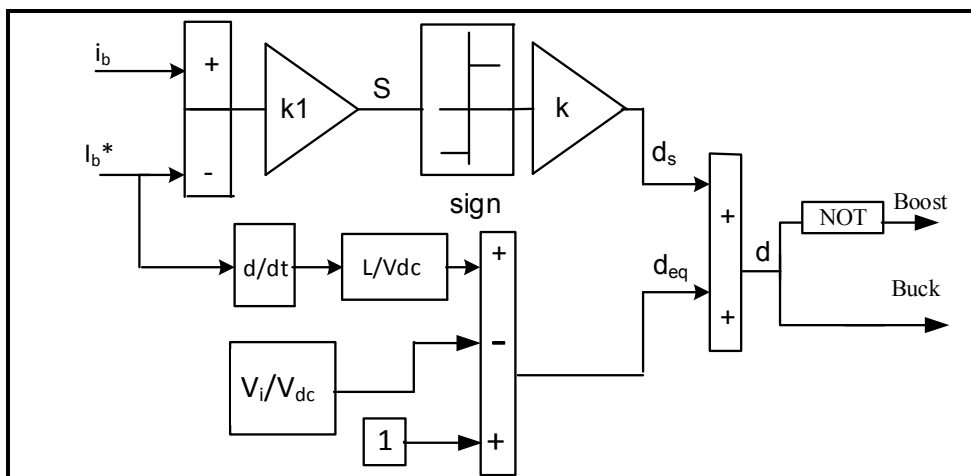


Figure 2.11 Bloc diagram of sliding mode control for battery charger

2.5.2 Modeling of the five level DC-AC bidirectional battery charger

The DC-AC five level converter is a part of PHEV battery charger mentioned previously is modeled using the Figure 2.12.

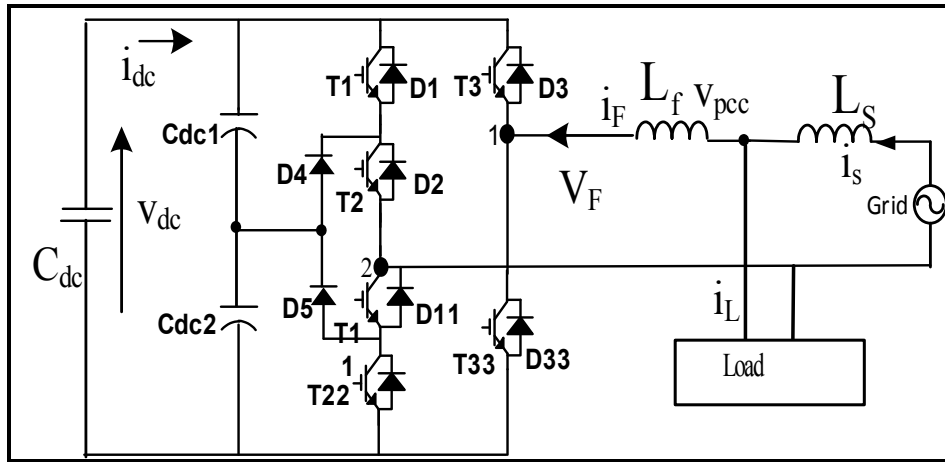


Figure 2.12 Five level dc-ac converter

The expression of the voltage and current of the converter are given by the following equations:

$$L_f \frac{di_f}{dt} = -d * v_{dc} + v_{pcc} \quad (2.35)$$

$$i_{dc} = C_{dc} \frac{dv_{dc}}{dt} = d^* i_f$$

$$L_f \frac{di_f}{dt} = -d * v_{dc} + v_{pcc} \quad (2.36)$$

$$i_{dc} = C_{dc} \frac{dv_{dc}}{dt} = d^* i_f$$

The necessary current reference to regulate the DC bus voltage is given by:

$$C_{dc} \frac{dv_{dc}}{dt} = \frac{d^* v_{dc}}{v_{dc}} i_{f0} = \frac{v_{pcc}}{v_{dc}} i_{f0} \quad (2.37)$$

Where i_{f0} is the active current to regulate the DC bus voltage. The sliding mode control is used to control the inverter current through the dynamic equation given in (2.37). Let's choose the sliding surface to be:

$$S = k(i_f - i_f^*) \quad (2.38)$$

The derivative of the sliding surface is given by:

$$\dot{S} = k \left(\frac{di_f}{dt} - \frac{di_f^*}{dt} \right) = k \left(\frac{-d_{eq}v_{dc} + v_{pcc}}{L_f} - \frac{di_f^*}{dt} \right) = 0 \quad (2.39)$$

The equivalent control law is given by:

$$d_{eq} = \frac{L_f}{v_{dc}} \left(\frac{v_{pcc}}{L_f} - \frac{di_f^*}{dt} \right) \quad (2.40)$$

To limit the control, a chattering control is used in the control law.

$$d_s = k_1 \text{sign}(S) \quad (2.41)$$

$$d = d_{eq} - d_s = d_{eq} - k_1 \text{sign}(S) \quad (2.42)$$

To ensure the stability of the sliding mode over the entire state space of the system, let's choose a Lyapunov function as:

$$V = \frac{1}{2} S S^T \quad (2.43)$$

One must show that a Lyapunov function is strictly positive definite, if its derivative is negative definite.

$$\dot{V} = S \dot{S} = S \left(k \left(\frac{-d_{eq}v_{dc} + v_{pcc}}{L_f} - \frac{di_f^*}{dt} - \frac{k_1 \text{sign}(S)}{L_f} \right) \right) = -\frac{kk_1}{L_f} S \cdot \text{sign}(S) \quad (2.44)$$

Using the inequality: $S \cdot \text{sign}(S) < |S|$

$$\dot{V} = -\frac{kk_1}{L_f} S \text{sign}(S) \leq -\frac{kk_1}{L_f |S|} \quad (2.45)$$

The stability condition of inequality (2.45) will be satisfied by appropriately selecting the sliding mode parameters $k_1 > 0$ and $k > 0$ on which the convergence rate of the state variables depend. The Table 2.3 shows the inverter state accordingly.

Table 2.2 Switching table of the inverter

| State | V_F | T_1 | T_2 | T_3 | T_{11} | T_{22} | T_{33} |
|-------|-------------|-------|-------|-------|----------|----------|----------|
| 1 | $-V_{dc}$ | 1 | 1 | 0 | 0 | 0 | 1 |
| 2 | $-V_{dc}/2$ | 0 | 1 | 0 | 1 | 0 | 1 |
| 3 | 0 | 1 | 1 | 1 | 1 | 0 | 0 |
| 4 | 0 | 1 | 1 | 1 | 0 | 0 | 0 |
| 5 | $V_{dc}/2$ | 0 | 1 | 1 | 1 | 0 | 0 |
| 6 | V_{dc} | 0 | 0 | 1 | 1 | 1 | 0 |

2.6 Simulation results of the Net Zero Energy House

The NZEH of 8 kW based on MG concept has been designed and tested experimentally (using laboratory hardware setup) in order to ensure an interruptible power supply for voltage regulation along with harmonic reduction, power factor correction and unbalanced load compensation. The system is simulated for different stages that are summarized as below:

- Simulation result of the bidirectional battery charge for plug-in hybrid electric vehicle;
- Simulation of the house with one source of energy, the electrical grid;
- Performance of the bidirectional battery charger for plug-in hybrid electric vehicle;
- Simulation of the Net Zero Energy House model by using photovoltaic system, electrical grid, plug-in hybrid electric vehicle to ensure an uninterruptible power supply over the year.

2.6.1 Simulation result of bidirectional battery charger for PHEV

Figure 2.13 and 2.14 show the validation by simulation of the bidirectional battery charger designed for PHEV and able to connect directly to dc or to ac source. The parameters V_s , i_s , i_{comp} , i_L and V_{dc} represent the source voltage, the source current, the compensator current, the load current and the dc bus voltage respectively. Figures 2.13 and 2.14 show the conversion from ac to dc current for charging the battery pack of PHEV. From $t = 0$ to $t = 0.05s$, there is no power exchange between the grid and the PHEV (I_b). From $t = 0.05s$ to $0.2s$, the battery is injecting power but the grid is still supplying small amount of power to the load. From $t = 0.2s$ to $0.3s$, the grid is supplying the load and charging the battery.

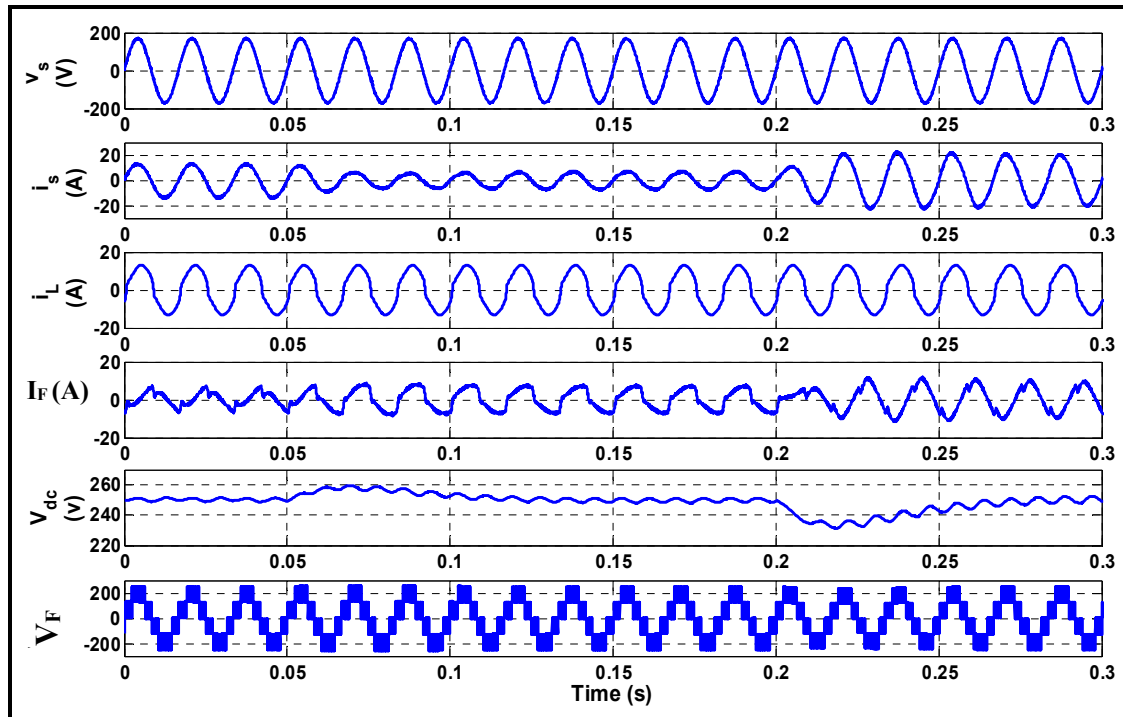


Figure 2.13 Five level battery charger for PHEV

The Figure 2.14 shows the simulation example of electric vehicle battery behavior during the charging and discharging for small variation.

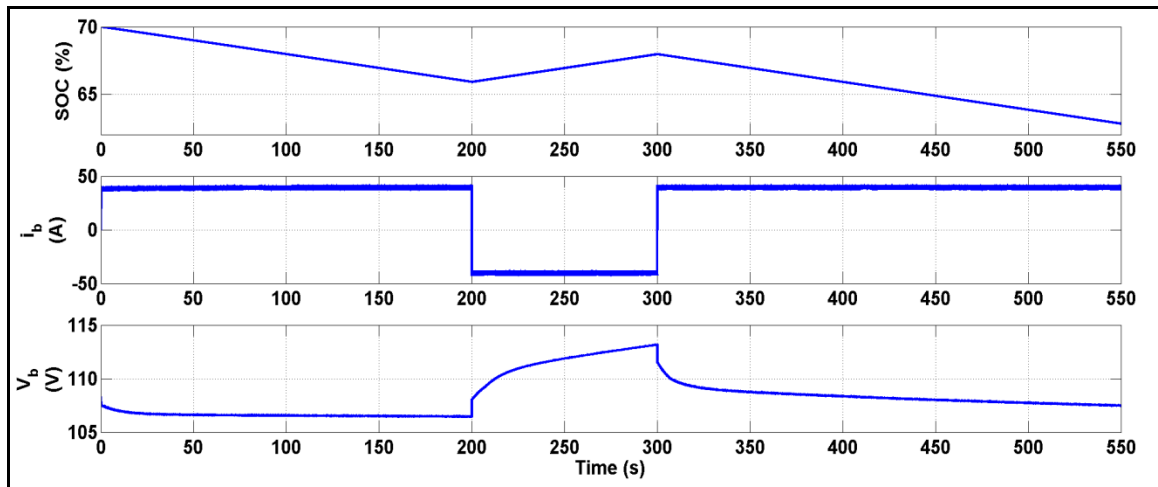


Figure 2.14 Charging and discharging of the battery

2.6.2 Simulation result of the house connected to the grid

The dynamic performance of the VSC-AHF to compensate harmonic current, reactive power and correct the unbalanced load is shown in Figure 2.15 and 2.16. Till $t = 0.05$ s, the VSC-AHF is not activated and the grid current (i_s) is distorted. From $t = 0.05$ s to $t = 0.35$ s, the VSC-AHF is activated, the harmonics current were immediately eliminated and the source current $i_s(abc)$ became sinusoidal. From $t = 0.2$ s to $t = 0.35$ s, an unbalance load is added, and the VSC-AHF was able to maintain the grid source balanced.

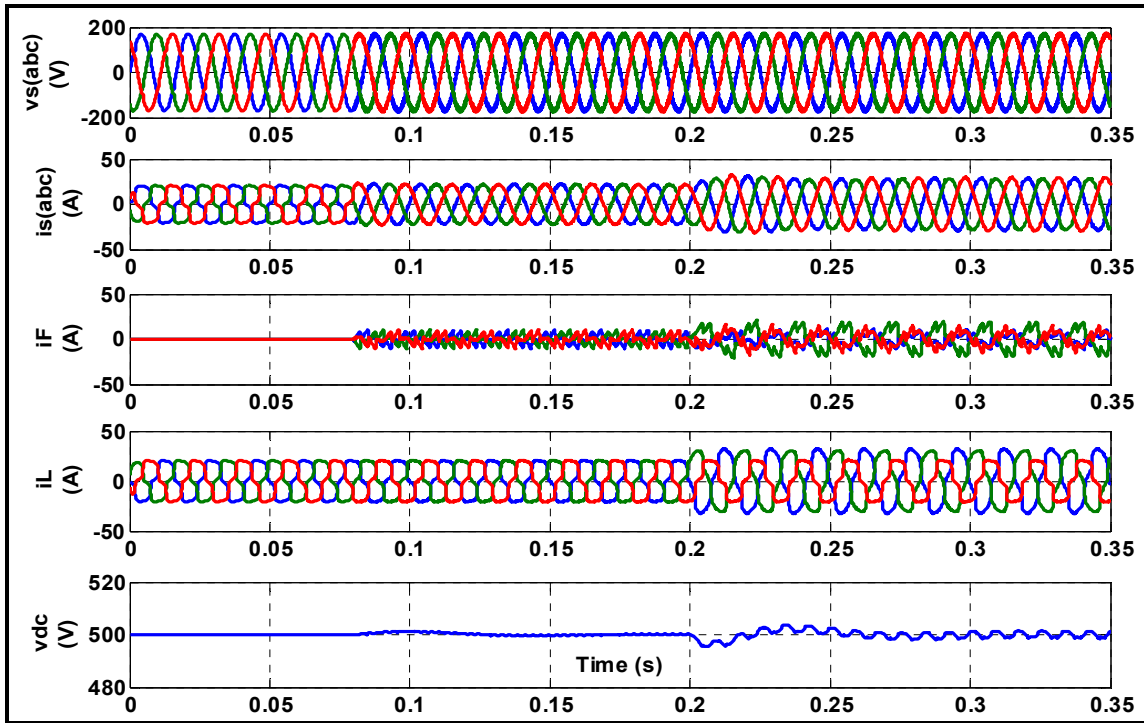


Figure 2.15 Testing the performance of VSC-AHF

Figure 2.16 shows the power flow and power management of the NZEH. The parameters Q_s , Q_L , Q_F represent respectively the reactive power of the source, load and VSC-AHF, P_s , P_L and P_F are the active power of source, load and VSC-AHF. Till $t = 0.07$, the reactive power required by the load (Q_L) is taken from the grid because the VSC-AHF is not yet activated. From $t = 0.07$ to 0.2 , the VSC-AHF generates all the amount of reactive power needed and the power factor is became the unity.

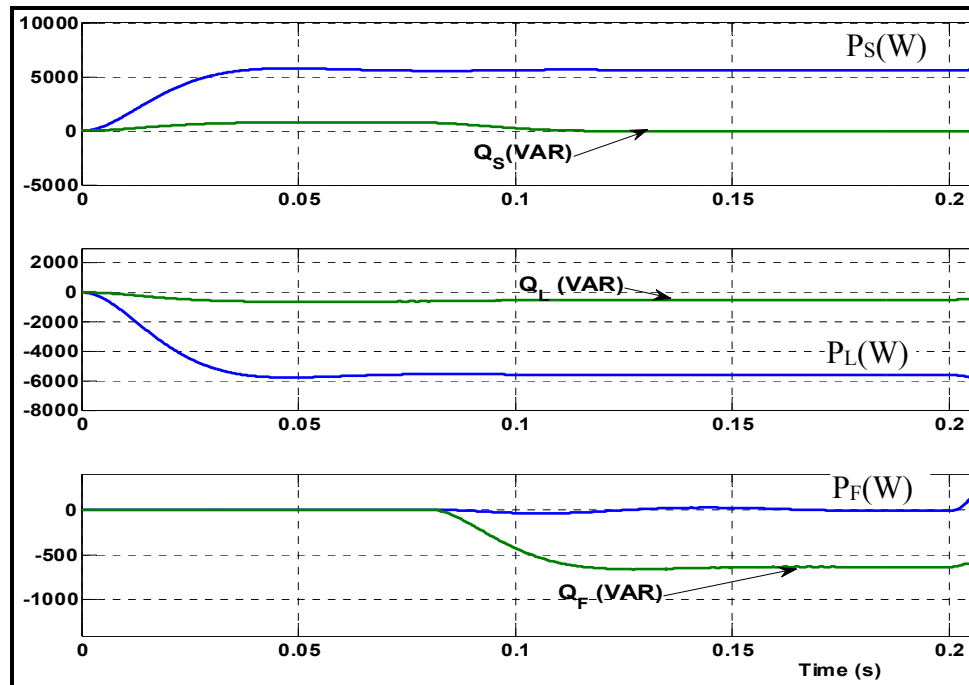


Figure 2.16 Power flow and reactive power control

2.6.3 Simulation of Net Zero Energy House for ON/OFF grid operation

Figure 2.17 shows the result of NZEH that is able to operate when connected to the grid or in standalone system (see the zoom in Figure 2.18 and 2.19). The different energy sources used for this test are the PHEV, battery for emergency, PVS and the electrical grid. The power flow between these different sources and NZEH is managed by the VSC-AHF using the new proposed control approach.

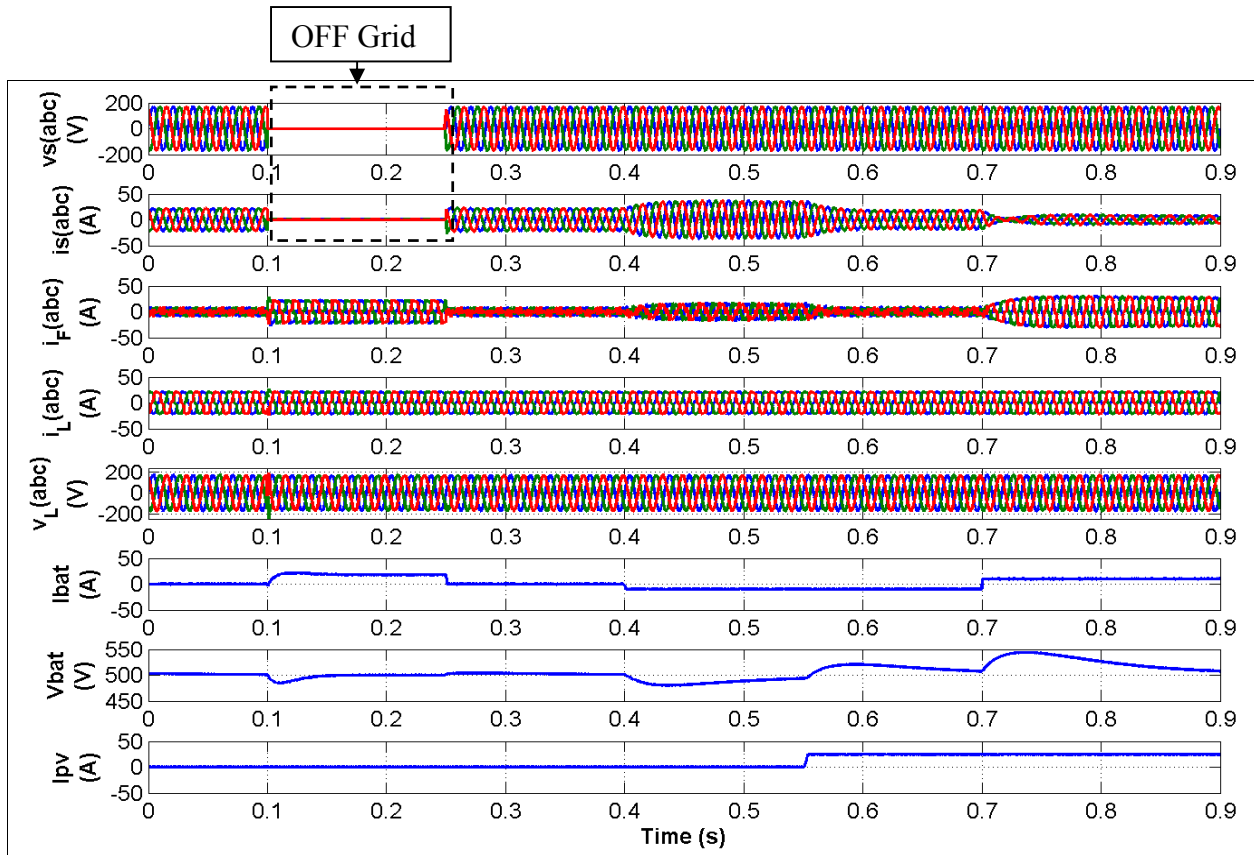


Figure 2.17 Net Zero Energy House operating in ON/OFF Grid

It is shown in the zoom of Figure 2.18, Figure 2.19, till $t = 0.1$ s, $I_{pv} = 0$, $I_{bat} = 0$, the grid is supplying alone the NZEH. From $t = 0.1$ s to $t = 0.25$ s, the grid is disappeared and the PVS do not generate any power, the battery of PHEV is starting to supply immediately the NZEH in standalone mode. The ac voltage at the PCC is well regulated and the transition between the OFF grid and standalone mode was smooth without any disturbances. From $t = 0.25$ s to $t = 0.9$, the grid is established and starts contributing by charging the battery and feeding the load.

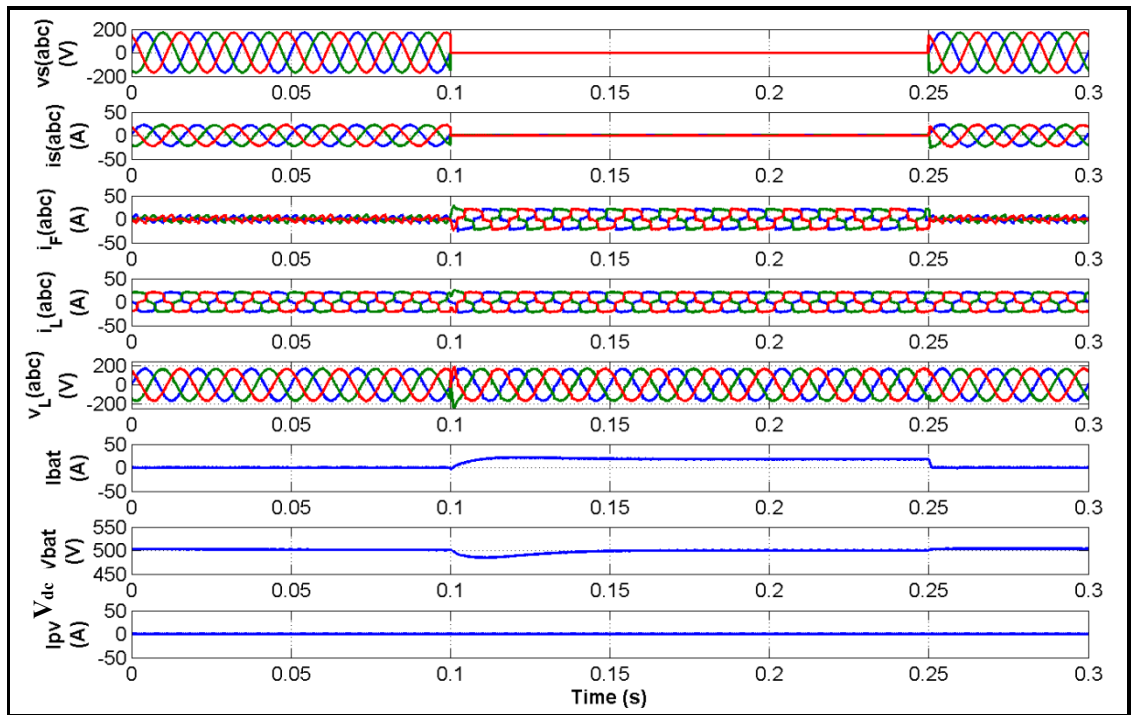


Figure 2.18 Zoom of figure 2.17

Figure 2.19 shows the zoom of Figure 2.17. From $t = 0.55$ to $t = 0.9$ s, the PVS starts generating the power, one remarks that the contribution of the grid is decreasing. In order to take care of the battery life, they are used only for emergencies.

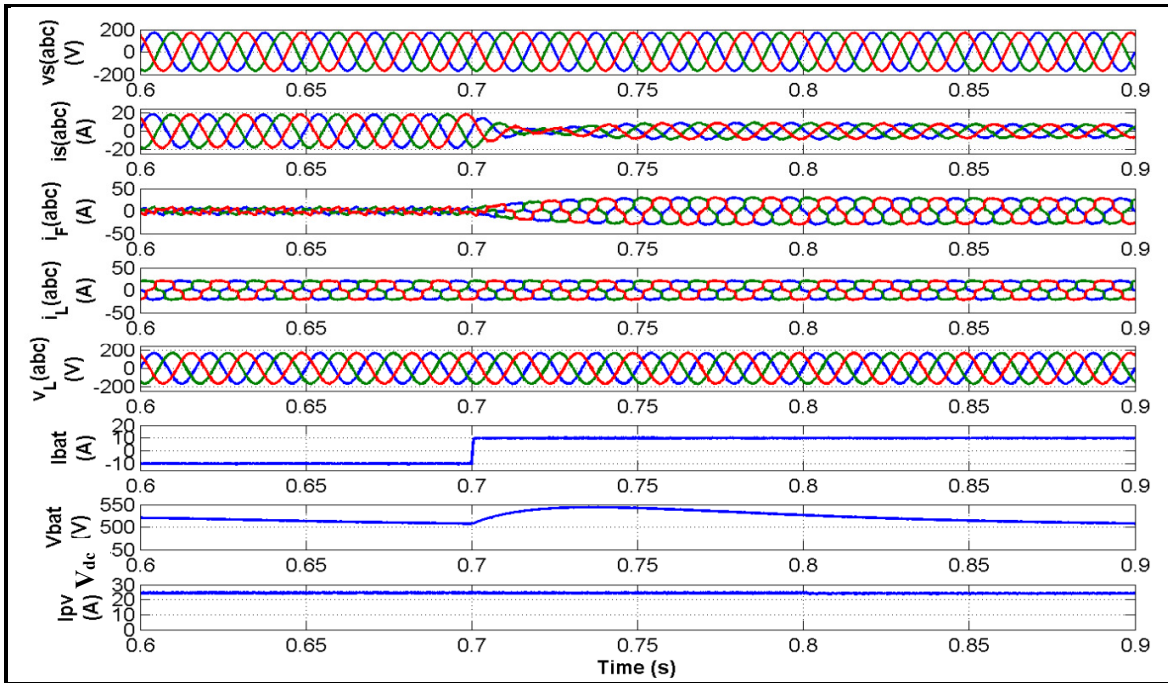


Figure 2.19 Zoom of Figure 2.17

The Figure 2.20 shows the performance of the control to compensate the unbalance when a single-phase battery charger is connected to the three phase.

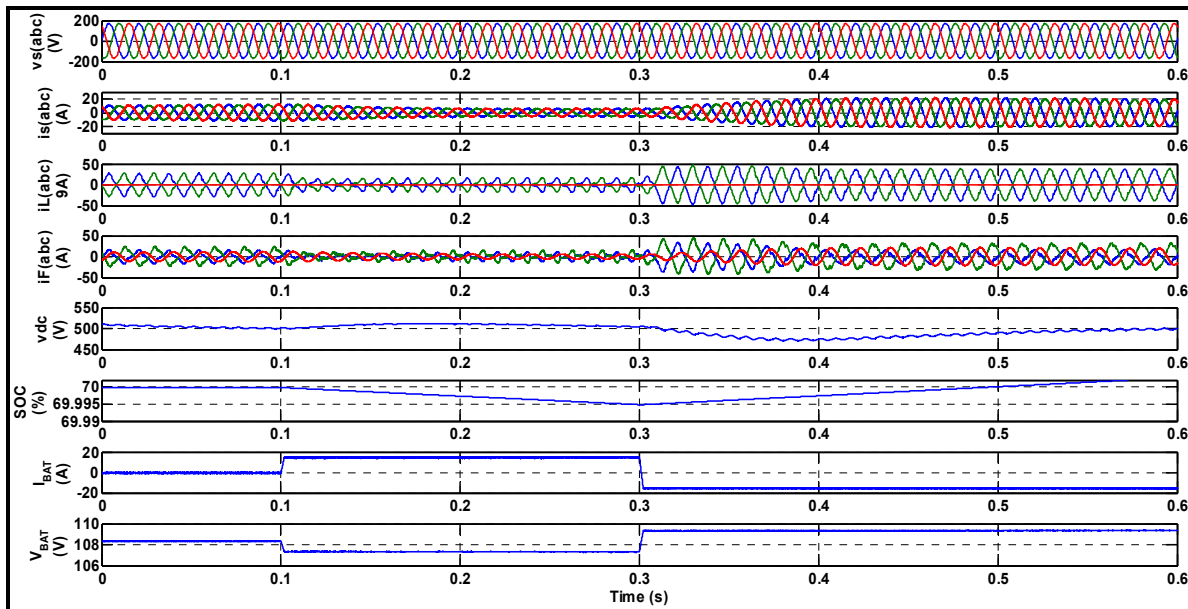


Figure: Unbalance compensation when a single phase battery charger connected to the three phase

2.7 Economic analysis using PV*Sol software

The economic analysis of the NZEH is done based on the data of city Oum-Hadjer in Republic of Chad (see Figure 2.21) using the “PV*SOL” software. PV*SOL is the solar software design tool for simulating photovoltaic system performance. It is a fully-featured program to model shading and visualize the landscape. PV*SOL enables definition of costs; performance indicators and CO2 fuel savings for a wide range of variables and optimize solar PVS performance.

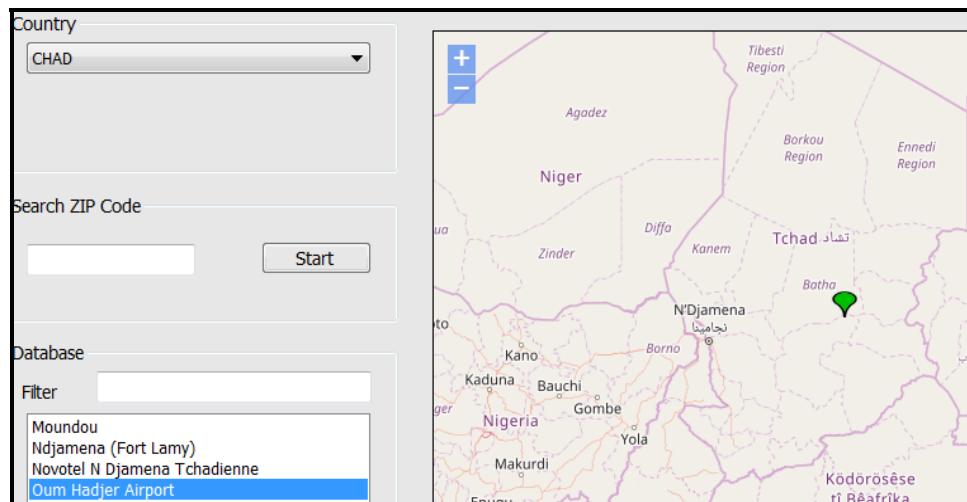


Figure 2.20 Climate Data for Oum-Hadjer City

The Figure 2.22 shows the implementation of NZEH in PV*Sol. A configuration of two inverters are used, this minimizes the risk of a total blackout in case of incident. The meters is used to calculate the amount of energy sent or received from the grid.

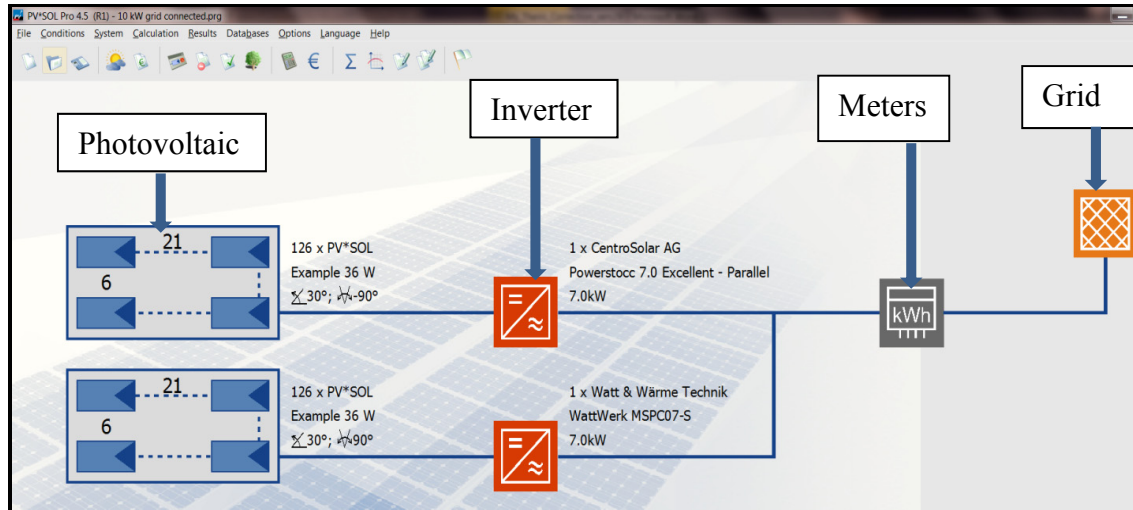


Figure 2.21 Model of the PVS connected to the grid in 2D

2.7.1 System Check and optimisation

Figure 2.23 shows the simulation and the compatibility of interconnection between different blocks of the system. The following message “simulation is not possible until you have checked and corrected the system parameters! Please observe any design recommendations made by the manufacturer” means during the system check errors are found that have to be corrected before simulation can take place. The message appears if the capacity of inverter is less than 90% or more than 110%. If the PVS output is larger than the inverter’s nominal output, the inverter must reduce the output to the inverter’s nominal output. If the PVS output is significantly less than the inverter’s nominal output, the inverter works at a low efficiency rate.

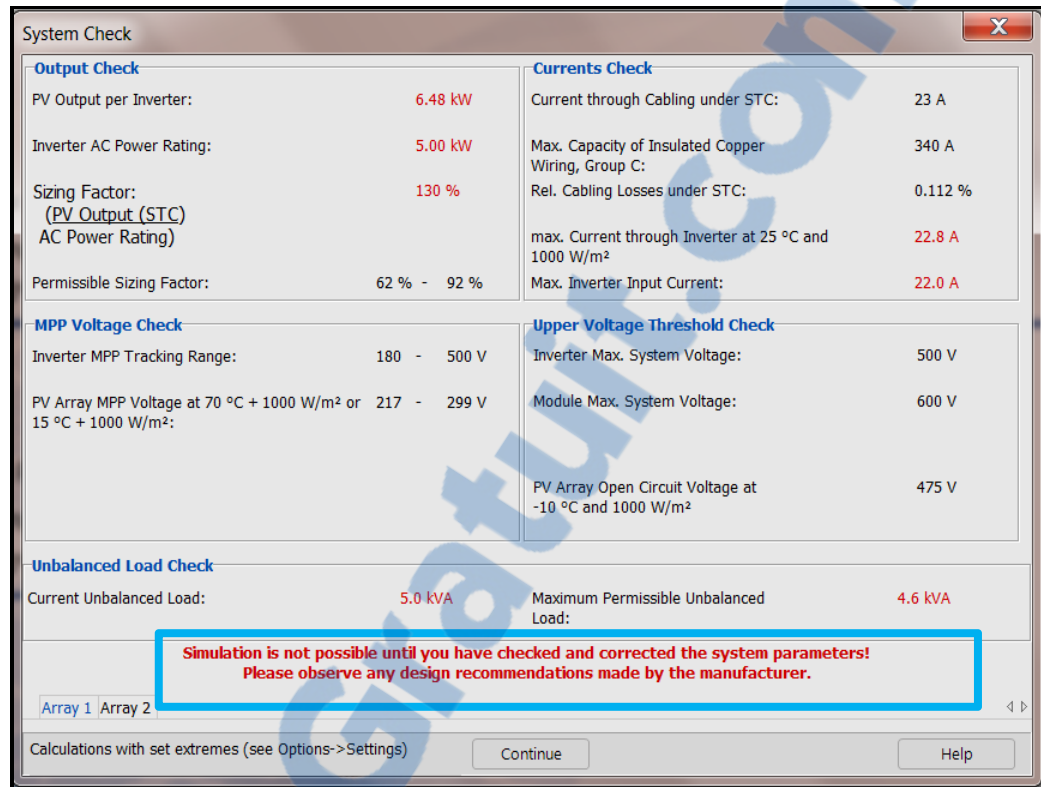


Figure 2.22 Check for the compatibility of the system

Figure 2.24 shows the new simulation with optimization parameters and replaced the previous Figure 2.23 and the problems of incompatibility have been solved.

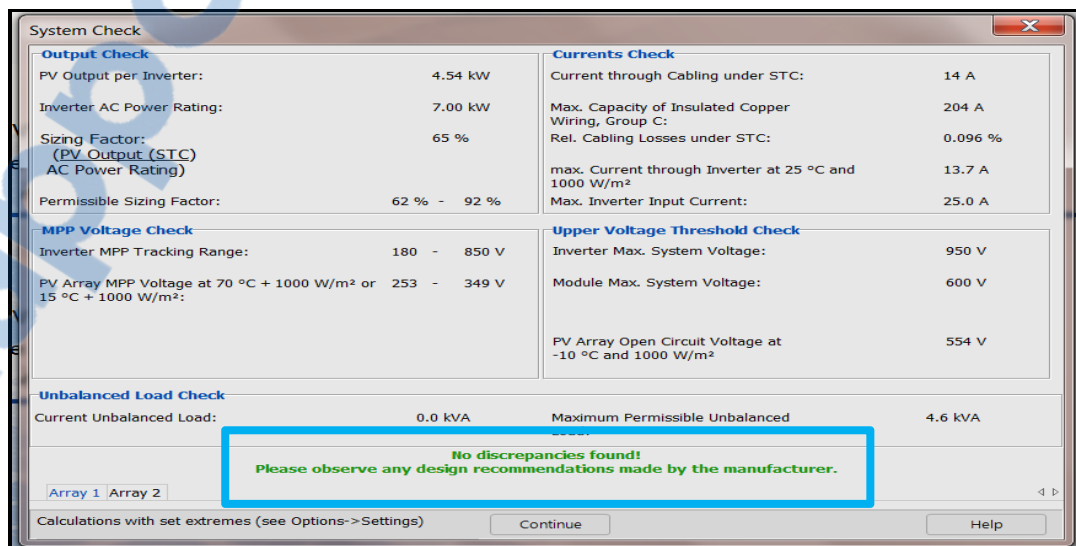


Figure 2.23 Check for compatibility of the system and optimization

2.7.2 Economic Efficiency Calculation and report

The Table 2.4 resumes the economic efficiency of the NZEH including the payback period of capital investment. The PV*Sol software has optimised the PV output power to 9.07 kWp.

Table 2.3 Report for economic efficiency calculation

| System Data | |
|--|---------------|
| System Operating Start | 01/01/2017 |
| Electricity Feed-in: | |
| Grid Concept: | Full Feed-in |
| For the First 25 Years | 0.3000 \$/kWh |
| Thereafter | 0.3000 \$/kWh |
| Basic Economic Efficiency Parameters | |
| Assessment Period | 25 Years |
| Interest on Capital | 0.00 % |
| Income and expenditure | |
| Investments | 30,000.00 \$ |
| Operating Costs | 500.00 \$/a |
| Consumption Costs | 1,000.00 \$/a |
| Other Costs | 1,000.00 \$/a |
| One-off Payments | 45.36 \$ |
| Other Income/Savings | 2,000.00 \$/a |
| Feed-in Payment Received in First Year | 3,793.70 \$/a |
| Tax | |
| Tax Rate: / from Year 10 | 5.0 % |
| Depreciation Period | 10 Years |
| | |
| Results According to Net Present Value Method | |
| Net Present Value | 55,446.36 \$ |
| Payback Period | 9.2 Years |
| Electricity Production Costs | 0.29 \$/kWh |

The Figure 2.25 shows that the profitability of the project will start after the payback period (9.2 years) of the initial investment. However, the project remains profitable because the life cycle of the PV modules is estimated to 25 years.

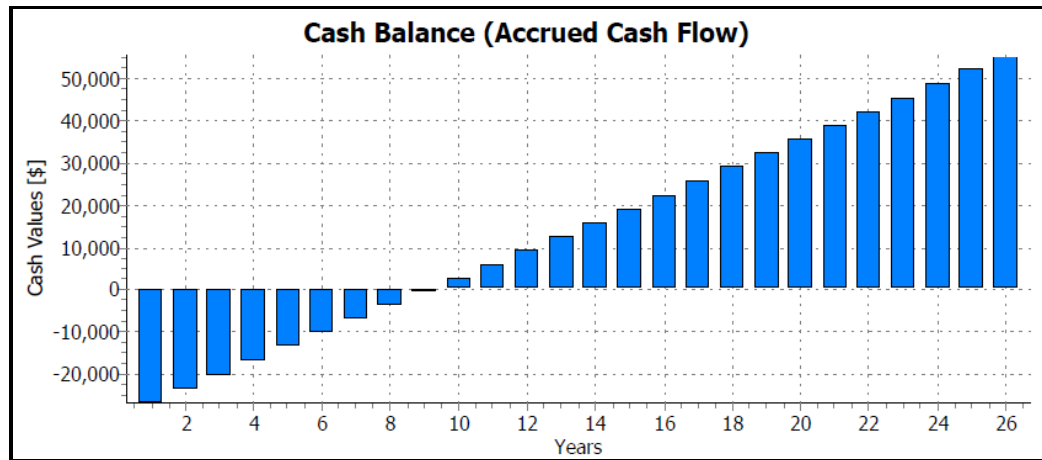


Figure 2.24 Project profitability after 9 years

2.8 Conclusion

The design and control of the Net Zero Energy House based on MG concept has been successfully carried out. Different type of control approach have been investigated in order to get the best combination of algorithm to ensure an interruptible power supply over the year, to reduce the sensors, to reduce the degree of control complexity and overall cost of the system. Promising results have been obtained by simulation for the two mode of operation: 1) ON grid operation mode: when the NZEH house is connected to the grid, the SRF control applied to VSC-AHF is activated in order to eliminate harmonics current, compensate reactive power, unbalance load and manages the power flow; 2) OFF grid operation mode: If the grid is disconnected for any reason, the second control is automatically activated to allow the system working on the standalone mode. The voltage at the PCC remains constant as shown in the simulation results. On the other hand, the developed sliding mode control for the onboard battery charger allows PHEV connecting to the dc or ac source side depending on the available socket. An economic study to determine the profitability of the NZEH has been done using the software PV*Sol. The payback period of the initial investment is estimated to 9.2 years. The project is considered to be economically profitable because the lifetime of the photovoltaic modules is at least 25 years.

CHAPTER 3

SMART HYBRID ENERGY MANAGEMENT OF STANDALONE SYSTEM BASED ON MICROGRID CONCEPT

3.1 Introduction

MG is attracting considerable attention as a solution to energy deficiency, especially, in remote areas. In order to enhance power quality and energy management reliability, MG needs optimization in terms of control and size reduction of components. This chapter analyzes three aspects: 1) Developing a new approach of active damping technique based on mathematical model of VSC without any additional sensors; 2) Reducing the size of the output LC filter by shifting the frequency and adjusting the active damping coefficient; 3) Building a fuzzy logic supervisor for smart energy management.

3.2 System description

The system under study (Figure 3.1) consists of PVS, DC-DC converter to extract maximum power from the PVS, VSC to convert the dc power to the ac power to supply the residence, regulates the ac and frequency of the output voltage. Gas generator Set is used for emergency case in order to maintain an uninterruptible power supply; dc water pump is used as damping load to absorb the extra power when the battery is fully charged. The electric vehicle can be used to maintain power supply of the load in case of emergency when the GGS and the PV are out of operation.

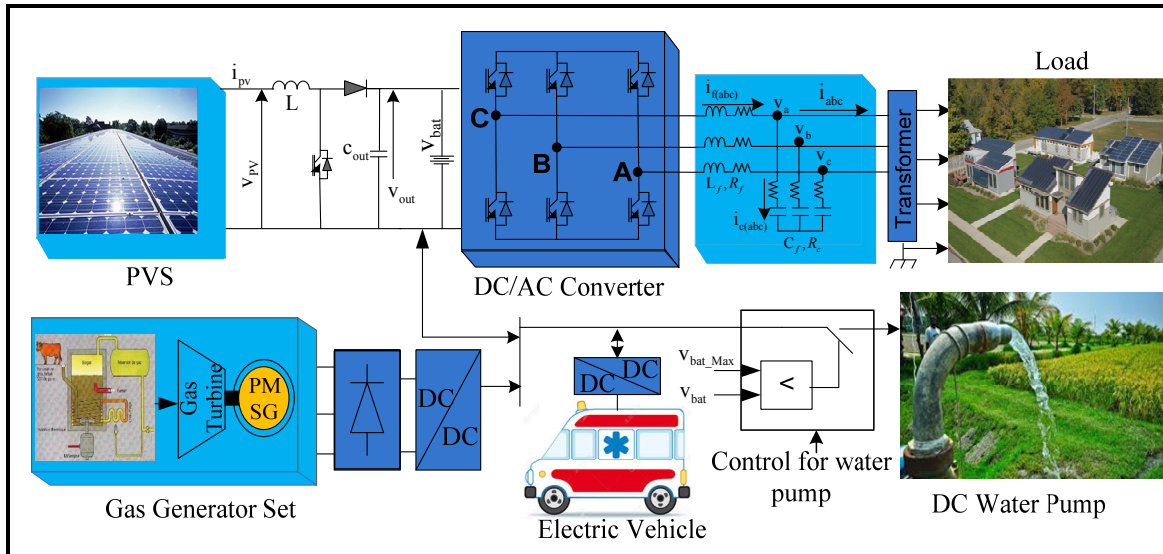


Figure 3.1 Smart MG system designed for remote area

3.3 Step for calculation of total energy demand and power supply

An optimal design of MG system for remote area requires detailed knowledge of climate data, load profile and daily energy consumption in order to define the right size and the right choice among the available energy resources.

3.3.1 Estimated daily energy consumption and specification of the load

The load is represented by many small houses. The daily energy consumption is calculated by the Equation (3.1) and recapitulated in Table 3.1.

$$E_L = \sum_{i=1}^k P_i \cdot t_i \cdot n_i, \quad (3.1)$$

Where P_i : nominal power of appliance (W);

t_i : operation time per day (h/day);

n_i : Number of appliances;

The number of appliances and the corresponding daily energy consumption are recapitulated in the Table 3.1 (Tidjani, 2012).

Table 3.1 Daily energy required for the load

| Type of appliances | Number of appliances | Total Power (P_{load}), w | Operation hour per day, hr/day | Daily load consumption, (Whr/day) |
|--|----------------------|-------------------------------|--------------------------------|-----------------------------------|
| AC load | | | | |
| Refrigerator | 10 | 800 | 24 | 19200 |
| Split solar air conditioner (1200 BTU) | 15 | 6000 | 10 | 60000 |
| TV | 10 | 800 | 3 | 2400 |
| Computers | 10 | 4000 | 4 | 32000 |
| Washer/dryer | 10 | 1100 | 1 | 11000 |
| vacuum cleaner | 10 | 7700 | 1 | 7700 |
| Lighting economic | 75 | 900 | 5 | 4500 |
| Dishwasher | 5 | 5000 | 2 | 10000 |
| E_{L_AC} (Whr) | | | | 136 000 |
| DC load | | | | |
| Batteries | | 2000 | 7 | 14000 (E_{bat}) |
| Electric vehicle | 1 | 5000 | 6 | 30000 |
| E_{L_DC} (Whr) | | | | 44 000 |
| Total daily energy E_L (Whr) | | | | 180 000 |

E_{L_AC} is the sum of the daily AC load and E_{L_DC} is the sum of the daily DC load. The total daily energy consumption $E_L = E_{L_AC} + E_{L_DC} = 180\ 000$ Whr.

3.3.2 Size evaluation of photovoltaic array

Knowing the total daily energy consumption of the load E_L , we can evaluate the optimal size of PVA using the following parameters:

Table 3.2 shows the characteristic of the photovoltaic module used for the size evaluation.

Table 3.2 Characteristics of choosing PV module X21-345

| | |
|--|--------------------------------------|
| Nominal Power P_{PV_module} | 345 W |
| Avg. Panel Efficiency | 21.5% |
| V_{mpp}(Rated Voltage) | 57.3 V |
| Rated Current (I_{mpp}) | 6.02 A |
| Open-Circuit Voltage | 68.2 V |
| Short-Circuit Current | 6.39 A |
| PV module dimensions | 1559mm x 1046mm =1.63 m ² |

The Table 3.3 resumes the different formula to calculate the size of photovoltaic array required for the installation.

Table 3.3 Calculation of peak power of photovoltaic array

| | |
|---|---|
| Calculation of average daily energy E_{PVA} required from photovoltaic system. Taking the efficiency of 95% for the dc-ac inverter and dc-dc converter | $E_{PVA} = \frac{E_L}{\eta_{dc-ac} \cdot \eta_{dc-dc}} = \frac{180000}{0.9025} = 199500 \text{ Wh}$ |
| Define the peak power of photovoltaic to install. T (4.9 hr) is the average daily number of hours for an irradiation of 1000 W/m ² and it is taken to be corresponded to month when the solar irradiation is the minimum in order to ensure the energy supply along the year (see Figure 2.2). C_p (0.95) represents the different power electronics losses. | $P_{PVA} = \frac{E_{PVA}}{T \cdot C_p} = 42 \text{ k W}$ |
| Define the total number of photovoltaic module N_t to be installed. N_p and N_s are the module connected in parallel and in series respectively. $P_{PV_module} = 345 \text{ W}$ (see Table 3.2). | $N_t = N_p \cdot N_s$ $N_s = \frac{V_{PVA}}{V_{mpp}} = \frac{220}{57.3} = 4$ $N_p = \frac{P_{PVA}}{P_{PV_module} \cdot N_s} = \frac{48000}{345 \cdot 4} = 35$ $N_t = 4 \cdot 35 = 140$ $A_{total} = A_{PVA_Array} \cdot N_T = 1.63 \cdot 140 = 228 \text{ m}^2$ |

3.3.3 Battery energy storage system capacity

Selection of battery consists to determine the capacity and voltage of battery.

The capacity of the battery is given by using the following expression.

$$C_B = \frac{E_T}{\eta_B \cdot DOD \cdot V_b} \cdot N_a = \frac{180000}{0.85 \cdot 0.85 \cdot 500} \cdot 0.5 = 250 \text{ Ah} \quad (3.2)$$

C_b = battery capacity (Ah)

E_T = daily energy consumption (Wh)

η_B = battery charging efficiency (normally 0.8 to 0.95)

V_b = battery voltage (Volt)

N_a = number of days to be operated without sunshine (Autonomy Days)

DOD = Depth of Discharge.

3.4 Modeling and control strategy of the under study system

The modeling and control strategy of the under study is presented as follows.

3.4.1 Modeling and control of photovoltaic system

A photovoltaic array is built from the connection of many photovoltaic modules. The photovoltaic module is consisted of solar cell connected in series and parallels. The Figure 3.2 shows the different steps to build a photovoltaic array.

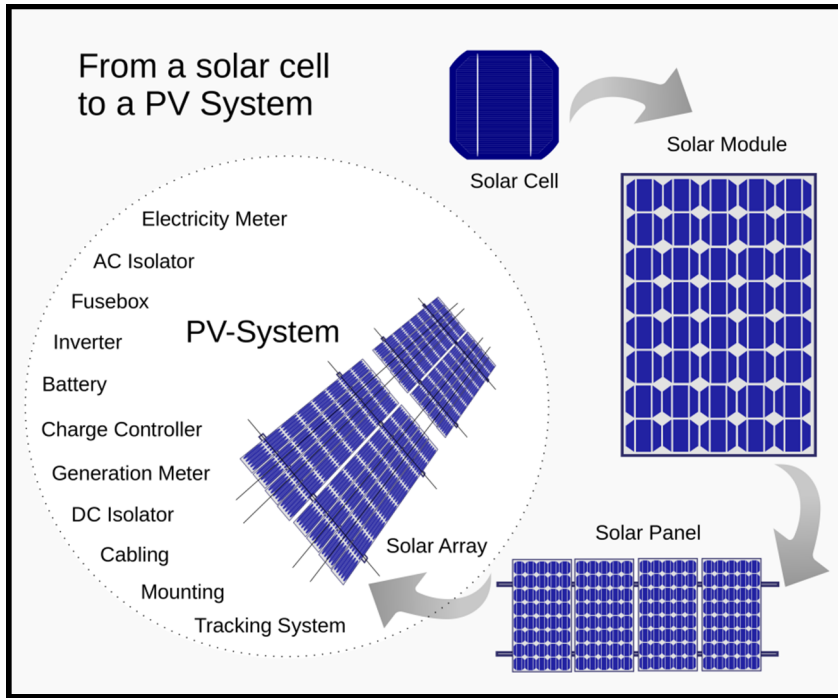


Figure 3.2 From a solar cell to the PVS

3.4.1.1 Mathematic model of solar cell

The equivalent circuit model of a solar cell is shown in Figure. 3.3.

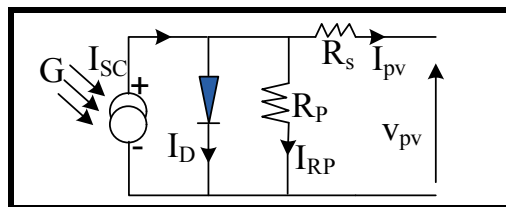


Figure 3.3 Equivalent circuit for solar cell

The mathematical model of the solar cell is given as following (Villalva, Gazoli, & Filho, 2009):

$$\begin{cases} i_D = \frac{V_{PV}}{R_P} + \frac{R_S}{R_P} I_{PV} \\ I_{PV} = I_{SC} - I_0 (e^{\frac{v_D}{v_T}} - 1) - \frac{v_D}{R_P} \\ v_D = V_{PV} + R_S I_{PV} \end{cases} \quad (3.1)$$

Where I_{SC} - short-circuit current; I_{PV} output current; v_D – Diode voltage with open circuit; I_D – current diode and it is defined as: $I_D = I_0 (e^{v_D/v_T} - 1)$; I_0 - saturation current, v_T - Thermal voltage (26 mV to 300 °K); R_P and R_S – are the parallel and series resistors respectively; V_{PV} - solar cell voltage; T - cell temperature; T_r , -reference temperature; G - solar irradiance; i_{rr} - saturation current; K_i - short-circuit temperature coefficient; q - charge of an electron; Q - total electron charge; K_b - Boltzmann's constant, E_g - band-gap energy of the material; A - Ideality factor.

3.4.1.2 Modeling of photovoltaic module

A photovoltaic module is a set of photovoltaic cells connected in series and parallel to obtain the desired voltage and current. From equation (3.1), we can write for one solar cell the following equation:

$$\begin{cases} v_D = \frac{V_{PV}}{N_S} + \frac{R_S}{N_P} I_{PV} \\ I_{PV} = N_P I_{SC} - N_P I_0 (e^{\frac{v_D}{v_T}} - 1) - \frac{V_{PV} + R_S I_{PV}}{R_P} \end{cases} \quad (3.2)$$

With $N_P = N_S = 1$

For a photovoltaic module, we can rewrite the equation (3.2) with N_P and $N_S > 1$

$$I_{PV} = N_p I_{SC} - N_p I_0 \left(e^{\frac{V_{PV} + R_s I_{PV}}{N_s} \frac{R_s I_{PV}}{N_p}} - 1 \right) - \frac{V_{PV}}{R_p} - \frac{R_s I_{PV}}{R_p} \tag{3.3}$$

The Figure 3.4 and 3.5 show the model of photovoltaic module implementation in Matlab Simpower system and some result of simulation. Figure 3.5 shows the example of simulation results of the photovoltaic module (in Watt) under different amount of solar irradiation.

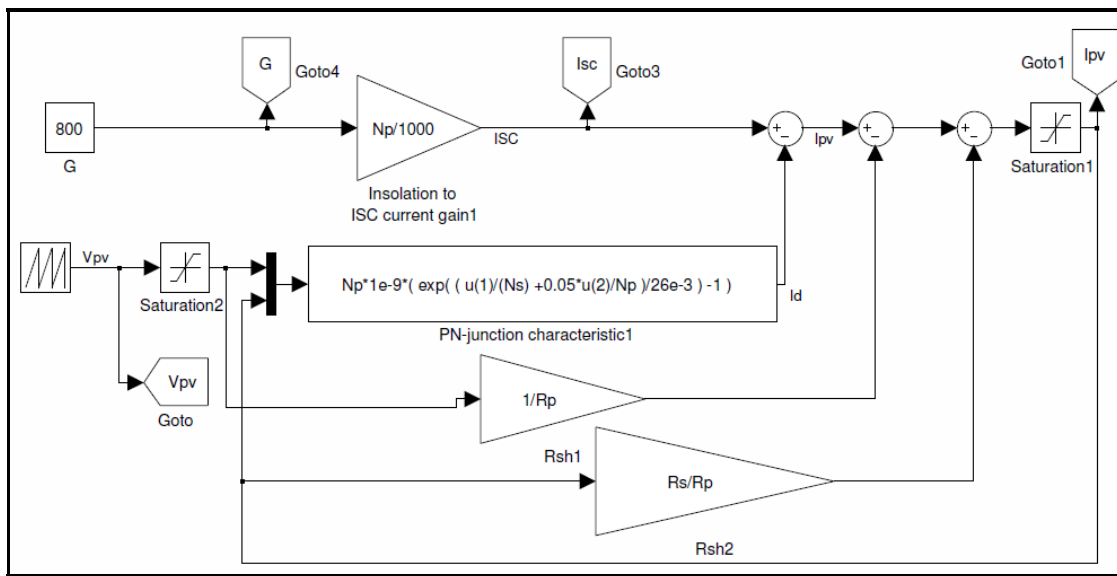


Figure 3.4 Implementation of photovoltaic module in Matlab

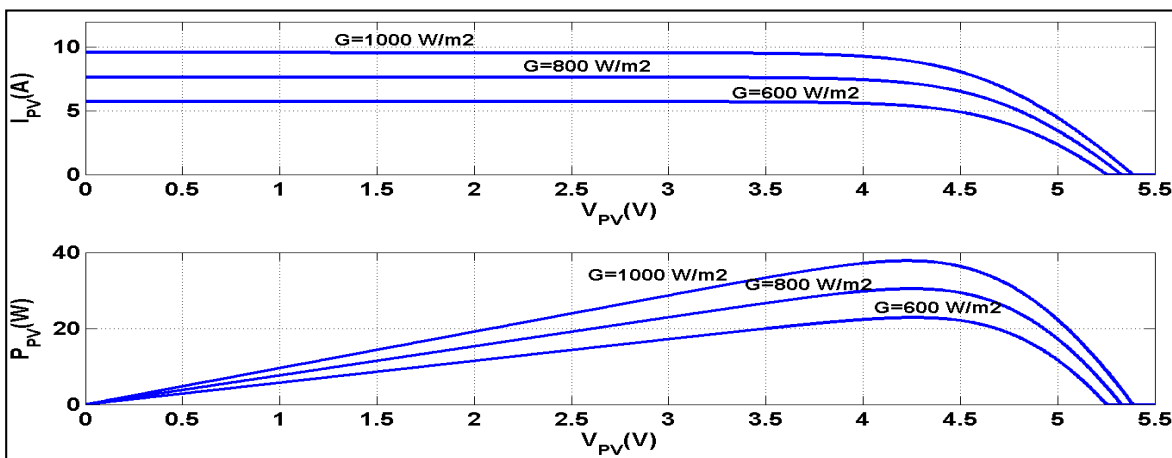


Figure 3.5 Result of PV module implementation

3.4.2 Gas generator set and its advantages

The gas generator set (GGS) with natural gas or biogas as a fuel is efficient and widely used. Natural gas is cleaner, less expensive than other non-renewable fuels, and is considerably efficient but is extremely explosive and its production requires more investment. However, biogas is a cheaper technology and the production can be carried out through many small plants or one large plant. A single cow can provide enough waste material within a day to power a light bulb the entire day. For this project, biogas is chosen as a fuel to operate the gas generator set.

3.4.2.1 Control strategy of GGS

The control strategy of GGS (Figure 3.6) is based on power balance technique between the power generated by the photovoltaic system (PVS) and the load demand. This is allowing to control GGS speed and gas injection in order to generate only the needing power when the PVS is not able to satisfy the demand. The power balance technique is given in Equation 3.4.

$$P_{GGS} = P_{PVS} - P_{Load} \quad (3.4)$$

The transfer function of the GGS is given by (Rezkallah, Chandra, & Singh, 2013).

$$\frac{T_{mec}(s)}{\Delta N_{gas}(s)} = \left(\frac{T_1 s + 1}{T_2 s + 1} \right) \left(\frac{1}{T_3 s + 1} \right) e^{-T_D s} \quad (3.5)$$

where ΔN_{gas} is the quantity of gas injection, T_{mec} -mechanical torque, T_D - dead time. T_1 , T_2 and T_3 represent the gain. The input of PI is the difference between ω_{ref} and ω that represents the reference and measured speed respectively.

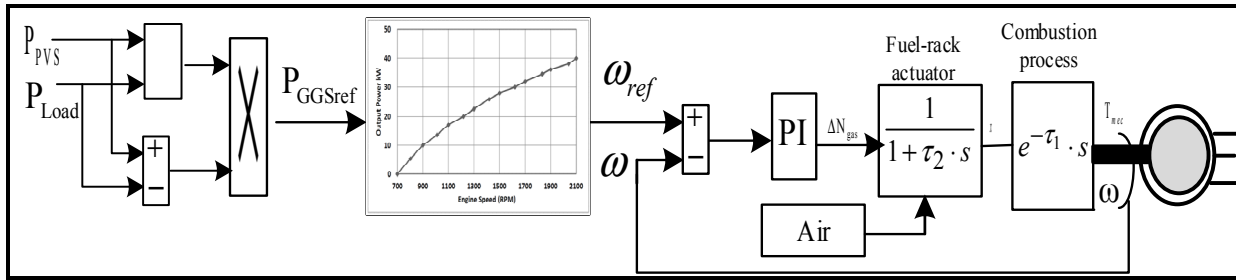


Figure 3.6 Control diagram of GGS

3.5 Developing of active damping approach for VSC

The VSC are intended to provide a controlled sinusoidal voltage with low total harmonic distortion (THD). A common practice to reduce the switching harmonics in the output voltage of the converter is to insert an LCL filter between the terminal of the inverter and the common AC bus. The presence of the LCL filter brings the risk of harmonic resonance of the filters. Many methods have been proposed to improve the stability of an LCL filtered VSC among which the passive and active damping approaches. The passive damping approach utilizes a damping resistor in series or shunt with the filter capacitor / inductors. The passive damping resistor is robust and sometimes introduces un-acceptable power loss. Active damping approach involves only change in the control loops and does not bring additional power loss. However, the performance of the active damping depends on the used approach. In this section, an active damping method (without any additional sensor) equivalent to the implementation of resistors R_c (see Figure 3.7) is suggested and it is shown that the bandwidth of the LCL filter with the proposed damping method can be extended further than that with a conventional passive damping. The idea is either to limit the bandwidth of the current controller so that the PWM converter does not excite the resonance of the LCL filter or to actively damp the resonance with feedback, from the LCL filter capacitor voltage or current.

Before introducing the effectiveness of the active damping control, one mentioned the disadvantage of passive damping technique (Cho, Lee, & Sul, 2015; Geng et al., 2017; Samanes & Gubía, 2017).

The idea is either to limit the bandwidth of the current controller so that the PWM converter does not excite the resonance of the $L_f C_f$ filter or to actively damp the resonance with feedback, from the $L_f C_f$ filter capacitor voltage or current. Before introducing the effectiveness of the active damping control, one mentioned the disadvantage of passive damping technique.

3.5.1 Passive damping approaches and their disadvantages

The $L_f C_f$ filter with passive damping resistor R_c is shown in Figure 3.7 (Hamoud, Doumbia, & Chériti, 2015).

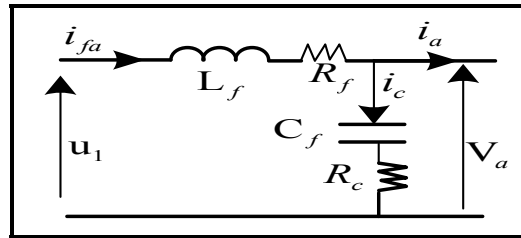


Figure 3.7. Output filter with damping resistor R_c

The transfer function extracted from Figure 3.7 is deduced as follow:

$$\frac{V_a}{u_1} = \frac{R_c + \frac{1}{jC_f \omega}}{R_c + \frac{1}{jC_f \omega} + jL_f \omega + R_f} = \frac{jR_c C_f \omega + 1}{j^2 L_f C_f \omega^2 + j\omega(R_c C_f + jR_f C_f) + 1} \quad (3.6)$$

Using Laplace parameter $s = j\omega$, the transfer function becomes:

$$G_0 = \frac{sR_c C_f + 1}{s^2 L_f C_f + s(R_c C_f + R_f C_f) + 1} \quad (3.7)$$

For the value of $L_f = 1.5e-3$ mH; $C_f = 20$ μ F; $R_f = 0.1$ Ω and for different values of damping resistor $R_c = [0 \ 5 \ 10]$ Ω .

3.5.2 Power losses calculation in the damping resistor R_c

The power losses for the damping resistor $R_c = 10$ Ω are calculated as follows:

$$I_c = \frac{V_{LL} / \sqrt{3}}{Z_T} = 2.7 \text{ A} \quad (3.8)$$

$$\text{where } Z_T = \sqrt{R_c^2 + \left(\frac{1}{C_f \omega}\right)^2} = \sqrt{100 + \left(\frac{1}{20 \cdot 10^{-6} * 377}\right)^2} = 133 \text{ } \Omega \quad (3.9)$$

So the power losses in one phase are calculated as:

$$P_{R_c} = R_c \cdot I_c^2 = 10 \cdot (2.7)^2 = 72.9 \text{ W} \quad (3.10)$$

The total power losses in three phases are deducted as:

$$P_{3\phi R_c} = 3 \cdot P_{R_c} = 3 * 72.9 = 218.7 \text{ W} \quad (3.11)$$

These losses are present 24 hours regardless of the loading condition. One remarks in Figure 3.8, the intersection point for different values of R_c is the same, it is meaning there is no flexibility in the resonant frequency to reduce the output filter size and reducing the power losses.

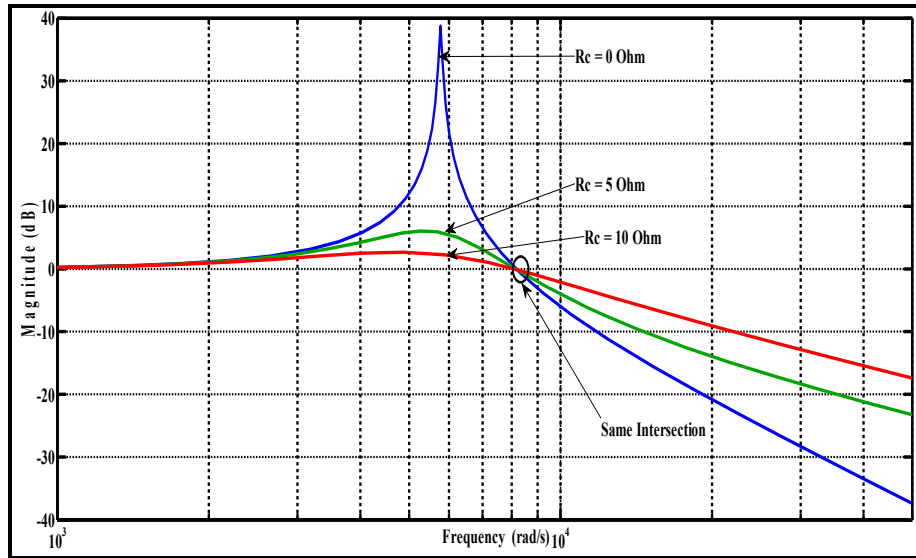


Figure 3.8. Bode diagram of output filter with damping resistor R_c

3.5.3 Development of active damping approach

Figure 3.9 shows the new configuration of $L_f C_f$ filter without passive damping resistor R_c . The objective is to develop a modeling approach to integrate the active damping technique in the control of the VSC without any additional sensors. The major benefit of active damping is its adaptive nature, which also makes it effective against disturbances originating from the grid. In addition it helps decreasing the losses caused by the physical passive damping resistor, improving the voltage quality at the PCC.

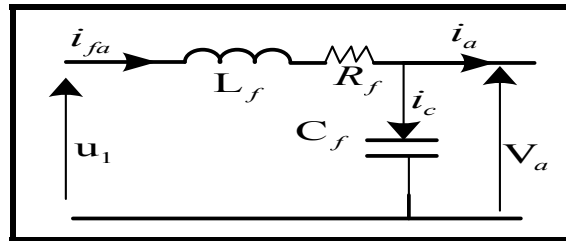


Figure 3.9 Output filter without damping resistor

The theory of active damping is based on mathematical model of VSC given by the following equations (Tidjani et al., 2014):

$$\left\{ \begin{array}{l} L_f \frac{di_{fa}}{dt} + R_f i_{fa} = u_1 - v_a \rightarrow u_1 = v_a + u_{fa} \\ L_f \frac{di_{fb}}{dt} + R_f i_{fb} = u_2 - v_b \rightarrow u_2 = v_b + u_{fb} \\ L_f \frac{di_{fc}}{dt} + R_f i_{fc} = u_3 - v_c \rightarrow u_3 = v_c + u_{fc} \end{array} \right. \quad (3.12)$$

where u_1 , u_2 and u_3 are the control laws; v_a , v_b and v_c the load voltage; i_{fa} , i_{fb} , and i_{fc} the filter currents; u_{fa} , u_{fb} and u_{fc} are the equivalent inputs.

The capacitors currents $i_{c(abc)}$ are given by the following equation:

$$\left\{ \begin{array}{l} i_{ca} = C_f \frac{dv_a}{dt} = i_{fa} - i_a \\ i_{cb} = C_f \frac{dv_b}{dt} = i_{fb} - i_b \\ i_{cc} = C_f \frac{dv_c}{dt} = i_{fc} - i_c \end{array} \right. \quad (3.13)$$

The regulation of the load voltage using dynamic Equation (3.13) with PI controller estimates the reference capacitor currents i_{ca}^* ; i_{cb}^* ; i_{cc}^* and given as follows:

$$\left\{ \begin{array}{l} i_{ca}^* = C_f \frac{dv_a}{dt} = i_{fa}^* - i_a \rightarrow i_{fa}^* = i_{ca}^* + i_a \\ i_{cb}^* = C_f \frac{dv_b}{dt} = i_{fb}^* - i_b \rightarrow i_{fb}^* = i_{cb}^* + i_b \\ i_{cc}^* = C_f \frac{dv_c}{dt} = i_{fc}^* - i_c \rightarrow i_{fc}^* = i_{cc}^* + i_c \end{array} \right. \quad (3.14)$$

Replacing Equation (3.14) in (3.12), one obtains:

$$L_f \frac{d\left(C_f \frac{dv_a}{dt} + i_a\right)}{dt} + R_f \left(C_f \frac{dv_a}{dt} + i_a\right) = u_1 - v_a \quad (3.15)$$

Rearranging the Equation (3.15), one gets:

$$L_f C_f \frac{d^2 v_a}{dt^2} + R_f C_f \frac{d v_a}{dt} + v_a = u_1 - R_f i_a - L_f \frac{d i_a}{dt} \quad (3.16)$$

$$v_a = \frac{u_1}{(L_f C_f s^2 + R_f C_f s + 1)} - \frac{(R_f + s L_f)}{(L_f C_f s^2 + R_f C_f s + 1)} i_a = G_1 * u_1 + G_2 * i_a \quad (3.17)$$

To study the relation between v_a and u_1 , one set $i_a = 0$, so the transfer functions is written as:

$$\left. \frac{v_a}{u_1} \right|_{i_a=0} = \frac{1}{C_f L_f s^2 + R_f C_f s + 1} = \frac{1}{s^2 + \frac{R_f}{L_f} s + \frac{1}{C_f L_f}} \quad (3.18)$$

The resonant frequency of the $L_f C_f$ filter is defined as:

$$\omega_0 = \frac{1}{\sqrt{L_f C_f}} = \frac{1}{\sqrt{1.5 \cdot 10^{-3} * 20 \cdot 10^{-6}}} = 5773.5 \text{ rad / s} \quad (3.19)$$

Let us define the Equation (3.16) which gives the transfer function from u_1 to v_a by neglecting the current i_a and is considered as a perturbation (Kanaan, 2002).

$$L_f C_f \frac{d^2 v_a}{dt^2} + R_f C_f \frac{d v_a}{dt} + v_a = u_1 \quad (3.20)$$

Let's introduce the expression $k_c i_c$ in the right side of the dynamic Equation (3.20), one obtains the following equation given by:

$$L_f C_f \frac{d^2 v_a}{dt^2} + R_f C_f \frac{d v_a}{dt} + v_a = u_1 - k_c i_c \quad (3.21)$$

Replacing $i_c = C_f \frac{d v_a}{dt} = C_f \cdot s \cdot v_a$ in Equation (3.21). The new open loop transfer function $G_1(s)$ of the plant given by:

$$G_1(s) = \frac{v_a}{u_1} = \frac{1}{L_f C_f s^2 + (R_f + k_c) C_f s + 1} = \frac{\frac{1}{L_f C_f}}{s^2 + \frac{(R_f + k_c)}{L_f} s + \frac{1}{L_f C_f}} \quad (3.22)$$

One chooses the damping factor $\zeta = 0.7$ then the choice of k_c is calculated as follows:

$$2\zeta\omega_0 = \frac{(R_f + k_c)}{L_f} \quad (3.23)$$

$$k_c = 2\zeta\omega_0 L_f - R_f = 2 \cdot 0.7 \cdot 5773.5 \cdot 0.0015 - 0.1 = 12 \quad (3.24)$$

In Figure.3.10, when the k_c increases, the damping as well as the pass band are reduced. This will help to increase the resonant frequency and to reduce the size of the output filter by choosing the appropriate value of k_c in order to increase the attenuation.

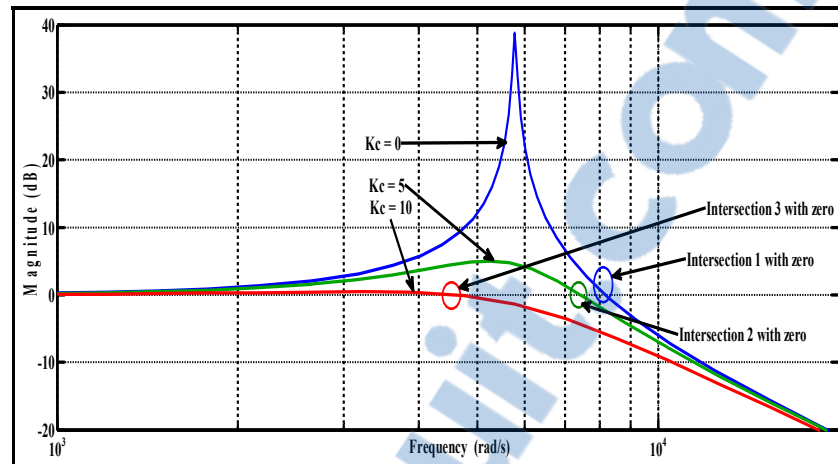


Figure 3.10 Output filter with active damping coefficient

The Figure 3.11 illustrates the comparison between the damping resistor R_c and active damping coefficient k_c . One notices during the variation of R_c , the intersection point remains the same (constant band pass), while with active damping k_c the band pass is reduced. The active damping technique gives the flexibility to choose the optimal band pass to reduce the size of output filter $L_f C_f$ and to improve the voltage quality (Tidjani et al., 2017).

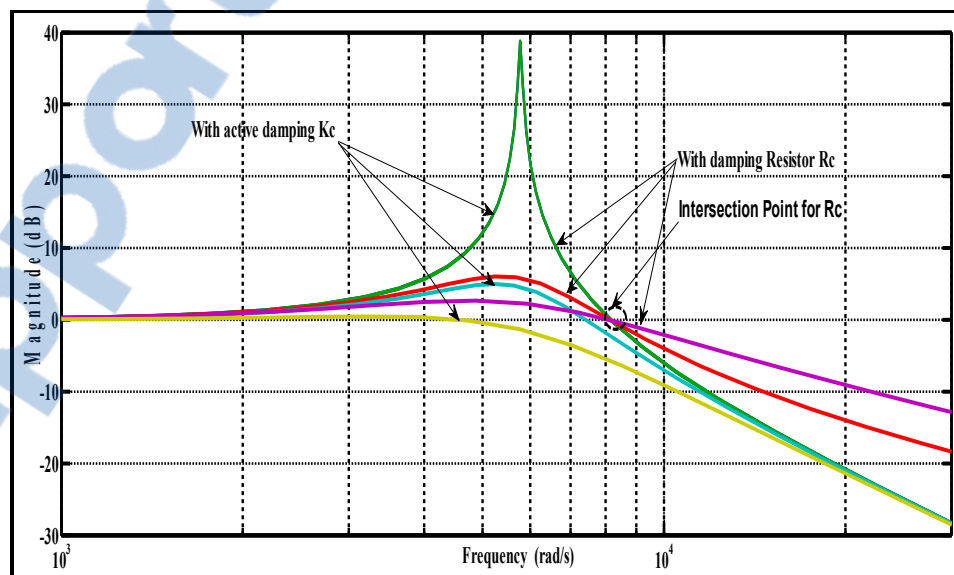


Figure 3.11 Bode Diagram of R_c and k_c

In addition, Figure 3.12 shows the performance of the active damping coefficient k_c in term of power quality. So, till $t = 0.05$, k_c is activated in the control shown and one sees the output voltage is perfectly sinusoidal. However, when the k_c was removed, the voltage is suddenly distorted from $t = 0.05$ s to 0.08 s,.

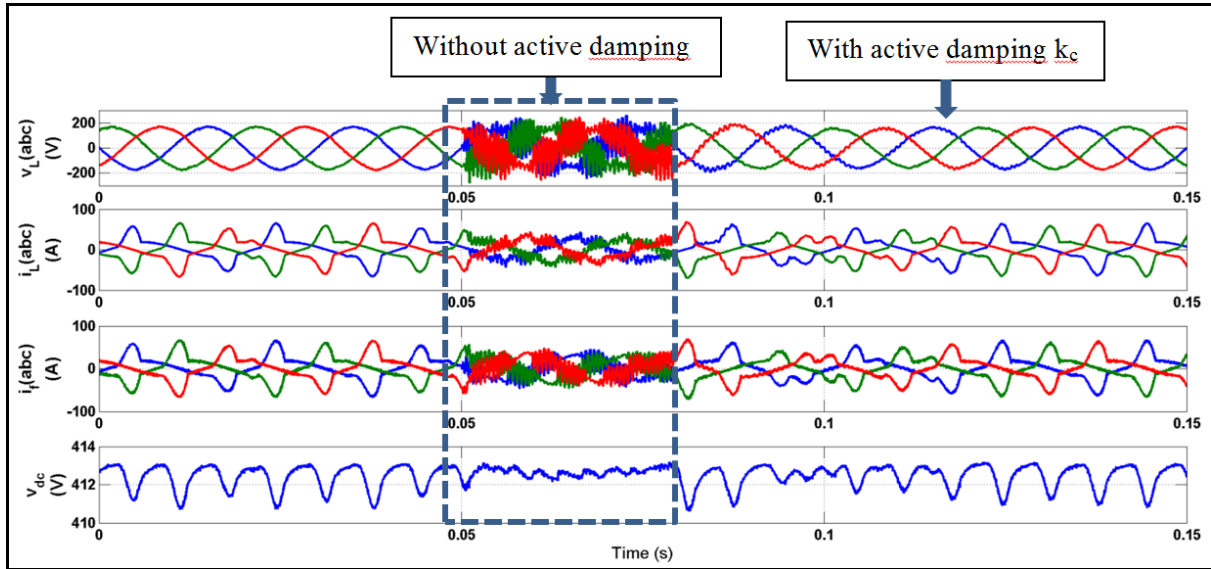


Figure 3.12 Performance of the VSC with and without active damping techniques

3.5.4 Approach for reducing the value of output filter $L_f C_f$ using active damping technique

In order to reduce the size of the $L_f C_f$ filter, knowing that the inverter will compensate until the twenty fifth harmonics order as shown in Figure.3.13, let's say $25 \times 60 = 1.5$ kHz. In Figure 3.14, the high harmonic frequency of the voltage inverter starts from 3.3 kHz, thereby, the resonant frequency is chosen at this value.

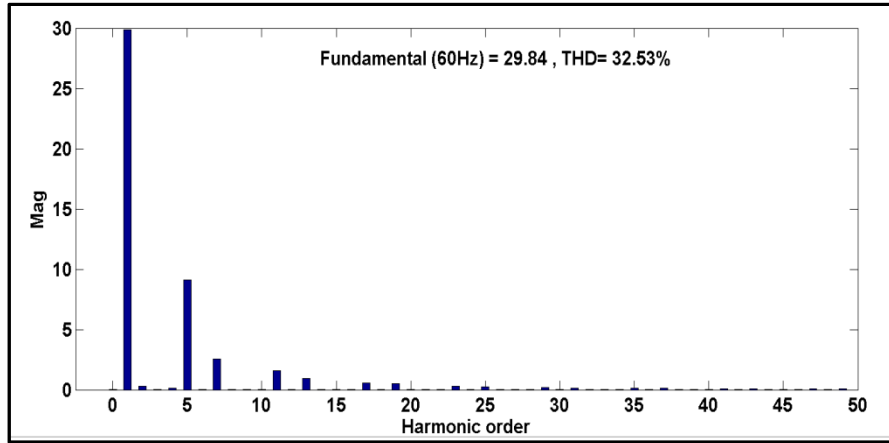


Figure 3.13 Harmonic spectrum of load current

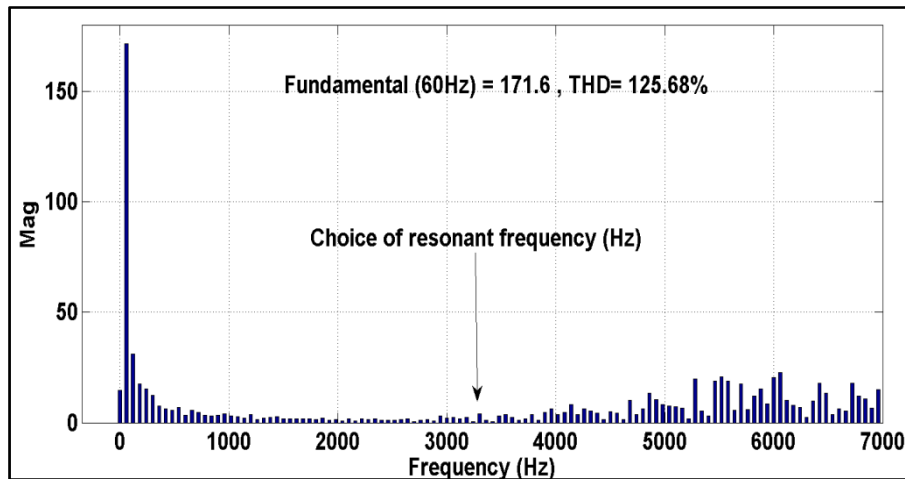


Figure 3.14 Harmonic spectrum of inverter voltage

For fixed capacitor $C_{f1} = 7.5 \mu\text{F}$, the new value of L_{f1} is calculated as follows:

$$\omega_{01} = \frac{1}{\sqrt{L_{f1}C_{f1}}} \rightarrow L_{f1} = \frac{1}{(\omega_{01})^2 C_{f1}} = \frac{1}{(21000)^2 * 7.510^{-6}} = 0.3\text{mH} \tag{3.25}$$

With this new resonant frequency ω_{01} , the coefficient $k_{c1} = 8.7$ for the value of $\zeta = 0.7$. From Figure 3.15, this value of k_{c1} does not give complete satisfactory attenuation and filtering. For better attenuation and for good response one needs to increase the value of k_{c1} by

increasing the damping factor value to be $\zeta = 2.1$. The new value of k_{c1} is then calculated as follows:

$$k_{c1} = 2\zeta\omega_{01}L_{f1} - R_f = 2 * 2.1 * 21000 * 0.0003 - 0.1 = 26 \quad (3.26)$$

In Figure 3.15, it is shown that the proposed approach technique based on active damping reduces the inductor value L_f by five times. The resonant frequency is shifted from ω_0 for value of $k_c = 20$ to ω_{01} for $k_{c1} = 26$. For both curves with $k_c = k_{c1} = 5$, one remarks that the phase margin is inside in its optimal value, this confirms the stability when shifting the resonant frequency. The value of $k_{c1} = 26$ gives better attenuation and contribute to the voltage quality improvement. In order to prove the good choice of the new parameters of the output filter, the results of Pole-Zero Map are shown in Figure 3.16. For the new resonant frequency, three values of active damping coefficient k_{c1} are plotted in pole-zero maps. When k_{c1} increases, the pole of the transfer function of the filter starts initially with complex poles ($k_{c1}=5, k_{c1}=10$) and then for $k_{c1}=26$, the poles become real.

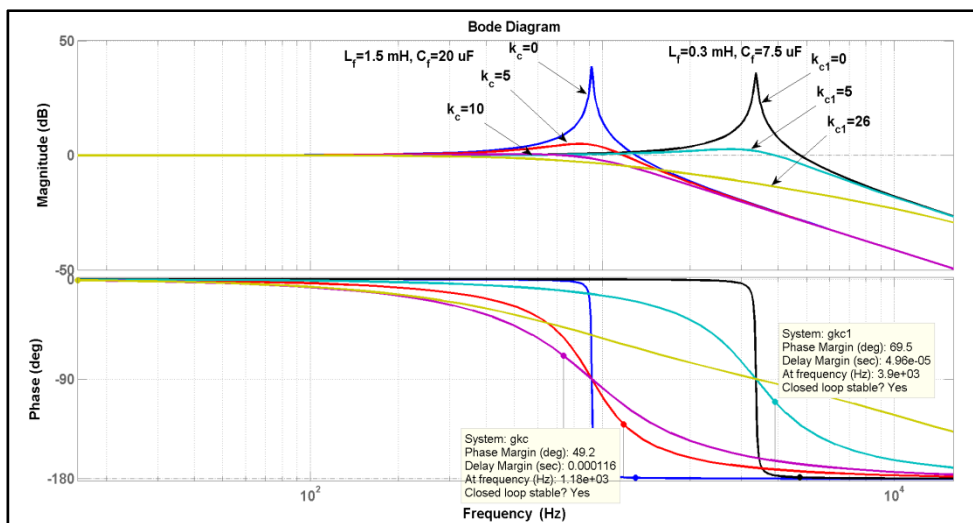


Figure 3.15 New value of output filter $L_{f1}C_{f1}$ with new damping factor

This confirms that the shift of the resonant frequency from 0.92 kHz to 3.3 kHz does not affect the stability of the system, but allows reducing considerably the size of the $L_f C_f$ filter.

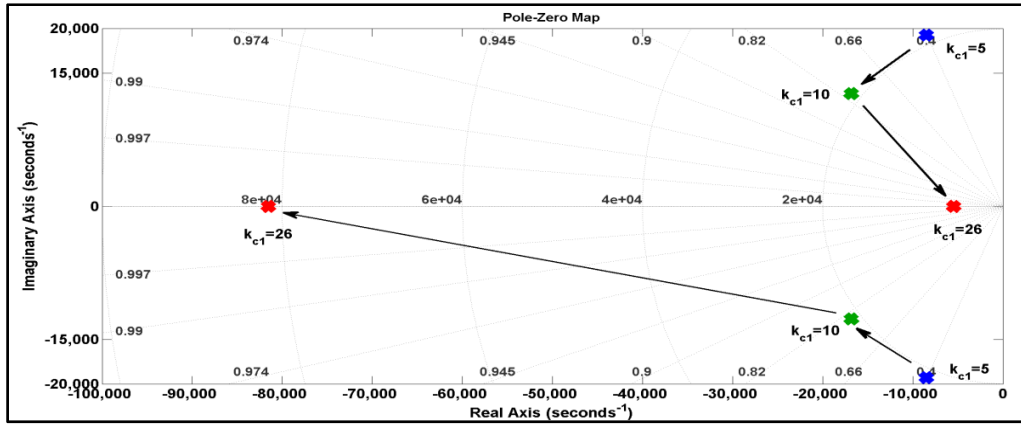


Figure 3.16 Zero and pole maps for transfer functions of the $L_f C_f$ before and after value reduction

The new control approach of VSC including the proposed active damping technique is implemented in Figure. 3.17.

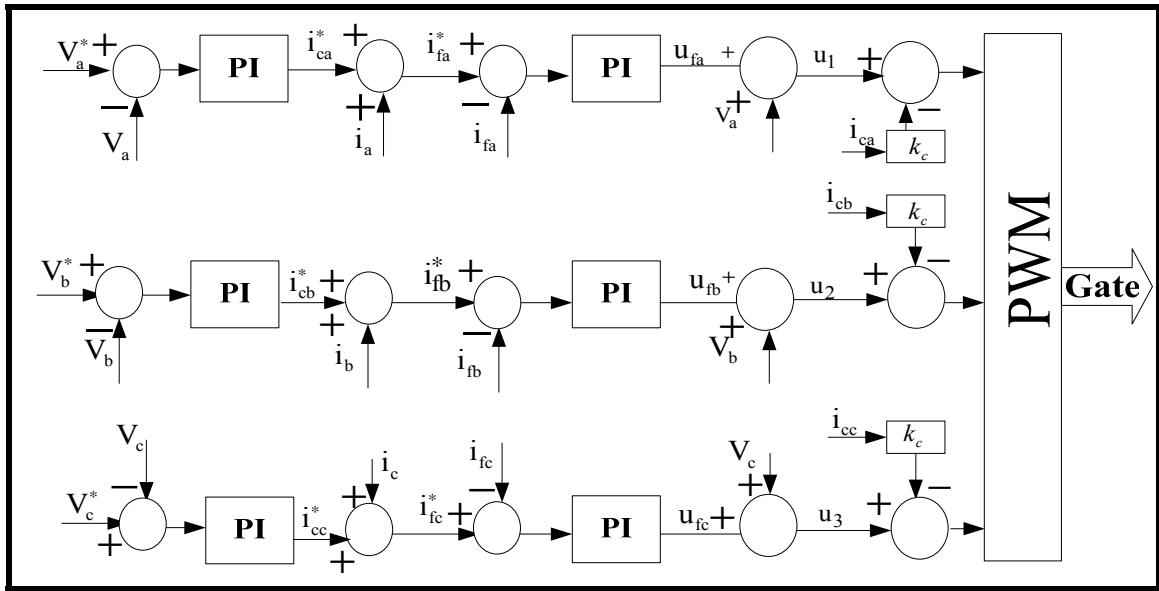


Figure 3.17 Control of VSC inverter with active damping coefficient

3.6 Fuzzy logic supervisor and its application domain

Fuzzy logic supervisor (FLS) is an approach to computing based on "degrees of truth" rather than the usual "true or false" (1 or 0) Boolean logic on which the modern computer is based. Pioneering study on fuzzy logic is done by Lotfi Zadeh in 1965 and then the first working group on fuzzy systems has been in Japan by Toshiro Terano in 1972 (Zadeh, 1965). During the past several years, FLS has emerged as one of the most active and fruitful areas for research in the applications of fuzzy set theory, especially in the realm of industrial processes, which do not lend themselves to control by conventional methods because of a lack of quantitative data regarding the input-output relations. Fuzzy control is based on fuzzy the logical system which is much closer in spirit to human thinking and natural language than traditional logical systems. Fuzzy logic has a high capability to deal with the uncertainties in the system through a simple rule of "IF-THEN" based approach, thereby eliminating the need for a mathematical model of the system. This is very useful in complex systems for which a complete mathematical model representation may not be possible. The fuzzy logic controller (FLC) based on fuzzy logic provides a means of converting a linguistic control strategy based on expert knowledge into an automatic control strategy (Lee, 1990). The fuzzy logic supervisor is using largely in energy management for hybrid wind/photovoltaic power generation unit, plug-in hybrid electric vehicle and heat pump for household applications (Breban, 2017).

The operation of FLS can be resumed into three steps as shown in Figure 3.18a

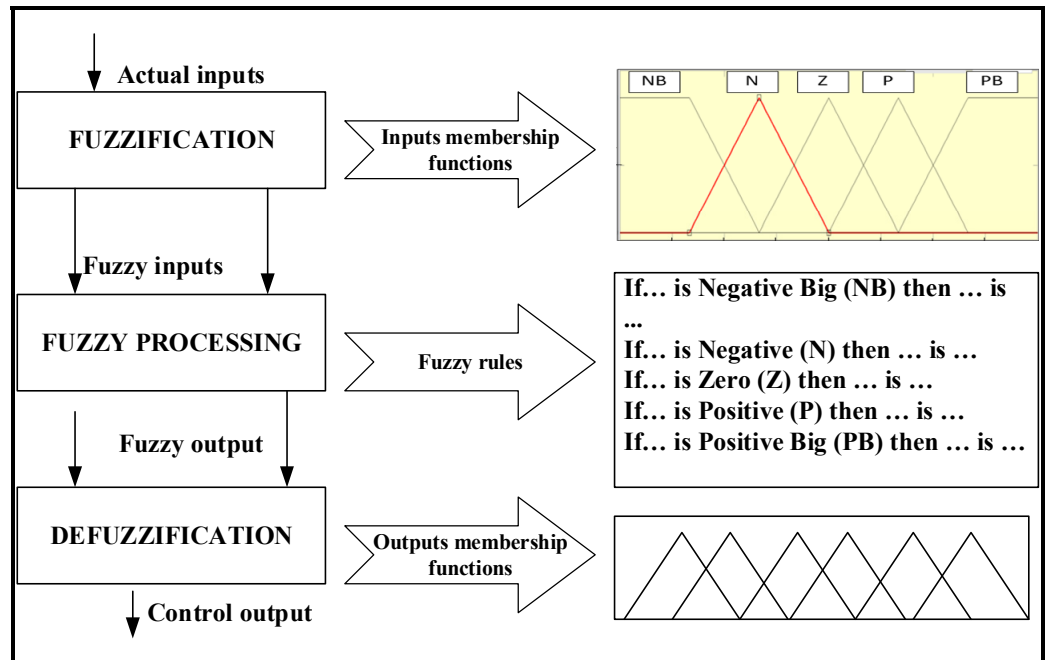


Figure 18a Operation of a fuzzy controller (Reznik, 1998)

- 1) Fuzzification: The fuzzification interface converts the binary logic inputs into fuzzy variables. The actual inputs are fuzzified to obtain the fuzzy inputs;
- 2) Fuzzy processing: processing fuzzy inputs according to the rules set and producing fuzzy outputs;
- 3) Defuzzification: The defuzzification interface converts the fuzzy variables into binary logic outputs.

This conversion is achieved by means of a membership function. The rule based on the IF-THEN rules describes the control strategy where the output from each one is deduced by the inference logic to get the output of each membership function (Singh, 2012).

3.6.1 Fuzzy logic energy management used for the proposed system

The fuzzy logic energy management is developed with the aim of managing effectively the power flow between the different energy resources and load and then increasing the global efficiency of the system.

The objective of using FSL in this chapter is to build a smart control that takes into account the interaction between generation sources and the load demand, and regulates the SOC of batteries. The developed FLS was built on 25 fuzzy rules given in Table 3.4.

The FLS inputs variables of regulation is:

$$P_{\text{reg}} = P_{\text{pvs}} - P_{\text{pump}} - P_L$$

where P_{reg} : the power regulation; P_{pump} : the power of water pump used as a damping load; SOC (%): the battery state of charge.

Table 3.4 Fuzzy logic rules for the power management of the system

| | NB | N | Z | P | PB |
|----|----|----|---|---|----|
| VL | PB | PB | M | Z | Z |
| L | PB | PB | M | Z | Z |
| M | PB | M | Z | Z | Z |
| H | M | Z | Z | Z | Z |
| VH | M | M | Z | Z | Z |

Where NB: Negative Big; N : Negative; Z : Zero; P : Positive; PB : Positive Big; VL:Very Low; L:Low; M:Medium; H:High; VH: Very High.

An example of explanation of FLS rules for the first line of Table 3.4 is as following, where P_{GGS} is the GGS power representing the output variable (see Figure 3.18b).

- If P_{reg} is NB and SOC is VL then P_{GGS} is PB, the GGS supplies entirely the full load;
- If P_{reg} is N and SOC is VL then P_{GGS} is PB, the GGS supplies the load power demand and also charges the battery;
- If P_{reg} is Z and SOC is VL then P_{GGS} is M, PV solar will supply alone all the load power and the battery will be charged by the P_{GGS} ;
- If P_{reg} is P and SOC is VL then P_{GGS} is Z, PV solar will supply the load demand and the difference is sent to the battery;

- If P_{reg} is PB and SOC is VL then P_{GGS} is Z, here the battery and the water pump will take additional power delivered by the PVS solar.

One deduces that if P_{reg} is negative and the power generated is not sufficient because the solar PVS is not delivering the required power. In this case a contribution of gas generator is essential to deliver the power difference. If it is positive, then extra power is delivered by the solar PVS, and in some cases, it may be used to charge the battery. The characteristic of GGS is used for power management in order to extract the exact power needed by the load. Figure 3.18b presents the two inputs and one output of the FLS.

Figures 3.19 -3.21 present the membership functions (MFs) of the two inputs and output. The implementation of the fuzzy logic supervisor is done using Fuzzy logic toolbox and Matlab/ Simulink software. It should be noted that those membership functions are built considering the maximal load power of 40 kW peak and the maximum SOC of battery charging as 98%.

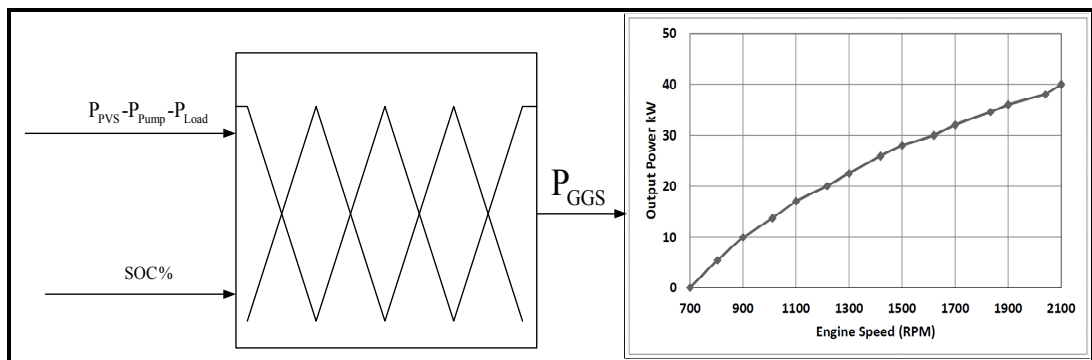


Figure 3.18b FLS and typical variable speed of GGS

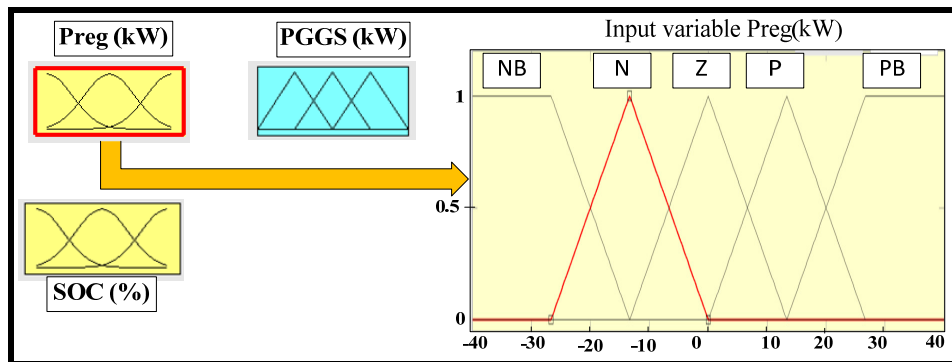


Figure 3.19 Membership function of input variable P_{reg}

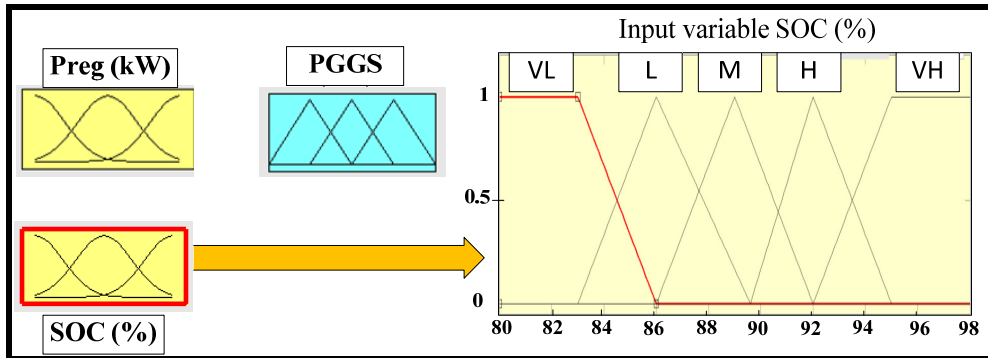


Figure 3.20 Membership function of input variable SOC(%)

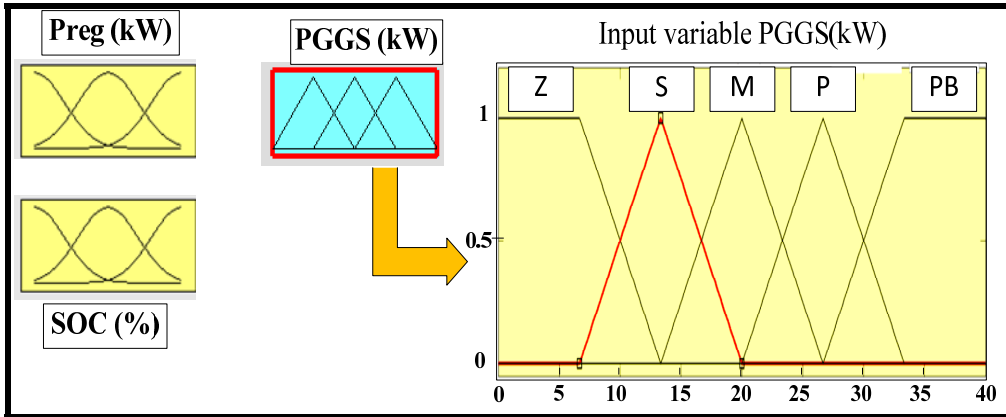


Figure 3.21 Membership function of input variable P_{GGS}

3.6.2 Battery overcharging and system protection using water pump

To protect the battery against overcharging and to avoid the extra power losses, a dc water pump is used as a dump load. As shown in preview main Figure 3.1, the starting condition of the water pump is integrated in the control by comparing the measured battery voltage V_{Bat} and the maximum allowed battery voltage $V_{Bat-Max}$. If overvoltage or overcharging of the battery occurs, a control signal is sent to the switch to activate the water pump. The pump will be deactivated when the battery voltage returns to the normal value and there is no extra power generation.

3.7 Simulation results of standalone complete system based on MG concept

The system under study was validated by simulation using Simpower System. The parameters of the system used in the simulation are shown in the ANNEXE II.

Figure 3.22 shows the performance of the FLS for power management of different DERs. The power is following perfectly the rules imposed by the FLS described in the Table 3.4. The FLS provides the corresponding speed of GGS to deliver exactly the power to balance the system in case of insufficient solar power generation and may also charge the batteries. The FLS also controls the charging of batteries via SOC. When the battery is full charged and there is no load power demand, the water pump is activated to consume the extra power.

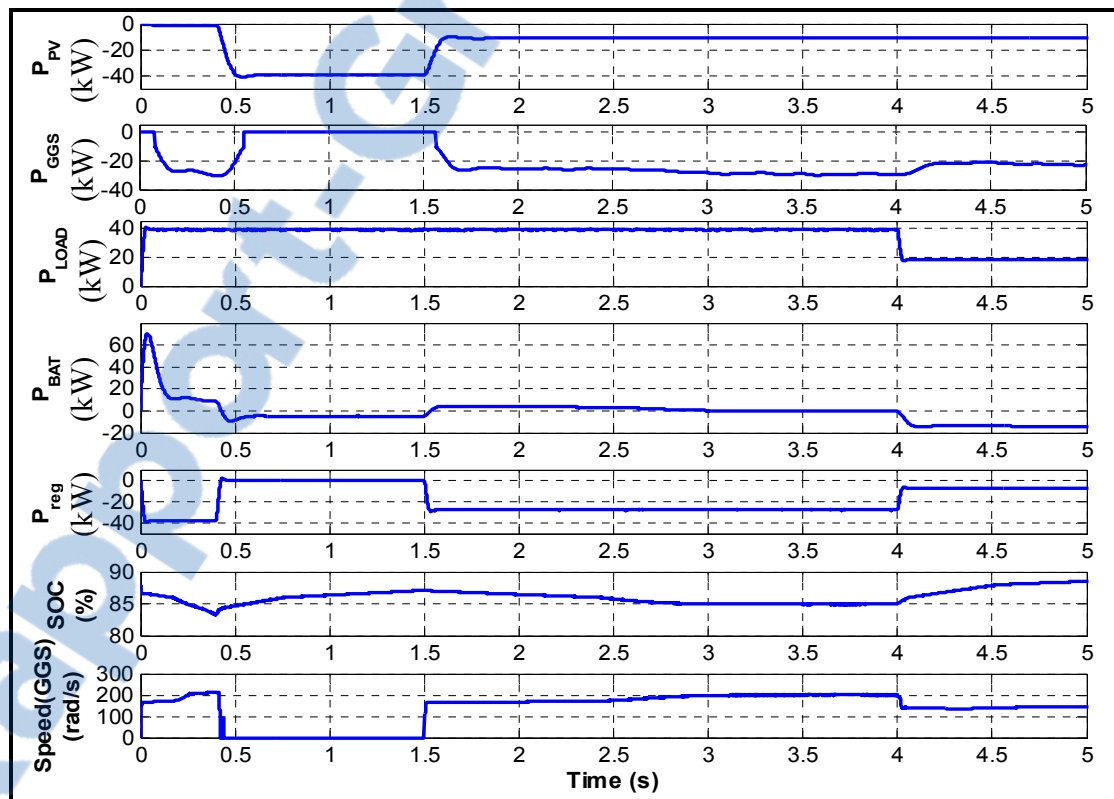


Figure 3.22 Power flow and speed of the GGS

During the transient start-up, the battery supplies alone the load power demand, the PVS is not contributing and the GGS is turned off. From $t = 0.1$ to 0.5 s the GGS is switched ON and

shares the power demand with the battery. From $t = 0.5$ to $t = 1.5$ s, the PVS started delivering the power demand (40 kW), SOC of the battery remains constant and the GGS is then shutdown automatically. From $t = 1.5$ to $t = 4$ s, the PVS generates only 10 kW, the GGS is then delivering the difference needed by the load. From $t = 4$ s to 5s, some loads are disconnected, the PVS is still delivering 10 kW, the GGS generates 20 kW to feed load and to charge the battery.

Figure 3.23 shows the performance of the system to keep the voltage constant at the PCC during load variation.

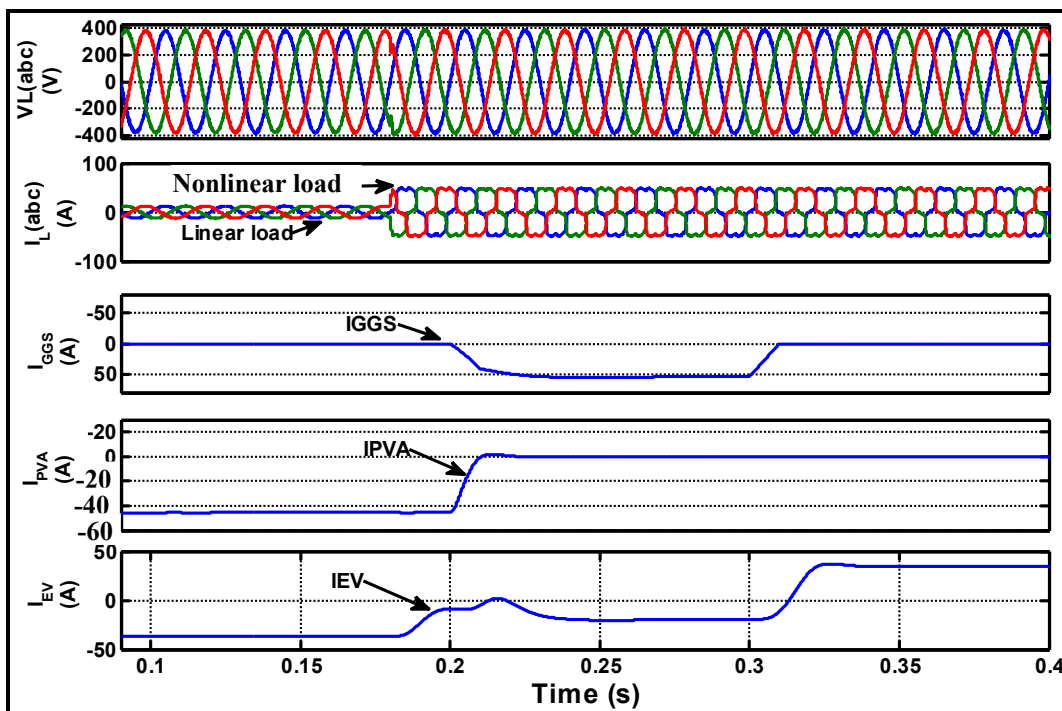


Figure 3.23 Power management and power quality

3.8 Conclusion

In this chapter, three aspects have been studied for standalone system based on MG concept.

- A new approach of active damping control technique without using any additional current sensor has been developed in order to reduce the losses in output filter and also to reduce the size of the VSC;

- Development of the shifting resonance technique to reduce five times the size of LiCr filter without affecting the stability of the system;
- Development of a smart power management using the fuzzy logic supervisor built on 25 rules.

In addition, the controlled interaction between PVS and gas generator set has contributed in the battery size reduction while ensuring an uninterruptible power supply. The feasibility and effectiveness of this MG system for remote area were evaluated with different simulation and have been validated experimentally in the laboratory setup.

CHAPTER 4

EXPERIMENTAL REALIZATION OF NZEH AND STANDALONE SYSTEM BASED ON MICROGRID CONCEPT

4.1 Introduction

This chapter describes the hardware implementation of Net Zero Energy House and Standalone System based on MG concept. The system parameters of the simulation and hardware implementation are shown in ANNEX II. The schematic designing of NZEH implementation was built in many steps as described in section 4.2. The experimental setup of standalone system is described in section 4.3. The semikron SKiiP1013 inverter assembly is used for the main test of the project. Part of hardware implementation and algorithm validation was achieved in collaboration with the industrial company Power survey.

4.2 Net Zero Energy House hardware implementation

The hardware implementation of NZEH was implemented in three steps. More details about the hardware setup are illustrated in ANNEX III.

4.2.1 Step1: Test of dc-dc boost converter with small photovoltaic module

This setup (Figure 4.1) is consisted of small photovoltaic module (20 W), microcontroller eZdsp F28335, DC-DC converter, IGBT gate drive, power supply and load. During the test, the output current of the used PV module is small and it was decided it by a powerful DC source in order to test adequately the system.

The used microcontroller is Texas Instrument C2000 family eZdsp F28335 shown in Figure 4.2. More details are described in ANNEX III. The experimental validation of the DC-DC boost converter is shown in the Figure 4.3.

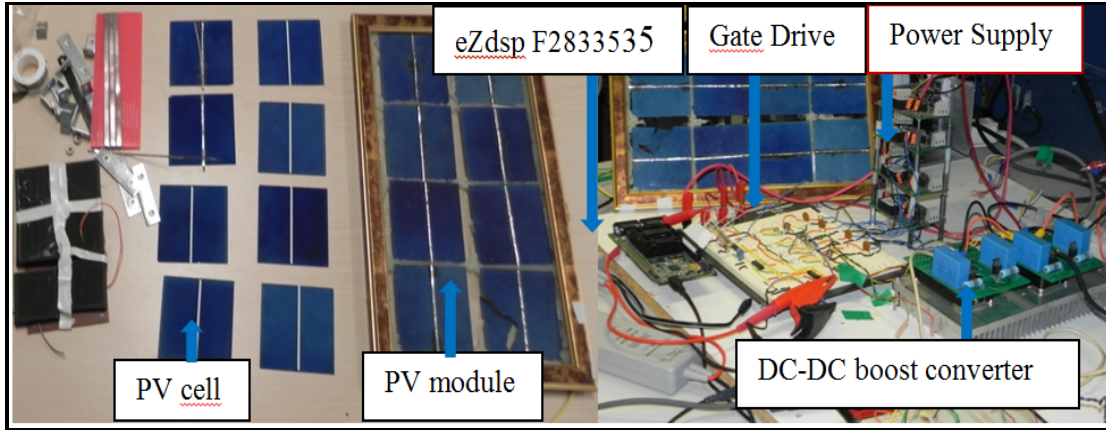


Figure 4.1 Mini Setup of NZEH (First step)

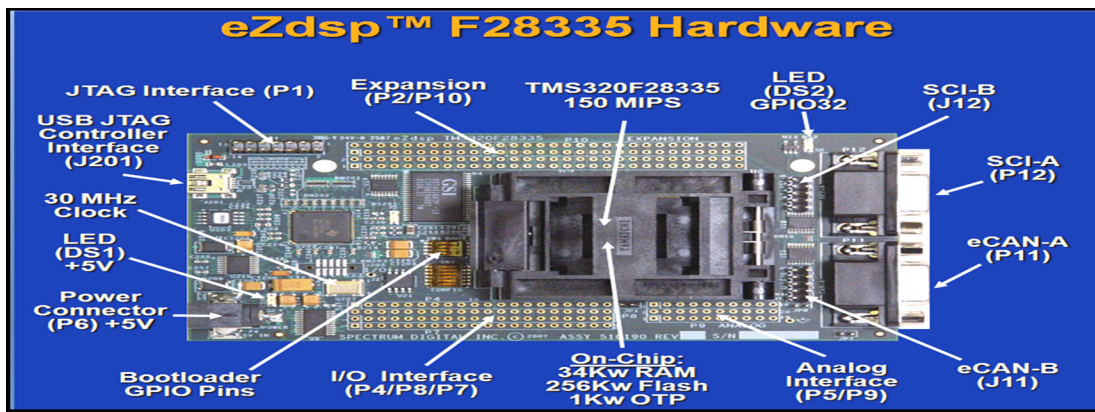


Figure 4.2 eZdsp F28335 description

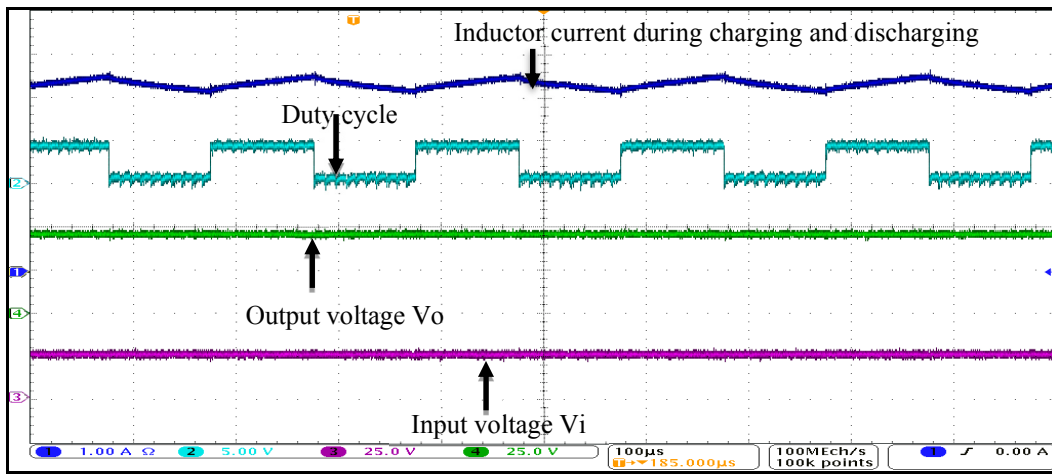


Figure. 4.3. DC-DC boost converter

4.2.2 Step2: Test of NZEH with the single phase VSC-AHF

After the validation of the boost functionality, the second step is to build and add to the system the single phase DC-AC converter and other components (load, grid, control box, inductor) as shown in Figure 4.4.

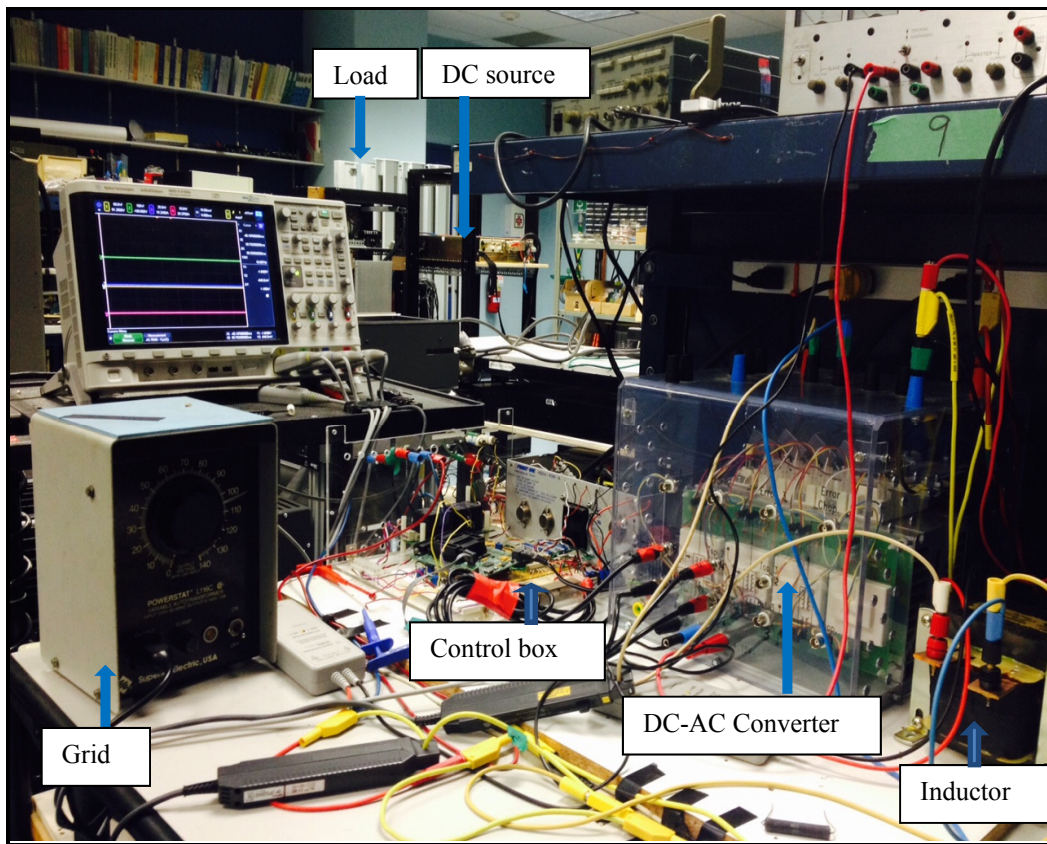


Figure 4.4 Laboratory setup for experimental validation (Second step)

Figures 4.5 and 4.6 show the experimental result of the single phase VSC-AHF to compensate the current harmonic and the reactive power. The dc bus voltage V_{dc} is regulated to its reference and is chosen twice greater than the maximum grid voltage. From the top to the bottom, the Figure 4.5 shows the dc bus voltage V_{dc} , the grid voltage V_s , the load current i_L and the active filter current i_f .

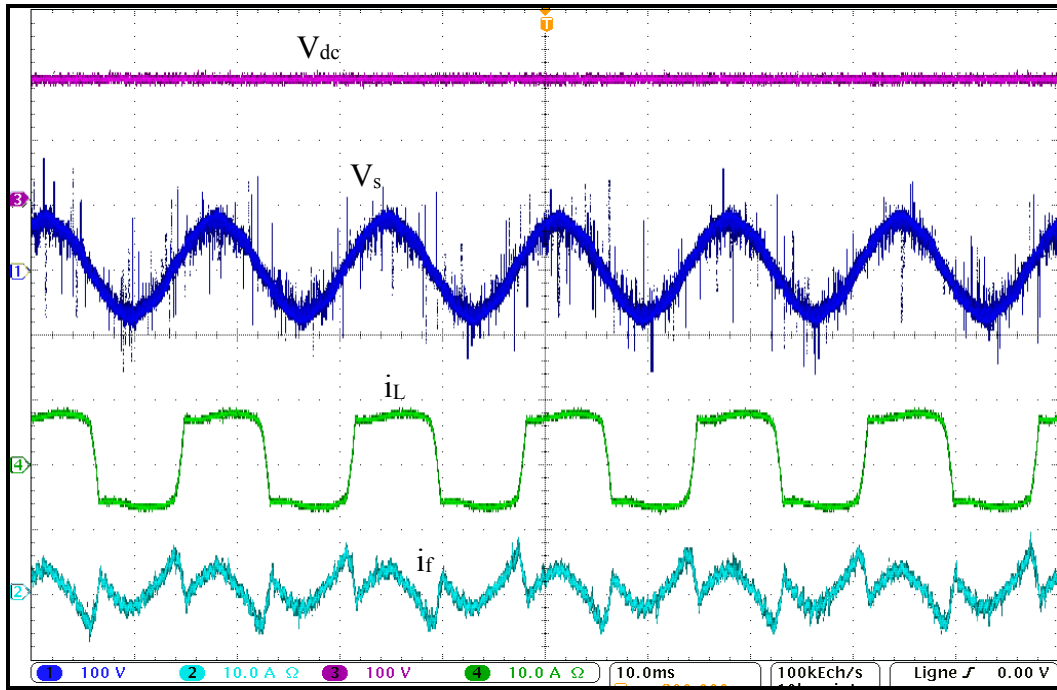


Figure 4.5 Result of single phase VSC-AHF connected to the grid

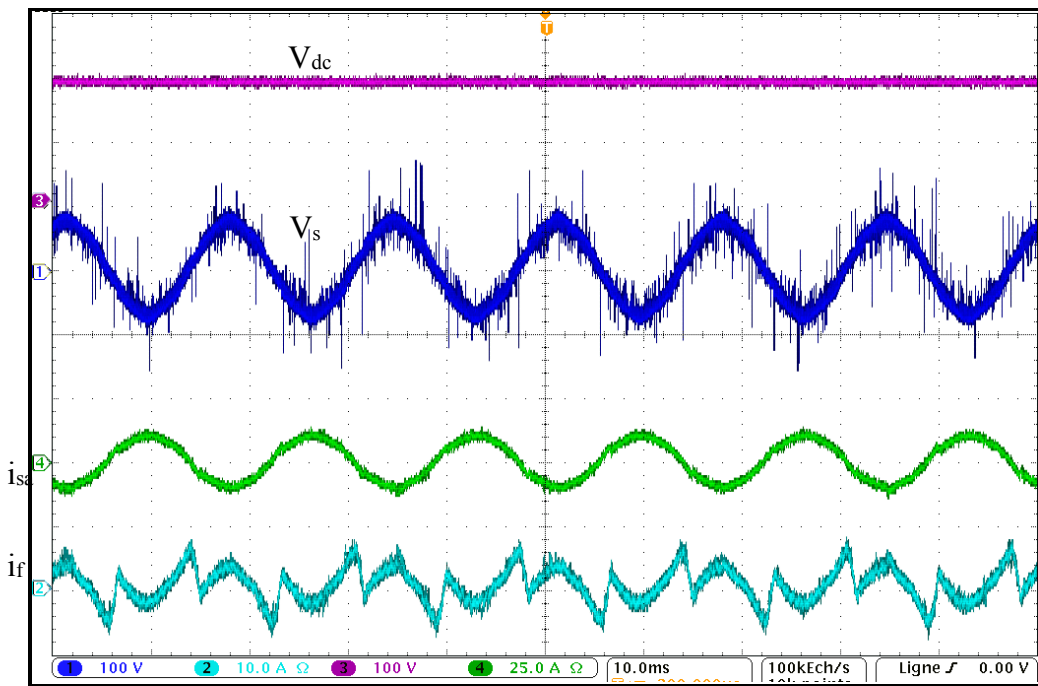


Figure 4.6 Result of single phase VSC-AHF connected to the grid

4.2.3 Step3: Improvement and performance of NZEH with industrial point of view

Step 3 is based on the performance of the previous system and was done in collaboration with the industrial company Power Survey Inc. Figures 4.7 and 4.8 show the experimental setup of the NZEH and its control box respectively. More details are explained in the next under sections were the control box component (sensors card, interface card and protection) with different printed circuit board conception and algorithm implementation are discussed.

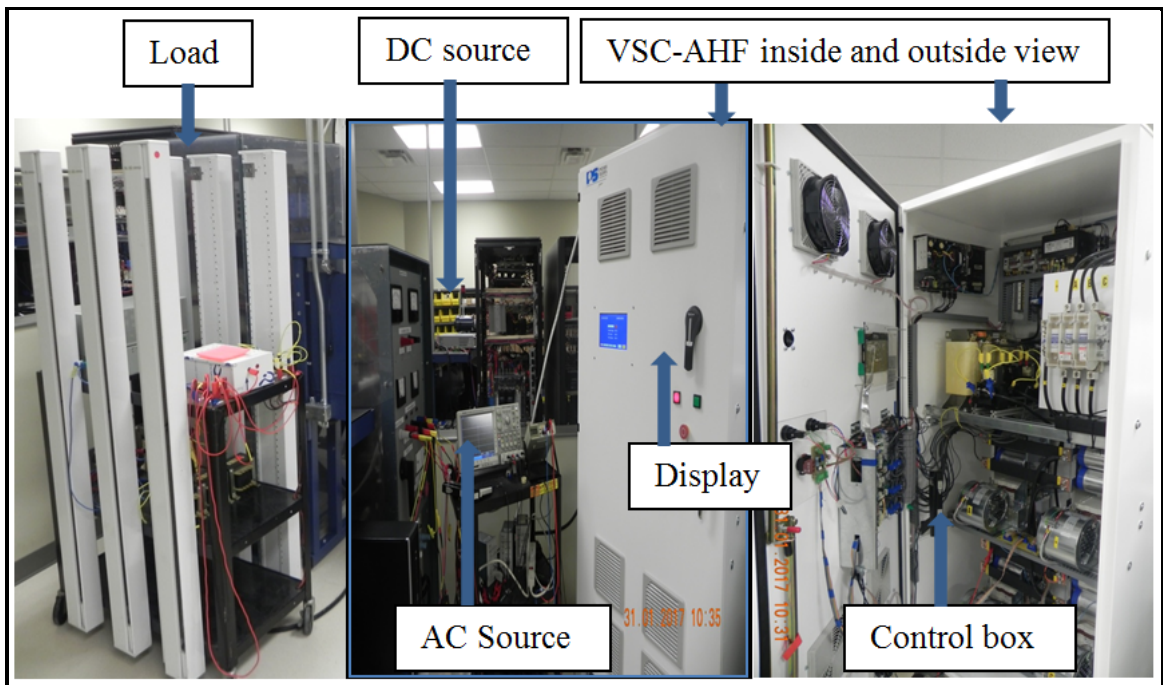


Figure 4.7 Experimental setup of NZEH

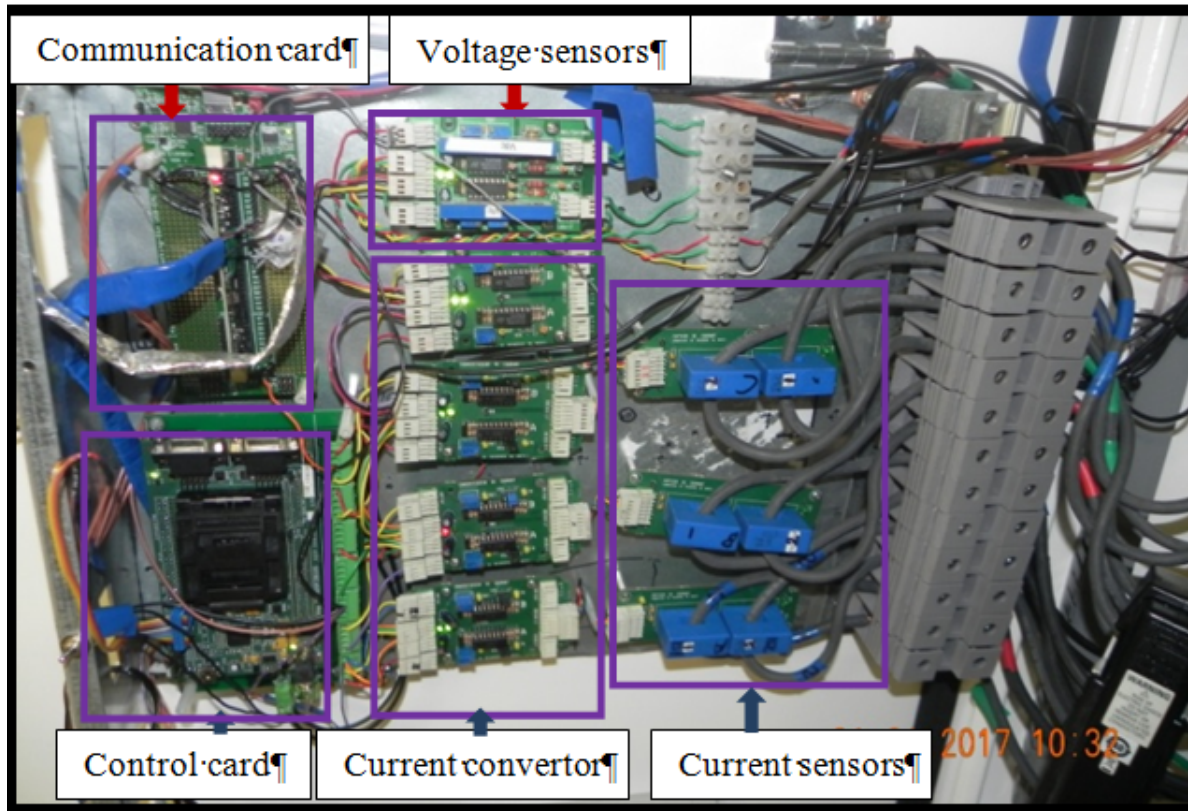


Figure 4.8 Control Box

4.2.3.1 Design of printed circuit board for sensing and regulating the signal of V_s , V_{dc} , i_s , i_F and i_L

The symbols V_s , V_{dc} , i_s , i_F and i_L represent the sensing output signal of the voltage source, dc bus voltage, current source, VSC-AHF current and current load. In order to control adequately the system, the input parameters value of the DSP is regulated by using the printed circuit board (PCB) designed in Altium designer software. The PCB is designed in two steps: the first step is the design of schematic circuit and then the PCB as shown in Figure 4.9 and Figure 4.10.

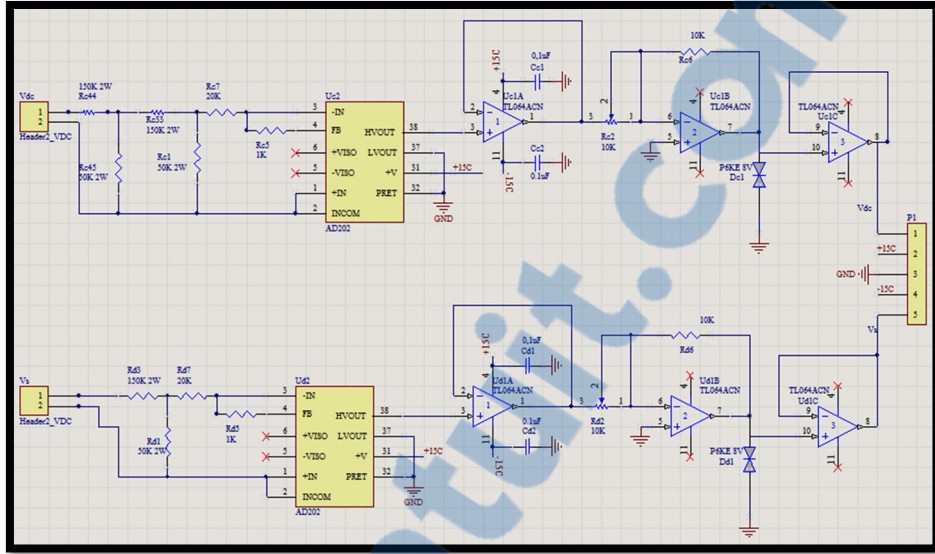


Figure 4.9 Schematic for V_{dc} and V_s

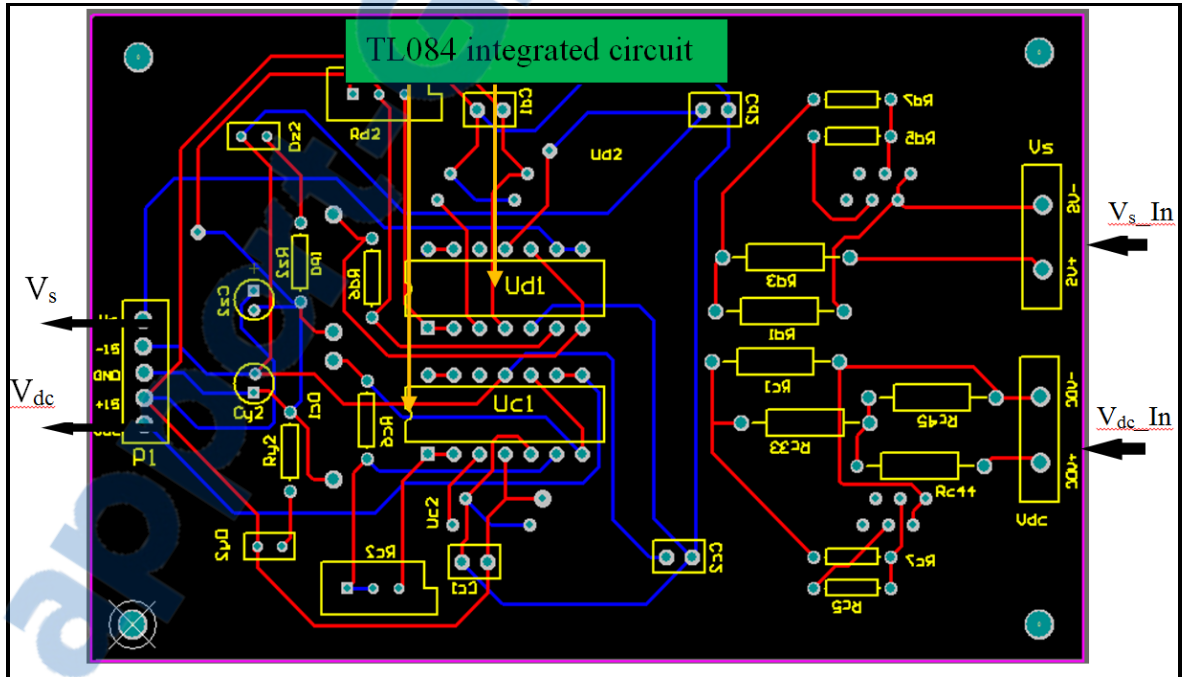


Figure 4.10 PCB for sensing and regulating V_s and V_{dc} output signal

Figure 4.11 and 4.12 show the schematic and PCB circuit for regulate the sensor current i_L and i_F to the amplitude of ± 1.5 .

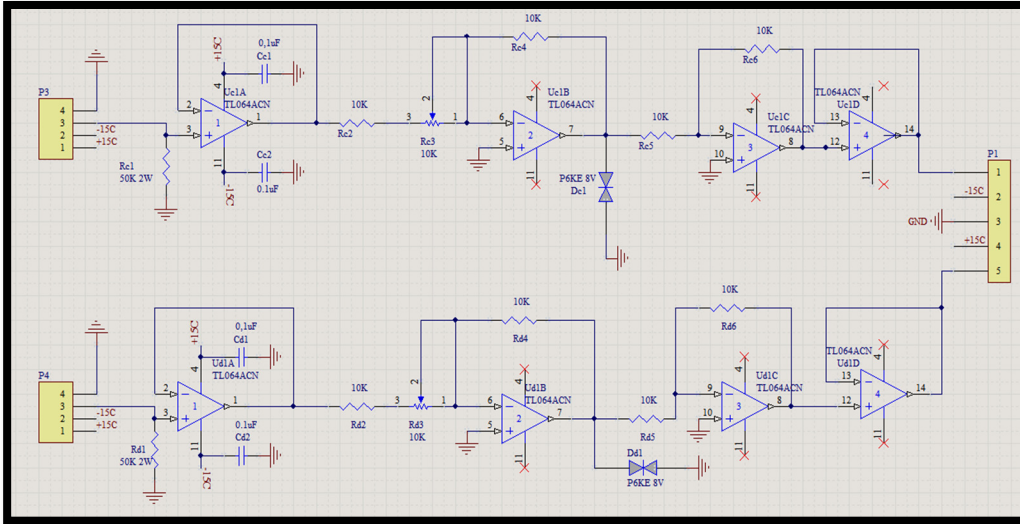


Figure 4.11 Schematic for signal i_L and i_F

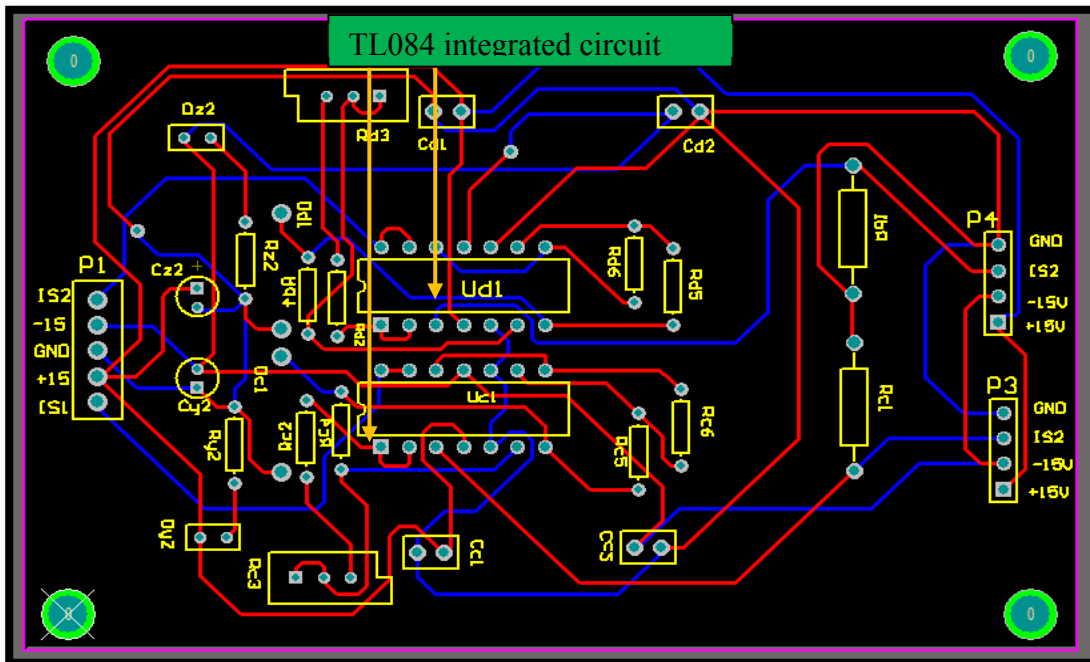


Figure 4.12 PCB for regulating the output signal of i_L and i_F

4.2.3.2 Offset of the input ADC signal and protection technique of the DSP

An important requirement concerning the ADC input signal is to be positive and limited between 0 and 3 V (maximum 3.3 V). Figure 4.13 shows the schematic design for the offset signal to the value between 0 and 3 V using the integrated circuit AD8648.

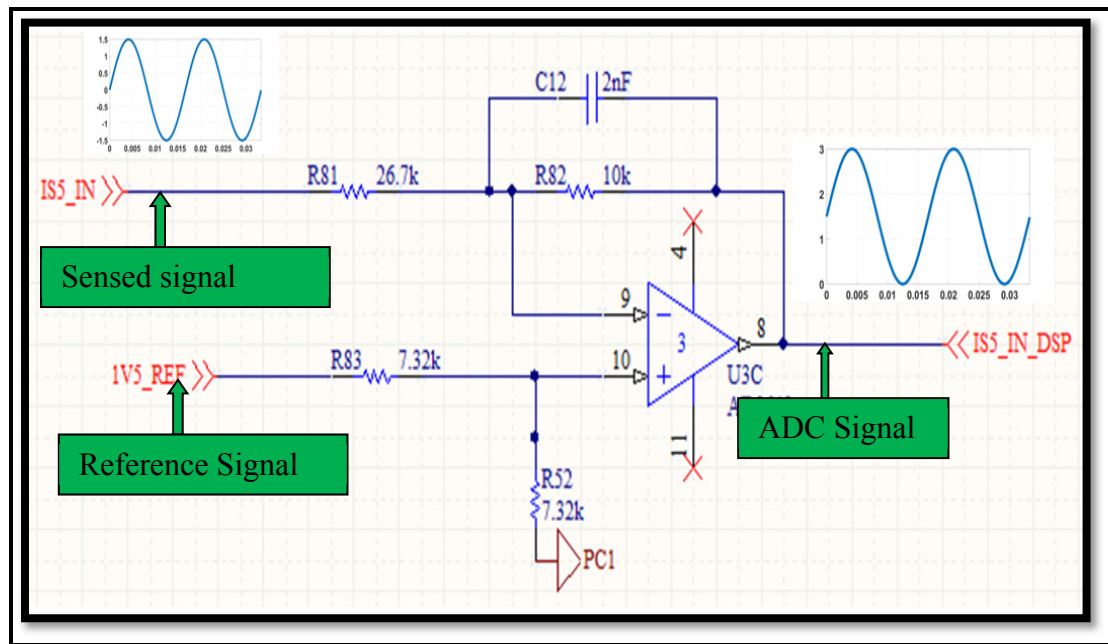


Figure 4.13 Schematic circuit for offset signal from ± 1.5 to 3V

If the input ADC signal exceeds the maximum value of 3.3V, the DSP may be damaged. Two measurements are used to protect the DSP against undesired overrun signal. The first is to power the integrated circuit of the offset AD8648 with 3.3 V and the second is the integration of zener diode. Figures 4.14 and 4.15 show the simulation and experimental validation of the DSP protection. In the both case, the overrun signal is automatically blocked and cut-off.



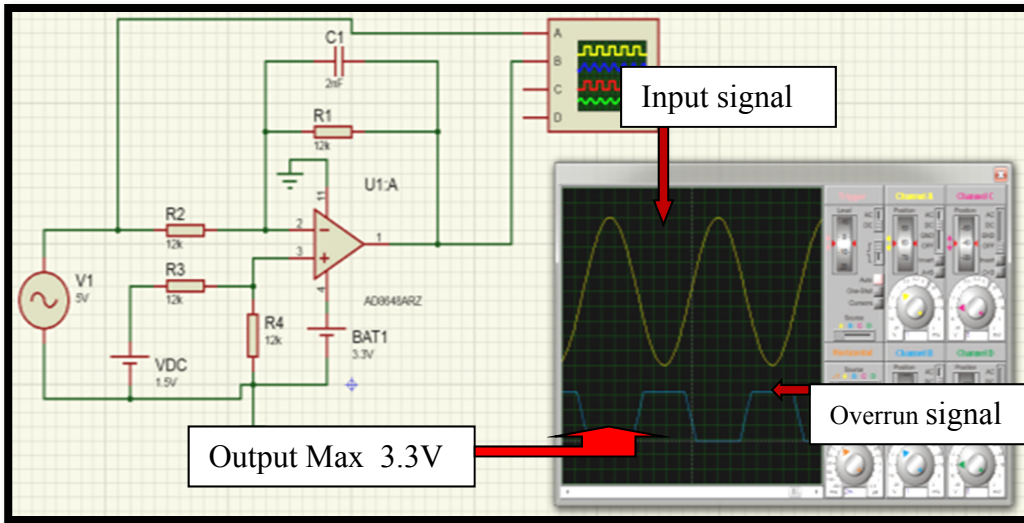


Figure 4.14 Simulation of the DSP protection

Figure 4.15 shows the real-time validation of the DSP protection when the signal exceeds 3.3 V. The over signal is then automatically blocked.

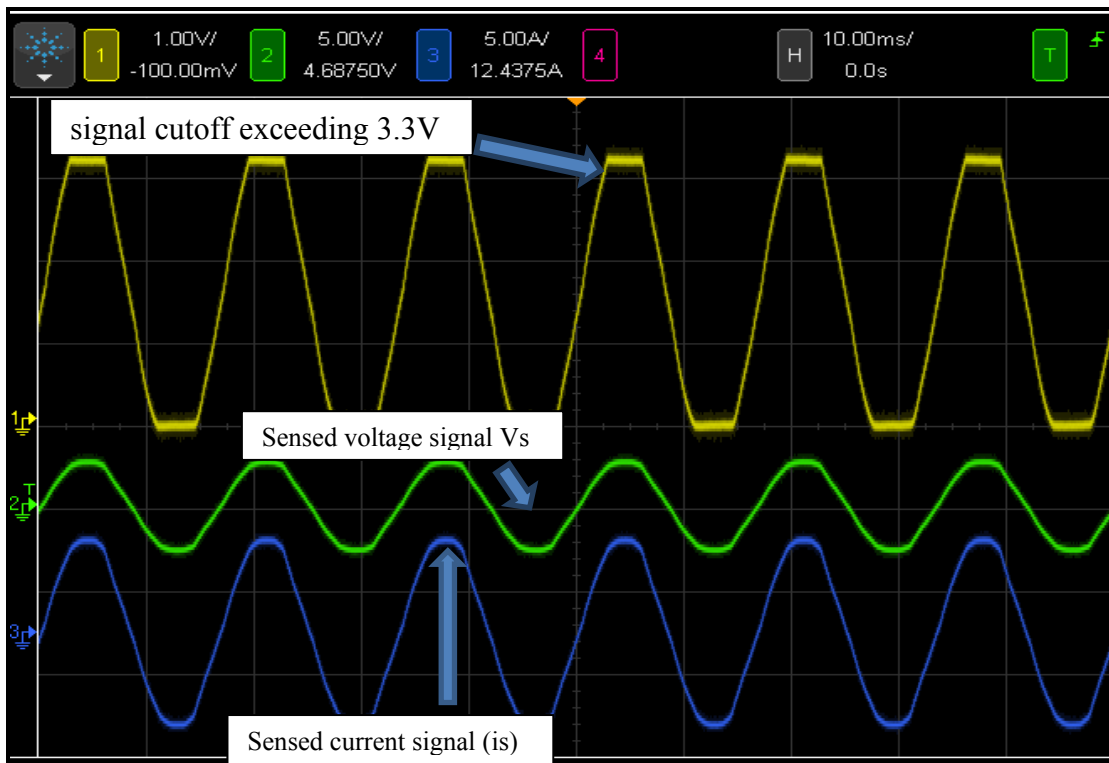


Figure 4.15 Experimental result of the DSP protection

4.2.3.3 PCB interface card for the microcontroller eZdsp F28335

Figure 4.16a and 4.16b show the second and third PCB version of interface card of eZdsp F28335 including the protection and offset circuit. To eliminate high frequencies noises, decoupling capacitors are used and also the analogical ground is isolated from the digital.

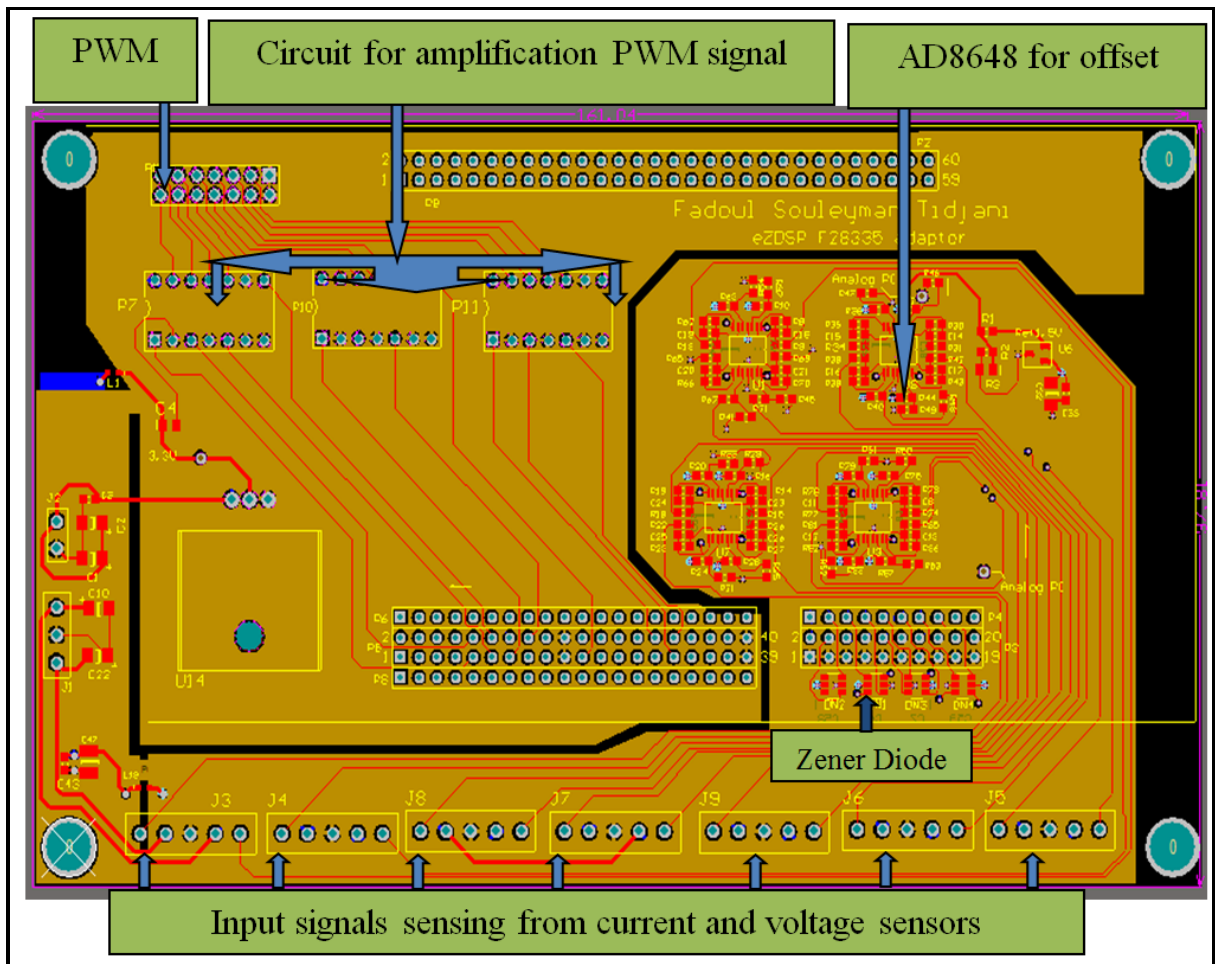


Figure 4.16 a) PCB interface card (version2) of eZdsp F28335

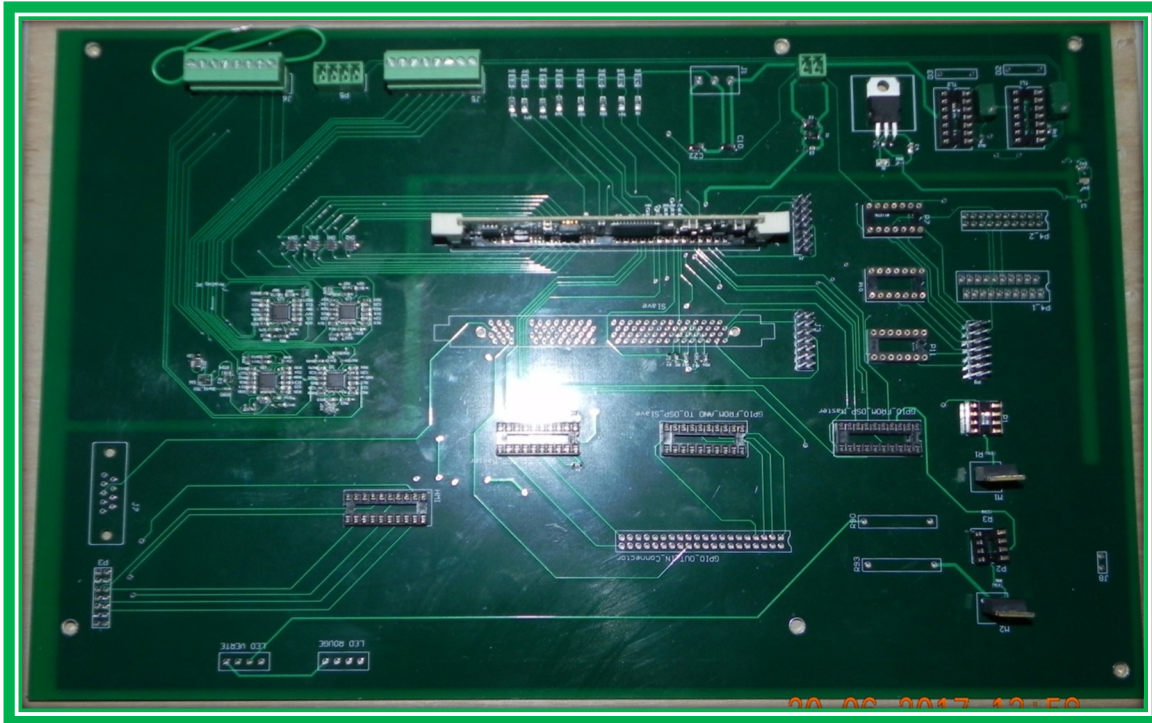


Figure 4.16 b) PCB interface card (version3) of eZdsp F28335

4.2.3.4 Implementation of the control algorithm of NZEH

The developed algorithm is implemented in two steps: 1) the implementation of algorithm in Matlab Simulink using the Texas Instrument optimized bloc of the eZdsp F28335, 2) The second step is the generation of the C code using Code Composer Studio (CCS) software. The CCS receives all parameters of variables from Matlab Simulink and then converts them in C languages compatible with the eZdsp F28335 functionality. The CCS is the integrated development environment for Texas Instrument's (TI) for the DSPs, microcontrollers and application processors. CCS includes compilers for each of TI's device families, source code editor, project build environment, debugger, profiler, simulators and many other features. The Figure 4.17 shows the main menu of CCS V.3 with its important icons.

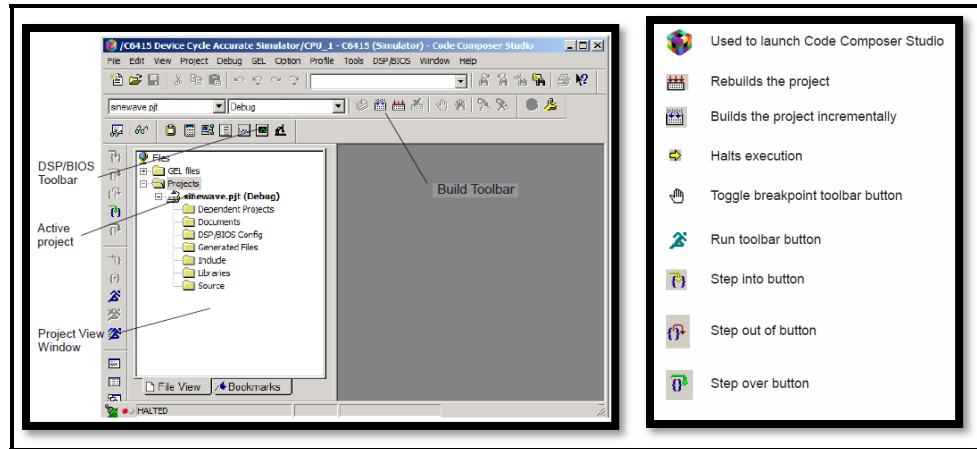


Figure 4.17 Code composer studio V.3 with its main icons on the right

Figure 4.18 shows the graphical display and visualization of the result in real time on the computer using the CCS window.

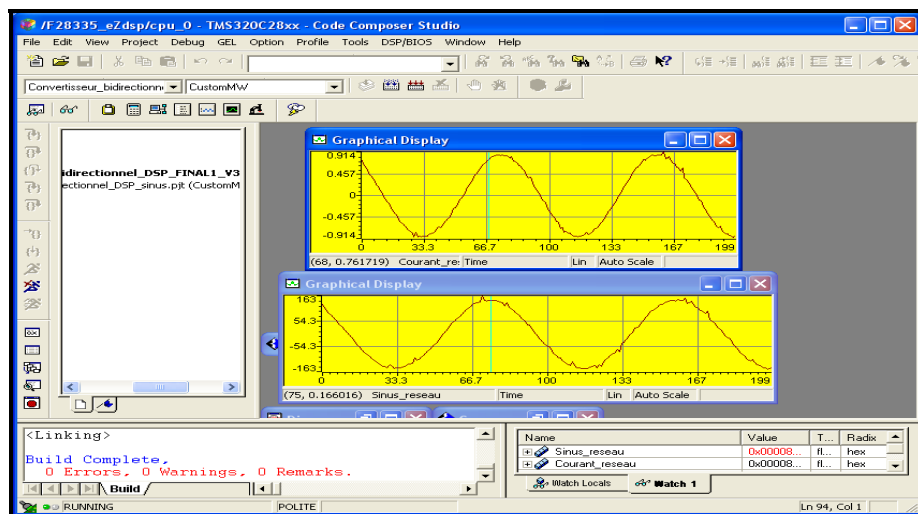


Figure 4.18 Graphical display with CCS

The signal processing from the sensors to the PWM passes through various steps:

- Regulating the output sensor signal to ± 1.5 V and then offsetting to the value; between 0 to 3V that representing the input signals to the DSP;
- Regulating the signal of the dc bus voltage to the value between 0-3V;
- Generating PWM signal for controlling the VSC-AHF.

The Figure 4.19 resumes the signal processing steps from ADC input to PWM output.

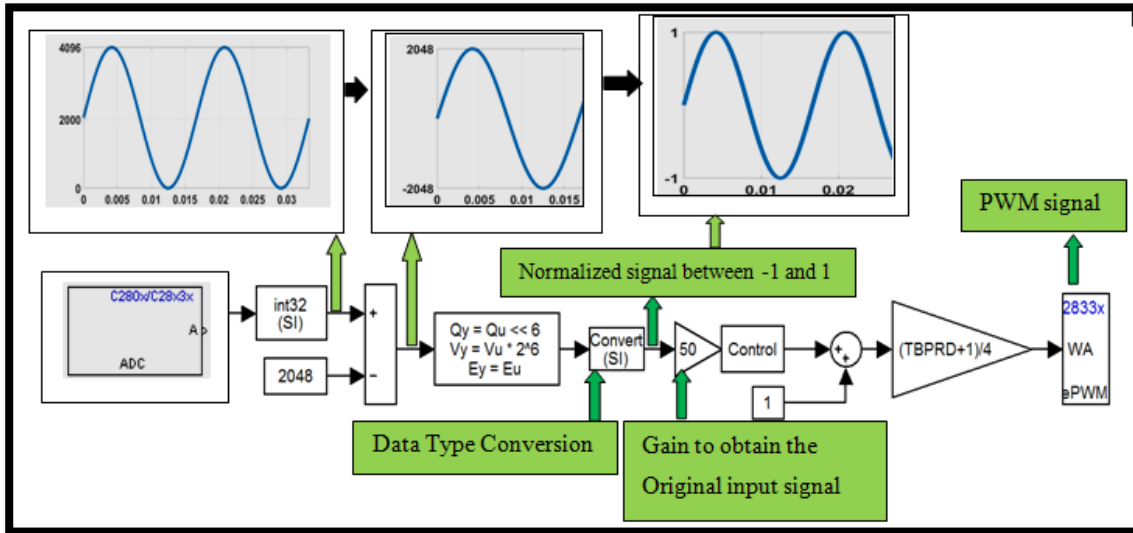


Figure 4.19 Input and output of signal from ADC to PWM

The complete diagram of the control algorithm for the NZEH is shown in Figure 4.20.

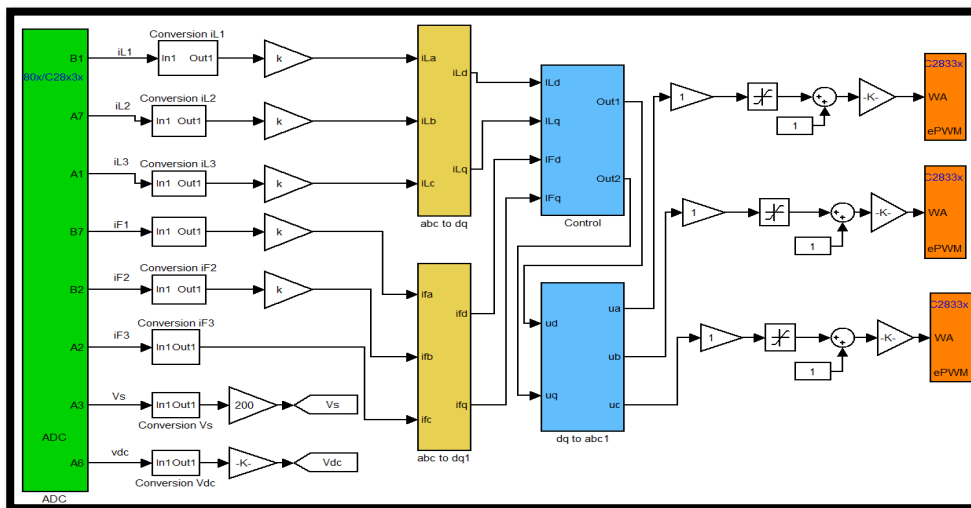


Figure 4.20 Control algorithm Diagram

4.2.3.5 Experimental result of NZEH

The used parameters for the experimental setup are shown in the ANNEXE III, Table 5. The result of Net Zero Energy House is focused on operation performance of the system and power management. Figure 4.21 shows the performance of the system with nonlinear load connection. The parameters V_{dc} , V_s , i_L and i_{sa} are very well controlled.

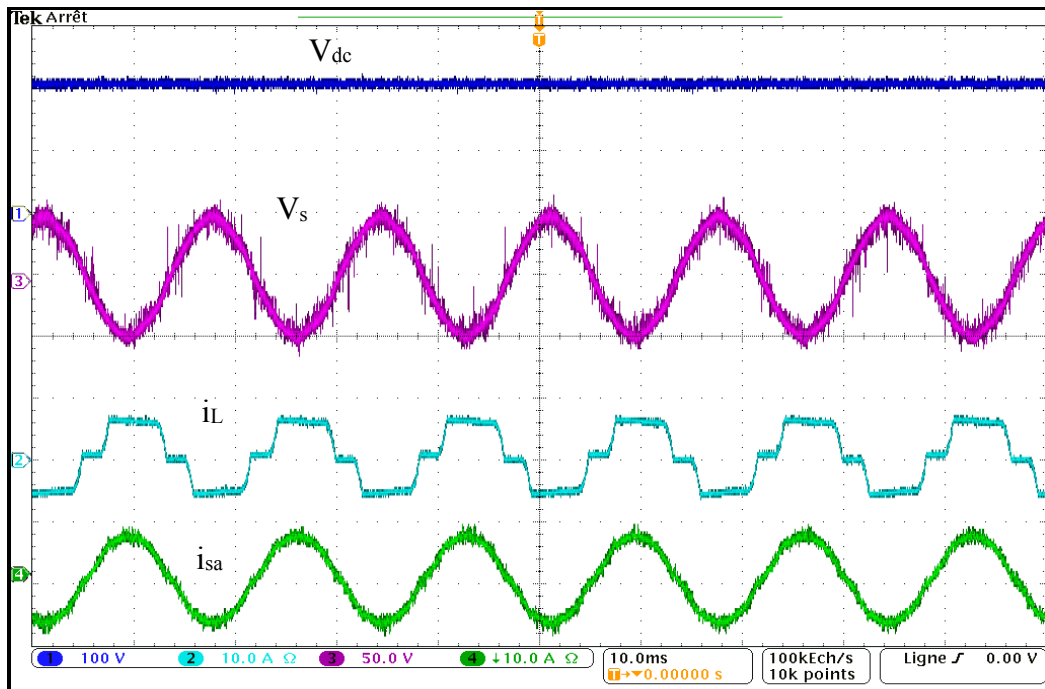


Figure 4.21 Result of VSC-AHF connected to the grid and load (V_{dc} , V_s , i_L , i_{sa})

Figure 4.22 shows the capability and robustness of the system during the load variation. The parameters V_{dc} , V_s , i_f , i_{sa} follow the instruction of algorithm control.

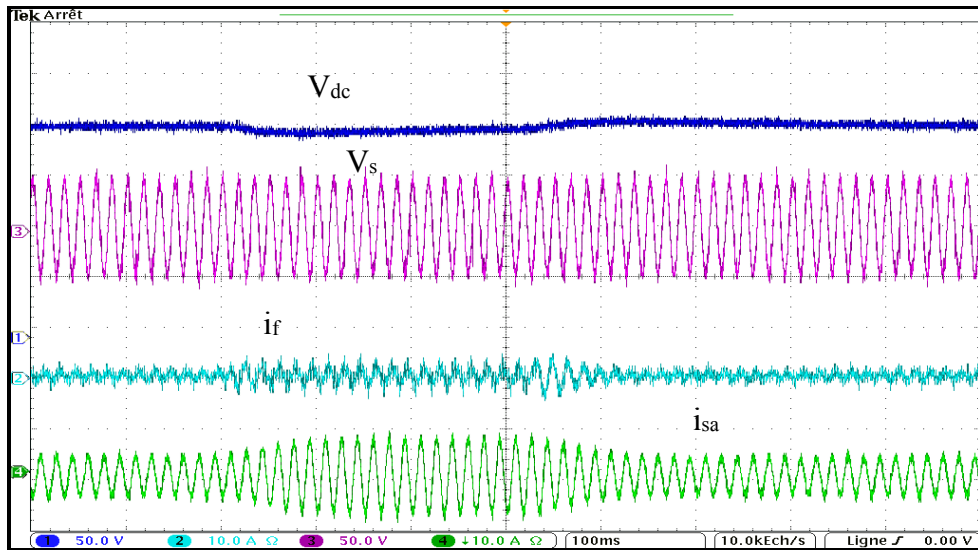


Figure 4.22 Result of VSC-AHF connected to the grid and load (V_{dc} , V_s , i_f , i_{sa})

1- Steady state response

The steady state of the V_{dc} , V_s , i_{sa} , and i_f are shown in the Figure 4.23.

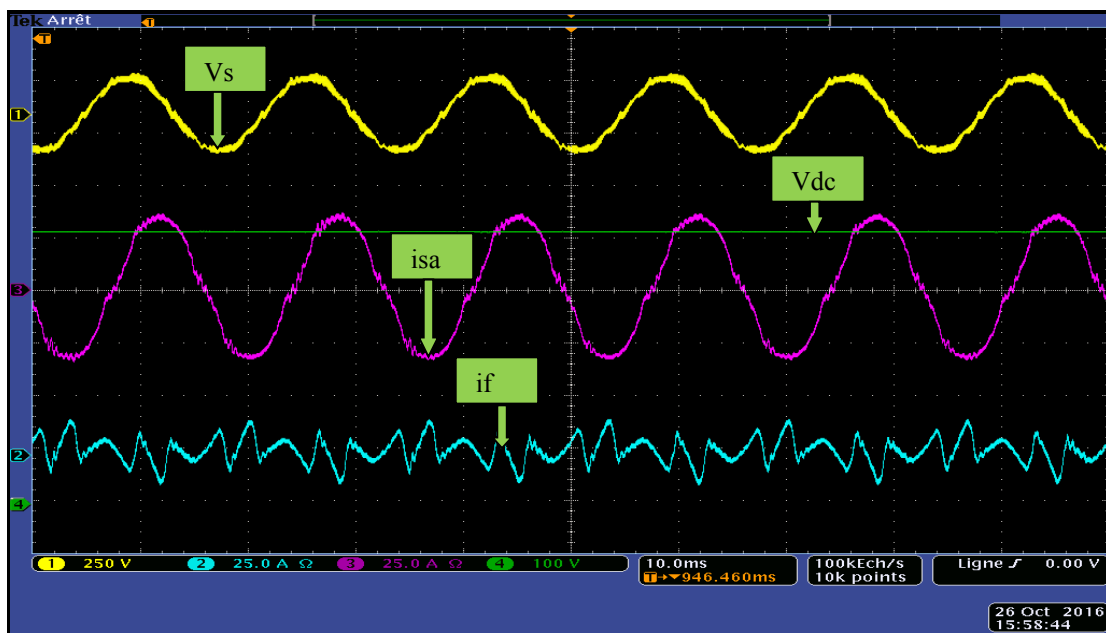


Figure 4.23 Steady state response of VSC-AHF

2- Experimental result of the NZEH during the startup of the system

During startup, the pre-load circuit (see chapter 2, Figure 2.11) is used to charge at first the dc capacitor at certain voltage level and then start the VSC-AHF as shown in Figure 4.24 where. This is to avoid a high inrush current that could damage the system.

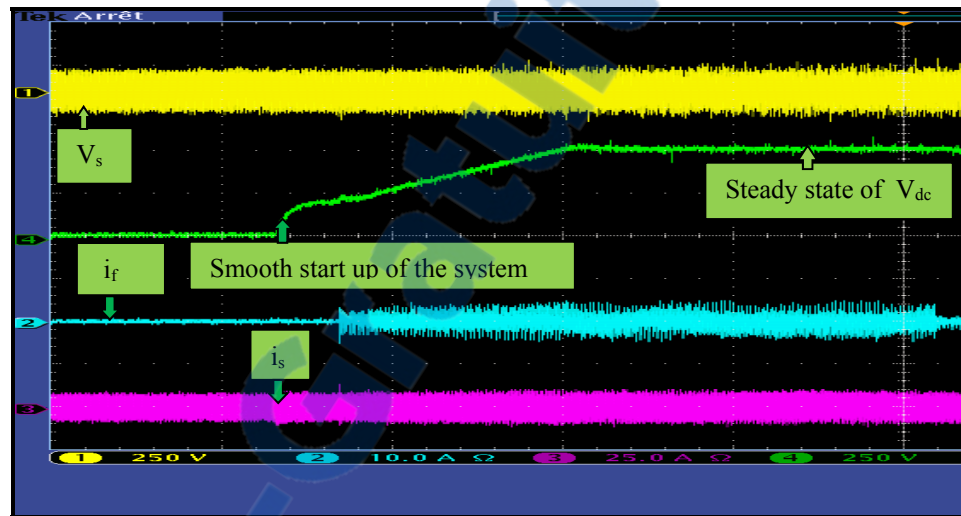


Figure 4.24 Experimental result for start from transient to steady state

The Figure 4.25 shows a zoom during the startup of the system.

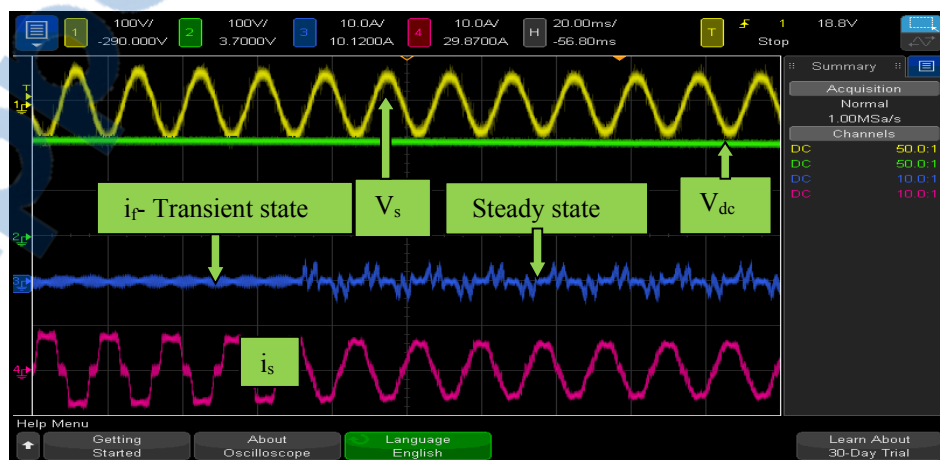


Figure 4.25 Experimental result for transient and steady state of the startup

3- Result of NZEH during the stop

The Figure 4.26 shows the experimental results of the V_{dc} , V_s , i_s and i_f during the VSC-AHF shutdown. In case of overload, the integration protection system forces decreasing at first the DC bus voltage gradually with a predefined slope until a certain voltage level and then canceling the VSC-AHF current and finally the dc capacitor will completely discharged via a resistor of relay3 (Figure 2.11 of chapter2).

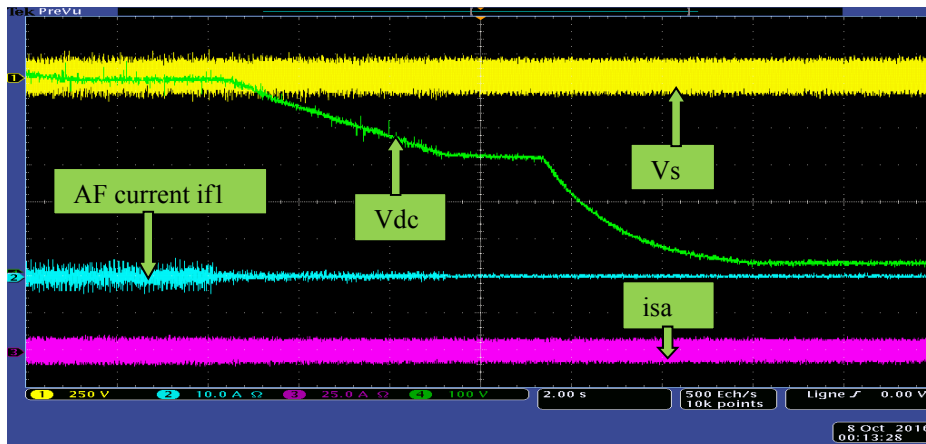


Figure 4.26 Experimental validation of the VSC-AHF during a shutdown

4- Operation of the NZEH from start time until stop

The Figure 4.27 shows the performance of the VSC-AHF during the start and stop. The experimental results of the V_{dc} ; V_s ; i_s and i_f during the stop and start demonstrates the high performance and protection of the system during the start and stop.

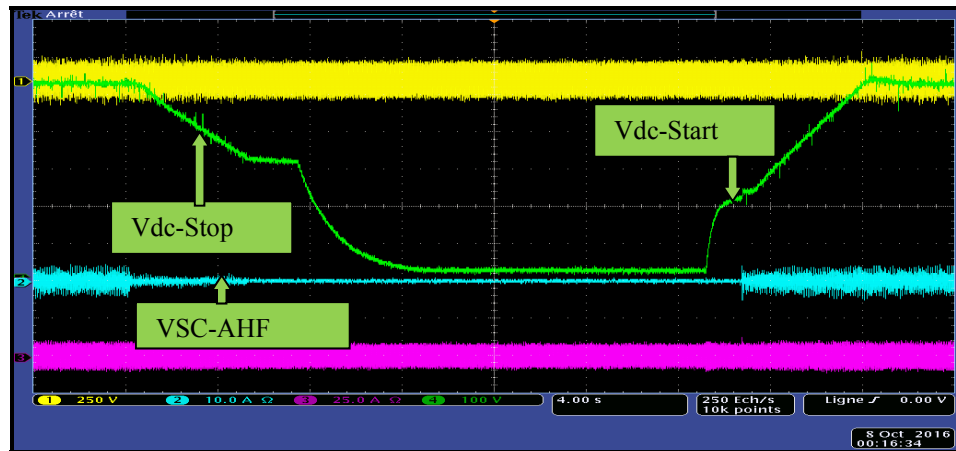


Figure 4.27 Experimental validation of the VSC-AHF during stop and start

5- Experimental result of NZEH with PVS and grid

The Net Zero Energy House is tested and validated experimentally using two sources of energy (photovoltaic and grid). In Figure 4.28, are shown different experimental results where i_L , i_F vs and v_{dc} are respectively the load current, the source current, the VSC-AHF current, the voltage source and the dc bus voltage. Figure 4.28a shows steady state response of the system. Figure 4.28b shows the dynamic response during the injection of the power from PVS to the load, one sees that the source current is decreased. In Figure 4.28c-d the PVS generated more power than the load demand and extra power is sent to the grid. In Figure 4.28e, at the beginning the PVS starts generating the power needed by the load and one remarks the grid do not contribute but at the end, the PVS generates power less than the load demand; the difference is taken from the grid.

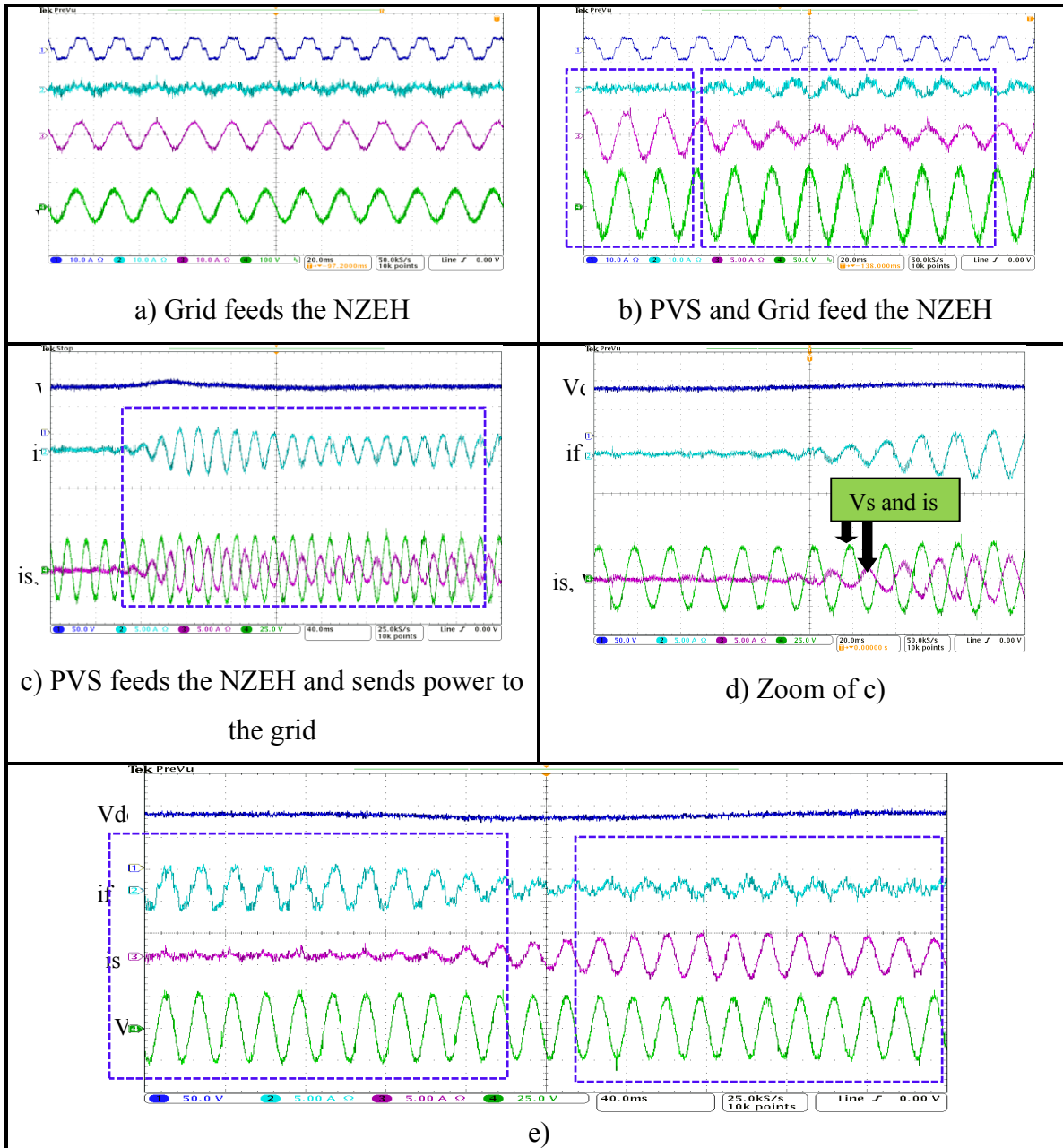


Figure 4.28 Experimental validation of the NZEH with PVS and grid

4.3 Experimental results for Chapter 3 (standalone system for remote area)

The experimental setup of the proposed standalone system (Figure 4.29) is based on PVS represented by the DC source, GGS, battery pack of PHEV, three phase convertor and load

(including dump load as a pump). The parameters specifications are given in ANNEXE1 (Table 5.4).

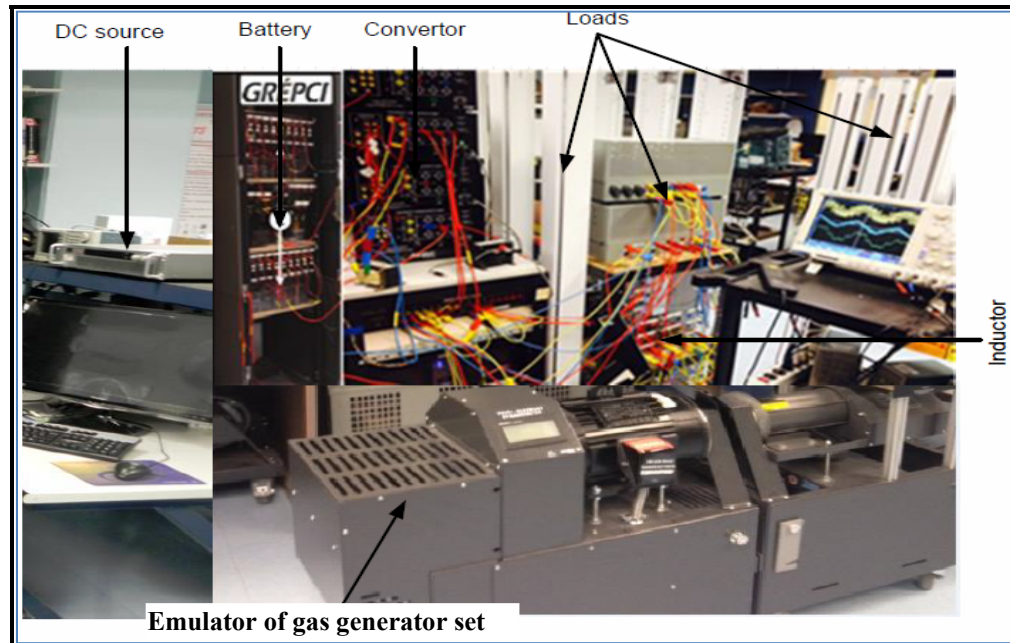


Figure 4.29 Experimental setup for standalone PVS, PHEV and GGS system

Figure 4.30 shows the experimental results for steady state operation of the system with linear load. v_f , v_a and i_a representing the output voltage of VSC, the load voltage and the load current respectively. The good quality of the load voltage (THD = 3%) and in phase with the load current confirms the good performance of the output filter.

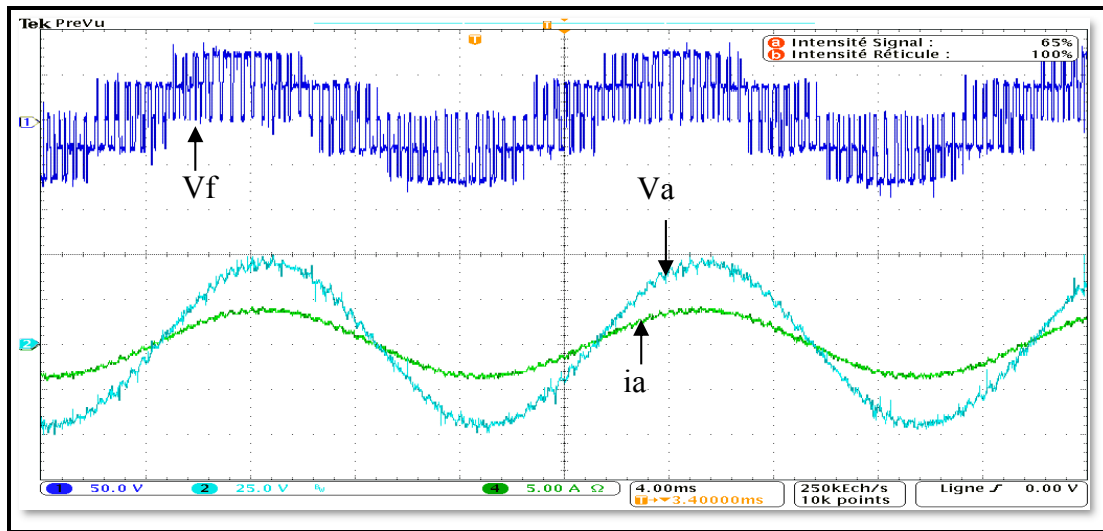


Figure 4.30 Steady state response of the system

Figure 4. 31 shows the dynamic response of the system during the variation of the output reference voltage. The output voltage follows exactly the reference variation, satisfying the performance of the control algorithm. The dynamic response shows the fast response of the output voltage during the variation of the reference voltage.

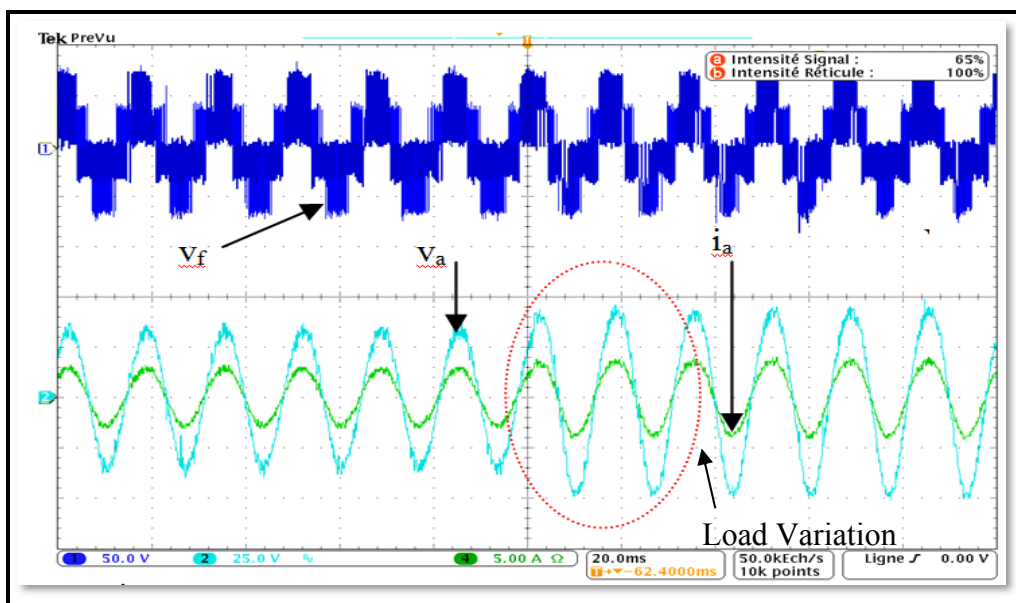


Figure 4.31 Reference load voltage variation from 30 to 45 V

In Figure 4.32, the system is tested for interaction between PVS, PHEV and GGS. At the beginning, the GGS is set to zero, the PVS generates more power than the load demand; the extra power is sent to charge the battery. When the PVS does not generate any power and GGS is still zero, the battery starts immediately sending power to satisfy the load demand. The battery is usually used to supply power for small applications such as lighting and TV at night.

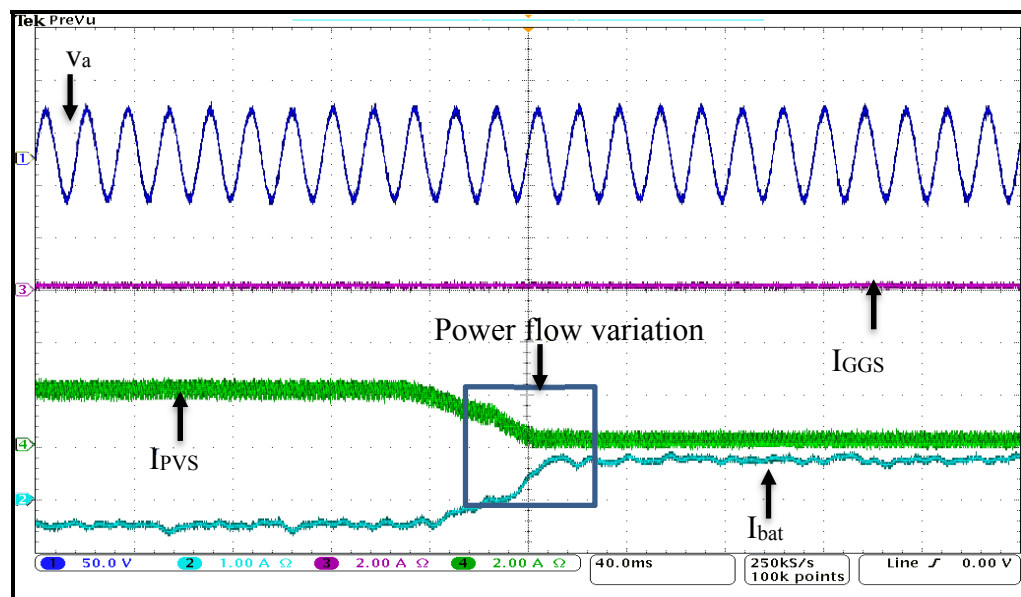


Figure 4.32 Feeding of load from PVS and batteries of PHEV

The Figure 4.33 shows the dynamic response of the system when I_{PVS} is zero, the GGS is turned on automatically to satisfy the load demand and also charges the battery. When the GGS is switched OFF, the battery will alone feed the load and the PVS is still OFF.

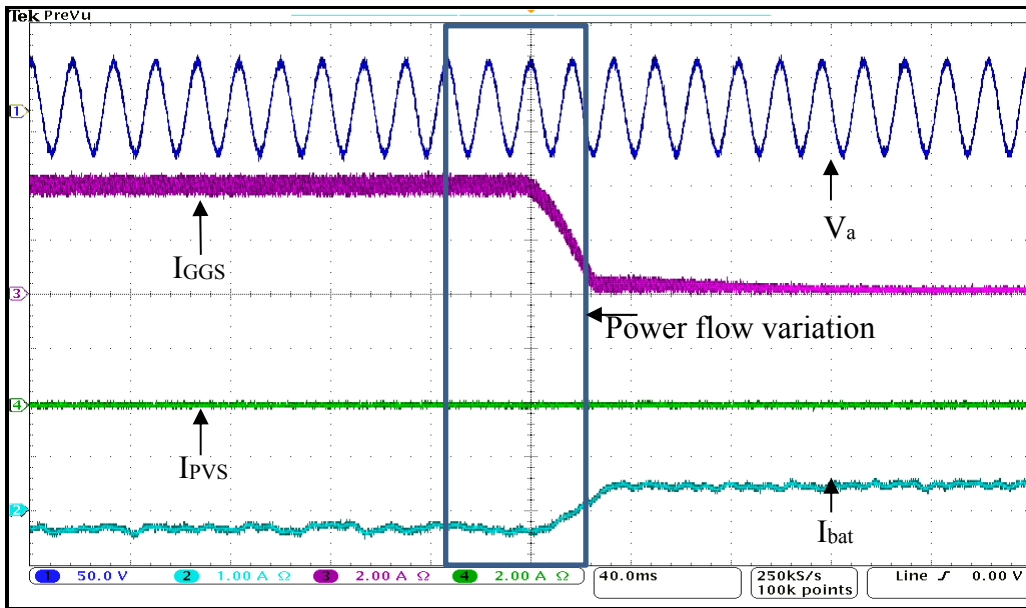


Figure 4.33 Load voltage with GGS and batteries without PVS

Figure 4.34 shows the perfect regulation of the voltage at the PCC during the removing of one phase load. This kind of unpredictable change did not influence the functionality of the system due to the robustness of the control.

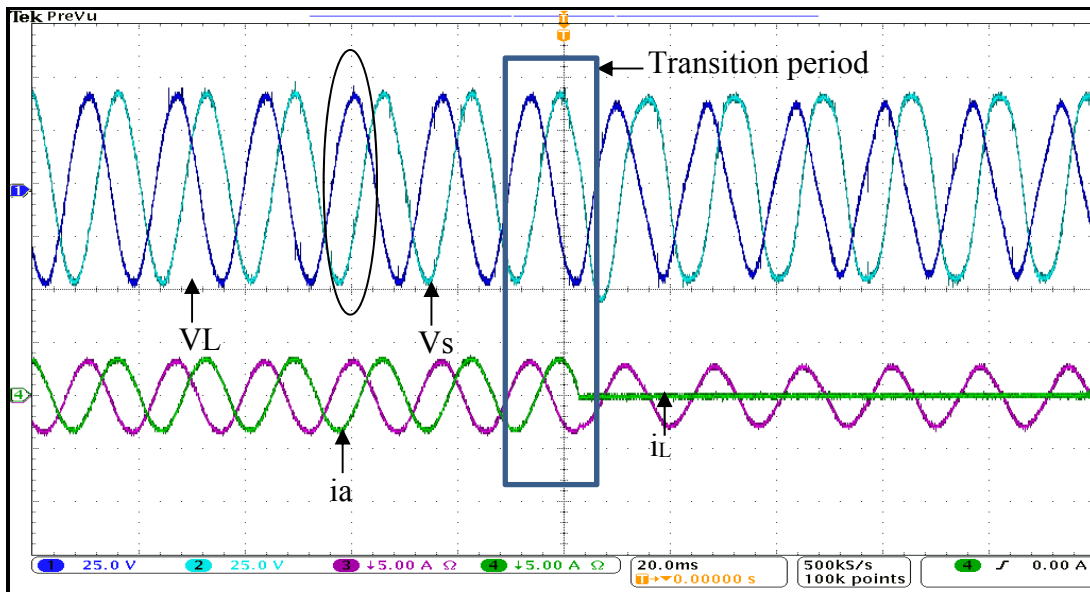


Figure 4.34 Experimental results with disconnection of one phase of the load

In Figure 4.35, the system is tested with a nonlinear load and without active damping control. The load voltage is highly distorted, which means that the entire current harmonics are flowing through the capacitor of the output filter C_f which generates voltage harmonic.

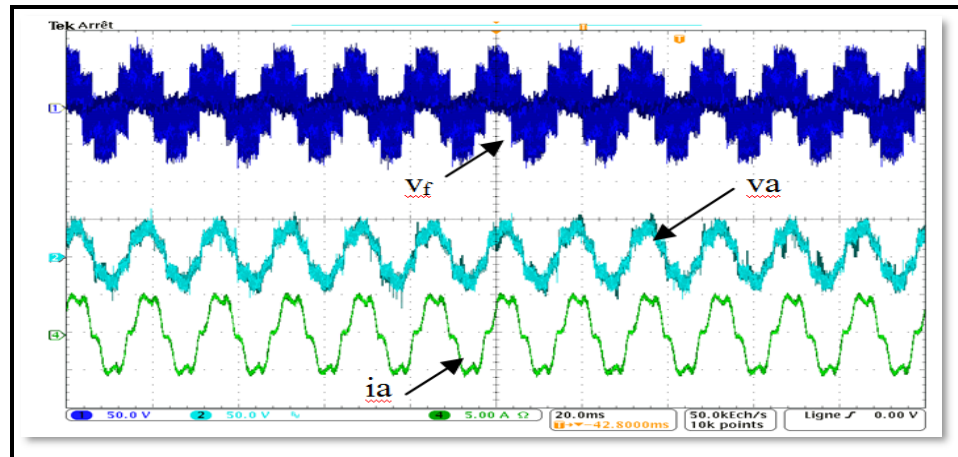


Figure 4.35 Voltage Quality of system without active damping

In Figure 4.36, the system is tested with a nonlinear load including active damping control. The distortion of load voltage is significantly reduced, that means the current harmonics flows through the capacitor are much reduced, because the value of the capacitor C_f is reduced to C_{fi} hence the impedance is increased which limits the current harmonics flowing through it.

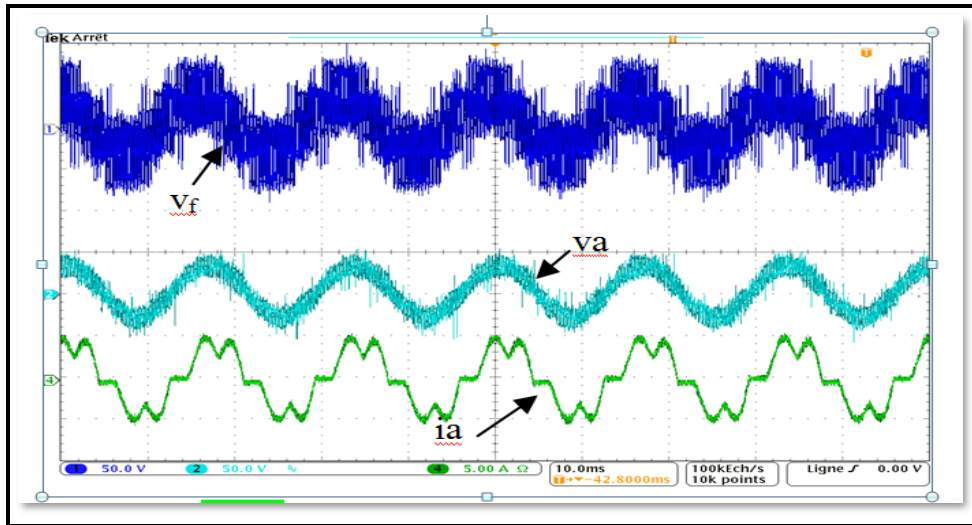


Figure 4.36 Voltage Quality of system with active damping

4.4 Conclusion

The design and control of the Net Zero Energy House based on micro grid concept has been successfully validated experimentally. For ON grid operation mode the VSC-AHF is controlled to flow the power from PVS to feed the load and sends the extra power to the grid. The VSC-AHF also used to charge the PHEV from the grid and eliminate harmonics current, compensates reactive power, unbalance load and manages the power flow. For the OFF grid operation mode, the proposed algorithm is able to force the system working on the standalone mode. The voltage at the PCC remains constant.

For standalone system, the experimental validation has demonstrated the proposed control algorithm for active damping technique without using any additional sensor. This technique has allowed reducing the number of physical components by eliminating the damping resistor. In addition, the size of LC filter of the VSC is reduced five time by shifting the resonant frequency to 21000 rad/s. Finally, the power management of the system has been controlled using fuzzy logic supervisor built on 25 rules. The smart interaction between PVS and GGS has contributed to reduce the size of energy storage system of battery while ensuring an uninterruptible power supply.

CONCLUSION AND RECOMMENDATIONS

Conclusion

This thesis presents a comprehensive research work in the area of micro-grid enhancement utilizing renewable energy resources. It addresses the control and real-time implementation aspects of MG for practical applications. Several new algorithms and concept are introduced, supported by thorough analytical studies and approved by means of offline simulation and validated through real-time experimental implementation. Furthermore, the scope of presented work covers voltage source converter with single and three phase using as an active harmonic filter, bidirectional battery charger with five level converter for electric vehicle, photovoltaic system, gas generator set, water pump and electrical grid.

The most significant conclusions of this research work are briefly summarized as follow:

- A thorough literature review of the past and the most recent research works in the development of MG and its reliability was conducted. A conceptual analysis to understand the functionality of the main element in MG control is carried out. Based on the given analytical study, a mathematical model is set up from which the control law of MG concept was extracted. Reported literatures on the power quality, energy management for standalone and grid connected system application based on MG concept were evaluated. A brief review on power factor and harmonic current compensation technique was also conducted;
- Extended reviews along with the feasibility of the ON and OFF grid mode of operation for the NZEH to ensure an uninterruptible power supply and to improve the power quality of the system were investigated. Furthermore, many controls algorithms have been investigated in order to find the best way to reduce the sensors' number, the degree of control complexity, while keeping a better power quality as well as the system reliability. The NZEH based on MG concept was validated theoretically and

experimentally for different scenarios of ON and OFF mode of operation. For ON grid mode, the standard norm of power quality is respected, the unbalance load, the harmonic and reactive power are respectively compensated adequately. The energy management between different sources is well evaluated and controlled depending on load demand. For OFF grid operation mode, the load voltage is kept clean and constant and the house remains continuously supplied even when the grid is disconnected;

- The new approach of bidirectional battery charger base on buck-boost converter and single dc-ac multilevel converter has been developed and tested in order to allow plug-in hybrid electric vehicle to be charged directly from dc or from ac source depending on availability of charging mode. A sliding mode approach has been developed to control the charging and discharging the PHEV and the stability were carried out and validated;
- The development of active damping control technique without using any additional sensor has allowed reducing the losses of the output filter, reducing the component of the system by eliminating the passive damping resistor and finally contributing in the voltage quality improvement;
- The proposed technique of resonant frequency shifting had allowed reducing five times the size of $L_f C_f$ output filter of the voltage source converter while keeping high performance of operation. This is providing an additional option for the hardware MG optimization;

The smart energy management was achieved through the developed fuzzy logic supervisor built on 25 rules. The mixed operation of photovoltaic system and gas generator set has contributed in the battery size reduction while ensuring an uninterruptible power supply. The Gas Generator Set was integrated successfully with other energy sources to ensure uninterruptible power supply. The experimental results are promising and could be a benchmark for the MG many countries. Finally, the economic study has approved the

reliability of the proposed MG system, and especially more reliable for the developing countries like African Central States;

In summary, this thesis dissertation puts forward a novel approach and newly developed adapted control strategies for MG which not only contributes in the scientific and technical development for energy management and power quality improvement, but also reduces the overall system cost. It also proves that with a minutely adapted controller and a proper dispatch of locally available energy resources, significant advantages can be achieved. The research work reported in this thesis along with experimentally validated results would certainly be considered as a remarkable development in the field of microgrid technologies for remote area and grid connected mode and helps reaching the concept of Net Zero Energy House expected by many people worldwide.

Recommendations for future researchers

This thesis provides the comprehensive aspects of the Microgrid system based on renewable energy to ensure an uninterruptible power supply for remote area and support the public network.

This section presents some guidelines to extend the research work as it stands now. A brief discussion on the directions for possible future work is also outlined.

Although the simulation and the experimental validation of this work show satisfactory results, some recommendations for future research work are important for the performance and more reliability. The recommendations for thesis work extension are summarized as follows:

- In the proposed topologies, a power generated by the gas generator set is converted to the dc using rectifier and boost converter to feed a dc load and then reconverted to the ac via a voltage source inverter to feed the ac load. These multiple stages of conversion may increase losses. It is recommended a deep study of control and topology that could

connect the same unit of gas generator set into the ac load without any conversion of power and into dc load side with at most one conversion;

- Renewable energies as solar, wind and biogas are more accessible and emerging as alternate sources of electricity. The power management of different source of energy connected together and their reliability mode of operation is a great and complex task which required more and more research the real smart grid concept. However, for increasing the efficiency of the system, it is recommended to investigate the new concept of power management as a Big Data-analysis of real customer consumption data from distribution grids, knowledge regarding the customer behaviour, as well as suggest how a future categorization based on the consumption pattern of each individual customer can look like. The aim is to integrate how the customer gets incentivized in this categorization, and thereby aiding the creation of more efficient tariffs;
- Improvement of NZEH based on MG to meet the standard as:
 - ANSI/ASHRAE/IESNA Standard 90.1, *Energy Standard for Buildings Except Low-Rise Residential Buildings*
 - ANSI/ASHRAE/IESNA Standard 100, *Energy Efficiency in Existing Buildings*
 - ANSI/ASHRAE Standard 105, *Standard Methods of Determining, Expressing, and Comparing Building Energy Performance and Greenhouse Gas Emissions*
 - ANSI/ASHRAE/IESNA Standard 189.1, *Standard for the Design of High-Performance Green Buildings Except Low-Rise Residential Buildings*
 - "ASHRAE Vision 2020, Producing Net Zero Energy Buildings," ASHRAE 2008.
 - Energy Independence and Security Act of 2007 (EISA)
 - Executive Order 13693, "Planning for Federal Sustainability in the Next Decade"
 - *International Energy Conservation Code (IECC)*
 - Title 24—2008 *California's Energy Efficiency Standards for Residential and Non-Residential Buildings*

ANNEX I

OPTIMISATION OF THE DC-AC INVERTER USING SEMISEL SOFTWARE

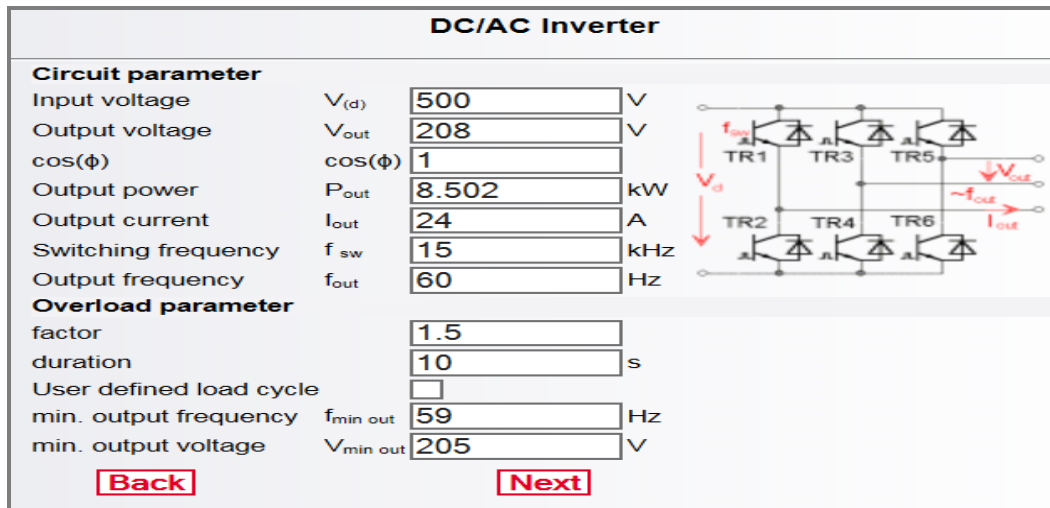


Figure-A I-1 Input parameters of VSC DC/AC

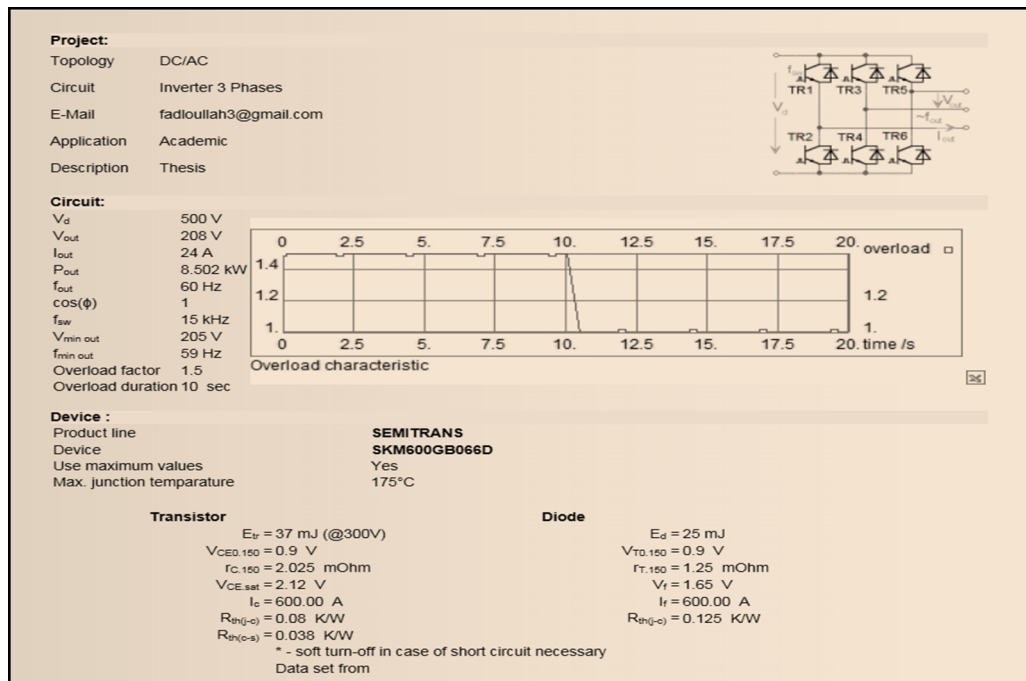


Figure-A I-2 Overload characteristics

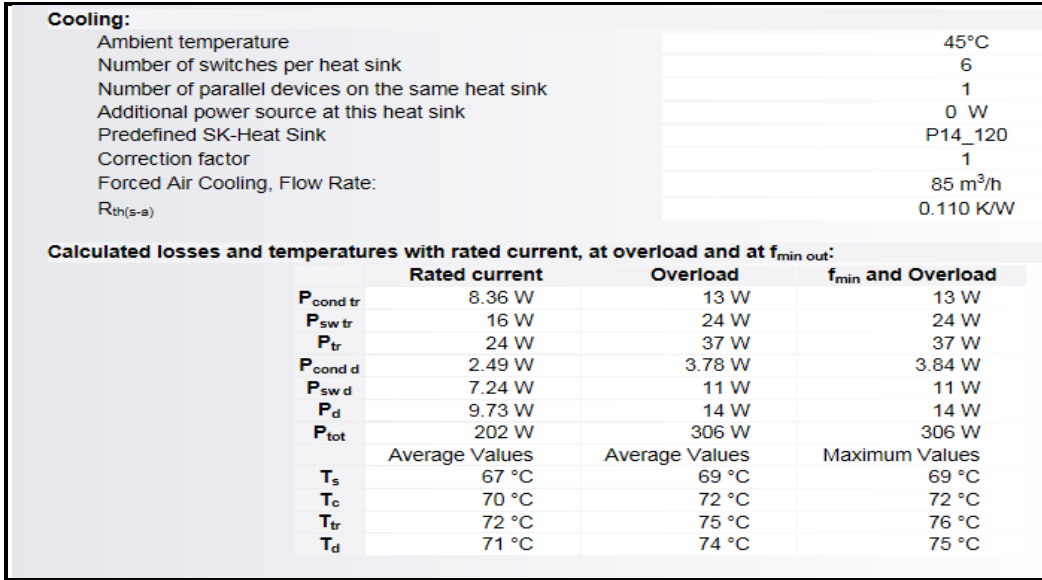


Figure-A I-3 Losses calculation

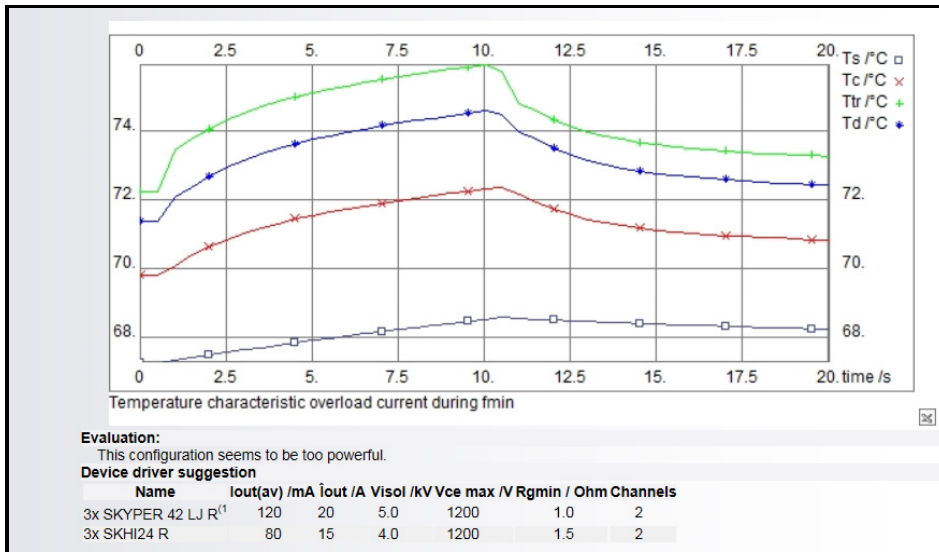


Figure-A I-4 Temperature characteristics

ANNEX II

SYSTEM PARAMETERS

Table-A II-1 Parameters used in the experimental validation of NZEH

| | |
|--|--------------|
| Line source voltage, V_s | 208 V |
| Source frequency, f_s | 60 Hz |
| Switching frequency | 15 kHz |
| Inductor of FA, L_f | 1.43 mH |
| Capacitor of AF, C_{dc} | 5000 μ F |
| THD of the load current, | 27% |
| THD of the source current | 5.4% |

Table-A II-2 Parameters used in simulation for standalone system

| Parameters | Values |
|--|----------------------------|
| Load voltage frequency | 60 Hz |
| Inductive filter (L_f) | 1.5 mH |
| Inductive filter (L_{fl}) | 0.3 mH |
| Switching frequency | 5 kHz |
| Rectifier nonlinear load (R_L and C_L) | 10 Ω , 1000 μ F |
| DC capacitor (C_{dc}) | 5000 μ F |
| PVA output | 40 kW |
| GGS | 40 kW |

Table-A II-3 Parameters used in experimentation setup for standalone system

| | |
|---|----------------------------|
| Load voltage frequency | 60 Hz |
| Inductive filter (L_f) | 1.5 mH |
| Inductive filter (L_{fl}) | 0.3 mH |
| Battery nominal voltage | 100 V |
| Switching frequency | 5 kHz |
| Nonlinear load (R_L and C_L) | 40 Ω , 1000 μ F |
| DC capacitor (C_{dc}) | 5000 μ F |

ANNEX III

HARDWARE SETUP DETAILS

Figure A.III-1 shows the mechanical design of the Rack of VSC-AHF.

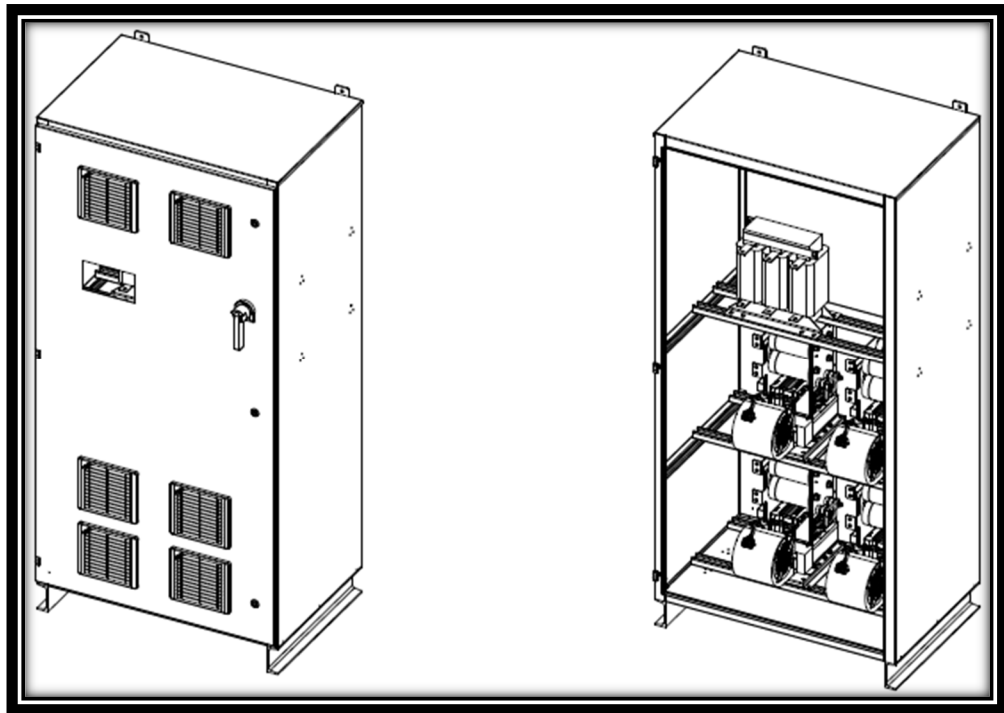


Figure-A III-1 Rack of VSC-AHF

A concept drawing of the one IGBT leg of SKiiP1013 assembly including gate driver, heatsink and bus dc sensor is shown Figure A.III-2.

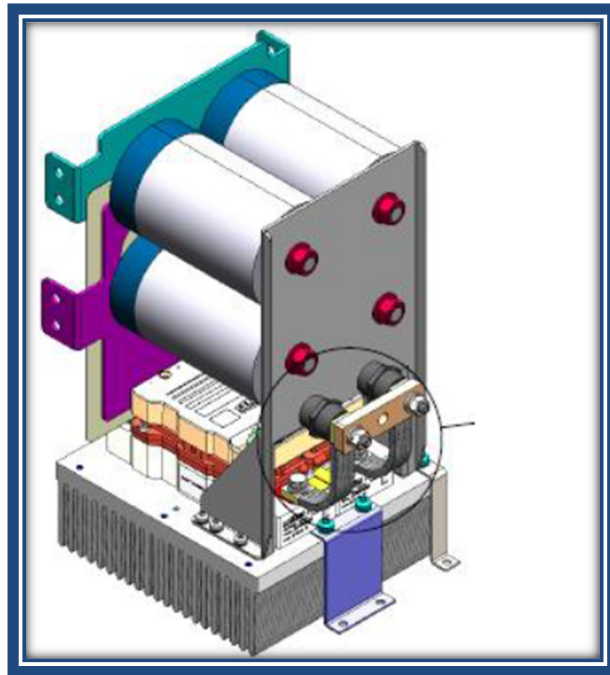


Figure-A III-2 One IGBT leg of SKiiP1013 assembly including gate driver, heatsink and bus dc sensor

Figure-A III-3a and Figure-A III-3b show more component of SKiiP1013 inverter assembly including gate driver, heatsink, capacitors, fan and bus dc sensor.

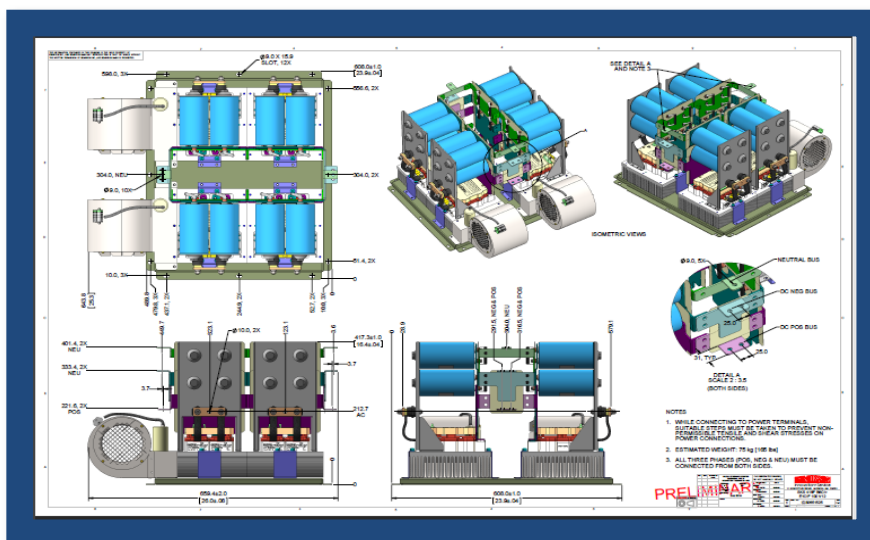


Figure-A III-3a SKiiP1013 inverter assembly including gate driver, heatsink, capacitors, fan and bus dc sensor

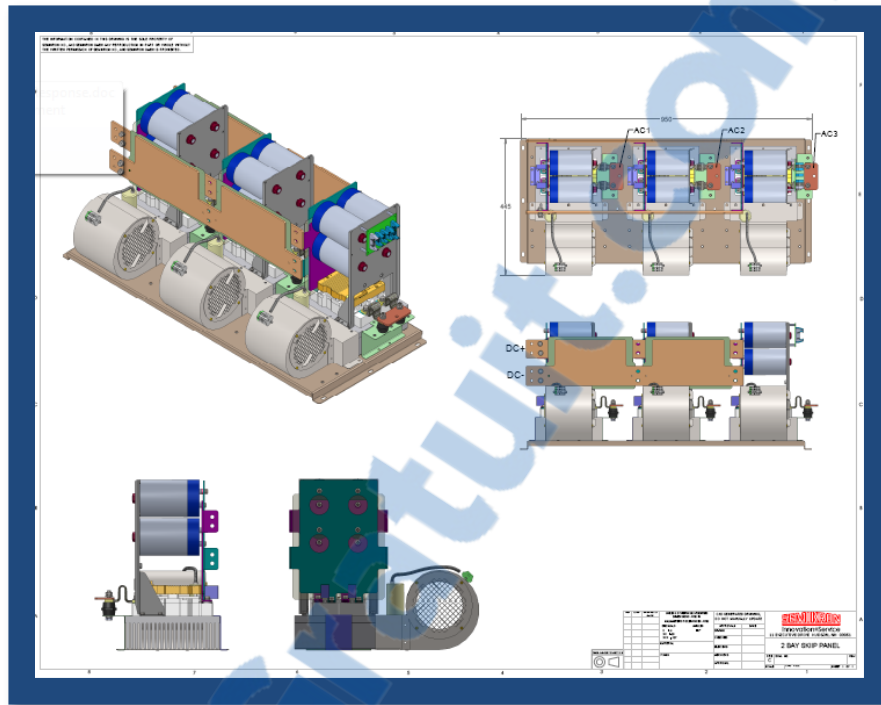


Figure-A III-3b SKiiP1013 inverter assembly including gate driver, heatsink, capacitors, fan and bus dc sensor

Figure-A III-4 to A III-6- show the overview of gate driver board of SKiiP1013 assembly and its functionality.

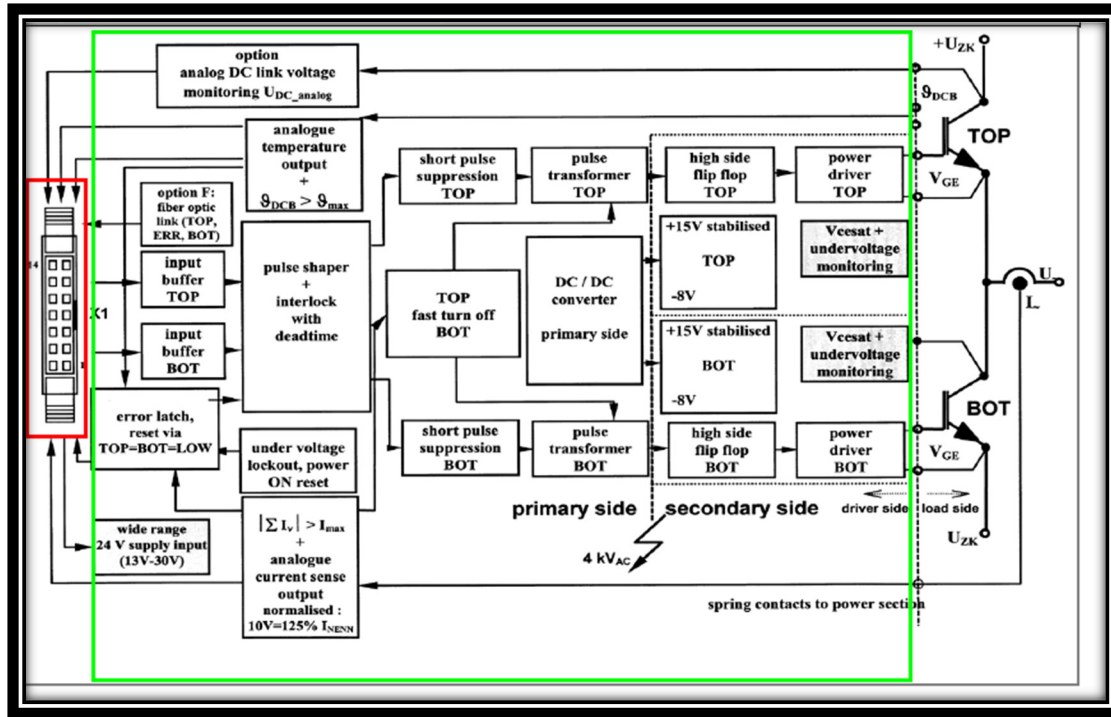


Figure-A III-4 Gate Driver Board block diagram of SKiiP1013

| Picture | Pin Description | Dimensions |
|---------|--|------------|
| | shield 1 ERROR HB1 OUT 3 BOT HB2 IN 5 TOP HB2 IN 7 ERROR HB3 OUT 9 Overtemp.OUT 11 Ubc ana out 13 +24Vdc IN 15 +15Vdc OUT 17 GND 19 GND aux 21 GND aux 23 GND aux 25 | |
| | 2 BOT HB1 IN 4 TOP HB1 IN 6 ERROR HB2 OUT 8 BOT HB3 IN 10 TOP HB3 IN 12 reserved 14 +24Vdc IN 16 +15Vdc OUT 18 GND 20 Temp. ana OUT 22 I ana OUT HB1 24 I ana OUT HB2 26 I ana OUT HB3 | |

Figure-A III-5 Connector DIN41651, GD Type, male plug, vertical, top view

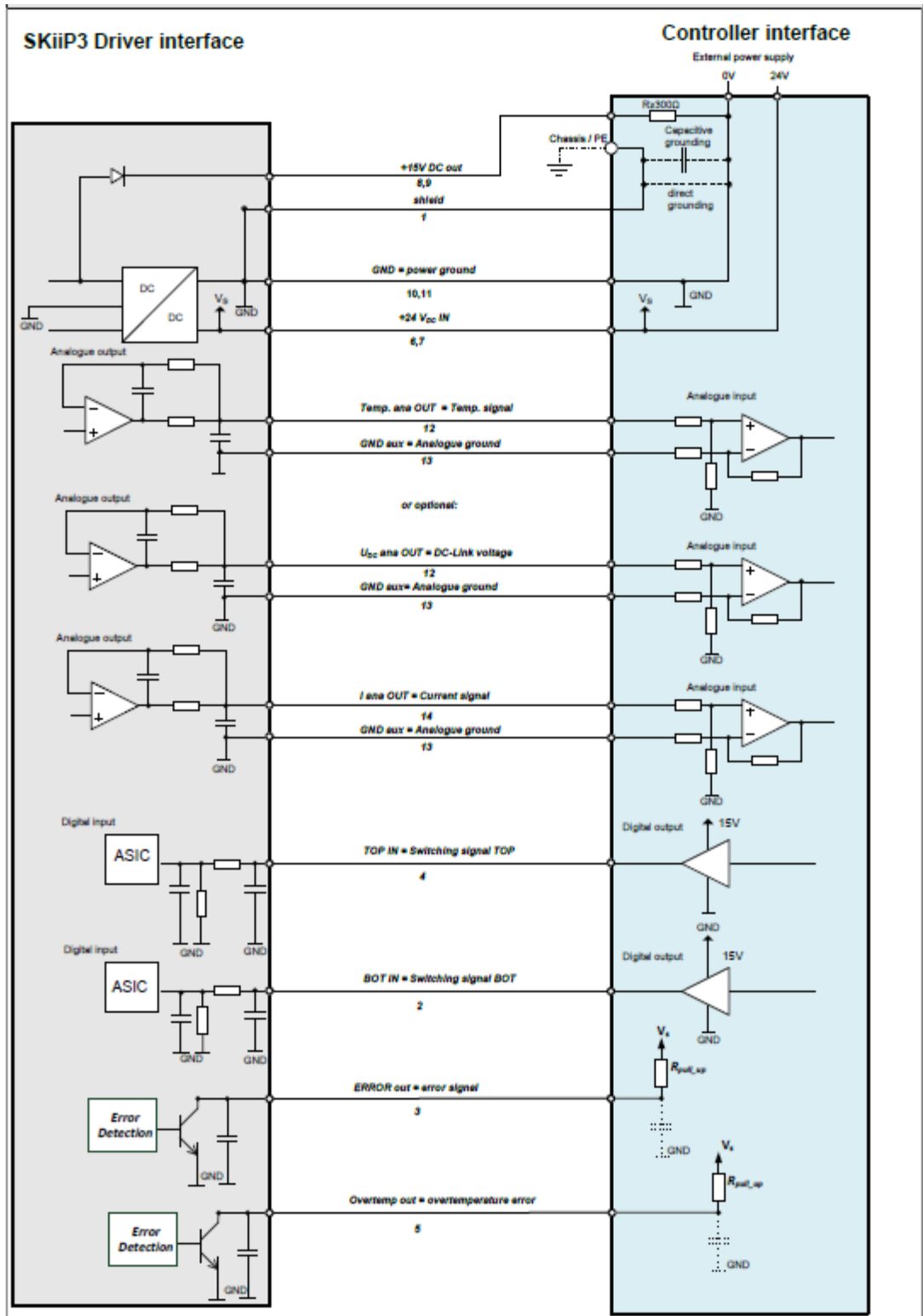
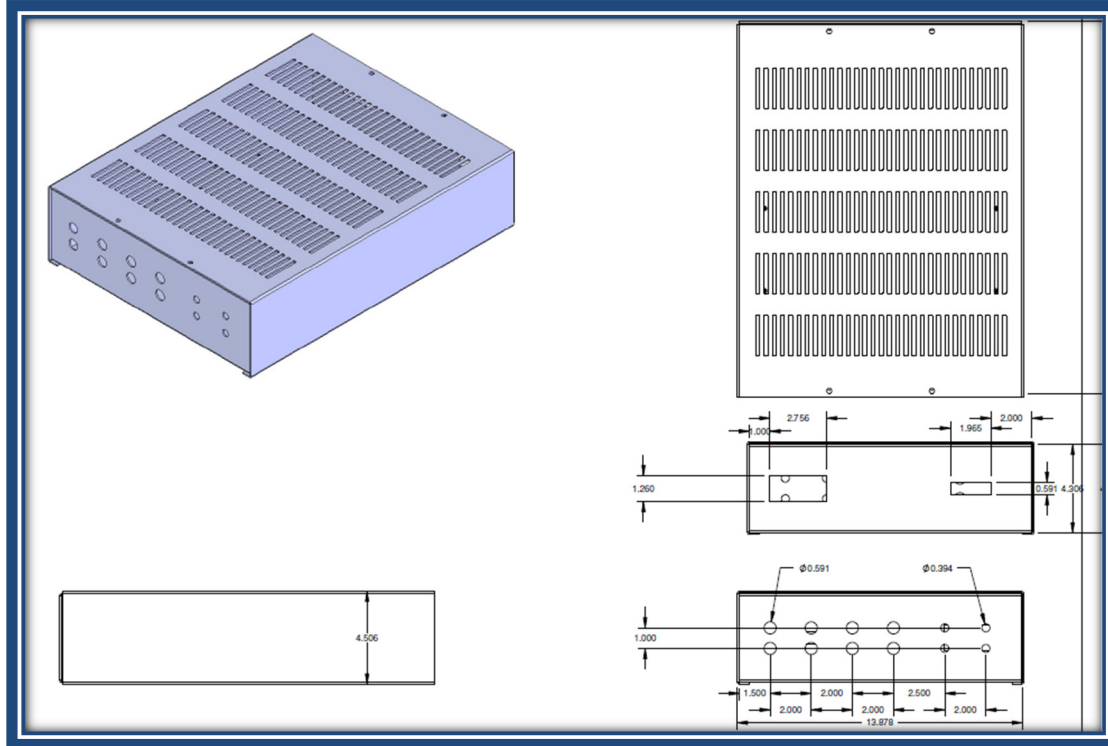


Figure-A III-6 Overview schematics of gate driver

Figures-A III-7 and A III-11 show the different component of control box.



Figures-A III-7 Rack of the control box

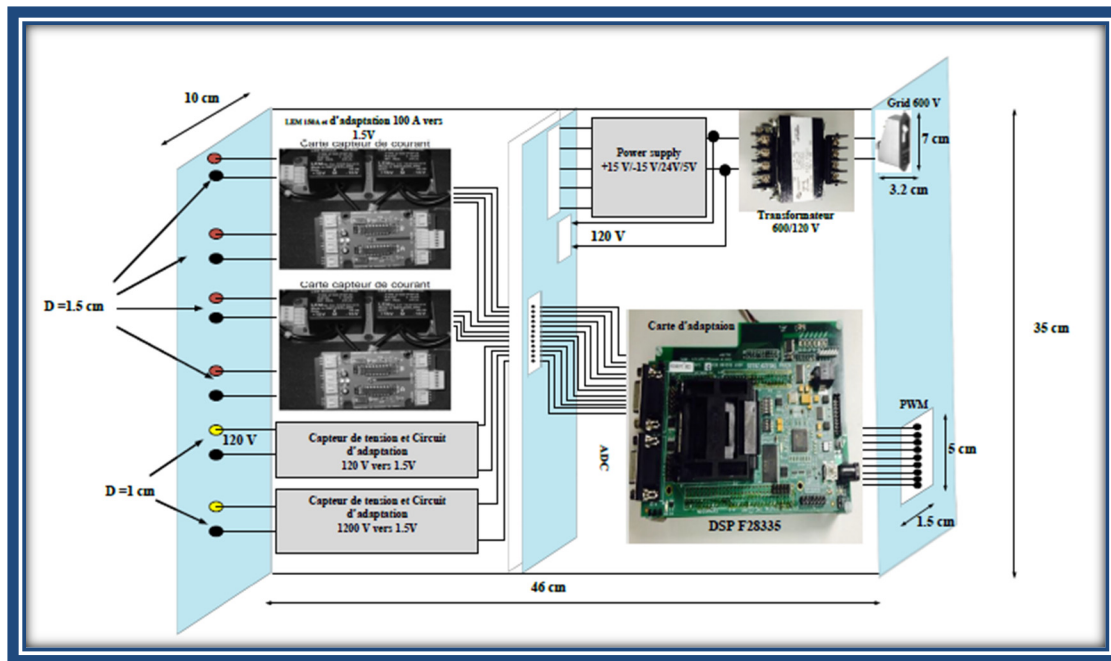


Figure-A III-8 Inside of the control box

Comparing to others models, the eZdsp F28335 is one of powerful and high performance controllers of C200 family. eZdsp F28335 has six independent enhanced PWM (ePWM) modules with two output channel each: ePWMxA and ePWMxB. More details are shown in Figure-A III-9 to A III-11 and Table-A III-1 to A III-2.

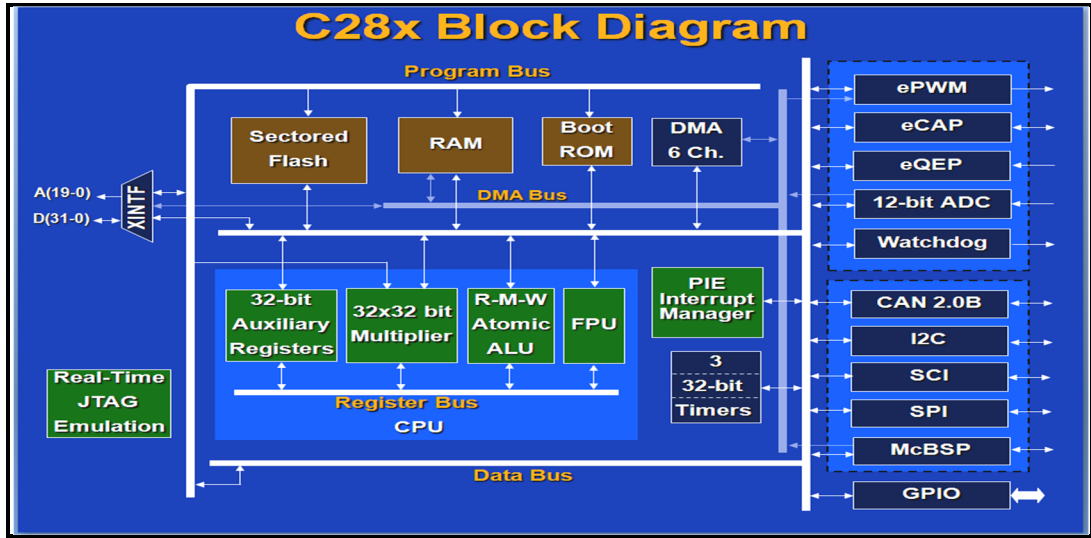


Figure-A III-9 Block diagram of DSP C28x family

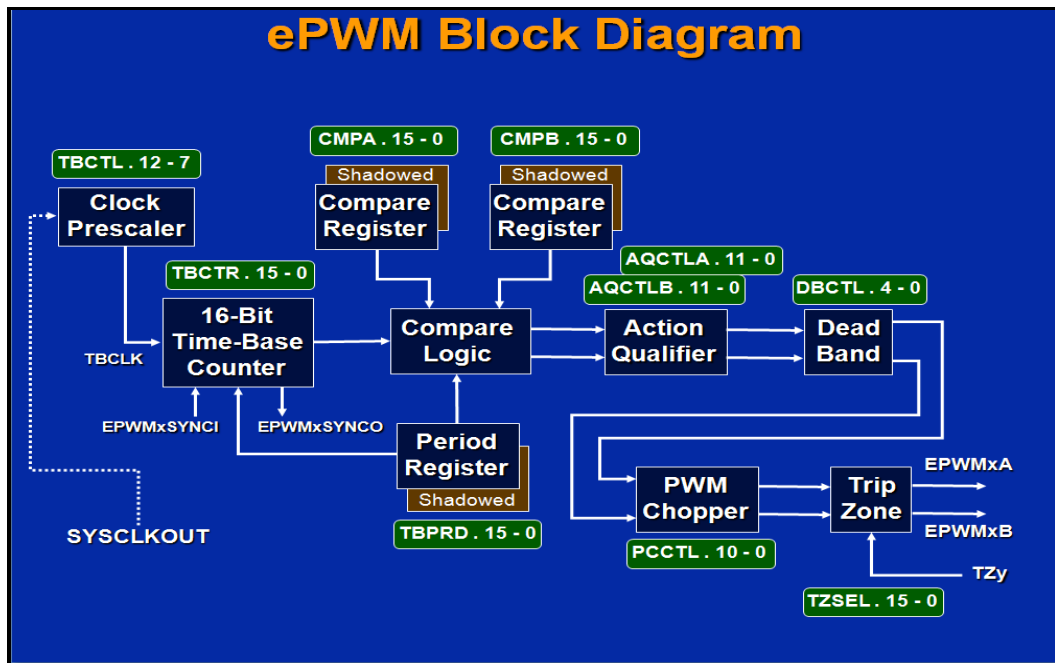


Figure-A III-10 PWM block diagram

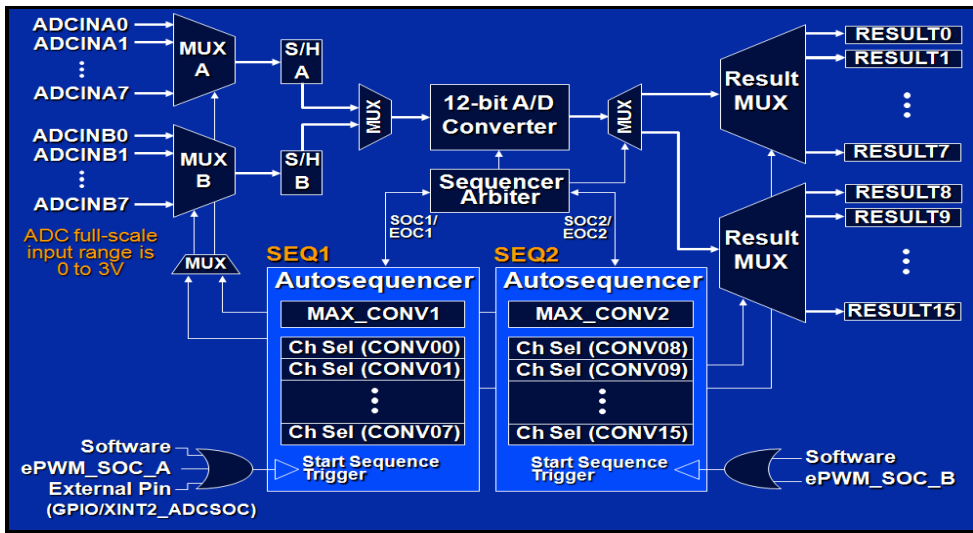


Figure-A III-11 ADC input channels of eZdsp F28335 from inside view

Table-A III-1 Comparison between different models of C2000 DSP family

| | MHz | FPU | Flash | RAM | DMA | PWM/ HRPWM | CAP/ QEP | Communication Ports |
|--------|-----|-----|-------|-----|-----|---------------|-------------|--|
| F28335 | 150 | Yes | 256 | 34 | Yes | 18/6 | 6/2 | SPI, 3x SCI, I ² C, 2x McBSP, 2x CAN |
| F28334 | 150 | Yes | 128 | 34 | Yes | 18/6 | 4/2 | SPI, 3x SCI, I ² C, 2x McBSP, 2x CAN |
| F28332 | 100 | Yes | 64 | 26 | Yes | 16/4 | 4/2 | SPI, 2x SCI, I ² C, McBSP, 2x CAN |
| | | | | | | | | |
| F28235 | 150 | No | 256 | 34 | Yes | 18/6 | 6/2 | SPI, 3x SCI, I ² C, 2x McBSP, 2x CAN |
| F28234 | 150 | No | 128 | 34 | Yes | 18/6 | 4/2 | SPI, 3x SCI, I ² C, 2x McBSP, 2x CAN |
| F28232 | 100 | No | 64 | 26 | Yes | 16/4 | 4/2 | SPI, 2x SCI, I ² C, McBSP, 2x CAN |

The eZdsp F28335 has a block diagram of the ADC module containing 16 analog input channels as shown in Table A III-2.

Table A III-2 ADC input channels of eZdsp F28335

| Input chanel ADCINA_i | Input chanel ADCINB_i |
|--|--|
| ADCINA0 | ADCINB |
| ADCINA1 | ADCINB1 |
| ADCINA2 | ADCINB |
| ADCINA3 | ADCINB3 |
| ADCINA | ADCINB4 |
| ADCINA5 | ADCINB5 |
| ADCINA6 | ADCINB6 |
| ADCINA7 | ADCINB7 |

LIST OF BIBLIOGRAPHICAL REFERENCES

- (A.P.E.S), A. E. S. (2012). *Geothermal Energy*. Retrieved from <https://sites.google.com/site/corsiscramsite/energy-resources-consumption/renewable-energy>
- A. de Almeida, L. M. J. D. (2003). *Power Quality Problems and New Solutions*. University of Coimbra, Pólo II 3030-290 Coimbra (Portugal).
- Abouelmahjoub, Y., Giri, F., Abouloifa, A., Chaoui, F. Z., Kissaoui, M., & Naitali, A. (2014, 8-10 Oct. 2014). *Nonlinear adaptive control of single phase half bridge shunt active power filter*. Paper presented at the 2014 IEEE Conference on Control Applications (CCA).
- Agency, I. R. E. (2015a). Africa 2030: Roadmap for a renewable energy future. Retrieved from http://www.irena.org/DocumentDownloads/Publications/IRENA_Africa_2030_REmap_2015_low-res.pdf.
- Agency, I. R. E. (2015b). *BATTERY STORAGE FOR RENEWABLES: MARKET STATUS AND TECHNOLOGY OUTLOOK*. Retrieved from http://www.irena.org/documentdownloads/publications/irena_battery_storage_report_2015.pdf
- Akagi, H. (2005). Active Harmonic Filters. *Proceedings of the IEEE*, 93(12), 2128-2141.
- Akagi, H., Srianthumrong, S., & Tamai, Y. (2003, 12-16 Oct. 2003). *Comparisons in circuit configuration and filtering performance between hybrid and pure shunt active filters*. Paper presented at the 38th IAS Annual Meeting on Conference Record of the Industry Applications Conference, 2003.
- A. A. Akhil, G. Huff, A. B. Currier, B. C. Kaun, D. M. Rastler, S. B. Chen, *et al.*, *DOE/EPRI 2013 electricity storage handbook in collaboration with NRECA*: Sandia National Laboratories Albuquerque, NM, 2013.
- Aredes, M., Hafner, J., & Heumann, K. (1997). Three-phase four-wire shunt active filter control strategies. *Power Electronics, IEEE Transactions on*, 12(2), 311-318.
- Asiminoaei, L., Blaabjerg, F., & Hansen, S. (2005, 6-10 March 2005). *Evaluation of harmonic detection methods for active power filter applications*. Paper presented at the Twentieth Annual IEEE Applied Power Electronics Conference and Exposition, 2005. APEC 2005.

- Awaar, V. K., Jugge, P., & Tara Kalyani, S. (2016, 14-17 Dec. 2016). *Mitigation of voltage sag and Power Quality improvement with an optimum designed Dynamic Voltage Restorer*. Paper presented at the 2016 IEEE International Conference on Power Electronics, Drives and Energy Systems (PEDES).
- Banerji, A., Biswas, S. K., & Singh, B. (2016a). Enhancing Quality of Power to Sensitive Loads With Microgrid. *IEEE Transactions on Industry Applications*, 52(1), 360-368. doi:10.1109/tia.2015.2478884.
- Banerji, A., Biswas, S. K., & Singh, B. (2016b). *Enhancing Quality of Power to Sensitive Loads With Microgrid*. (52). (1).
- B. Bolund, H. Bernhoff, and M. Leijon, "Flywheel energy and power storage systems," *Renewable and Sustainable Energy Reviews*, vol. 11, pp. 235-258, 2007.
- Bedir, A., Ozpineci, B., & Christian, J. E. (2010a, 19-22 April 2010). *The impact of plug-in hybrid electric vehicle interaction with energy storage and solar panels on the grid for a zero energy house*. Paper presented at the Transmission and Distribution Conference and Exposition, 2010 IEEE PES.
- B. C. Steele and A. Heinzl, "Materials for fuel-cell technologies," *Nature*, vol. 414, pp. 345-352, 2001.
- Bedir, A., Ozpineci, B., & Christian, J. E. (2010b, 19-22 April 2010). *The impact of plug-in hybrid electric vehicle interaction with energy storage and solar panels on the grid for a zero energy house*. Paper presented at the IEEE PES T&D 2010.
- Benchaita, L., Saadate, S., & Salem nia, A. (1999). A comparison of voltage source and current source shunt active filter by simulation and experimentation. *Power Systems, IEEE Transactions on*, 14(2), 642-647.
- Bevrani, H., Habibi, F., Babahajyani, P., Watanabe, M., & Mitani, Y. (2012). Intelligent Frequency Control in an AC Microgrid: Online PSO-Based Fuzzy Tuning Approach. *IEEE Transactions on Smart Grid*, 3(4), 1935-1944. doi:10.1109/tsg.2012.2196806.
- Bidram, A., & Davoudi, A. (2012). Hierarchical Structure of Microgrids Control System. *IEEE Transactions on Smart Grid*, 3(4), 1963-1976. doi:10.1109/tsg.2012.2197425.
- Bor-Ren, L., Yuan-An, O., & Tsung-Yu, Y. (2004, 2-4 Sept. 2004). *Shunt active power filter with three-phase switch-clamped inverter*. Paper presented at the Proceedings of the 2004 IEEE International Conference on Control Applications, 2004.
- Bustamante, F., Bitemas, J., Borjas, J., Vilorio, L., Edwards, J., Chavez, J., & Haa, A. (2006, 15-18 Aug. 2006). *Cascade Protection with Transient Voltage Surge Suppressors (TVSS) in Variable Speed Drive for Electro-Submersible Pumps*. Paper presented at

the 2006 IEEE/PES Transmission & Distribution Conference and Exposition: Latin America.

Cai, N., Xu, X., & Mitra, J. (2011, 24-29 July 2011). *A hierarchical multi-agent control scheme for a black start-capable microgrid*. Paper presented at the 2011 IEEE Power and Energy Society General Meeting.

Chaoyong, H., Xuehao, H., & Dong, H. (2010, 24-28 Oct. 2010). *Hierarchical control techniques applied in micro-grid*. Paper presented at the 2010 International Conference on Power System Technology.

Cho, B. G., Lee, Y., & Sul, S. K. (2015, 22-25 June 2015). *Active damping method equivalent to series resistor effect for LCL filters in a grid-connected PWM converters*. Paper presented at the 2015 IEEE 6th International Symposium on Power Electronics for Distributed Generation Systems (PEDG).

Dörfler, F., Simpson-Porco, J. W., & Bullo, F. (2016). Breaking the Hierarchy: Distributed Control and Economic Optimality in Microgrids. *IEEE Transactions on Control of Network Systems*, 3(3), 241-253. doi:10.1109/tens.2015.2459391.

Eddin, M. A. (2002). *Contribution à l'Etude des Compensateurs Actifs des Réseaux Electriques Basse Tension*. Louis Pasteur – Strasbourg I École Doctorale Sciences Pour l'Ingénieur. Retrieved from http://green.univ-lorraine.fr/data/theses/alali_2002.pdf

Edremitlioglu, H. H. (2010). *ECONOMICAL, ENVIRONMENTAL OUTCOMES OF WIND ENERGY PRODUCTION IN TURKEY*. (Bachelor of Science), WORCESTER POLYTECHNIC INSTITUTE. Retrieved from [Econ_and_Eviron_outcomes_of_Wind_Energy_Production_in_Turkey.pdf](#).

Emadi, A. (2011). Transportation 2.0. *IEEE Power and Energy Magazine*, 9(4), 18-29. doi:10.1109/mpe.2011.941320.

Energy, S. R. (2012). *How Hydropower Generation Works*. Sky Renewable Energy. Retrieved from <http://www.skyrenewableenergy.com/renewable-energy/hydro/>.

Erb, D. C., Onar, O. C., & Khaligh, A. (2010, 21-25 Feb. 2010). *Bi-directional charging topologies for plug-in hybrid electric vehicles*. Paper presented at the Applied Power Electronics Conference and Exposition (APEC), 2010 Twenty-Fifth Annual IEEE.

Escobar, G., Valdez, A. A., Torres-Olguin, R. E., & Martinez-Montejano, M. F. (2007). A Model-Based Controller for A Three-Phase Four-Wire Shunt Active Filter With Compensation of the Neutral Line Current. *Power Electronics, IEEE Transactions on*, 22(6), 2261-2270.

- Etemadi, A. H., & Iravani, R. (2013). Overcurrent and Overload Protection of Directly Voltage-Controlled Distributed Resources in a Microgrid. *IEEE Transactions on Industrial Electronics*, 60(12), 5629-5638. doi:10.1109/tie.2012.2229680.
- Etz, R., Patarau, T., Daraban, S., & Petreus, D. (2012, 9-13 May 2012). *Microgrid model for fast development of energy management algorithms*. Paper presented at the Electronics Technology (ISSE), 2012 35th International Spring Seminar on.
- Ferraro, M., Sergi, F., Antonucci, V., Guarino, F., Tumminia, G., & Cellura, M. (2016, 7-10 June 2016). *Load match and grid interaction optimization of a net zero energy building through electricity storage: An Italian case-study*. Paper presented at the 2016 IEEE 16th International Conference on Environment and Electrical Engineering (EEEIC).
- Ferreira, F., Monteiro, L., Afonso, J. L., & Couto, C. (2008, 10-13 Nov. 2008). *A control strategy for a three-phase four-wire shunt active filter*. Paper presented at the 2008 34th Annual Conference of IEEE Industrial Electronics.
- Freire, R., Delgado, J., Santos, J. M., & de Almeida, A. T. (2010, 19-22 Sept. 2010). *Integration of renewable energy generation with EV charging strategies to optimize grid load balancing*. Paper presented at the Intelligent Transportation Systems (ITSC), 2010 13th International IEEE Conference on.
- Fujita, H., Yamasaki, T., & Akagi, H. (2000). A hybrid active filter for damping of harmonic resonance in industrial power systems. *Power Electronics, IEEE Transactions on*, 15(2), 215-222.
- Gawande, S. P., Pardeshi, S. M., Kadwane, S. G., Ramteke, M. R., Daigavane, M. B., Debre, P. D., & Bagde, B. Y. (2016, 14-17 Dec. 2016). *Capacitor voltage balancing techniques for three level capacitor clamped multilevel inverter under load compensation*. Paper presented at the 2016 IEEE International Conference on Power Electronics, Drives and Energy Systems (PEDES).
- Geng, Y., Yun, Y., Chen, R., Wang, K., Bai, H., & Wu, X. (2017). Parameters Design and Optimization for LC-Type Off-Grid Inverter with Inductor-Current-Feedback Active-Damping. *IEEE Transactions on Power Electronics*, PP(99), 1-1. doi:10.1109/TPEL.2017.2664812.
- Gous, M. G. F., & Beukes, H. J. (2004). *Sliding mode control for a three-phase shunt active power filter utilizing a four-leg voltage source inverter*. Paper presented at the Power Electronics Specialists Conference, 2004. PESC 04. 2004 IEEE 35th Annual.
- Grino, R., Cardoner, R., Costa-Castello, R., & Fossas, E. (2007). Digital Repetitive Control of a Three-Phase Four-Wire Shunt Active Filter. *Industrial Electronics, IEEE Transactions on*, 54(3), 1495-1503.

- Gupta, K. K., & Jain, S. (2014). Comprehensive review of a recently proposed multilevel inverter. *IET Power Electronics*, 7(3), 467-479. doi:10.1049/iet-pel.2012.0438
- Gupta, K. K., Ranjan, A., Bhatnagar, P., Sahu, L. K., & Jain, S. (2016). Multilevel Inverter Topologies With Reduced Device Count: A Review. *IEEE Transactions on Power Electronics*, 31(1), 135-151. doi:10.1109/TPEL.2015.2405012.
- HAMADI, A. (2010). *CONTRIBUTION À L'ÉTUDE DES FILTRES HYBRIDES DE PUISSANCE UTILISÉS POUR AMÉLIORER LA QUALITÉ DE L'ÉNERGIE DANS LE RÉSEAU ÉLECTRIQUE DE DISTRIBUTION*. ÉCOLE DE TECHNOLOGIE SUPÉRIEURE, ETS.
- Hamadi, A., Al-Haddad, K., & Rahmani, R. (2006, 9-13 July 2006). *Series active filter to mitigate power quality for medium size industrial loads (multi Pulses Transformer and modern AC drive)*. Paper presented at the 2006 IEEE International Symposium on Industrial Electronics.
- Hamadi, A., Javadi, A., Ndtoungou, A., Rahmani, S., & Al-Haddad, K. (2017, 22-25 March 2017). *Modeling and control to enhance a grid on/off operation of a single-phase system*. Paper presented at the 2017 IEEE International Conference on Industrial Technology (ICIT).
- Hamoud, F., Doumbia, M. L., & Chériti, A. (2015, 23-25 Nov. 2015). *Power factor improvement in WECS using cascade PI control of passive damping LCL-filter*. Paper presented at the 2015 International Conference on Sustainable Mobility Applications, Renewables and Technology (SMART).
- Harkouss, F., Fardoun, F., & Biwole, P. H. (2016, 13-15 July 2016). *Optimization of design parameters of a net zero energy home*. Paper presented at the 2016 3rd International Conference on Renewable Energies for Developing Countries (REDEC).
- Hauser, J., & Bamieh, B. (2015, 15-18 Dec. 2015). *Dynamics of a driven Stirling engine*. Paper presented at the 2015 54th IEEE Conference on Decision and Control (CDC).
- Hirve, S., Chatterjee, K., Fernandes, B. G., Imayavaramban, M., & Dwari, S. (2007). PLL-Less Active Power Filter Based on One-Cycle Control for Compensating Unbalanced Loads in Three-Phase Four-Wire System. *IEEE Transactions on Power Delivery*, 22(4), 2457-2465. doi:10.1109/tpwrd.2007.893450.
- H. Ibrahim, A. Ilinca, and J. Perron, "Energy storage systems—characteristics and comparisons," *Renewable and sustainable energy reviews*, vol. 12, pp. 1221-1250, 2008.

- Horak, J. (2006, 21-24 May 2006). *Power Quality: Measurements of Sags and Interruptions*. Paper presented at the 2005/2006 IEEE/PES Transmission and Distribution Conference and Exhibition.
- Hybrid power plant; http://www.dlr.de/vt/en/desktopdefault.aspx/tabid-9006/18909_read-15119/).
- IRENA. (2012). *Biomass for power generation*. International Renewable Energy Agency. Retrieved from https://www.irena.org/DocumentDownloads/Publications/RE_Technologies_Cost_Analysis-BIOMASS.pdf.
- Jayawarna, N., Jenkins, N., Barnes, M., Lorentzou, M., Papthanassiou, S., & Hatziagyriou, N. (2005, 18-18 Nov. 2005). *Safety analysis of a microgrid*. Paper presented at the 2005 International Conference on Future Power Systems.
- K.C. Divya, J. Ø. (2009). *Battery energy storage technology for power systems—An overview*. ELSEVIER.
- Kanaan, H. (2002). *CONTRIBUTION À LA MODÉLISATION ET AU RÉGLAGE DES REDRESSEURS TRIPHASÉS NON POLLUANTS UNIDIRECTIONNELS DE TYPE ÉLÉVATEUR ET À FRÉQUENCE DE COMMUTATION FIXE*. ÉCOLE DE TECHNOLOGIE SUPÉRIEURE UNIVERSITÉ DU QUÉBEC Retrieved from <http://espace.etsmtl.ca/id/eprint/810>.
- Karugaba, S., Muetze, A., & Ojo, O. (2012). On the Common-Mode Voltage in Multilevel Multiphase Single- and Double-Ended Diode-Clamped Voltage-Source Inverter Systems. *IEEE Transactions on Industry Applications*, 48(6), 2079-2091. doi:10.1109/TIA.2012.2226223.
- Kedjar, B., & Al-Haddad, K. (2008, 4-7 May 2008). *LQ control of a three-phase four-wire shunt active power filter based on three-level NPC inverter*. Paper presented at the 2008 Canadian Conference on Electrical and Computer Engineering.
- Khadkikar, V., & Chandra, A. (2008). A New Control Philosophy for a Unified Power Quality Conditioner (UPQC) to Coordinate Load-Reactive Power Demand Between Shunt and Series Inverters. *IEEE Transactions on Power Delivery*, 23(4), 2522-2534. doi:10.1109/tpwr.2008.921146.
- Khan, S. (2009). *Introduction To Microgrid*. Slide Share. Retrieved from <https://www.slideshare.net/Shahabkhan/microgrid-presentation>.

- Komurcugil, H. (2007). Globally stable control of three-phase three-wire shunt active power filters. *Electrical Engineering*, 89(5), 411-418.
- Komurcugil, H. (2009). *Integral sliding mode control of a single-phase current-source inverter*. Paper presented at the Industrial Electronics, 2009. IECON '09. 35th Annual Conference of IEEE.
- Komurcugil, H., & Kukrer, O. (2005). A new control strategy for single-phase shunt active power filters using a Lyapunov function. *Industrial Electronics, IEEE Transactions on*, 53(1), 305-312.
- Kramer, B., Chakraborty, S., & Kroposki, B. (2008, 10-13 Nov. 2008). *A review of plug-in vehicles and vehicle-to-grid capability*. Paper presented at the Industrial Electronics, 2008. IECON 2008. 34th Annual Conference of IEEE.
- http://www.dlr.de/vt/en/DesktopDefault.aspx/tabid-9006/18909_read-15119/gallery-1/gallery_read-Image.29.27161/
- Lab, B. *Microgrid at Berkeley Lab*. Retrieved from https://building-microgrid.lbl.gov/sites/all/files/styles/maximage/public/schematics_0.png?itok=6OdUr4Dw.
- Lee, C. C. (1990). Fuzzy logic in control systems: fuzzy logic controller. I. *IEEE Transactions on Systems, Man, and Cybernetics*, 20(2), 404-418. doi:10.1109/21.52551.
- Leijon, M. (2014). *Flywheel energy and power storage systems*. *Renew Sustain Energy Uppsala University, Renewable and Sustainable Energy Reviews*. Retrieved from https://www.researchgate.net/publication/223071124_Flywheel_energy_and_power_storage_systems_Renew_Sustain_Energy_Rev_112235.
- Lilienthal, P. (2013). *How to Classify Microgrids: Setting the Stage for a Distributed Generation Energy Future*. Homer Energy. Retrieved from <http://microgridnews.com/how-to-classify-microgrids-setting-the-stage-for-a-distributed-generation-energy-future/>.
- Longo, M., Roscia, M. C., & Zaninelli, D. (2015, 16-18 June 2015). *Net zero energy of smart house design*. Paper presented at the 2015 International Conference on Clean Electrical Power (ICCEP).
- Mahale, S. D., & Patil, R. J. (2016, 9-10 Sept. 2016). *Comparative analysis of various impedance source inverters*. Paper presented at the 2016 International Conference on Automatic Control and Dynamic Optimization Techniques (ICACDOT).

- Marin S. H, J. C. E. (2006). *Supercapacitors: A Brief Overview*. Retrieved from WWW: <http://www.mitre.org/tech/nanotech>.
- Matas, J., de Vicuna, L. G., Miret, J., Guerrero, J. M., & Castilla, M. (2008). Feedback Linearization of a Single-Phase Active Power Filter via Sliding Mode Control. *Power Electronics, IEEE Transactions on*, 23(1), 116-125.
- Mehrizi-Sani, A., & Iravani, R. (2012). Online Set Point Modulation to Enhance Microgrid Dynamic Response: Theoretical Foundation. *IEEE Transactions on Power Systems*, 27(4), 2167-2174. doi:10.1109/tpwrs.2012.2190532.
- Mendalek, N. (2009). *Modeling and control of three-phase four-leg split-capacitor shunt active power filter*. Paper presented at the Advances in Computational Tools for Engineering Applications, 2009. ACTEA '09. International Conference on.
- Mendalek, N., Al-Haddad, K., Fnaiech, F., & Dessaint, L. A. (2003). Nonlinear control technique to enhance dynamic performance of a shunt active power filter. *Electric Power Applications, IEE Proceedings* -, 150(4), 373-379.
- Mendalek, N., Al-Haddad, K., Kanaan, H. Y., & Hassoun, G. (2008). *Sliding mode control of three-phase four-leg shunt active power filter*. Paper presented at the Power Electronics Specialists Conference, 2008. PESC 2008. IEEE.
- Missanda, A., Al-Haddad, K., & Mendalek, N. (2016, 14-17 March 2016). *Nonlinear control of three-phase three-level four-wire NPC converter*. Paper presented at the 2016 IEEE International Conference on Industrial Technology (ICIT).
- Mukhopadhyay, S., Maiti, D., Banerji, A., S. K, B., & Deb, N. K. (2017). A New Harmonic Reduced 3-phase Thyristor Controlled Reactor for Static VAR Compensators. *IEEE Transactions on Industrial Electronics, PP(99)*, 1-1. doi:10.1109/TIE.2017.2694409.
- Nava-Segura, A., & Carmona-Hernandez, M. (1999). A detailed instantaneous harmonic and reactive compensation analysis of three-phase AC/DC converters, in abc and α ; β coordinates. *Power Delivery, IEEE Transactions on*, 14(3), 1039-1045.
- Nikkhajoeei, H., & Lasseter, R. H. (2007, 24-28 June 2007). *Microgrid Protection*. Paper presented at the 2007 IEEE Power Engineering Society General Meeting.
- Olivares, D. E., Cañizares, C. A., & Kazerani, M. (2011, 24-29 July 2011). *A centralized optimal energy management system for microgrids*. Paper presented at the 2011 IEEE Power and Energy Society General Meeting.

- Ota, Y., Taniguchi, H., Nakajima, T., Liyanage, K. M., Baba, J., & Yokoyama, A. (2012). Autonomous Distributed V2G (Vehicle-to-Grid) Satisfying Scheduled Charging. *Smart Grid, IEEE Transactions on*, 3(1), 559-564. doi:10.1109/tsg.2011.2167993
- Pal, Y., Swarup, A., & Singh, B. (2008). *A Review of Compensating Type Custom Power Devices for Power Quality Improvement*. Paper presented at the Power System Technology and IEEE Power India Conference, 2008. POWERCON 2008. Joint International Conference on.
- Parhizi, S., Lotfi, H., Khodaei, A., & Bahramirad, S. (2015). State of the Art in Research on Microgrids: A Review. *IEEE Access*, 3, 890-925. doi:10.1109/ACCESS.2015.2443119.
- Park, J. D., & Candelaria, J. (2013). Fault Detection and Isolation in Low-Voltage DC-Bus Microgrid System. *IEEE Transactions on Power Delivery*, 28(2), 779-787. doi:10.1109/tpwrd.2013.2243478.
- Pavinatto, E. F., Peres, M., Reis, P. D., Pereira, L. S., & Salles, F. P. (2008). Small power generation. *IEEE Industry Applications Magazine*, 14(6), 62-68. doi:10.1109/MIAS.2008.929326.
- Prasai, A., Du, Y., Paquette, A., Buck, E., Harley, R., & Divan, D. (2010, 12-16 Sept. 2010). *Protection of meshed microgrids with communication overlay*. Paper presented at the 2010 IEEE Energy Conversion Congress and Exposition.
- Puthenpurakel, S. P., & Subadhra, P. R. (2016, 1-3 Sept. 2016). *Identification and classification of microgrid disturbances in a hybrid distributed generation system using wavelet transform*. Paper presented at the 2016 International Conference on Next Generation Intelligent Systems (ICNGIS).
- Rastogi, M., Naik, R., & Mohan, N. (1994). A comparative evaluation of harmonic reduction techniques in three-phase utility interface of power electronic loads. *IEEE Transactions on Industry Applications*, 30(5), 1149-1155. doi:10.1109/28.315225.
- Reigosa, D., Arbolea, P., Gonzalez-Moran, C., González-Morán, C., Gomez-Aleixandre, J., & Gómez-Aleixandre, J. (2009, 15-18 Nov. 2009). *An improved control scheme based in droop characteristic control for microgrid converters*. Paper presented at the 2009 International Conference on Electrical Machines and Systems.
- Rezkallah, M., Chandra, A., & Singh, B. (2013, 10-13 Nov. 2013). *Three-leg four-wire voltage source inverters for hybrid standalone system feeding unbalanced load*. Paper presented at the IECON 2013 - 39th Annual Conference of the IEEE Industrial Electronics Society.

- L. Reznik, "Fuzzy controller design: recommendations to the user," in *Knowledge-Based Intelligent Electronic Systems, 1998. Proceedings KES'98. 1998 Second International Conference on*, 1998, pp. 609-616.
- Rivas, D., Moran, L., Dixon, J. W., & Espinoza, J. R. (2003). Improving passive filter compensation performance with active techniques. *Industrial Electronics, IEEE Transactions on*, 50(1), 161-170.
- Roy, J., Xia, Y., & Ayyanar, R. (2016, 18-22 Sept. 2016). *A single phase transformerless string inverter with large voltage swing of half-bridge capacitors for active power decoupling*. Paper presented at the 2016 IEEE Energy Conversion Congress and Exposition (ECCE).
- Rutherford, M. J., & Yousefzadeh, V. (2011, 6-11 March 2011). *The impact of Electric Vehicle battery charging on distribution transformers*. Paper presented at the Applied Power Electronics Conference and Exposition (APEC), 2011 Twenty-Sixth Annual IEEE.
- S. Chowdhury, S. P. C. a. P. C. (2009). *Microgrids and Active Distribution Networks*. IET RENEWABLE ENERGY.
- Samanes, J., & Gubía, E. (2017, 26-30 March 2017). *Sensorless active damping strategy for parallel interleaved voltage source power converters with LCL filter*. Paper presented at the 2017 IEEE Applied Power Electronics Conference and Exposition (APEC).
- Sawant, R. R., & Chandorkar, M. C. (2009). A Multifunctional Four-Leg Grid-Connected Compensator. *IEEE Transactions on Industry Applications*, 45(1), 249-259. doi:10.1109/tia.2008.2009704.
- Setel, A., Gordan, I. M., & Gordan, C. E. (2016, 6-9 Nov. 2016). *Use of geothermal energy to produce electricity and heating at average temperatures*. Paper presented at the Mediterranean Conference on Power Generation, Transmission, Distribution and Energy Conversion (MedPower 2016).
- Sharma, V., Saini, P., Garg, S., & Negi, B. (2016, 16-18 March 2016). *Comparative analysis of VSI, CSI and ZSI fed induction motor drive system*. Paper presented at the 2016 3rd International Conference on Computing for Sustainable Global Development (INDIACom).
- S. Breban, I. Gros, C. Marginean, and P. Teodosescu, "Fuzzy Logic Energy Management for a Residential Power System Using Renewable Energy Sources," in *Modern Fuzzy Control Systems and Its Applications*, ed: InTech, 2017.

- Singh, B., Jayaprakash, P., & Kothari, D. P. (2008a). A T-Connected Transformer and Three-leg VSC Based DSTATCOM for Power Quality Improvement. *Power Electronics, IEEE Transactions on*, 23(6), 2710-2718. doi:10.1109/tpel.2008.2004273.
- Singh, B., Jayaprakash, P., & Kothari, D. P. (2008b). A T-Connected Transformer and Three-leg VSC Based DSTATCOM for Power Quality Improvement. *IEEE Transactions on Power Electronics*, 23(6), 2710-2718. doi:10.1109/tpel.2008.2004273.
- Srianthumrong, S., Fujita, H., & Akagi, H. (2002). Stability analysis of a series active filter integrated with a double-series diode rectifier. *Power Electronics, IEEE Transactions on*, 17(1), 117-124.
- Sunan, E., Kucuk, F., Goto, H., Guo, H. J., & Ichinokura, O. (2014). Three-Phase Full-Bridge Converter Controlled Permanent Magnet Reluctance Generator for Small-Scale Wind Energy Conversion Systems. *IEEE Transactions on Energy Conversion*, 29(3), 585-593. doi:10.1109/TEC.2014.2316471.
- Singh, M., Kumar, P., & Kar, I. (2012). Implementation of vehicle to grid infrastructure using fuzzy logic controller. *IEEE Transactions on Smart Grid*, 3(1), 565-577.
- Szasz, R. (2008, 14-18 Sept. 2008). *Fuel cell technology: A promising alternative for extended back-up power run time for telecommunication sites*. Paper presented at the INTELEC 2008 - 2008 IEEE 30th International Telecommunications Energy Conference.
- Talei, H., Zizi, B., Abid, M. R., Essaaidi, M., Benhaddou, D., & Khalil, N. (2015, 10-13 Dec. 2015). *Smart campus microgrid: Advantages and the main architectural components*. Paper presented at the 2015 3rd International Renewable and Sustainable Energy Conference (IRSEC).
- Tangtheerajaronwong, W., Hatada, T., Wada, K., & Akagi, H. (2007). Design and Performance of a Transformerless Shunt Hybrid Filter Integrated Into a Three-Phase Diode Rectifier. *IEEE Transactions on Power Electronics*, 22(5), 1882-1889. doi:10.1109/tpel.2007.904166.
- Thounthong, P., Chunkag, V., Sethakul, P., Davat, B., & Hinaje, M. (2009). Comparative Study of Fuel-Cell Vehicle Hybridization with Battery or Supercapacitor Storage Device. *Vehicular Technology, IEEE Transactions on*, 58(8), 3892-3904.
- Tidjani, F. S., & Chandra, A. (2012, 25-28 Oct. 2012). *Integration of renewable energy sources and the utility grid with the Net Zero Energy Building in Republic of Chad*. Paper presented at the IECON 2012 - 38th Annual Conference on IEEE Industrial Electronics Society.

- Tidjani, F. S., Hamadi, A., Chandra, A., & Pillay, P. (2014, Oct. 29 2014-Nov. 1 2014). *Control strategy for improving the power flow between home integrated photovoltaic system, plug-in hybrid electric vehicle and distribution network*. Paper presented at the IECON 2014 - 40th Annual Conference of the IEEE Industrial Electronics Society.
- Tidjani, F. S., Hamadi, A., Chandra, A., Pillay, P., & Ndtoungou, A. (2017). Optimization of Standalone Microgrid Considering Active Damping Technique and Smart Power Management Using Fuzzy Logic Supervisor. *IEEE Transactions on Smart Grid*, 8(1), 475-484. doi:10.1109/TSG.2016.2610971.
- Ustun, T. S., Ozansoy, C., & Ustun, A. (2013). Fault current coefficient and time delay assignment for microgrid protection system with central protection unit. *IEEE Transactions on Power Systems*, 28(2), 598-606. doi:10.1109/tpwrs.2012.2214489.
- Ustun, T. S., Ozansoy, C., & Zayegh, A. (2011, 17-20 Oct. 2011). *Implementation of Dijkstra's algorithm in a dynamic microgrid for relay hierarchy detection*. Paper presented at the 2011 IEEE International Conference on Smart Grid Communications (SmartGridComm).
- Vigneshkumar, L., & Prabakaran, R. (2016, 25-27 May 2016). *Implementation of multilevel topology using 4 H-bridges*. Paper presented at the 2016 International Conference on Advanced Communication Control and Computing Technologies (ICACCCT).
- Villalva, M. G., Gazoli, J. R., & Filho, E. R. (2009). Comprehensive Approach to Modeling and Simulation of Photovoltaic Arrays. *Power Electronics, IEEE Transactions on*, 24(5), 1198-1208. doi:10.1109/tpel.2009.2013862.
- Wiroj, T., Hatada, T., Keiji, W., & Akagi, H. (2007). Design and performance of a transformerless shunt hybrid filter integrated into a three-phase diode rectifier. *IEEE Transactions on Power Electronics*, 22(5), 1882-1889.
- Yacoubi, L., Al-Haddad, K., Dessaint, L. A., & Fnaiech, F. (2006a). Linear and Nonlinear Control Techniques for a Three-Phase Three-Level NPC Boost Rectifier. *IEEE Transactions on Industrial Electronics*, 53(6), 1908-1918. doi:10.1109/TIE.2006.881990.
- Yacoubi, L., Al-Haddad, K., Dessaint, L. A., & Fnaiech, F. (2006b). Linear and Nonlinear Control Techniques for a Three-Phase Three-Level NPC Boost Rectifier. *Industrial Electronics, IEEE Transactions on*, 53(6), 1908-1918.
- Yonghua, S., Xia, Y., & Zongxiang, L. (2010, 25-29 July 2010). *Integration of plug-in hybrid and electric vehicles: Experience from China*. Paper presented at the Power and Energy Society General Meeting, 2010 IEEE.

- Zabihi, S., & Zare, F. (2006). *Active Power Filters with Unipolar Pulse Width Modulation to Reduce Switching Losses*. Paper presented at the Power System Technology, 2006. PowerCon 2006. International Conference on.
- L. A. Zadeh, "Fuzzy sets," *Information and control*, vol. 8, pp. 338-353, 1965
- Zhang, R., Prasad, V. H., Boroyevich, D., & Lee, F. C. (2002). Three-dimensional space vector modulation for four-leg voltage-source converters. *Power Electronics, IEEE Transactions on*, 17(3), 314-326.
- Zhang, Y., & Qu, C. (2015). Table-Based Direct Power Control for Three-Phase AC/DC Converters Under Unbalanced Grid Voltages. *IEEE Transactions on Power Electronics*, 30(12), 7090-7099. doi:10.1109/tpel.2014.2387694.
- Zhaoan, W., Qun, W., Weizheng, Y., & Jinjun, L. (2001). A series active power filter adopting hybrid control approach. *Power Electronics, IEEE Transactions on*, 16(3), 301-310.
- Zubieta, L. E. (2016). Are Microgrids the Future of Energy?: DC Microgrids from Concept to Demonstration to Deployment. *IEEE Electrification Magazine*, 4(2), 37-44. doi:10.1109/MELE.2016.2544238.